conference & workshop

PROGRESSIVE ROCK FAILURE

monte verità

June 5 - 9 2017

creep and stress corrosion

long term strength limits

progressive slope failure

environmental drivers

subsurface infrastructure

EXTENDED ABSTRACTS

www.prf2017.ethz.ch

An ISRM Specialized Conference

ISRM

Published by ETH Zurich, Zurich, Switzerland

Edited by Kerry Leith, Martin Ziegler, Matthew Perras and Simon Loew.

An ISRM Specialized Conference

Printed in Switzerland, by ETH Zürich

PRF 2017

Progressive rock failure conference 2017
Monte Verità
5–9 June 2017
Extended abstracts
www.prf2017.ethz.ch

PREFACE

Geological materials change their strength properties through time, which has significant implications for the stability of natural and artificial slopes, surface or subsurface excavations, and deep boreholes used for energy production. While some of these mechanical property changes lead to slow phenomena like creep, others lead to rapid and hazardous deformations and failure of geological materials. Time-dependent aspects of weakening and failure in natural systems are, however, difficult to study as internal damage is not visible to the naked eye and the underlying processes can last from several seconds to many thousands of years. Better understanding and predicting of these processes represents a great challenge to those involved in the preservation of existing structures, future development of critical transport and energy infrastructure, and the assessment of natural hazards in response to a changing climate. By bringing together participants from diverse backgrounds, PRF 2017 provides an exciting opportunity to address processes controlling the degradation and failure of brittle rock across an exceptional range of spatial and temporal scales.

Three days of seminars/discussions and one day of integrated excursions, are arranged around five core themes: creep and stress corrosion, long term strength limits, progressive slope failure, environmental drivers, and subsurface infrastructure. The core themes will allow practitioners and researchers from diverse backgrounds to progress beyond current knowledge barriers, and lay out a framework for the future evaluation of time-dependent weakening and failure of brittle rocks. Participants will present recent insights derived from:

- field observations in both surface and sub-surface environments (43%),
- laboratory testing (17%),
- theory and conceptual modeling (17%), and
- advanced numerical methods (23%).

A one-day workshop, arranged as a follow-up to the meeting, will demonstrate practical approaches to observing and modelling progressive damage evolution and brittle failure using industry-leading tools and software.

SPONSORS

ETH zürich

Congressi
Stefano Franscini

FNSNF
Swiss National Science Foundation

Schweizerische Eidgenossenschaft
Confédération suisse
Confederazione Svizzera
Confederaziun svizra

Eidgenössisches Nuklear-sicherheitsinspektorat ENSI

SFIG	SCHWEIZERISCHE FACHGRUPPE FÜR INGENIEURGEOLOGIE
GSGI	GROUPEMENT SUISSE DE LA GEOLOGIE DE L'INGENIEUR

ITASCA
Consulting Group, Inc.

ISRM International Society for Rock Mechanics

TABLE OF CONTENTS

Lab investigations

Theory and conceptual modelling

State-of-the-art numerical modelling

Numerical modelling workshop

Time-dependent weakening and failure in the crust: subcritical crack growth and brittle creep

Philip Meredith[1*], Nicolas Brantut[1], Michael Heap[2] and Patrick Baud[2]

[1] Rock & Ice Physics Laboratory, Department of Earth Sciences, University College London, London, UK
[2] Géophysique Expérimentale, EOST (UMR7516 CNRS), Université de Strasbourg, Strasbourg, France
* p.meredith@ucl.ac.uk

Earthquake ruptures and volcanic eruptions are the most dramatic manifestations of the dynamic failure of a critically stressed crust. However, these are actually very rare events in both space and time, and most of the crust spends most of its time in a highly stressed but subcritical state.

Under upper crustal conditions, most rocks accommodate applied stresses in a brittle manner through cracking, fracturing and faulting. Such cracks can grow at all scales from the grain scale to the crustal scale, and under different stress regimes. Under tensile stress, single, long cracks tend to grow at the expense of shorter ones. By contrast, under all-round compression deformation of rocks in the brittle field proceeds by the progressive growth and coalescence of many microcracks. Under nominally dry environmental conditions and rapid loading, crack growth is primarily governed by the applied stresses. Indeed, laboratory experiments show that rock strength is essentially time independent under such conditions (Paterson & Wong 2005). At the microscopic scale, time independence means that the crack growth criterion is well modeled by the concept of constant fracture toughness, i.e., a critical stress intensity factor at microcrack tips.

However, at lower strain rates and in the presence of aqueous fluids, i.e., under more realistic upper crustal conditions, experiments show that brittle rock deformation becomes time-dependent. This is well demonstrated by the fact that rocks can fail by static fatigue, following a preceding period of creep deformation, under conditions of constant applied stress (e.g., Scholz 1968; Kranz 1980; Baud & Meredith 1997; Heap et al. 2009; Brantut et al. 2013). Time-dependent crack growth arises from chemically activated subcritical crack growth processes, such as stress corrosion reactions (see Atkinson 1984; Atkinson & Meredith 1987). This process allows deformation of the crust to proceed over a wide range of strain rates, from the very low rates associated with tectonic loading up to the very high rates associated with earthquake rupture or impact events. Overall, cracking in the crust can therefore occur over a spatial scale spanning some 12 orders of magnitude, and a temporal scale spanning some 18 orders of magnitude. Establishing quantitative links between microscopic, grain-scale subcritical cracking and macroscopic, sample-scale to crustal scale brittle creep behavior is a key challenge for our understanding of the time-dependent mechanics of the Earth's crust.

Experimental rock deformation provides us with several ways to investigate time-dependent brittle deformation. Two main types of experiments can be distinguished: (1) "constant strain rate" experiments in which stress varies as a result of deformation and (2) "creep" experiments in which deformation and deformation rate vary over time as a result of an imposed constant stress. In the latter case, when a rock is held at constant stress (i.e., both the differential stress and the effective confining pressure, denoted P_{eff}, are maintained constant), it deforms typically in the manner depicted in Fig. 1. This phenomenon of brittle creep has been observed in all major rock types, including granite, basalt limestone and sandstone. Such curves have commonly been described as exhibiting three phases, based solely on the observed macroscopic strain-time behavior: an initial decelerating stage, termed primary creep, followed by an apparent constant strain rate stage, termed secondary creep, and finally an accelerating tertiary creep stage, after which the sample fails. It is apparent from Fig. 1 that the rock experiences a wide range of strain rates as deformation proceeds. Such experiments therefore have the ability to convey very rich information on the time-dependency of the brittle deformation process.

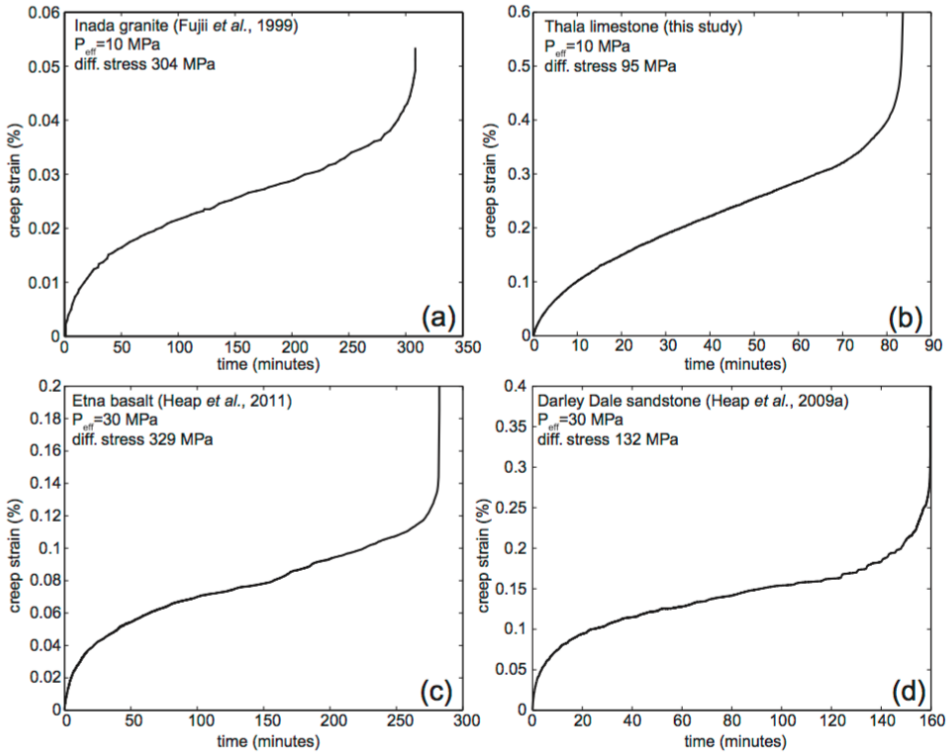

Figure 1. Experimentally derived brittle creep curves for (a) granite, (b) limestone, (c) basalt and (d) sandstone. The constant applied differential (creep) stress and effective confining pressure (P_{eff}) for each experiment are indicated in each panel. Figure from: Brantut et al. (2013).

However, for a consistent description of time-dependent brittle deformation to be determined, it should be able to explain both creep (constant stress) and constant strain rate deformation in a unified manner. We show how the increasing importance of microcrack interactions as deformation proceeds is able to produce the switch from decreasing to increasing crack growth rate during deformation at constant stress (i.e., the transition from primary to tertiary creep). It is the same process that is in fact responsible for the existence of a peak stress in deformation experiments performed at an imposed constant strain rate (Brantut et al. 2012).

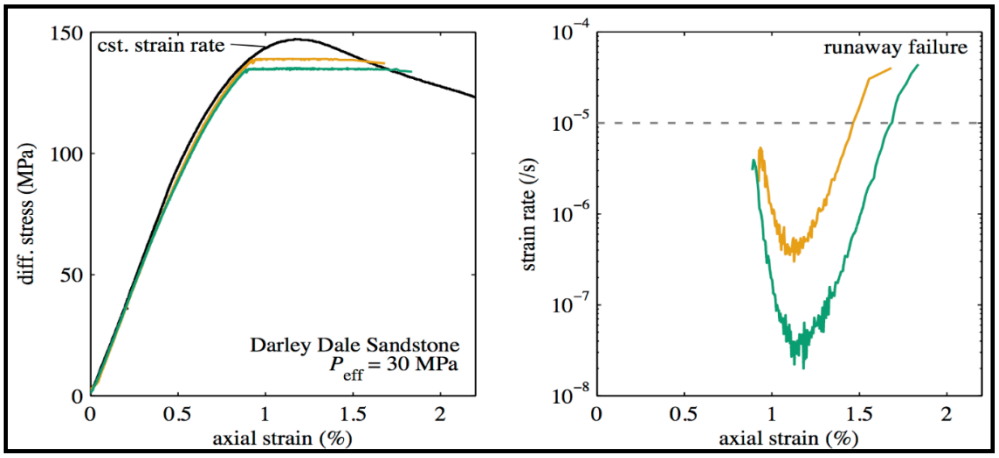

Figure 2. Comparison of the deformation of Darley Dale sandstone under constant strain rate (black curve) and constant stress (creep) conditions. Constant creep stresses were set at 95% of peak stress (orange curve) and 92% of peak stress (green curve). Data from: Brantut et al. (2014).

Fig. 2 shows the differential stress and axial strain rate as functions of axial strain for one constant strain rate experiment (in black) and two creep experiments (in orange and green) performed on samples of Darley Dale sandstone at 30 MPa effective confining pressure. As expected, the behavior

is the same during the loading stage, since the imposed condition (a constant strain rate of 10^{-5} s^{-1}) is the same. In the creep experiments, once the pre-determined creep stress is reached, the stress is maintained constant. By contrast, the differential stress keeps evolving during the constant strain rate experiment; first increasing until it reaches a peak (around 147 MPa), after which it decreases gradually. No macroscopic dynamic stress drop occurred, since the machine stiffness was high enough to prevent runaway deformation in the strain-softening regime. A striking observation is that the creep samples, deformed under constant stress, fail macroscopically (i.e., the deformation rate increases in an uncontrollable manner) when the two curves (constant strain rate and constant stress) intersect each other.

Several other fundamental observations can be made from the data of Fig. 2. First, the creep strain rate is never constant, as suggested in many earlier studies. There is simply a point of inflexion when decelerating creep reaches a minimum strain rate, after which it increases and accelerates to failure. So, the apparent period of secondary (often erroneously called “steady state”) creep does not actually exist. Second, the minimum creep strain rate is achieved exactly at the point where the stress difference (between constant strain rate and creep tests) is largest, i.e., when the differential stress is at the peak during the constant strain rate test.

These observations of slow cracking have profound implications for the evolution and dynamics of the Earth’s crust. We therefore present a model to describe the process that is based on micromechanics, but also provides an adequate description at the macroscopic or crustal scale. We do this by establishing a relationship between the internal, microstructural state of the rock and the macroscopically observed external parameters. We present examples that attempt to reconcile these ideas through external measurements of stress and strain evolution during deformation with simultaneous measurements of the evolution of key internal variables such as elastic wave speeds, acoustic emission output, porosity and permeability. Overall, the combined data are able to explain both the complexity of stress-strain relations during constant strain rate loading and the shape of creep curves during constant stress loading, thus providing a unifying framework to describe the time-dependent mechanical behavior of crustal rocks.

Finally, we present some ongoing work that attempts to bridge the gap between feasible laboratory strain rates and times-scales, and natural tectonic strain rates, by using the stable environment of the deep-sea to perform ultra-long-term creep experiments with durations from months to years.

Reference list

Atkinson, BK. 1984. Subcritical crack growth in geological materials, J. Geophys. Res., 89(B6), 4077–4114.

Atkinson, BK, Meredith PG. 1987. The theory of subcritical crack growth with applications to minerals and rocks. In B. K. Atkinson (ed.), Fracture Mechanics of Rock, 111–116, Academic Press, London.

Baud, P, Meredith PG. 1997. Damage accumulation during triaxial creep of Darley Dale sandstone from pore volumometry and acoustic emission, Int. J. Rock Mech. Min. Sci., 34(3–4), 371.

Brantut, N, Baud, P, Heap, MJ, Meredith PG. 2012. Micromechanics of brittle creep in rocks, J. Geophys. Res., 117, B08412, doi:10.1029/2012JB009299.

Brantut, N, Heap, MJ, Meredith PG, Baud P. 2013. Time-dependent cracking and brittle creep in crustal rocks: A review, J. Struct. Geol., 52, 17–43.

Brantut, N, Heap, MJ, Baud, P, Meredith PG. 2014. Rate- and strain-dependent brittle deformation of rocks, J. Geophys. Res. Solid Earth, 119, 1818–1836, doi:10.1002/2013JB010448.

Heap, MJ, Baud, P, Meredith, PG, Bell, AF, Main IG. 2009. Time-dependent brittle creep in Darley Dale sandstone, J. Geophys. Res., 114, B07203, doi:10.1029/2008JB006212.

Kranz, RL. 1980. The effects of confining pressure and stress difference on static fatigue of granite, J. Geophys. Res., 85(B4), 1854–1866.

Paterson, MS, Wong TF. 2005. Experimental Rock Deformation—The Brittle Field, 2nd ed., Springer-Verlag, Berlin Heidelberg.

Scholz, CH. 1968. Experimental study of the fracturing process in brittle rocks, J. Geophys. Res., *73*(4), 1447–1454.

Can long term rock erosion rates be predicted through fracture mechanics?

Martha Cary Eppes[1*], Russell Keanini[2], Gregory S. Hancock[3], Xiaofeng Chen[4] and Thomas A. Dewers[5]

[1] Department of Geography & Earth Sciences, University of North Carolina (UNC) at Charlotte, North Carolina, USA
* meppes@uncc.edu
[2] Department of Mechanical Engineering and Engineering Science, UNC Charlotte, North Carolina, USA
[3] Department of Geology, College of William and Mary, Virginia, USA
[4] Bureau of Economic Geology, University of Texas, Austin, USA
[5] Sandia Laboratories, Albuquerque, New Mexico, USA

1 Introduction

The *in situ* mechanical breakdown, or physical weathering, of rock at and near Earth's surface constitutes a critical component of a wide array of surface process systems ranging from river channels (Hancock et al. 2011) to mass wasting (Collins and Stock 2016) to long-term landscape evolution (Kirchner et al. 2006). The relative importance of various weathering processes (freezing, thermal cycling, mineral hydration, etc.) in contributing to these systems, however, remains unknown, resulting in an overall lack of understanding of the key driving and limiting factors of rock breakdown and erosion (Portenga and Bierman 2011). Here we take a new approach to evaluating mechanical weathering and associated rock erosion by exploring these processes in the context of climate-dependent subcritical crack growth.

The role that subcritical crack growth (a.k.a. time-dependent crack growth, progressive rock fracture) may play in mechanical weathering and subsequent rock erosion has never been substantially characterized. Based on a compendium of existing fracture mechanics data and theory (Eppes and Keanini, in prep), the following hypotheses arise: 1) subcritical crack growth is a viable, and likely common, mechanism of mechanical weathering acting in concert with all weathering-induced stresses at and near Earth's surface, 2) rates of subcritical crack growth in all weathering environments are climate–dependent, outside of climate's influence on individual stress loading via processes like freezing or mineral hydration, and therefore 3) rates of erosion for any given rock type will be strongly influenced by that rock's subcritical crack growth characteristics, such as its fracture toughness or its subcritical crack growth index (*n)*, the latter of which is itself also known to be climate-dependant. In testing these hypotheses we explore a potentially universal mechanism of rock breakdown at and near Earth's surface.

2 Methods

2.1 Numerical Modeling

We quantitively evaluate the role that subcritical crack growth plays in rock weathering and erosion by building a physically based numerical model that employs well-vetted rock-stress and rock cracking numerical relationships that we borrow from existing rock mechanics literature (e.g. Anderson 2005; Atkinson, 1987). We model subcritical crack growth through a novel combination of Paris' Law and Charles's Law (Eppes and Keanini, in prep.). This combination is necessary in order to take advantage of existing data for *n* that does not exist for the equivalant Paris Law exponent, *m*. The latter describes subcritical crack growth under cycling loading, which is characteristic of virtually all weathering-related stresses. Focusing only on a single source of stress, the simple but ubiquitous case of intergranular stresses that arise due to solar-induced thermal cycling, we then use realistic rock, environment and stress-loading parameters to quantify rates of subcritical crack growth and subsequent rock erosion.

2.2 Field Testing

In order to determine to what extent modeled erosion rates match measured ones, we apply the model to three different rock types that are characterized by varying 10Be-derived bare rock erosion rates (Hancock, in prep.) where they outcrop in the Blue Ridge Mountains of Virginia, USA. We also collected field data for the fracture characteristics (crack density, length, weathering) of natural outcrops of the three rock types, in order to document how subcritical crack growth may manifest as observable mechanical weathering. We have collected samples for determination of each rock type's fracture tougness and *n* values under dry and saturated conditions.

3 Preliminary results

Overall, our modeling results show that the magnitude of most weathering-related stresses, as quantified by us and others to date, are sufficient to result in subcritical crack growth-driven weathering. Furthermore, our modeling demonstrates the potentially strong climate dependence (both moisture and temperature) of mechanical weathering via subcritical crack growth. We calculate, for example, several orders of magnitude differences in erosion rate for a single rock type (granite) subjected to the same magnitude of stresses but different climate-averaged temperature and moisture conditions. We find, however, that calculated rock erosion rates are strongly dependent also on rock-specific thermal and mechanical parameters. These parameters also appear to influence the observed macro-fracture characteristics of the ridge-forming rock types of the Blue Ridge Mountains. Overall, our study highlights several novel means by which a fracture mechanics approach may specifically be applied to rock weathering and erosion at and near Earth's surface.

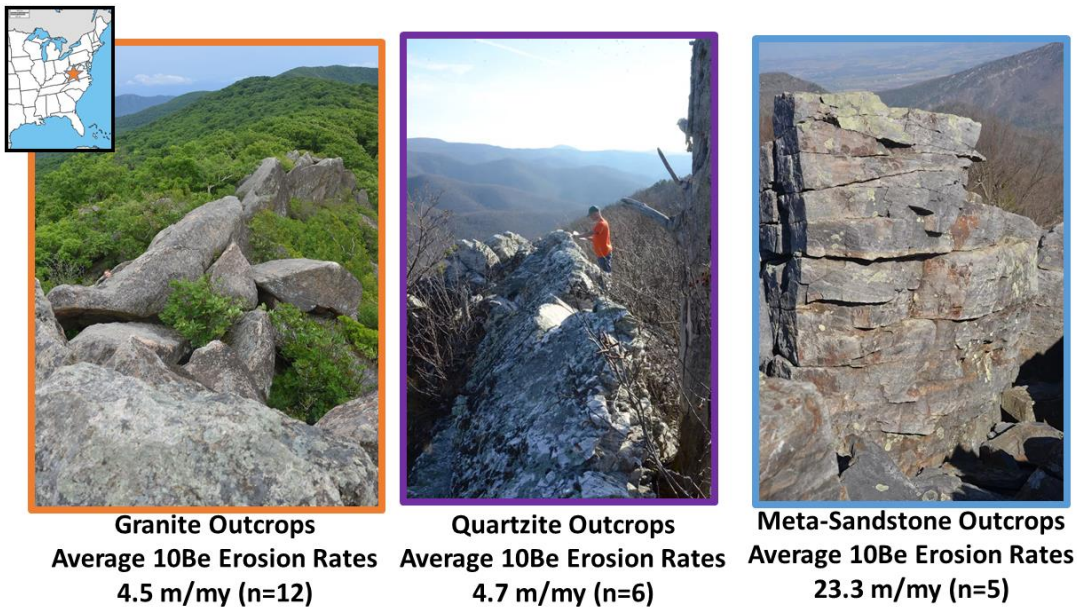

Figure 1. Photographs of typical outcrops and averaged erosion rates of the three rock types for which data was employed in this study. ^{10}Be Erosion Rate data is from Hancock (in prep.). (photograph © M.C.Eppes).

4 Reference list

Anderson, T. L., 2005, Fracture mechanics: fundamentals and applications, CRC press.

Atkinson, B. K., 1987, Fracture mechanics of rock, Academic press London.

Collins, B. D., and Stock, G. M., 2016, Rockfall triggering by cyclic thermal stressing of exfoliation fractures: Nature Geoscience.

Hancock, G. S., Small, E. E., and Wobus, C., 2011, Modeling the effects of weathering on bedrock-floored channel geometry: Journal of Geophysical Research: Earth Surface (2003–2012), v. 116, no. F3.

Kirchner, J. W., Riebe, C. S., Ferrier, K. L., and Finkel, R. C., 2006, Cosmogenic nuclide methods for measuring long-term rates of physical erosion and chemical weathering: Journal of Geochemical Exploration, v. 88, no. 1, p. 296-299.

Portenga, E. W., and Bierman, P. R., 2011, Understanding Earth's eroding surface with 10 Be: GSA Today, v. 21, no. 8, p. 4-10.

Progressive failure of brittle rock slopes: Field observations, modeling results and unknowns

Simon Loew[1*], Valentin Gischig[1], Franziska Glüer[1], Lorenz Grämiger[1]and Sophie Gschwind[1]

[1] Department of Earth Sciences, ETH Zurich, Switzerland
* simon.loew@erdw.ethz.ch

1 Introduction

In 1962 Karl Terzaghi describes in a seminal paper systematically the progressive damage of brittle rock slopes through geological time, driven by fluvial and subglacial glacial incision into steep slopes. According to Terzaghi the removal of lateral support of steep and fractured rock slopes leads to increased shear stresses in the rock mass and the breakage of “many cohesive bonds connecting the blocks between the joints”, driving the formation of a new fracture system and a basal rupture plane. He stresses that in the layer of frost penetration and of significant daily and seasonal temperature variations, the effective cohesion of the rock may be completely eliminated and failure is characterized by periodic rock fall activity. On the other hand, deep and delayed sliding is supposed to origin from a combined effect of the increase of shear stresses and a slow creep-deformation of the rock acting upon by these stresses. These processes are overlain by “cleft-water pressures reducing the frictional resistance along the joint walls” from rainfall and snow melt water infiltrating into the strongly damaged near surface layer, where the groundwater table (or pore pressures) show seasonal variations measured in “tens of feet”. These pressure variations are strongest during rapid snowmelt in spring, when “the exit of the joints are still plugged with ice”.

Terzaghi (1962) also discusses the successive stages in the evolution of slopes. He states that if the rate of fluvial or glacial down-cutting decreases, the slope angle of the valley walls is gradually reduced by weathering and removal of weathering products until the slope angle reaches a stable value defined by the orientations and friction angles of “continuous joint sets” and persistent faults. Special consideration is given to the exceptional conditions prevailing after the retreat of large valley glaciers, including the observation that strong variations in delayed response times after exposure to “all the agencies which weaken the slope” are observed.

While many of these ground-breaking concepts have been verified and refined in the following decades, several open key questions could not be clearly resolved until today. This lecture discusses the current understanding of Terzaghi’s concepts based on new field observations and modeling results carried out at the Chair of Engineering Geology in the last 10 years.

2 Paraglacial and periglacial processes

In the valley of the Great Aletsch Glacier (Switzerland), Grämiger (2017) has studied in detail thermo-hydro-mechanical induced stresses and resulting long-term rock slope damage during repeat glacial cycles. Following Lateglacial deglaciation, the surrounding valley rock slopes in the Aletsch region experienced several minor glacier cycles during the Holocene, which could be reconstructed in great detail. The foliated gneissic rock mass of the Aletsch valley contains several large rock slope instabilities with a concentration around the retreating, present-day glacier tongue (Fig. 1). The reaction of the individual slope compartments in the glacier tongue area shows strong variations primarily controlled by the structural pre-disposition from large scale faults. Ground surface temperature measurements, monitoring of subglacial water pressures in ice boreholes, regional spring-line mapping, and monitoring of rock slope deformation at Aletsch each contributed to parameterizing and validating thermal and hydraulic boundary conditions of a series of transient mechanical, thermo-mechanical and hydro-mechanical 2D discrete-element models.

The simulations of Grämiger et al. (2017) reveal that purely mechanical loading and unloading of rock slopes by ice during glacial cycles generates relatively limited new damage. The amount of initial damage, inherited from pre-glacial, ice-free topographic and in-situ stress conditions, strongly controls the susceptibility of the slope to new damage from ice loading. Thermal strain from long-term temperature changes induces stresses at depths exceeding 100 m, generating significantly more rock slope damage than predicted for purely mechanical loading cycles. Glacier loading cycles in parallel with long-term mountain water table variations generate substantial fracture propagation. Major damage occurs during initial ice occupation and first glacier retreat, while subsequent re-advances result in minor damage. Superposition of annual groundwater cycles (i.e., hydro-mechanical fatigue) strongly increases rock slope damage during glacial loading cycles, destabilizing the toppling-mode valley flank in our models.

Detailed investigations of active landslides around the toe of the Great Aletsch Glacier demonstrate that old (presumably Late-Glacial or early Holocene) landslides exposed by the downwasting glacial ice since the Little Ice Age (LIA climax around 1860), strongly react when the landslide toe area becomes ice-free. In the Moosfluh deep seated landslide (Fig. 1), the response to recent glacial unloading is very strong, leading to large displacements at the decameter scale and very intensive internal deformations. We can quantify the amount and type of internal strain, compare it to pre-LIA deformations and assess the long-term damage modeled by Grämiger (2017).

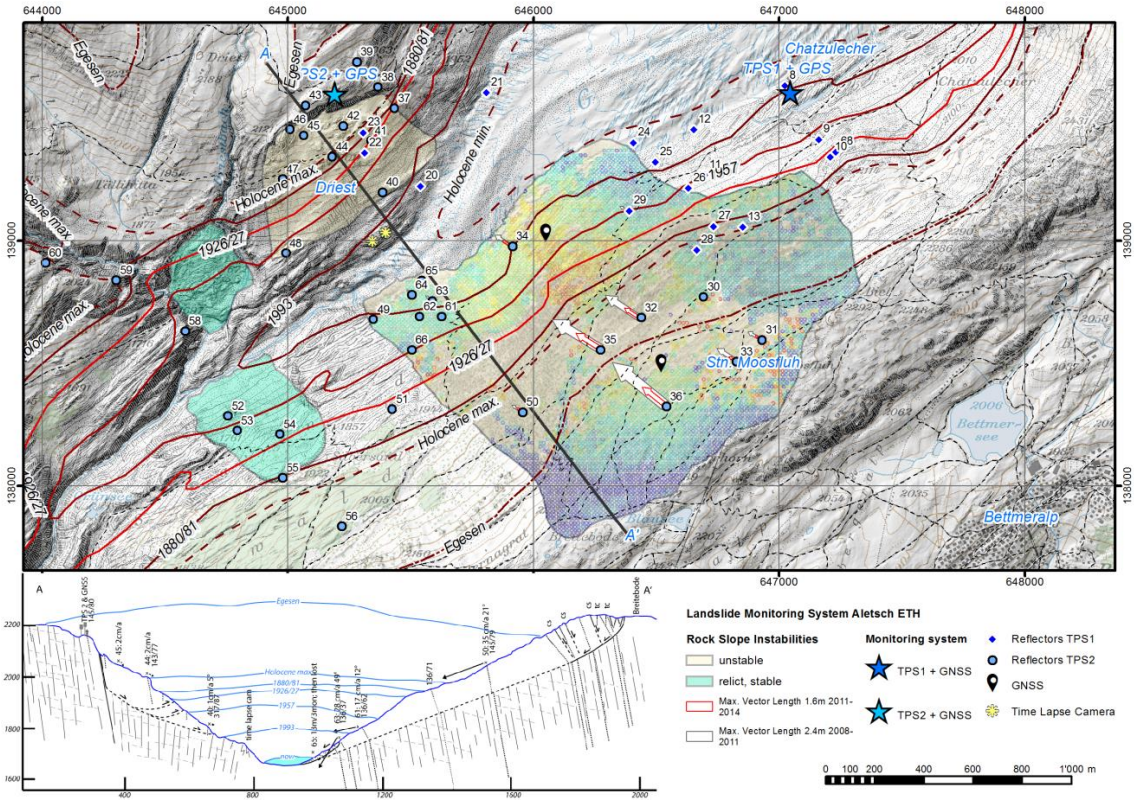

Figure 1. Active landslides around the current tongue of the Great Aletsch Glacier (Switzerland). Shown are displacement vectors and ice elevations since the Little Ice Age.

3 Displacement rates, creep curves and catastrophic failure

Today a 3-stage creep model is frequently used to describe the displacement behavior of landslides (e.g. Crosta and Agliardi 2003). It is composed of an initial non-linear acceleration phase related to stress re-adjustment to new boundary conditions of repeated retrogressive failures, typically lasting a few years. The second stage, with quasi-steady displacement velocities, can be related to slow micro-cracking and small incremental failures accumulated during many thermo-mechanical or pore-pressure cycle (Fig. 2). The duration of this stage is strongly variable, lasting from a few years to presumably thousands of years, when considering exposure ages of head scarps as determined at

several rockslides in the Alps and elsewhere. The third stage with accelerated creep could be the result of sudden micro-crack propagation at high stress levels. This stage - typically lasting again a few years in brittle rock - is often modeled with exponentially increasing displacements following the results of small scale fatique tests. However, detailed field observations show important deviations from this idealized exponential behavior (Fig. 3) and the time dependent accelerations. This stage is of fundamental importance for early warning systems, but can not be predicted with rigorous physics-based approaches. In addition, many deep instabilities in brittle rock never fail catastrophically and the underlying causes have only been studied by very few researchers.

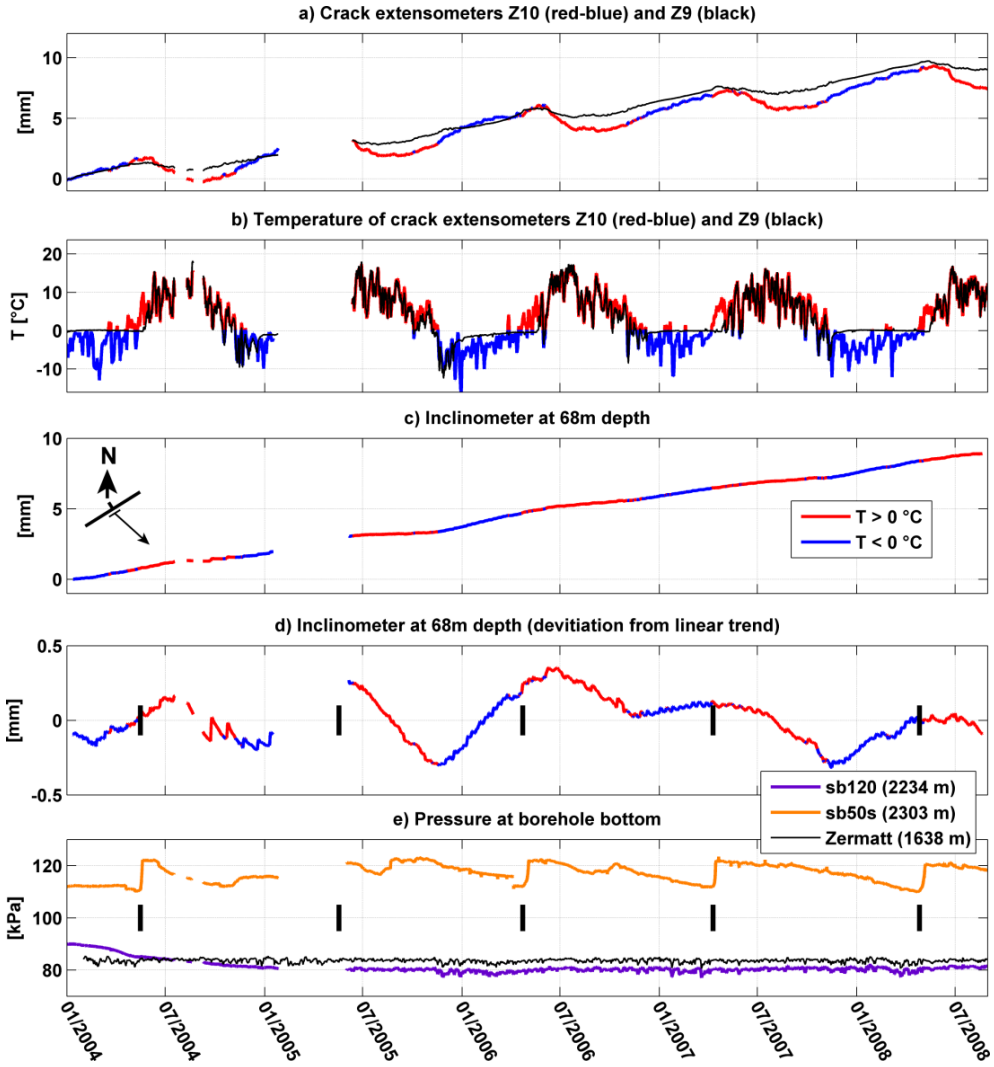

Figure 2. Monitoring data from the current Randa instability a) Crack extensometer data; the record from Z10 is colored according to temperature from its built-in sensor. Red colors are T > 0 °C, blue are T < 0°C. b) Temperature measured at fractures Z10 and Z9. c) Inclinometer data from 68 m depth in borehole sb120 colored according to the temperature. d) Inclinometer data with linear trend subtracted to emphasize temporal variations in the time series. e) Piezometric pressure from the bottom of borehole sb120 and sb50s, as well as barometric pressure from the nearby meteo-station in Zermatt. Black bars indicate the onset of snowmelt derived from piezometer data. From Gischig et al. 2011.

4 Cyclic loading from temperature and pore pressure variations

Deformation monitoring during the second (steady) creep stage at the rock slope instability above Randa (Switzerland) showed that relative dislocation rates across active fractures at surface and in depth of up to 68 m (i.e. in the entire instability) increase when near-surface rock temperatures drop in the fall and decrease after snowmelt as temperatures rise (Gischig et al. 2011, Fig.2). 2D discrete-element numerical modeling could support the interpretation of this seasonal deformation trend as

being controlled by thermomechanical (TM) effects driven by near-surface temperature cycles. It is expected that the time scale of secondary creep is strongly influenced by the criticality of fractures in the slopes and the efficacy of fatigue processes, as micro-cracking is commonly thought to initiate at stress levels between 30 and 50% of the unconfined compressive strength, while coalescence of micro-cracks occurs at about 70 to 90% of the rupture strength. Cyclic loading of intact rock at stress levels above the limit required for crack coalescence (e.g., through TM forcing) leads to accumulation of microscopic damage, and to progressive strength degradation (Attewell and Farmer, 1973). Thus, micro-scale cyclic fatigue can contribute to progressive failure of intact rock bridges and interlocking asperities. However, at the stress amplitudes and annual period typical for TM effects investigated here (<100 kPa below the thermal active layer), stress corrosion (sometimes referred to as static fatigue) may be equally important and also contribute to progressive failure (Scholz and Koczynski, 1979).

In comparison to Preonzo, where hydro-mechanical forcing is evident (Fig. 3), thermo-mechanical effects are especially important at Randa due to the absence of significant groundwater within the unstable rock mass. Differences in groundwater conditions between Randa and Preonzo can be attributed to the slope morphology around the instabilities (convex ridge at Randa, concave slope at Preonzo).

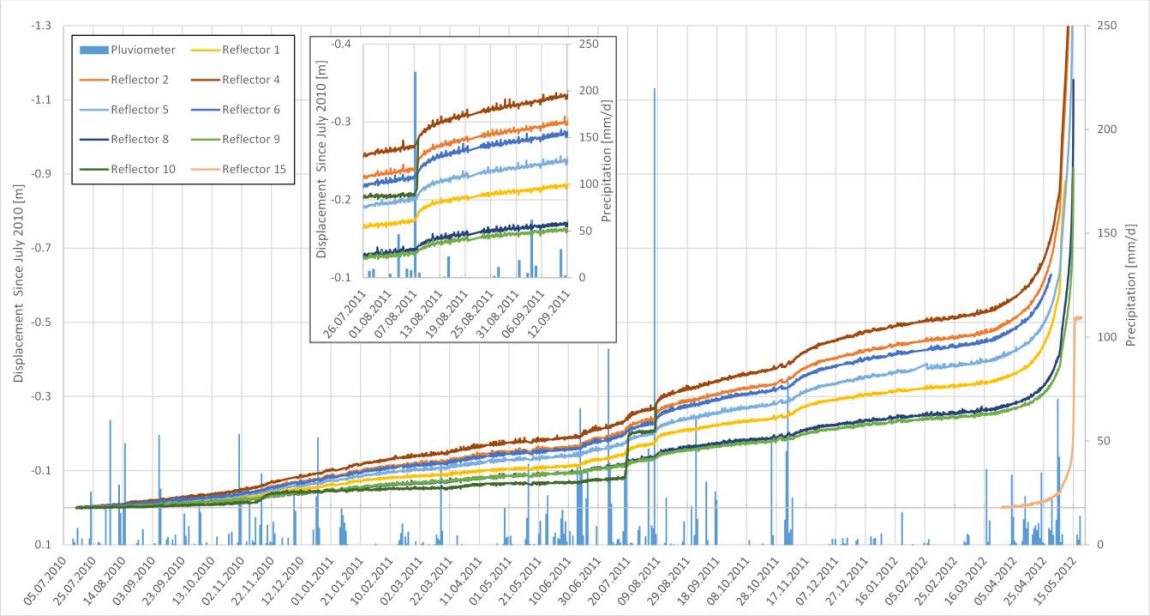

Figure 3. Displacements of reflectors located in the face of the Preonzo instability complex recorded by a Total Station during the period of acceleration. Superimposed are daily precipitations. From Loew et al. 2017.

5 Reference list

Attewell, P. B., and I. W. Farmer (1973), Fatigue behavior of rock, Int. J. Rock Mech. Min. Sci., 10, 1-9.

Gischig, V., Moore, J.R., Evans, K.F., Amann, F. and Loew, S., 2011. Thermo-mechanical forcing of deep rock slope deformation - Part II: the Randa rock slope instability. Journal of Geophysical Research. 116(F04011): pp. 17.

Grämiger, L. M., 2016. Beyond debuttressing: Thermo-hydro-mechanical rock slope damage during glacial cycles. Ph.D. thesis, ETH Zurich.

Grämiger, L. M., J. R. Moore, V. S. Gischig, S. Ivy-Ochs, and S. Loew 2017. Beyond debuttressing: Mechanics of parag-lacial rock slope damage during repeat glacial cycles, Journal of Geophysical Research: Earth Surface 122. doi:10.1002/2016JF003967.

Loew, S, Gschwind, S, Gischig, V, Keller-Signer, A, Valenti, G. 2017. Monitoring and early warning of the 2012 Preonzo catastrophic rockslope failure. Landslides, 14 (1), 141-154.

Scholz, C. H., and T. A. Koczynski (1979), Dilantancy Anisotropy and the Response of Rock to Large Cycling Loads, Journal of Geophysical Research, 84(B10), 5525-5534.

Terzaghi, K. 1962. Stability of steep slopes on hard unweathered rock. Géotechnique 12: 251–270

Progressive brittle damage processes and failure in rock

Mark Diederichs[1*], Jennifer Day[2], Ehsan Ghazvinian[3], Matthew Perras[4], Chrysothemis Paraskevopoulou[5] and Gabriel Walton[6]

[1] Dept. Geol. Sci. and Geol. Eng., Queen's University, Kingston, Canada
[2] Dept. of Earth Sciences, University of New Brunswick, Fredericton, Canada
[3] Mine Design Engineering, Kingston Canada
[4] Engineering Geology, Institute of Geology, ETH Zurich, Switzerland
[5] School of Earth and Environment, University of Leeds, UK
[6] Colorado School of Mines, USA
* diederim@queensu.ca

1 Background

In geological vocabulary, the term "brittle" is used to describe deformation behaviour in which the rock loses continuity (Van der Pluijm & Marshak 2004), or as the permanent change that occurs in a solid material due to the growth of fractures and/or due to sliding on fractures after the rock stresses exceed some critical value (Davis & Reynolds 1996). Brittle structures can be identified at many scales. Within crystal grains, microfractures can initiate either at the grain boundary where atomic disorder is higher, creating nucleation sites, or within the grain along cleavage or initiated by inclusions (pores or impurities). Grain boundaries themselves can exhibit brittle separation, dilation and shear displacement. At the micro-scale, such fractures or cracks can propagate across or between multiple grains and can be extensional, sheared or a combination. Coalescence of brittle microstructures can lead to macroscopic fractures (a general term) including cracks and ultimately joints in extension or shear fractures of different scales. Infilling of such features over time with vein minerals restores continuity in an engineering sense but does not change the geological designation of these "brittle" structures. Ultimately larger scale discontinuities can result from the interconnection of joints, bedding weakness planes (Perras 2014) and shear fractures resulting in shear zones or larger scale extensional partings. The orientation of these macro structures is controlled by primary anisotropy, induced fabric (Ghazvinian 2015) and/or by paleo- and neo-tectonic stresses.

The geological designation of brittle is related only to a disruption at any scale to the physical continuity of the solid material at any point in the deformation process. In true ductile or plastic deformation, there is at no time a physical break in the solid continuum at any scale (atomic bonding is transferred or replaced but never broken). This is very different from the definition of "brittle, plastic and ductile" used in typical engineering applications. In a very basic engineering usage, brittle behaviour refers to a significant loss of strength after elastic limits are exceeded. Plastic or ductile behaviour refers to a sustained level of strength, after elastic deformation limits and after yield begins, for a sustained set of boundary conditions including confinement. The terms strain-weakening or -hardening are appended to indicate a measured loss or gain of strength, respectively. This designation still makes a distinction between moderate weakening and significantly brittle behaviour. This phenomenological description, however, does not address the micromechanics behind the yield behaviour and does not capture the processes in which progressive accumulation of small-scale brittle damage-processes or ductile creep that ultimately lead to delayed macroscopic brittle failure.

At high confinements, macroscopically ductile or plastic behaviour in rock can be the result of microscopic brittle damage accumulation and evolution without significant macroscopic dilation (Diederichs 2003). In addition, time dependent behaviour can be the result of viscous creep (true solid flow) or can originate from subcritical brittle crack growth. Likewise, both microscopic fracture damage and macroscopic brittle failure can result from true ductile creep processes that lead to strain incompatibility within a heterogeneous material at the grain scale and rockmass scale (Paraskevopoulou 2016). It is reasonable, then to conclude without contradiction, that brittle damage

processes can lead to progressive deformations and that the yield process and failure can be simultaneously brittle and progressive in nature.

2 Progressive brittle processes in underground engineering

This presentation will address the progressive nature of brittle damage and failure at different scales from microscopic, to laboratory scale, to excavation and rock slope scale. In underground environments, spalling is a well-recognized but until recently poorly understood phenomenon. The processes that lead to visible spall damage in underground excavations are typically progressive, although the time scale varies under different boundary and environmental conditions.

Progressive damage processes that are measureable over time through deformation or acoustic emission can set the stage for violent energy releases (rockbursts). In brittle rocks, it is often difficult to separate out the instantaneous expression of failure from the associated excavation rate-dependent and pure time-dependent processes. The interplay of these progressive processes becomes even more complex in heterogeneous ground under high stress (Day 2016).

In both underground excavations and in rock slopes, progressive movement along pre-existing brittle structures can lead to overloading of remnant asperities or rock bridges over time, causing sudden failure which is instantaneous in expression but which can be considered progressive in development. The delay that results from these progressive damage processes can make prediction and management of the ultimate dynamic rupture events a major challenge (Diederichs et al. 2013).

In situations with variable confinement such as rock pillars and abutments, different confinement levels lead to fundamentally different behaviours in neighbouring rock zones. Progressive deformation and damage within the confined core of a pillar, for example, can be macroscopically ductile but can lead to brittle fracture and spalling in the rock adjacent to the excavation (Walton 2014). Understanding the interplay between progressive damage and deformation is necessary to analyze the processes and design accordingly. In addition, environmental factors and cycling can lead to subcritical crack growth and an apparent progression of brittle damage and ultimately fracture.

These concepts will be developed with some discussion of fundamental fracture theory complimented by examples from a variety of underground environments. The effect of stress path, geometry and construction sequencing on the nature of brittle yield in underground works, as well as the important role that progressive brittle damage evolution plays in defining and controlling the nature and timing of rock-burst hazards in tunnelling will be discussed. Issues of stand-up time and support design will also be covered.

3 Reference list

Davis G., Reynolds, S. 1996. Structural Geology of Rocks and Regions. 2nd Edition. Wiley. USA.

Day, J. 2016. The influence of healed rockmass structure on the behaviour of deep excavations in complex rockmasses. PhD Thesis, Queen's University.

Diederichs, M.S. 2003. Rock fracture and collapse under low confinement conditions. Rock Mechanics and Rock Engineering . v36:5:p339-381

Diederichs, MS., Eberhardt E., and Fisher. B. (2013). Consideration of stress and structural influence on. Proceeding of the World Tunnel Congress, ITA, Geneva, Switzerland.

Ghazvinian, E. 2015. Fracture Initiation and Propagation in Low Porosity Crystalline Rocks: Implications for Excavation Damage Zone (EDZ) Mechanics. PhD Thesis, Queen's University.

Paraskevopoulou, C. 2016. Time-dependency of rocks and implications associated with tunnelling. PhD Thesis, Queen's University.

Perras, M. 2014. Understanding and predicting excavation damage in sedimentary rocks:A continuum based approach. PhD Thesis, Queen's University.

Van der Pluijm, B., Marshak, G. 2004. Earth Structure. 2nd Edition. Norton. USA

Walton, G. 2014. Improving continuum models for excavations in rockmasses under high stress through an enhanced understanding of post-yield dilatancy. PhD Thesis, Queen's University.

Consequences of daily and annual thermal cycles on fracture propagation and rock slopes stability

Véronique Merrien-Soukatchoff[1*] and Muriel Gasc-Barbier[2]

[1] GeF, EPN01, Cnam, Paris, France
* veronique.merrien@lecnam.net
[2] Cerema, Aix en Provence, France

1 Introduction

Natural temperature variations are thought to play a role in rock slope instabilities. Thermal and and geotechnical in situ measurements have been carried out in sites were the succession of thermo-mechanical effects are suspected to have led progressively to failure. Parallel laboratory tests show the damage of specimens subjected to thermal fatigue. Site and laboratory observations are briefly described below and elements of interpretation are proposed.

2 In situ observations

In situ observations accredited the role of temperature variations in the progressive destabilization of rock slopes. We refer below to 2 French sites, but Vargas et al. (2004, 2009) made similar observation in Brazil.

2.1 A gneissic rock mass

For several years, thermal and geotechnical in situ measurements have been collected at the “Rochers de Valabres” site (Southern French Alps), a gneissic rockmass, to examine surface thermomechanical phenomena and their potential contribution to rock fall triggering. In fact, in May 2000 (Fig. 1) the site experiments a 2000 m^3 rock fall during a period with any particular rainfall event, seismic activity, or freeze-thaw period and we suspect it could be linked to the repetition of thermal variation (Gunzburger et al. 2005). The site was monitored with different equipment to record the temperature variation in the rock-mass and the potential induced effect. The measured data were analyzed based on analytical solutions and numerical modelling.

Figure 1. Consequence of a rock rupture attributable to the effect of temperature

2.2 A limestone cliff

At “La Roque Gageac”, a village located near Bergerac at the right bank of the Dordogne, a cliff composed of sandy limestone was subjected to rupture accredited to temperature fluctuations.

The site experienced 4 rock falls since 1920, which resulted in three deaths. Among the potential causes for these rock falls, temperature variations were considered as one of the possible preparatory factor and the site is monitored with temperature gauges and strain measurement and under study.

3 Laboratory tests

Experiments conducted by Gasc-Barbier et al. (2014) showed that the damage of limestone specimens subjected to thermal fatigue (cycles varying between 10 and 50 ° C) significantly increase after about 300 cycles (decrease in the velocities of the compression waves). Macro-cracking was observable after about 400 cycles (Fig. 2).

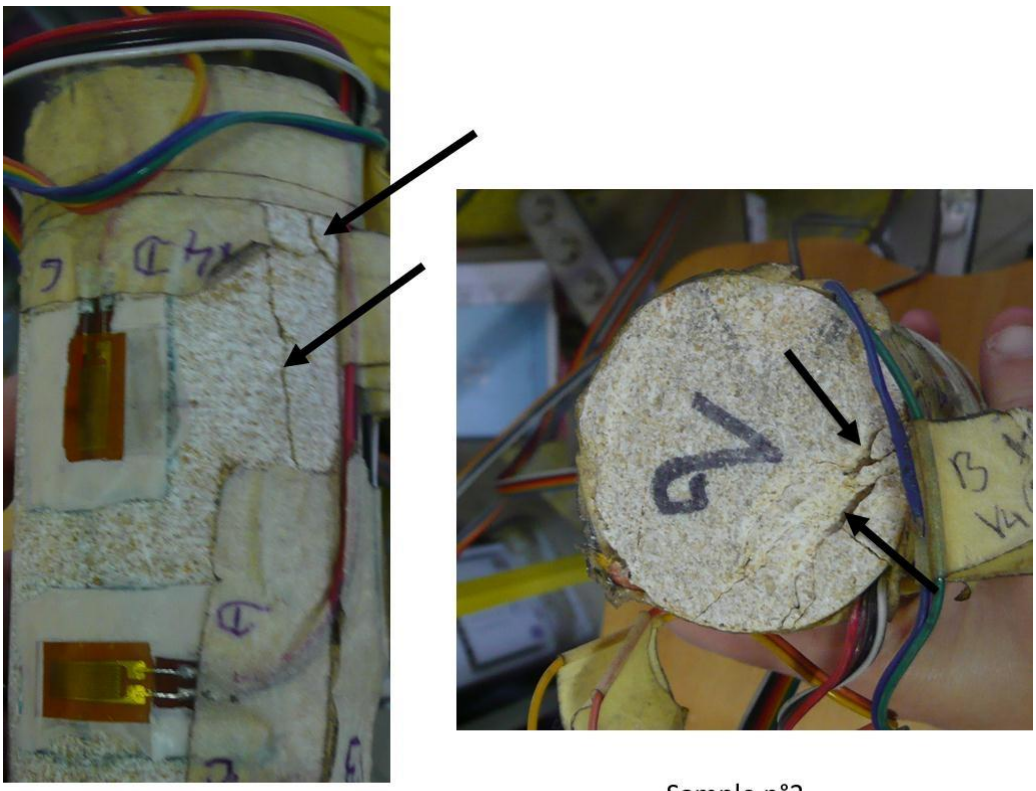

Figure 2. Photograph showing damage of 2 specimens after 400 thermal cycles after Villarraga et al. 2016

4 Possible mechanisms

Several mechanisms may coexist to explain initiation and progressive failure due to temperature variation: thermal shock, creation and pervasion of fractures between minerals at the surface linked to differences in their light-transmissivity, and thermal fatigue. It is possible to show that the critical tensile stress intensity factor (K_I) can be the same order of magnitude as fracture toughness (K_{Ic}) which can explain the fracture propagation. Some extension strain criterion (instead of stress criteria) could also be temporarily reached due to temperature variations and so explain the fracture propagation.

5 Reference list

Gasc-Barbier, M., Girma, G., Gendre, V, 2014 Laboratory analysis of thermal fatigue in limestone. Eurock 2014, Vigo (Espagne)

Gunzburger, V., Merrien-Soukatchoff, V., Guglielmi, Y. 2005. Influence of daily surface temperature fluctuations on rock slope stability: case study of the Rochers de Valabres slope (France). International Journal of Rock Mechanics and Mining Sciences, 42, 331-349.

Merrien-Soukatchoff V, Gunzburger, Y, Clément, C, 2010. Natural thermal strains close to surface of rock slopes: Measurement and modelling of the "Rochers de Valabres" case. Rock Slope Stability Conference; 2010 24-25 November 2010; Paris (France).

Vargas JR, E. A., Chavez, E., Gusmão, L., Amaral, C., 2009. Is thermal fatigue a possible mechanism for failures of some rock slopes in Rio de Janeiro, Brazil? 43rd U.S. Rock Mechanics Symposium and 4th U.S.-Canada Rock Mechanics Symposium, 2009 Asheville, NC.

Vargas Jr, E., Castro, J. T., Amaral, C, Figueiredo, R. P., 2004. On mechanisms for failure of some rock slopes in Rio de Janeiro, Brazil: Thermal fatigue? In: Lacerda W., E. M., Fontoura S.A.B., Sayao A.S.F, ed. Landslides: evaluation and stabilization, Proceedings of the Ninth International Symposium on Landslides, une 28 -July 2, 2004 2004 Rio de Janeiro. Taylor & Francis Group, 1007-1011.

Villarraga, CJ., Gasc, M., Gendre, V., Vaunat, J., 2016, The effect of thermal fatigue in a limestone - A laboratory study ISL 2016 Paper n°357.

Progressive thermally induced fracture of an exfoliation dome: Twain Harte, California, USA

Brian D. Collins[1*], Greg M. Stock[2], and Martha C. Eppes[3]

[1] Landslide Hazards Program, U.S. Geological Survey, Menlo Park, California, USA
* bcollins@usgs.gov
[2] Yosemite National Park, U.S. National Park Service, El Portal, California, USA
[3] Dept. of Geography and Earth Sciences, University of North Carolina at Charlotte, North Carolina, USA

1 Introduction

The well-documented 2014-2016 exfoliation of Twain Harte Dome, located in the western foothills of California's Sierra Nevada Mesozoic granitic batholith, provides an unprecedented opportunity to study progressive fracture of exfoliation domes. The dome seemingly spontaneously fractured on five occasions during the late summer of 2014, with subsequent fracturing in the summers of 2015 and 2016. The warm-weather timing of all events strongly suggests that thermally-induced environmental conditions are responsible for triggering exfoliation. Some of the exfoliation events consisted of rock slabs being thrust ~40 cm into the air in a matter of seconds, with both audible and observable explosive-like energy release. We initiated a research project to investigate the triggering conditions and fracture mechanics of dome exfoliation under this active setting to serve as a proxy for understanding precursor signals that might occur prior to rock falls on near-vertical cliffs. Here we present the portion of our data that captures the collapse of the slab that was deformed during the 2014 events. The data suggest that the collapse and other ongoing deformation is occurring as a result of progressive fracture driven by diurnal heating and cooling.

2 Exfoliation sheet monitoring

Following the August 2014 fracture events, we installed three vibrating-wire-type strain gauge "crackmeters" (Geokon modified 4420; see Collins & Stock 2016) between a newly detached portion of the uppermost slab of the dome and the intact rock beneath (Fig. 1). Two crackmeters monitored open fractures and a third crackmeter acted as a control to differentiate between thermal strains in the instrumentation verses thermal strains in the granitic slab. We also deployed pendent-type temperature and light sensors (Onset Hobo UA-002-08) to act as a proxy for surface rock temperatures. Our instrumentation captured data at 5-minute intervals beginning on 22 August 2014 for 41 days until the upper slab detached and crushed the crackmeters.

3 Progressive failure and ongoing research

From the outset, the crackmeter data exhibited a continuous diurnal response of nearly 0.5 cm motion over a 24 hour cycle that was coincident with near-surface air temperature (Fig. 2). However, beginning September 18, the overall signal was damped for a period of 4 days, and then became elevated for 3 days, indicating first closing and then accentuated opening of the fractures. During the next 4 days, the slab responded directly to a period of cooling and eventually collapsed, crushing the crackmeters (data after September 24 are likely not reliable). We interpret these observations as direct evidence that cyclic thermal stresses were driving progressive fracture at the ends of the overlying slab where it was still attached to the rock mass below. We hypothesize that subcritical crack growth had been occurring under these conditions for many years such that the slab geometry reached a point where the critical stress intensity was exceeded. This resulted in the seemingly spontaneous fracturing events observed in 2014 through 2016. Based on these results, we have initiated a larger study to measure stress, deformation, and temperature conditions at this site to capture future events and identify potential precursors to slab detachment.

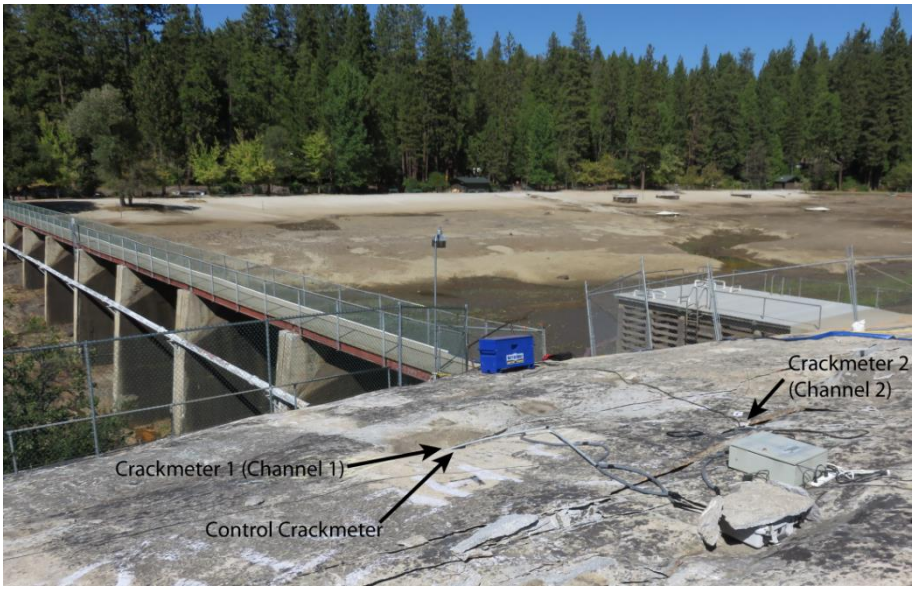

Figure 1. Photograph of part of the upper slab of Twain Harte Dome. The dome forms the left abutment for a multiple-arch concrete dam (middle-left); the reservoir impounded by the dam (background) was drained following the initial dome fracture events. Locations of the crackmeter instrumentation that measured the movement of the upper fractured slab are shown by arrows.

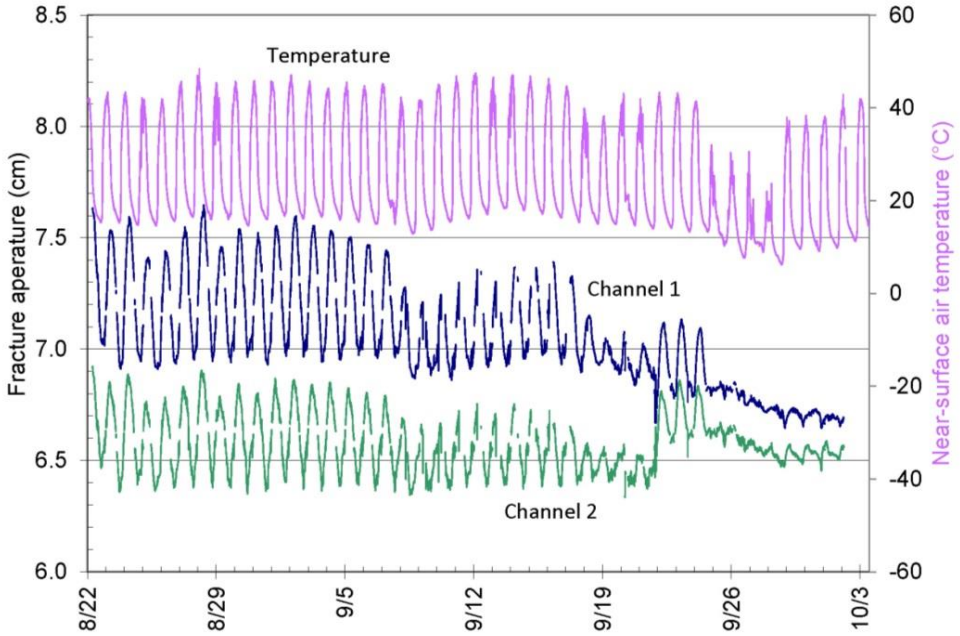

Figure 2. Graph of crackmeter data from the upper slab of Twain Harte Dome showing the diurnal displacement variation with temperature and eventual collapse of the slab during late September 2014. Date format is M/DD. Slab collapse on September 25 is coincident with several days of cooling, but notably occurred immediately after three days of pronounced fracture opening and closing.

4 Reference list

Collins, B.D., Stock, G.M. 2016. Rockfall triggering by cyclic thermal stressing of exfoliation fractures. Nature Geoscience 9, 395–400, doi:10.1038/ngeo2686.

5 Acknowledgments

The authors wish to thank Dennis Wyckoff, Lake Manager at Twain Harte Lake for his assistance and enthusiasm for this study. Any use of trade, firm, or product names is for descriptive purposes only and does not imply endorsement by the U.S. Government.

Development of a new thermally-induced fracture in a 12,000 year old bedrock surface

Kerry Leith[1*], Matthew Perras[1], Topias Siren[2], Tuomas Rantanen[2], Andrea Wolter[1], Suvi Heinonen[3], and Simon Loew[1]

[1]Department of Earth Sciences, Zurich, Switzerland
[2]Department of Civil Engineering, Aalto University, Finland
[3]Geological Survey of Finland, Finland
* kerry.leith@erdw.ethz.ch

1 Introduction

A long period of exceptionally high temperatures in Finland in the summer of 2015 was associated with the formation of large 'exfoliation' or 'sheeting' fractures on Långören Island in the Finnish Archipelago. A video of the event shows sharp fractures forming along the edge of a thin bedrock sheet several meters across (Sarpaneva 2014), while total vertical strain of one section of the pop-up was up to 100 mm, and observations following the event indicate a slab of approximately 50 m^2 was detached from the underlying bedrock. Long scratch marks ('striations') visible on the bedrock surface of the island are the result of boulders being dragged over the landscape during the last glacial period (>15 ka BP), hinting at the rarity of the recent events on the otherwise undamaged surfaces (Fig. 1).

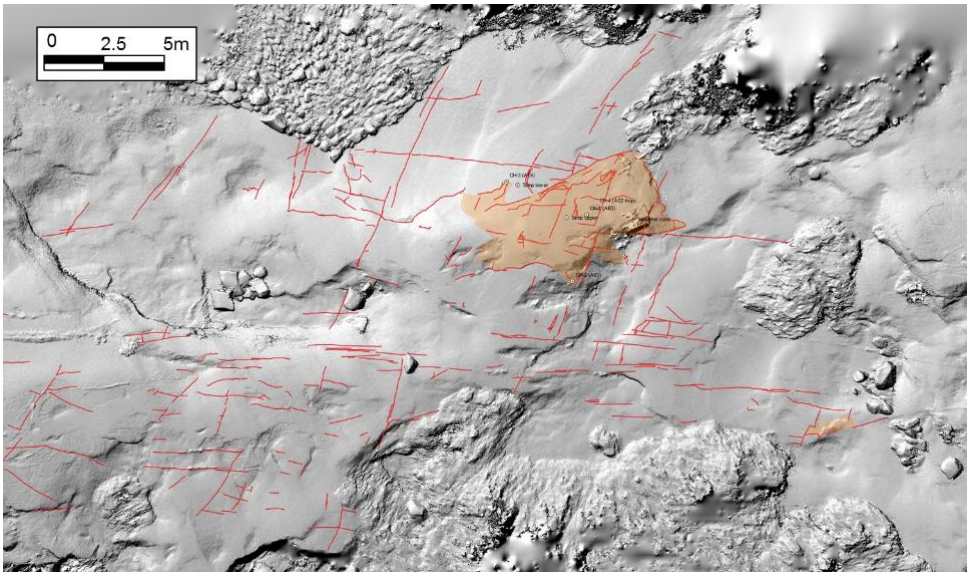

Figure 1. Structure-from-motion (SFM) derived hillshade image covering the area of two pop-ups formed during exceptionally hot weather in July 2014 (orange), and post-glacial fractures mapped during the field survey (red). Striations relating to LGM ice flow can be observed crossing from upper left to lower right. The present-day beach is marked by the boulder concentration and smooth DEM surface in the upper left corner.

2 Setting

Deglaciation of the region is bracketed by two moraine complexes dated at 15.2–13 ka BP and 13–11.5/6 ka BP, while flow lineations based on a reconstructed ice sheet topology and regional field mapping of drumlins indicate the present-day island was located on the eastern margin of a southward-flowing ice stream sourced in the center of the Weichselian Scandinavian ice sheet (Boulton et al. 2004, and references therein). The ice sheet in this region was around 2500 m thick during the estimated maximum for the Last Glacial Maximum at approximately 18.5 ka BP (Näslund 2006). Present-day isostatic uplift rates relative to sea level in the region are approximately 3.5–4 mm/a

(Ekman 1996). Tidal variations in the archipelago only cause a few centimeters of sea level change, and as a result, the slow emergence of the now 3.5 m – 4 m. a.s.l. bedrock surface can reasonably accurately be extrapolated back to 0.8–1 ka BP.

3 Extensional fracture formation

Better termed extensional fractures, these features form as a result of very high stresses acting parallel to the bedrock surface, while very low gravitational stresses hold the bedrock in place. Alternative examples of extensional fracture formation in various environments include A) 'Sheeting' fractures developing in relatively flat-lying topography B) 'Exfoliation' fractures forming on the side of a U-shaped glacial valley and C) 'Spalling' of highly stressed bedrock in a borehole or tunnel. (Leith et al. 2014). Much like a metal plate buckling on a hot element (often with a surprising "pop"), thermal expansion of horizontally confined rock surfaces causes an increase in horizontal stresses, and can lead to a buckling of bedrock once conditions become critical. Unlike the metal plate, however, joints separating the bedrock surface from underlying rock are generally not continuous, and many intact 'rock bridges' need to be broken before the surficial plate is large enough to "pop" (the stress required for buckling decreases as plates become larger). A pre-requisite for these spectacular events is therefore the destruction of rock bridges, which in this case likely occurred as a result of progressive strength degradation over the previous 1 ka, and surface-parallel stresses induced through thermal expansion, which cause loading at the tips of existing cracks to exceeded critical levels. The subsequent propagation of fractures sub-parallel to the ground surface will then increase the area of crack tips (thereby dissipating fracture energy) until either the fracture again becomes stable, or the sheet becomes large enough to buckle.

This process requires that crack-tip stress concentrations exceed the instantaneous or long-term fracture toughness of the gneissic bedrock on the island. In turn, this can be aided by stored elastic potential energy as a result of lithification in the deep brittle crust, exhumation, and horizontal tectonic strains during exhumation, as well as chemical potential energy and / or water present at the stressed crack tips to allow ion exchange and strength degradation. A process broadly termed 'stress corrosion'. In Finland, evidence derived from regional studies suggests maximum near-surface horizontal stress magnitudes in the south-west of the country are in the order of 10 – 20 MPa, while observations of conjugate fractures on the island that commonly terminate in intact rock indicate present-day horizontal stresses may approach the crack initiation threshold (approximately 20–30 MPa), with an ENE – WSW orientation similar to that observed elsewhere in the region (Andersson et al. 2007).

4 *In situ* monitoring and preliminary numerical model results

In order to investigate the drivers of extensional fracturing, we undertook a campaign to characterize the site of the fracture including a GPR survey, a SFM DEM survey, and a map of new and pre-existing fractures (Fig. 1). In addition, we installed a monitoring system on the buckled slab from July to September 2016. This included a weather station, acoustic emission sensors, and bedrock temperature strings installed to a depth of 1 m on both the fractured slab, and intact rock. Using weather data from the nearest permanent weather station (on Vänö Island) 13 km to the south of Långören, we were able to calibrate a 1D numerical model of bedrock temperature that accurately matches monitoring data from temperature strings installed during the 2016 campaign. This then allowed us to extrapolate back to evaluate temperatures during the 2014 event, and selecting the next hottest day in the record leading up to the predicted maximum temperature on the 25th of July 2014, initialize a 2D finite element model of a 4 m long, 0.25 m thick, flat bedrock slab subjected to three months of 'real' temperature fluctuations using COMSOL Multiphysics (Fig. 2). Preliminary results predict the buckling of our modelled slab during a warm period several weeks before our selected initialization temperature, and three days after the hottest day during this period (Fig. 2). This both indicates the criticality of conditions required for buckling of a flat slab, and is consistent with the two-day delay observed for the 2014 event, and a two day delay between a particularly hot day during our 2016 record and a 24 hour long period of enhanced acoustic emission observed on sensors at the site.

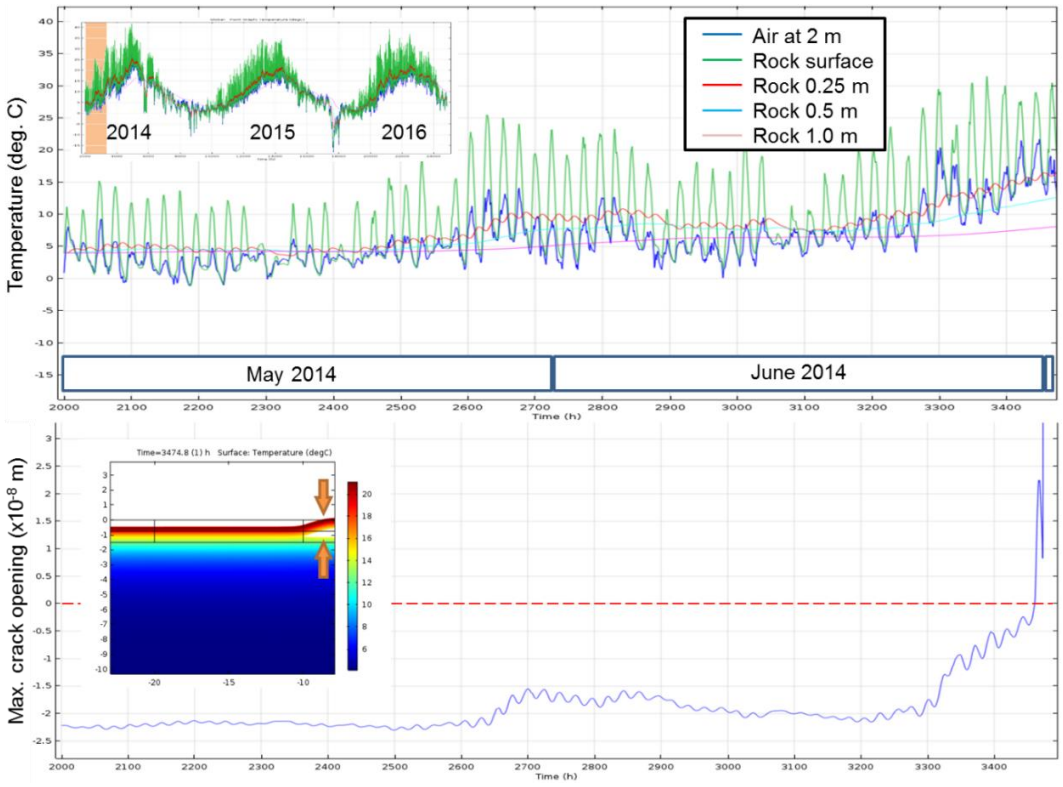

Figure 2. 1D thermal model and 2D thermo-mechanical model results for the period of interest (inset, upper), model temperatures leading up to the modelled fracture event (upper), geometry of the buckled slab (inset, lower), and crack opening during the same period (lower). Note the three-day delay between the peak temperature in late June 2014 and irrecoverable crack opening.

5 Conclusions

The gently undulating bedrock landscape of Långören Island is a classic example of a region that has evolved through erosion of hard, unweathered bedrock, and although heating and thermal expansion almost certainly triggered these events, the high pre-existing stresses resulting from millions of years of exhumation and tectonic strain, in association with 1000 years of progressive fracturing and stress corrosion were essential preparatory factors. As the long-term *in situ* stresses appear to be limited by the strength of the local bedrock, thermal stresses during the 2014 event were simply required to push loading conditions 'over the edge', providing enough additional stress to initiate the active fracturing process. The absolute magnitude of heating, and the resulting thermally-induced stress is therefore largely unrelated to the extensional fracture event, more important is the comparative magnitude with respect to previous events, and the rate of progressive fracture development.

6 Reference list

Andersson, J., Ahokas, H., and Hudson, J. A., 2007, Olkiluoto site description 2006.

Boulton, G. S., Dongelmans, P., Punkari, M., and Broadgate, M., 2004, Evidence of European ice sheet fluctuation during the last glacial cycle, in Ehlers, J., and Gibbard, P. L., eds., Developments in Quaternary Science, Volume Volume 2, Part 1, Elsevier, p. 441-460.

Ekman, M., 1996, A consistent map of the postglacial uplift of Fennoscandia: Terra Nova, v. 8, no. 2, p. 158-165.

Leith, K., Moore, J. R., Amann, F., and Loew, S., 2014, In situ stress control on micro-crack generation and macroscopic extensional fracture in exhuming bedrock: J. Geophys. Res., v. 119, no. 1, p. 594–615.

Näslund, J.-O., 2006. Ice-sheet dynamics, in Climate and climate-related issues for the safety assessment SR-Can, no. TR-06-23, pp. 33–56, Swedish Nuclear Fuel and Waste Management

Sarpaneva, A., 2014, Kallio repeää video, from Geologian tutkimuskeskus on Vimeo https://vimeo.com/103317646

The joy of breaking rocks and myths

Mauri McSaveney[1,2]

[1] GNS Science Ltd, Lower Hutt, New Zealand
[2] Visiting professor, SKLGP, Chengdu University of Technology, Chengdu, China
* m.mcsaveney@gns.cri.nz

1 Introduction

Some years ago, my PhD advisor described me as an iconoclast. Very early in my career, I found that if I wanted to build on someone else's hypothesis, it was necessary to ensure that I fully understood it, and was aware of and agreed with all of its assumptions. It was a defense mechanism to avoid being led astray by so-called experts straying off the topic of their supposed expertise. At that stage I had just encountered RL Shreve's air-layer lubrication (Shreve 1968) with some disbelief. Air-layer lubrication was a neat idea, but it was based on the assertion that the landslide mass falls on and traps a layer of air. It sounds so simple, so it 'must be true.' If rock avalanches behaved as Autumn leaves that's what they would do. There are some obvious differences in the behavior of falling rocks and falling leaves. Rock-avalanche behavior is dominated by momentum and is appropriately studied as a problem of ballistics and not aerodynamics. That is my first recollected experience in myth busting. My current efforts at myth busting also relate to masses of broken rock, one is the myth of fracture-surface energy, another is the myth of a fragmentation limit.

2 The myth of fracture-surface energy

Conventional wisdom has it that when rocks break they make fracture-surface energy. I was introduced to this wisdom by some wise and well meaning gentlemen who tried to tell me that rock breakage was an energy consuming process and could not possibly contribute to the apparent low friction of rock-avalanche long runout. I tend to ignore both wisdom and convention, especially when I cannot make sense of it. But I did attempt to track down the origin of this conventional wisdom because it seemed to be important. And so I was introduced to Griffith fracture theory (aka. Griffith failure criterion). Griffith fracture theory is more than a neat idea, it is a simple and useful concept which I can fully understand, but it has a useless appendix - it does not make fracture-surface energy.

Rocks break, but they do not do it unaided. In December 2016 I had the pleasure of assisting some synthetic rocks in their breakage, in a study of the relationship between input elastic strain and the creation of new surface area (see Davies et al. This conference). Under appropriate supervision according to the Health and Safety regulations of the University of Canterbury, I carried out unconfined compression tests on dry 10mm diameter and 20 mm long Pyrex (borosilicate glass) cylinders. I tried to get a cylinder to break at the highest possible load in the hope of creating the largest amount of new surface area on the broken fragments. The intent was to test what has become known as Griffith brittle facture theory after a hypothesis first presented in Griffith (1921). Many fine cylinders were harmed in the attempt.

Griffith (1921) presents a simple and elegant energy-balance analysis of the propagation of a hypothetical crack through an unspecified brittle solid. It postulates that a pre-existing crack propagates if the forces pulling the crack apart exceed the forces holding it together. It was developed to explain why battleships could break in two, a fact that had gained some embarrassing empirical support. It is an undisputed fact that a battleship will break apart if the sum of forces holding its potential cracks together is smaller than the sum of the forces pulling them apart. Rocks and battleships are alike in this behaviour, however unlike battleships, rocks can break many times, and counting the pieces still holds interest for some of us.

The postulate about the propagating crack is axiomatic and requires no test. The ultimate fate of the work done, however, is not axiomatic; the Griffith (1921) suggestion about its fate as surface energy is a hypothesis which has never been tested. Why? There are several reasons: 1) it is not central to the fracture theory; 2) it does not matter to the theory of fracture propagation where the strain energy might go to, so long as it goes somewhere (in an earlier era it could have gone to heaven, or to hell, but in early 20th Century science, surface energy was in vogue – that that is where Griffith sent it); and 3) it is not possible to determine that any energy goes to surface energy. In our experiments, much of energy went to make a loud bang and some of it left signatures on some fracture surfaces of its passage to escape out of the solid glass cylinder (Fig. 1).

3 Energy and fracture surfaces

3.1 Decibels, compressive strength and fragments

Apparently, not all dry 10mm diameter and 20 mm long borosilicate cylinders are alike in their response to compression to their breaking strength. Some respond with a weak “Pop!” and few fragments. Some few respond with a very loud “Bang!” and many fragments. Most responses lie in between. In the boring interludes of applying the loading, one can reflect on the strong positive correlation between loudness, compressive strength and number of fragments, and on why there can be so much variance in such a simple property as compressive strength of such a uniform material. Since there was more thrill in creating a loud bang and many fragments, we sought to increase the strength of the samples by annealing them in a furnace to 550°C for an hour to relieve possible stored stresses from their manufacture. Then we lubricated the ends to reduce friction against the platens as the diameters of the cylinders expanded through elastic strain. Perhaps these procedures helped us to reach greater loads, but mostly they allowed pleasant breaks in an otherwise repetitive task.

Did we successfully test the hypotheses of Griffith (1921)? I refer you to Davies et al. (This volume) for one opinion. But I also refer you to Fig. 1. The fracture surface on the largest glass shard in the figure has ripples on it; there are ripples on the ripples. When this crack was propagating in complete compliance with Griffith fracture theory, it was being steered by the internal stresses within the glass. This stress tensor was dynamic and fluctuating because waves of elastic strain were propagating through the glass, transiently altering the stress (and strain) tensor as the cylinder broke. The origin of these strain waves was the release of elastic strain from within the glass cylinder by the propagating cracks. These strain waves were on their way to making a loud bang, when they reached the edges of the exploding cylinder. These strain waves were a temporary dynamic property of the material mass of the glass cylinder in the process of being dispersed as heat energy and work in the relocation of glass fragments. If I could have seen inside the protective steel shield that trapped all the fragments, I would have see the cylinder suddenly explode, but I would have seen nothing of the processes by which it did this. Where in Griffith (1921) is the bit about propagation of transient elastic strain? It is not there!

If one wanted to do a real, as opposed to a hypothetical energy balance on the ***brittle fracture*** process there is a whole lot of complex surface chemistry to deal with, to account for the exothermic absorption of mostly water onto the new surfaces. Hypothetical battleships present a simpler problem ***when simplified to an elliptical pre-existing crack***.

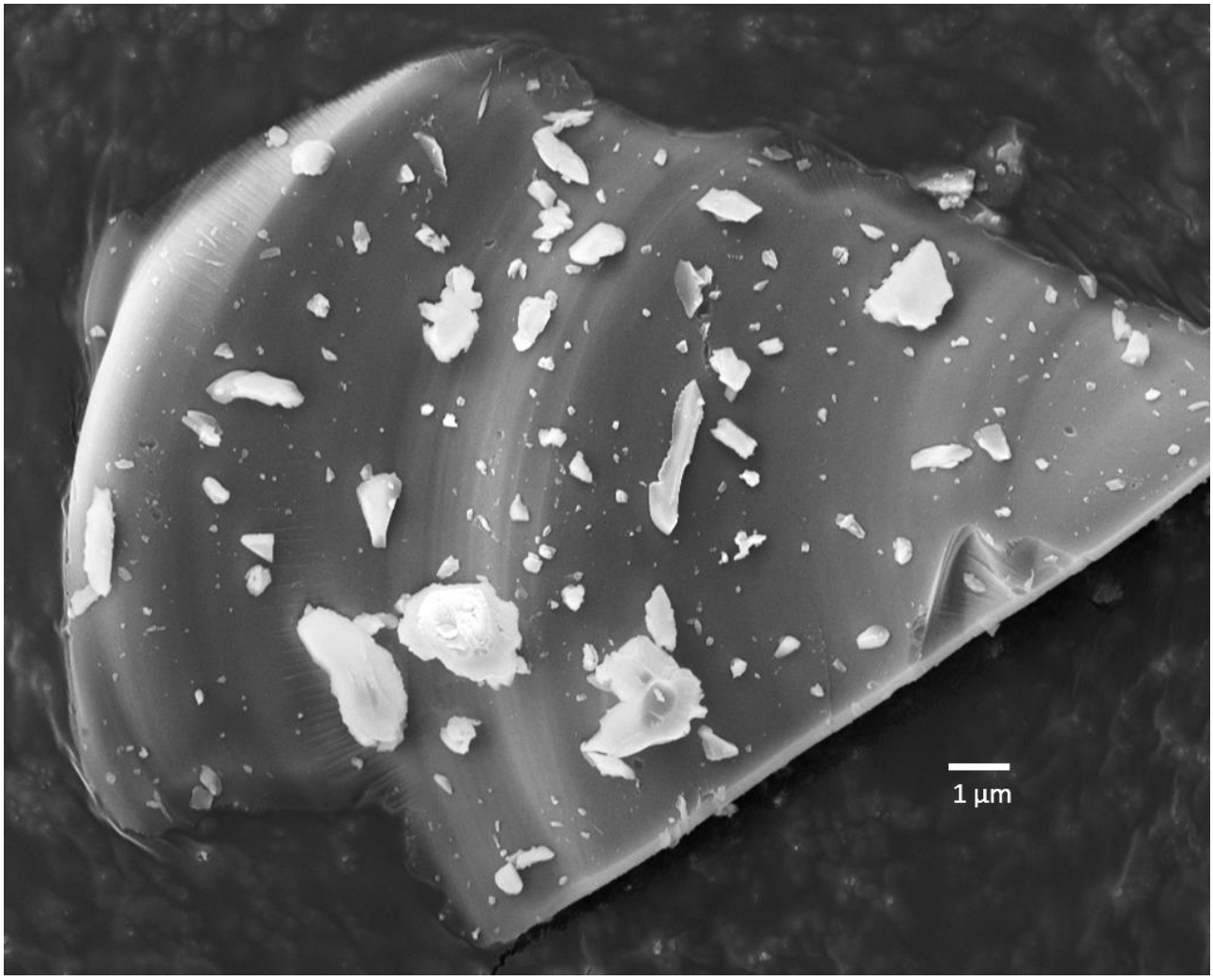

Figure 1. Scanning electron microscope image of fragments of borosilicate glass. The conchoidal fracture on the largest fragment is rippled because it encountered variations in stress orientation as it propagated through the brittle glass. These variations were caused by the transient elastic strain released by propagating cracks. Some researchers have suggested a minimum fragmentation size of >1µm which is not evident here (image by Natalya Reznichenko).

4 The myth of a fragmentation limit

Another piece of conventional wisdom that achieves unnecessary space in the scientific literature is the 'fragmentation limit'. This supposed limit to which materials can be fractured was introduced to us by some reviewers of ill-fated manuscripts of Tim Davies and I. Like air-layer lubrication, the myth of a fragmentation limit still persists as a theory despite somewhat compelling empirical evidence to the contrary, such as illustrated in Fig. 1. Why? My hypothesis is that it survives because it sounds correct, and it is easy to understand. The assumptions behind it are simple and logical., but they do not allow for Van der Waals forces or surface chemistry. Very small particles, in the nanometer range, do not maintain independent existence; they clump together forming larger particles called agglomerates. Agglomerates can be brittle too, and fragments of agglomerated fragments can be found among experimentally fragmented brittle materials. So, there is a limit on the size of fragment that can persist on its own, but there is no limit to the number of times a piece of brittle material can be strained until it breaks

5 Discussion

Why am I so fixated on breaking rocks? Better minds than mine have told me in no uncertain terms that the energy consuming process of breaking rocks can have no part in contributing to the apparently low frictional resistance of the major geophysical processes that make rocks break. I refer you to a very nerdy toy, commonly called a Newton's Cradle, but Isaac Newton had nothing to do with it. Wikipedia articles accurately describe it as demonstrating conservation of momentum. But not one description of it that I have seen, accurately describes how it works. It works by transferring energy as elastic strain waves back and forth though a line of rigid spheres.

I refer you now to an earthquake. You can choose any magnitude. Would you consider I was completely bonkers if I told you that it works by transfer of energy as elastic strain waves?

I am not fixated on breaking rocks. I am just incredulous that otherwise intelligent minds can close so tightly when an assortment of accepted facts are served to them in a different dish. It is not helped that the major ingredient is invisible transient elastic strain.

Rocks break. They do so in accordance with the Griffith fracture criterion by accumulating elastic strain until one or more cracks propagate through them. The accumulated elastic strain is released and radiates away from the propagating crack. For a seismologist, the radiating waves follow all the rules that seismic waves follow. For a physicist, they follow the rules that acoustic waves follow. They are the same rules dressed in a different jargon. When elastic strain waves pass through a granular material the energy is gradually attenuated. The reciprocal of the "seismic attenuation rate" is the coefficient of internal friction.

That is how the process of breaking rocks contributes to the apparently low frictional resistance of the major geophysical processes that make rocks break. It is not the only process contributing to low friction, but it is fully one of them.

6 Reference list

Davies T., McSaveney M. & Reznichenko N. 2017 The fate of elastic strain energy in brittle fracture. This Volume.

Griffith, AA. 1921. The Phenomena of Rupture and Flow in Solids. Philosophical Transactions of the Royal Society of London A 221, 163-198.

Shreve, R.L. 1968 Leakage and Fluidization in Air-Layer Lubricated Avalanches. Geological Socitey of America Bull. 79 no. 5 p. 653-658. doi: 10.1130/0016-7606(1968)79[653:LAFIAL]2.0.CO;2

Development of an ice-buttressed slope failure: Mueller Rockslide, New Zealand

Sam McColl[1*], Emma Cody[1], and Daniel Draebing[2]

[1] Physical Geography Group, Institute of Agriculture and Environment, Massey University, New Zealand
[2] Landslide Research Group, Technical University of Munich, Germany
* s.t.mccoll@massey.ac.nz

1 Introduction

The development of large rock slope failures within glaciated valleys is often assumed to be primed by steepening of topography from glacial erosion and by subsequent glacier retreat (McColl 2012). Glacier retreat removes confining stresses, changes hydrological, thermal, and weathering processes, and changes the interaction of co-seismic waves within the slope (e.g. Gischig et al. 2011; McColl et al. 2012; Grämiger et al. 2016), gradually lowering stability through strength degradation or a rise in destabilizing shear stresses. Few studies have documented the evolution of slope failure in glaciated valleys over historical time periods, and thus relatively little is known about how these processes interact to generate failures. For example, glacial debuttressing may cause catastrophic failures, as indicated by numerous post-glacial rock avalanche deposits in formerly glaciated valleys; but some of these failures may have occurred thousands of years following ice withdrawal (e.g. Ballantyne et al. 2014; Ostermann & Sanders, in press), suggesting that earthquake shaking or gradual strength degradation may also be responsible for triggering failure. It has also been suggested that the initial development of rock slope failures can proceed prior to the complete glacier withdrawal, and involve deformation of a buttressing glacier (McColl & Davies 2013).

This study takes the opportunity to investigate the long-term development of a large, active rock-slope failure that is still partially-buttressed by a glacier, with the aim to explore how failure develops over time and to assess the factors controlling movement and failure evolution.

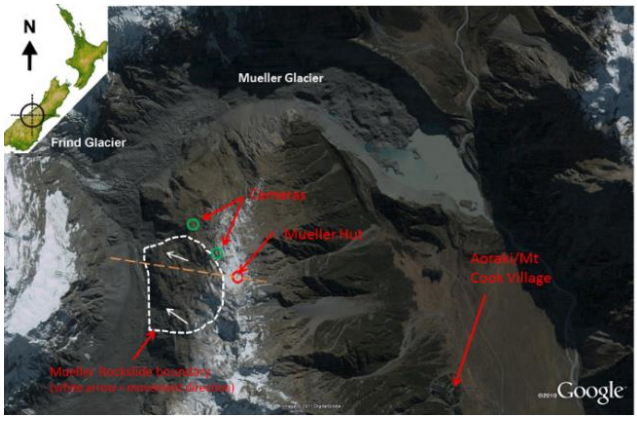

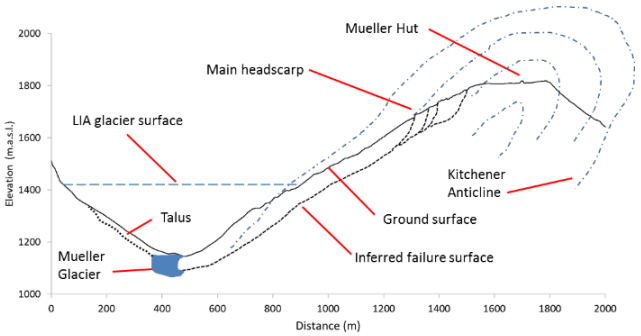

Figure 1 (left). Mueller rockslide, Aoraki/Mt Cook National Park. Figure 2 (right). X-section of rockslide along orange line in Fig. 1.

2 Study site

The study focusses on the Mueller Rockslide, in Aoraki Mt Cook National Park, in the central Southern Alps of New Zealand (Fig. 1). The rockslide, estimated to be ~150 Mm^3 in volume, occupies the dip slope of an overturned anticline in Mesozoic greywacke sandstone (Lillie & Gunn 1964) (Fig. 2). The rockslide toe is partly buttressed by the Mueller Glacier, which has thinned by ~100 m since the Little Ice Age. The glacier becomes narrow adjacent to the landslide toe, perhaps in part due to squeezing by the Mueller Rockslide (McColl & Davies 2013). There is no infrastructure on the active

landslide, but a popular alpine hut sits some 200 m behind the landslide crown, where large (> 1 m wide) pervasive cracks, indicate slope relaxation in this location.

3 Methodology

To investigate the causes and development of this failure, a geological model has been developed for the landslide (Fig. 2), and annual GPS surveys of surface monitoring pegs have been collected since 2010. In 2016 a time-lapse camera was installed to improve the temporal resolution of monitoring, and in 2017 an additional camera and crack-meters were installed. An existing climate station at the top of the ridge and in the nearby lower valley have provided a record of temperature and precipitation for the site during the study period. A continuous GPS station further along on the same ridge, provide an indication of the magnitude of regional tectonic deformation, and seasonal recoverable slope deformation resulting from snow loading, thermal, and hydrological changes.

4 Results

Movement data indicates total net downslope displacements in the central part of the landslide of more than 13 m (~9 m horizontally; 10 m vertically) between 2010 and 2017. The magnitude of annual displacement there appears to be relatively consistent, but possibly slowing (Fig. 3). The movement direction is consistent with movement in the dip direction of bedding, suggesting sliding along bedding planes.

Movement farther up slope, immediately below the ~30 m high landslide head scarp, has been much less, with a total net downslope movement of ~1 m between 2010 and 2017, but with a consistent or weakly accelerating trend. Crack dilation measurements and GPS surveys above the landslide crown show very little permanent displacement, of little more than several mm over the study period.

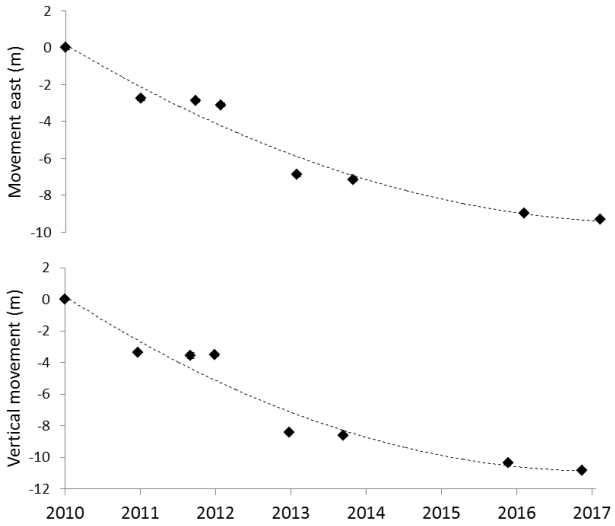

Figure 3. Relative movement of a survey mark positioned in the mid-lower slope, as measured by GPS. The rockslide appears to be slowing in this part of the slope.

While there is insufficient continuous monitoring data, as yet, to confidently link landslide displacement with external triggers, there is an indication provided by the GPS survey data that heavy rainfall events (or prolonged summer precipitation) may facilitate heightened annual displacements.

5 Discussion

While the timing of landslide initiation is unknown, crude extrapolation of linear movement rates and the amount of deformation represented by valley closure and head-scarp development, would suggest that the landslide begun moving within the last 300 years, consistent with debuttressing associated with post-LIA glacier downwasting. Proposed cosmogenic surface exposure age dating of the landslide head scarp and lateral moraine off-set by landslide movement may offer a means of better quantifying the timing of landslide development and the rates of pre-historical movement.

The ongoing movement and squeezing of the valley indicates that glacier deformation has accommodated movement, regulated the rate of movement, and possibly prevented a rapid, complete failure of the slope. This suggests that glacier ice plays a rather more complex role in the development of rock slope failures, beyond simple elastic debuttressing.

The movement data, albeit limited in temporal resolution, suggests a relationship with rainfall, indicating that once initiated, groundwater may also regulate the rate of slope movement. The continuous GPS further along the ridge, off the landslide, shows a ~50 mm seasonal recoverable displacement, suggesting that i) caution is needed to differentiate between permanent and cyclic deformation at the monitoring pegs; ii) the Mueller Rockslide might experience cyclic stresses that may further weaken the slope over time (e.g. Grämiger et al. 2016).

Weakening rock mass strength, groundwater changes, reducing glacier ice support, and the high seismic hazard of the tectonically-active region, may each provide a process that could lead to a rapid release of the slope. Further monitoring, subsurface investigation, and the development of stability models may help to predict the future development of this rockslide.

6 Reference list

Ballantyne, CK, Sandeman, GF, Stone, JO, Wilson, P. 2014. Rock-slope failure following Late Pleistocene deglaciation on tectonically stable mountainous terrain. Quaternary Science Reviews, 86, pp.144–157.

Gischig, VS, Moore, JR, Evans, KF, Amann, F, Loew, S. 2011. Thermo-mechanical forcing of deep rock slope deformation - Part II: the Randa rock slope instability. Journal of Geophysical Research: Earth Surface 116.F4.

Grämiger, L, Moore, JR, Gischig, VS, Loew, S. 2016. Paraglacial rock mass damage during repeat glacial cycles in preparing slope instabilities (Aletsch region, Switzerland). EGU GA Conference Abstracts (Vol. 18, p. 15114).

Lillie, AR, Gunn, BM. 1964. Steeply plunging folds in the Sealy range, Southern Alps. New Zealand Journal of Geology and Geophysics, 7(3), pp.403–423.

McColl, ST. 2012. Paraglacial rock-slope stability. Geomorphology, 153, pp.1–16.

McColl, ST, Davies, TR, McSaveney, MJ. 2012. The effect of glaciation on the intensity of seismic ground motion. Earth Surface Processes and Landforms, 37(12), pp.1290–1301.

McColl, ST, Davies, TR. 2013. Large ice-contact slope movements: glacial buttressing, deformation and erosion. Earth Surface Processes and Landforms, 38(10), pp.1102–1115.

Ostermann, M, Sanders, D. in press. The Benner pass rock avalanche cluster suggests a close relation between long-term slope deformation (DSGSDs and translational rock slides) and catastrophic failure. Geomorphology.

Insights into progressive rockfall failure from 4D scanning

Nick Rosser[1*], Jack Williams[1], Matthew Brain[1] and Richard Hardy[1]

[1] Department of Geography, Durham University, United Kingdom
* n.j.rosser@durham.ac.uk

1 Abstract

Our understanding of the nature of progressive failure of rockfall is in part limited by the temporal and spatial resolution, and coverage of monitoring data. We present a uniquely high-resolution 4D dataset that captures over 180,000 rockfall, largely < 1m^3. Of these rockfall, only a small portion show evidence of pre-failure deformation. We use our data to look in detail at the nature of deformation during the week prior to failure. We see multiple phases of movement that relate to weather conditions, in addition to pulses of movement immediately prior to collapse, which we hypothesize relate to the underlying progressive failure mechanism controlling the release of the rockfall.

2 Introduction

A series of studies using repeat surveys of actively failing rock slopes have revealed that rockfalls rarely occur as instantaneous events, and are often preceded by deformation or sequences of precursors (e.g. Rosser et al. 2007). It has been suggested that the behavior of a slope prior to failure reflects, at least in part, the underlying mechanisms, including progressive failure. For example, Royán et al. (2015) identify an accelerating pattern of small-scale movements prior to a larger rockfall, which the authors attribute to a progressive mode of failure. Similarly, Rosser et al. (2013) identified an increasing rate of increasingly large rockfalls preceding subsequent rock cliff collapse. Whilst these studies offer insight, they are limited by the frequency of data collection which is normally collected over intervals longer than the duration of changes, or they rely on fortuitously capturing precursors. To address this, here we present a uniquely long-term, high-resolution (space and time) monitoring dataset, captured using repeat laser scans over 9-months.

3 Methods

Our dataset comprises *c*. 9,880 scans captured at < 1 hr intervals. Each scan contains c. 1.8m points at point spacing ≈ 0.05 m. The scanning system is a Riegl vz1000 with a controls system that enables sequential scans of the monitored rockface (area = 9,592 m^2). Data is combined with contemporaneous weather conditions to assess controls on deformation. Data is processed using a set of algorithms developed specifically for optimizing the detection of fine-scale change in large archives of point cloud data. This method optimizes scans in the series *n-x*, where *n* is the current scan and *x* is previous scans, to build a point cloud with a minimal level of noise, against which the scan *n+1* is compared. Data is removed in areas where scanning is inconsistent and unreliable for change detection such as sharp topographic edges. Deformation is assessed using an evolution of the M3C2 algorithm (Lague et al. 2013). This data is capable of quantifying differences <3 mm at ranges of up to 350 m. More than 180,000 rockfall were captured using this data.

4 Results

In our inventory the mean rockfall size is 0.0015 m^3, and maximum 7.25 m^3, totaling over 110 m^3 of mass wasting. Only 18 rockfalls were > 1 m^3. Using a search zone equivalent to the aerial extent of each rockfall, we are able to identify precursors for only *c*. 30 rockfall (<0.01%), of which all are in the largest 0.01% by volume recorded. Therefore, precursors are only discernable for the largest events, which may in part be a function of our monitoring resolution, or may reflect a lack of precursors for the smallest events. Precursors are manifest as either deformation, generally movement of failing blocks forward from the cliff, or smaller rockfall that are sourced from within the footprint of a

later, larger event. For those events which show precursors, this deformation generally takes two forms, illustrated in Fig. 1.

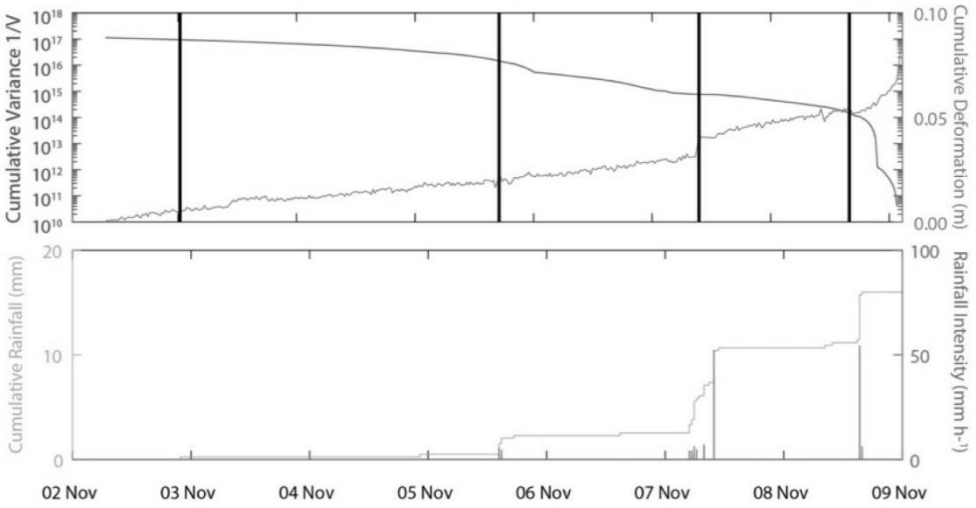

Figure 1. Example of development of deformation prior to a c. 3 m³ rockfall captured at 60 min intervals. Failure occurs on 9 November, with deformation measured during the preceding 7 days. Note a progressive increase in velocity that is coincident with rainfall. We also plot time-reverse cumulative variance, which highlights multiple stages in the tertiary creep period in the 9 hours prior to failure on 9 Nov.

Deformation includes firstly: (1) an increase in deformation rate, above background noise that appears to irreversibly ratchet up in response to rainfall events. This period of activity is visible for several days prior to failure. Second, (2), for the larger failures in our inventory (c. 1m^3), the pattern of deformation described in (1) transitions into a more characteristic hyperbolic acceleration of deformation rate normally over a period of *c*. 6 hours prior to failure. Plotting inverse velocity against time for this period yields a linear trend, as observed for far larger failures previously (e.g. Rosser et al. 2007). We explore descriptive statistics (time-reversed cumulative variance), to describe distinct periods of deformation within both (1) and (2) above, also shown in Fig. 1.

5 Discussion & Summary

Constant 4D monitoring allows us to capture deformation and precursors prior to relatively small (< 1 m^3) rockfall. We observe patterns of behaviour comparable to those more widely observed for larger-scale rockslope failures, and we are able to relate the rate of deformation to rainfall. Using the inventory, we are able to draw general conclusions across multiple events that give insight into the progressive development of rockfall. The resolution of this data provides new insight into deformation in the period prior to collapse, which we infer relates to failure mechanism. We observe a ratcheting effect, triggered by rainfall during secondary creep, the analysis of which could offer some insight on the controls on transition to tertiary deformation.

6 Reference list

Lague D., Brodu N., Leroux J. 2013. Accurate 3D comparison of complex topography with terrestrial laser scanner: application to the Rangitikei canyon (N-Z). Journal of Photogrammetry and Remote Sensing, 82,10 - 26.

Rosser, N.J., Brain, M.J., Petley, D.N., Lim, M. & Norman, E.C. 2013. Coastline retreat via progressive failure of rocky coastal cliffs. Geology, 41, 939 - 942.

Rosser, N.J., Lim, M., Petley, D.N., Dunning, S.A. & Allison, R. 2007. Patterns of precursory rockfall prior to slope failure. Journal of Geophysical Research : Earth Surface, 112, F04014.

Royán M., Abellán A., Vilaplana J. 2015. Progressive failure leading to the 3 December 2013 rockfall at Puigcercós scarp (Catalonia, Spain). Landslides.1-11.

Williams J., N. Rosser, R. Hardy. *in review.* Analysis of deformation from high-resolution 4D terrestrial laser scanning. Earth Surface Dynamics.

Exfoliation fracturing mechanisms and related stress conditions in the Aar Massif, Grimsel region

Martin Ziegler[1*] and Simon Loew[1]

[1] Department of Earth Sciences, ETH Zurich, Switzerland
* martin.ziegler@erdw.ethz.ch

1 Why do we study exfoliation joints?

Exfoliation joints are natural fractures limited to near the ground surface, i.e., they occur at a depth range important for rock extraction and engineering works. Exfoliation joints (also known as sheeting joints) follow the landscape surface at the time of their formation; the age of the associated landscape feature then provides a maximum age of exfoliation joints. While landscape forms can change through time, exfoliation joints preserve elements of former landscape morphologies by their undisturbed orientations.

Exfoliation fractures can play a key role in causing slope instabilities such as rockfalls and rockslides, increase the rates of rock mass weathering and erosion, but also, together with tectonic fractures, allow for economic extraction of dimension stones from a rock mass. Apart from this, we can use exfoliation joint properties (orientation, spacing, and fracture surface morphology) to constrain geologically recent and today's near-surface rock mass stresses, a rock mass state property that is essential for rock engineering. Furthermore, well-preserved fracture surface morphologies let us interpret fracture formation modes and processes.

2 What is special about the Grimsel region of the Central Alps?

The Grimsel region in Switzerland is well suited for analyzing the impact of erosional episodes, and accompanying stress changes, on exfoliation joint formation in granitic-gneissic rocks (Ziegler et al. 2013, 2014, 2016). Mapping above and below ground revealed that exfoliation joints are widespread and occur between valley bottoms and mountain crests within glacial (inner and hanging U-shaped trough valleys, glacial cirques, and steep mountain crests) and predominantly fluvial landforms (gently inclined linear slopes above the inner trough valleys, narrow inner-valley gorges, and steep V-shaped side gullies). Relating the mapped distribution and characteristics of exfoliation joints to identified erosional episodes and landscape features of known and inferred ages enabled us to distinguish four exfoliation joint generations in the Grimsel area, ranging from the lower Pleistocene (~1.5–1 Ma; generation 1) to the Late Glacial/Holocene (<0.02 Ma; generation 4). The most prominent and deepest exfoliation joint generation is associated with erosion of the inner glacial troughs of the upper Aar valley, which likely occurred during the 'mid-Pleistocene Revolution' (generation 2), followed by a joint generation with a minimum age dating to about the Last Glacial Maximum (generation 3).

3 Fracture surface morphology

The bulk of exfoliation joints shows prominent, common fracture surface markings (i.e., fractographic features): (1) radial plumose structures with distinct plume axes; (2) arrest marks superimposed by plumose striations; and (3) gradually-developing en échelon fringe cracks (Fig. 1). Multiple arrest marks reveal that exfoliation joints formed incrementally and, together with the absence of hackle fringes, suggest stable, subcritical (time-dependent) fracturing conditions. Assuming that plume axes formed parallel to the maximum principal compressive stress (σ1), active at the time of fracture formation, we inferred near-surface palaeostress orientations and compared them with classical borehole-based in-situ stress data. Our results indicate complex directional trends of near-surface σ_1 within the trough valleys of the Grimsel region. The majority of plume axes suggests (1) persistently

subhorizontal to slightly inclined σ_1-orientations at trough valley slopes and (2) near-surface variability of σ_1-orientations originating from topographic perturbation superimposed on the regional stress field (an example of an exfoliation joint plumose axes directions is given in Fig. 1).

In 2016 we conducted field investigations using an Unmanned Aerial Vehicle (UAV) to obtain high-resolution photographs and 3D fracture geometry models of exfoliation joints on steep glacial slopes. These data suggest that not only the direction of the plume axes is a valuable source of stress information, but that the 3D geometry of the fracture may allow us to also constrain the principal stress ratios, σ_1 to σ_2, during mode-I fracture propagation (Rickenbacher & Ziegler 2016).

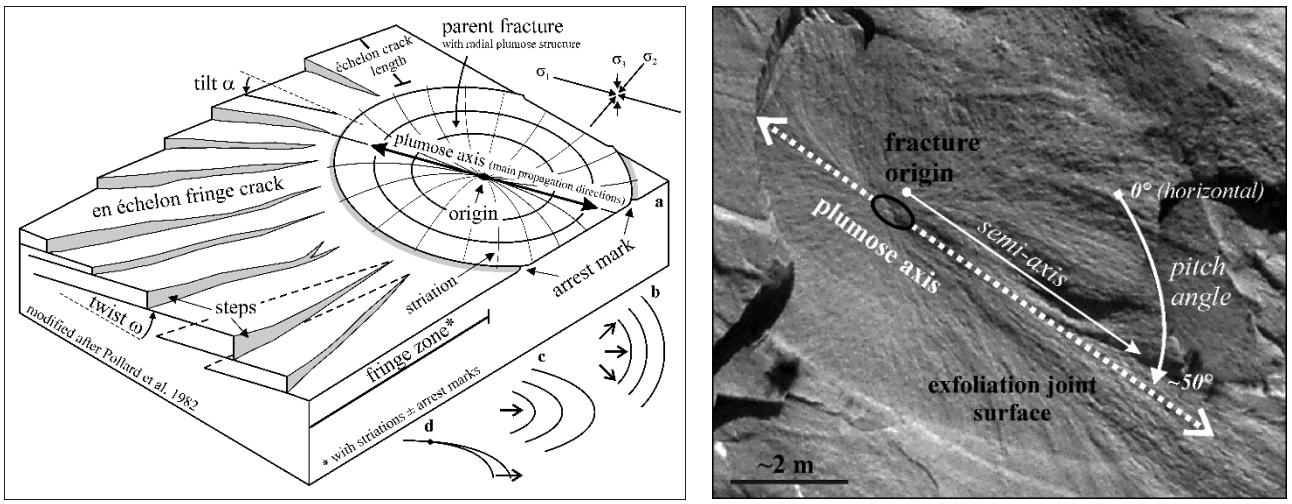

Figure 1. Left: Sketch (a) of fractographic features frequently encountered on exfoliation fractures in the Grimsel study area: (i) fracture origin; (ii) arrest marks; (iii) plumose structures with (iv) plumose axis on the parent plane, typically surrounded by (v) gradually-developing en échelon fringe cracks (here with consistently clockwise twist sense, as seen in direction of fracture propagation). Arrest marks can occur in form of concentric (b) or parabolic/elliptical furrows or ridges (c). In places, renewed fracture propagation only occurs along parts of existing fracture front lines (d). Right: Example of a radial plumose structure on a steep exfoliation joint in Central Aar Granite. Dotted arrows mark the plumose axis and major fracture propagation directions.

4 Numerical modeling

We used three-dimensional, elastic numerical modelling to investigate stress tensors at the near surface of the topographically complex Grimsel area. The model's dimensions are large (more than 10x10x10 km) and the upper model surface represents in fine details the bedrock morphology of the region (both the recent bedrock morphology and an assumed palaeo-landscape were incorporated). Model input properties for intact rock and rock mass were derived from laboratory rock testing (strength, elastic properties, density, and anisotropy) and field investigations (rock mass fracture mapping). The models were stepwise shortened in horizontal directions, isotropically and anisotropically, and near-surface stress tensors monitored. The model results strongly support our hypothesis: Plumose axes form parallel to σ_1 in an overall compressive (far-field) stress field. The model findings illustrate that superposition of topographic stresses with realistic horizontal strains reveals complex near-surface σ_1-trajectories that widely follow the patterns of exfoliation fracture plumose axes (a comparison between fractographically inferred and numerically modelled σ_1 trends is shown in Fig. 2). Thus, also the model results demonstrate large variations of stress orientations, which cannot be captured by small numbers of classical stress measurements. These investigations substantially increased our knowledge of near-surface stress orientations in Alpine slopes.

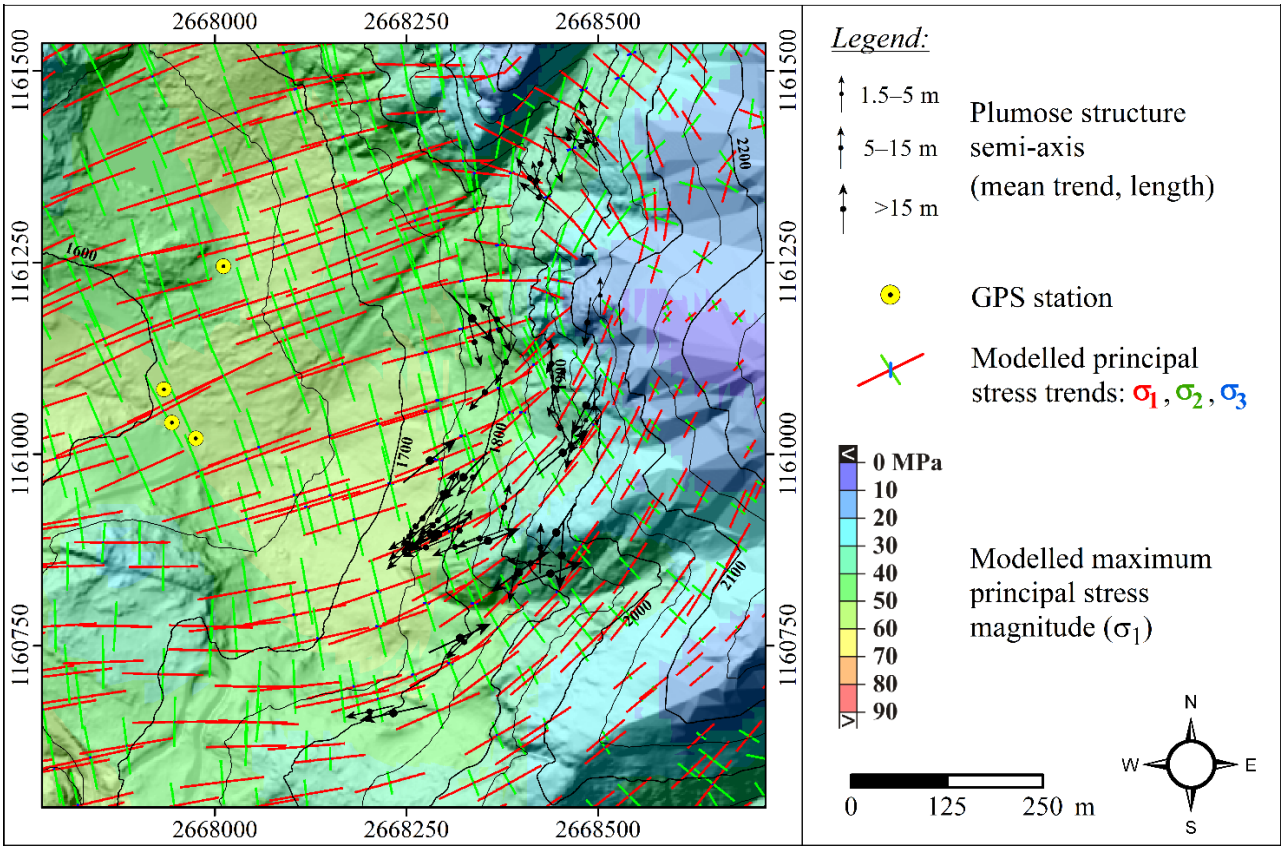

Figure 2. Comparison between fractographically inferred (black arrows) and numerically modelled maximum principal stress trends (red axes= σ_1) for a morphologically complex area in the Grimsel region.

5 Concluding summary

Our study shows:

- that knowledge of the distribution of exfoliation joint generations can reveal unique insights into the morphological evolution of an Alpine valley,
- that high landscape surface-parallel stress magnitudes exist in shallow rock mass at Grimsel,
- that exfoliation fractures of all mapped generations formed incrementally, suggesting stable, subcritical fracture propagation,
- that exfoliation fracture surface morphologies can be used to infer directional trends of fracture propagation and associated palaeostress orientations within Alpine valley slopes,
- that simplified numerical models support exfoliation fracture formation under compression and principal stress directions as inferred from the majority of in-situ stress measurements, and
- that exfoliation fracture plumose axes can be used as a proxy for principal stress orientations.

6 Reference list

Pollard, DD, Segall, P, Delaney, PT. 1982. Formation and interpretation of dilatant echelon cracks. GSA Bulletin 93, 1291–1303.

Rickenbacher, M, Ziegler, M 2016. Exfoliation fracture geometry as a new tool to infer principal stress ratios? Poster at 14th Swiss Geoscience Meeting, Geneva, 19–20 November 2016.

Ziegler, M, Amann, F, Loew, S 2016. Near-surface patterns of rock stress orientations in morphologically complex Alpine valleys – The Grimsel region of Switzerland as a case study. Rock Mech. Rock Eng. 85, 129–151.

Ziegler, M, Loew, S, Bahat, D 2014. Growth of exfoliation joints and near-surface stress orientations inferred from fractographic markings observed in the upper Aar valley (Swiss Alps). Tectonophysics 626, 1–20.

Ziegler, M., Loew, S., Moore, J.R. 2013. Distribution and inferred age of exfoliation joints in the Aar Granite of the central Swiss Alps and relationship to Quaternary landscape evolution. Geomorphology 201, 344–362.

Paraglacial history and structure of the Moosfluh Landslide (1880–2016)

Franziska Glueer[1*], Simon Loew[1], Dominik Zangerl[1] and Andrea Wolter [1]

[1] Department of Earth Sciences, ETH Zurich, Switzerland
* franziska.glueer@erdw.ethz.ch

1 Introduction

Often large-scale postglacial rock slope failures like rock-falls, rock-slides or deep-seated gravitational slope deformations (DSGSD, (Crosta et al. 2013)) can be found in formerly-glaciated alpine areas. It is supposed that failure in these alpine landscapes is directly conditioned by former glaciation and deglaciation (Ballantyne and Stone 2013; Clayton et al. 2017; Evans and Clague 1994; Holm et al. 2004; McColl 2012). Glacial steepening and deglaciation processes have been subject to many studies in the last decades (Grämiger et al. 2017). In contrast preparatory factors like daily, annual and interstadial climatic variations have rarely been studied as well as the historical evolution of failure processes in a paraglacial context since the little ice age (LIA, 1880). The interaction between the retreating glacier and the large DSGSD at Moosfluh is studied in this research. Based on historical data and recent landslide-monitoring and –mapping we present the progressively upslope development of a DSGSD into an active toppling-mode landslide.

2 Study site

Being located in the Swiss Alps, the Great Aletsch Glacier region with its long glacial history, its climate and geology, forms a scientifically unique study area. We are monitoring a rockslide with an estimated volume of about 0.2 km³ occupying the southern valley slope at the tongue of the glacier consisting of a steeply into the slope dipping Pre-Variscan Gneiss (Ambühl 1930).

The rockslide toe is buttressed by the Great Aletsch Glacier, which has thinned since LIA more than 300 m at the study location and lost more than three kilometers of length (Glaciological Reports, 1881-2013). The glacier tongue at the Moosfluh instability lies at 1700 m a.s.l., whereas the ridgetop with the Moosfluh cable car station, which is the only direct infrastructure on the active landslide, is located at 2330 m a.s.l. To be noticed is the damned lake Gibidum 3.5 km downstream the Massa which proceeds the Aletsch Glacier with a water volume of $9.2 \cdot 10^{-6}$ km³.

From the current point of knowledge (May 2017) according to morphological features and movement patterns the slope can be divided into three different sectors. These sectors are always characterized by a steep slope (around 35°) followed by a flat sector of 5-15°.

The lower slope sector with an average slope angle of 35° is characterized by glacially abraded bedrock partially covered with sediment. Since September 2016 the bedrock with its cover at the landslide toe shows fresh, uphill-facing scarps with throws of up to 2 m (Fig. 1, left). The top of the lower sector at Kalkofen is less inclined (5-10°) and shows extensional features with normal scarps and antislope scarps (Fig. 1, right). Within this sector a secondary landslide with a normal scarp of 15 m altitude developed in September 2016 and proceeded upwards in winter 2016/17 building another 15 m high scarp 100 m higher.

The medium sector of the slope is characterized by a rockfall area (average slope 37°) which again is topped by an area of extension at Alte Staffel (slope 10-15°) with normal and antislope scarps within close area. In a small extend the rockfall area beneath Alte Staffel and Kalkofen already exists in 1940, whereas the activation and massive rockfall only started in September 2016.

In the upper slope sector saw-tooth-surface due to several slope parallel NW-SE trending ridges of up to 1 km length can be observed. These ridges are characterized by depressions and steep upslope-facing surfaces which are dipping around 50° to the SE compared to the slope gradient of 25-30° to the NW. These upslope-facing surfaces of up to 4 m heights show fresh torn turfs of up to 0.8 m heights. These torn turfs also developed in September 2016 even though small torn turfs where recognized during field work in summer 2015. The ridge of the upper sector with the Moosfluh cable car station accents into a 150 m to 250 m broad graben, limited by several normal scarps as well as antislope scarps (see Fig. 2).

Figure 1. Left: Picture of a fresh uphill facing scarp at the lower sector cutting through rock and sediment cover (dimension 2 m). Right: Uphill facing scarp with a height (of around 0.5 m) and extension (of around 0.2 m) at Kalkofen area, notice tensioned roots.

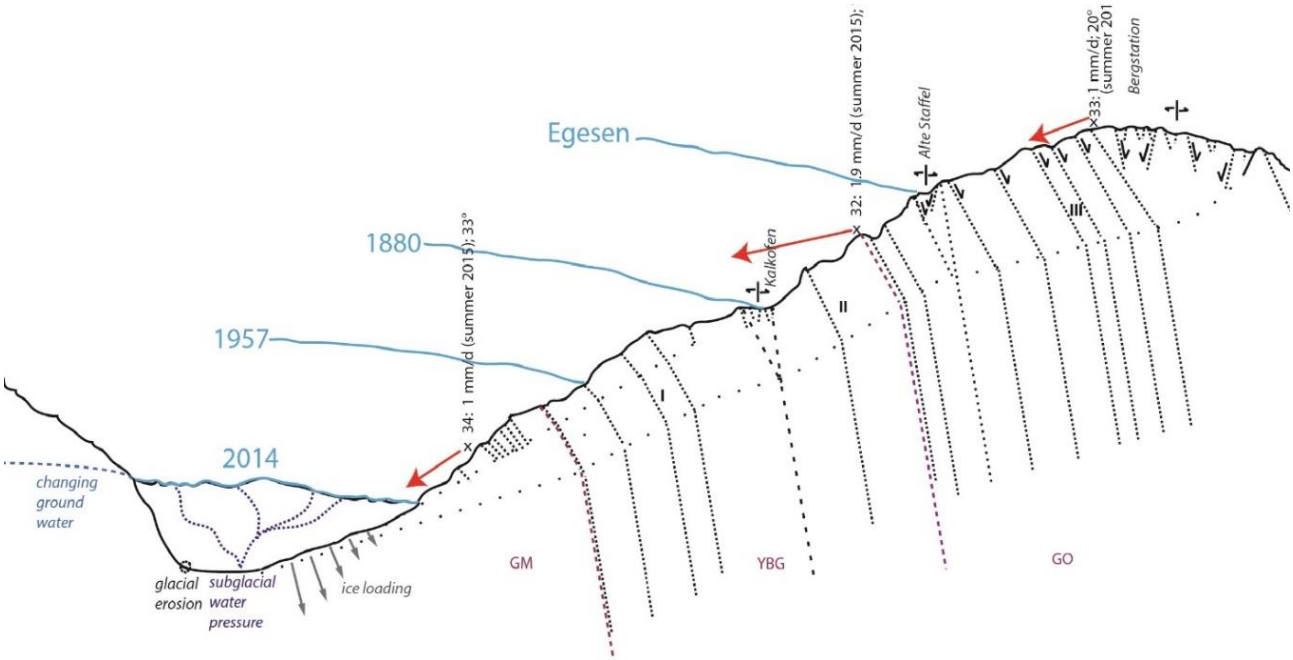

Figure 2. Profile of the Moosfluh instability in 2014. Drawn are glacial stages, geology, shistosity, the three sectors (I-III) and acting forces at the landslide toe. For location of profile see Fig. 3.

3 Methodology

Integration of the results obtained from different remote sensing and ground based monitoring techniques allowed us to investigate the long (multi-decadal) and short (seasonal) term evolution of the Moosfluh instability in a 75-year period (1940-2015). Analogue and digital photogrammetry (Kaab et al. 1997; Messerli 1968) of historic aerial photographs and digital image correlation (Kaab and Vollmer 2000) allowed us to do multi-temporal landslide mapping and slope stability studies for seven

stereographic image pairs from 1940-2009. Synthetic Aperture Radar Interferometry techniques (Kenner et al. 2016) help to detect and quantify small ground surface deformations. For the study area InSAR data from 1992 on exist and help determine the magnitude of displacement rates of the landslide (Kos et al. 2016; Strozzi et al. 2010).

The last and most accurate technique used for the Moosfluh instability are tachymeter and GPS measurements. A large set of high-accuracy three-dimensional topographic measurements captured by two robotized total stations (RTSs) and global positioning system receivers (GPS) was installed to identify ground movement with its seasonal trends and the kinematic behavior of the slope failure during the last three years.

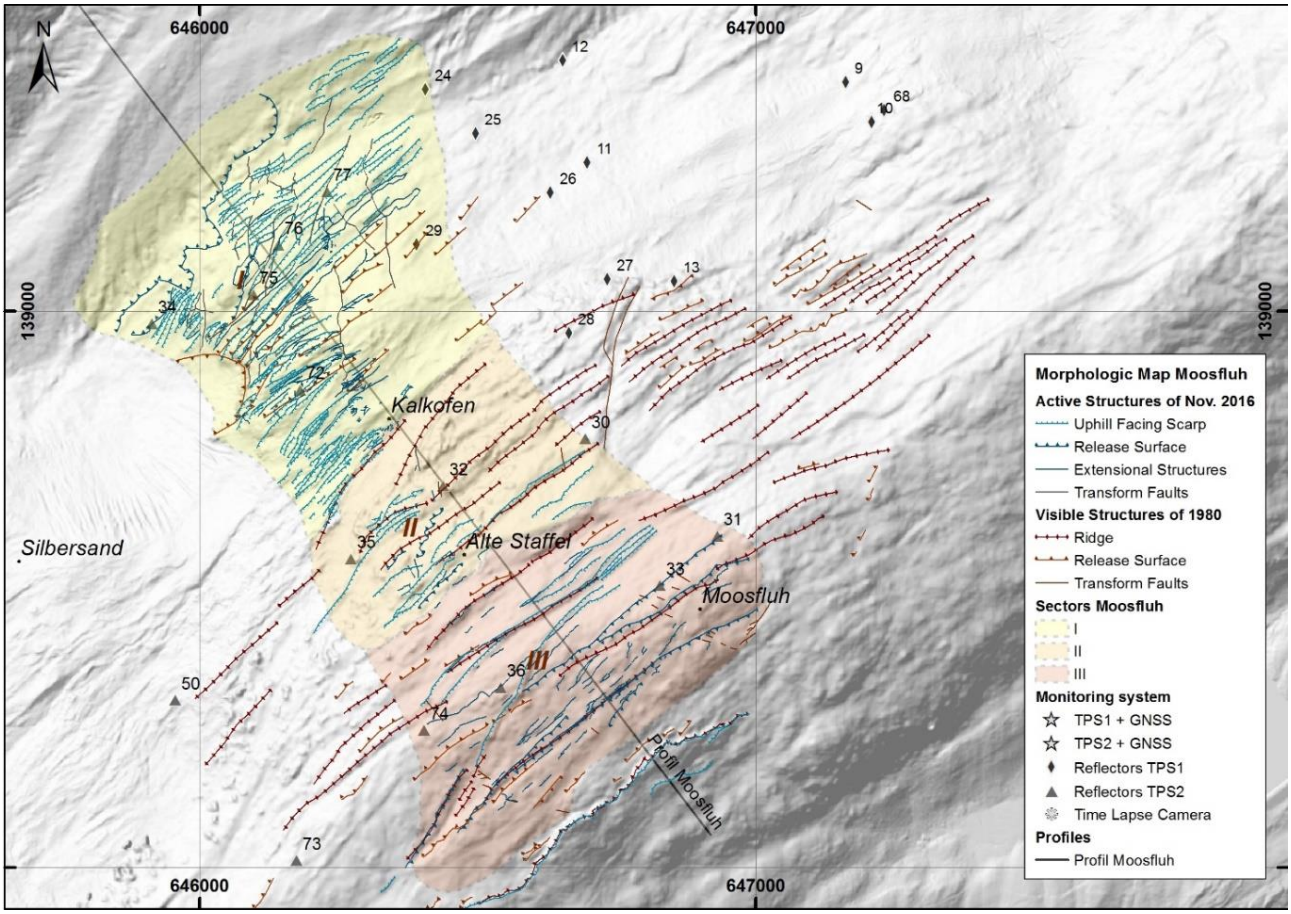

Figure 3. Morphologic map of the Moosfluh instability with data of the year 1980 (reddish colours) and 2016 (blue colours). Visible are all characteristic features like trenches, ridges, scarps and fault structures as well as the three different sectors. The features extend out of the current outline of the instability.

4 Results

The digital photogrammetry revealed a very slow movement of the landslide body between 1940 and 1995 (<1 cm/a). Already in 1940 the same morphologic structures as in 1990 are visible in the area not covered by glacial ice. During this time period the Great Aletsch Glacier has lost more than 100 m in thickness, exposing steep rock faces and drastic morphologic changes like steep walls, slope-parallel trenches and ridges. This leads to the conclusion that for the time interval between 1940 and 1990 all characteristic morphologic features observable in 1990 already existed in 1940 and no larger topographic changes during this time interval occurred. The visible morphologic structures of the year 1980 are displayed in Fig. 3 (reddish colours). Key questions here concern the differentiation between morpho-structures resulting from glacial erosion and tectonic activity compared to morpho-structures arising from progressive rock slope failure. Fig. 3 also shows the results of a high resolution 3D photogrammetric mapping with all active/re-activated structures from November 2016 in blue colours.

For the time span between 1992 and 2012 long-term satellite InSAR data show slope deformation from 3±2 cm/year up to 26 ±1.8 cm/year (Kos et al. 2016). Clearly the satellite data shows different departments of the instability moving at different time and speed, suggesting a feedback mechanism between landslide toe and landslide crown. This supports our model of three different slope, characterized each by a steep slope of 25° – 35° topped by a gentle plateau of 5° - 15° gradient, interacting each as reaction to the lowermost sector - for space and freedom created by toppling.

5 Reference list

Ambühl, E., 1930. Petrographie und Geologie des zentralen Gotthardmassivs südlich Andermatt. Dissertation ETHZ: 183.

Ballantyne, C.K. and Stone, J.O., 2013. Timing and periodicity of paraglacial rock-slope failures in the Scottish Highlands. Geomorphology, 186: 150-161.

Clayton, A., Stead, D., Kinakin, D. and Wolter, A., 2017. Engineering geomorphological interpretation of the Mitchell Creek Landslide, British Columbia, Canada. Landslides: 1-21.

Crosta, G.B., Frattini, P. and Agliardi, F., 2013. Deep seated gravitational slope deformations in the European Alps. Tectonophysics, 605: 13-33.

Evans, S.G. and Clague, J.J., 1994. RECENT CLIMATIC-CHANGE AND CATASTROPHIC GEOMORPHIC PROCESSES IN MOUNTAIN ENVIRONMENTS. Geomorphology, 10(1-4): 107-128.

Glaciological Reports, -. 1881-2013. "The Swiss Glaciers" Yearbooks of the Cryospheric Commission of the Swiss Academy of Sciences (SCNAT) published since 1964 by the Labratory of Hydraulics, Hydrology and Glaciology (VAW) of ETH Zürich, No. 1-126((http://glaciology.ethz.ch/swiss-glaciers/)).

Grämiger, L.M., Moore, J.R., Gischig, V.S., Ivy-Ochs, S. and Loew, S., 2017. Beyond debuttressing: Mechanics of paraglacial rock slope damage during repeat glacial cycles. Journal of Geophysical Research: Earth Surface, 122(4): 1004-1036.

Holm, K., Bovis, M. and Jakob, M., 2004. The landslide response of alpine basins to post-Little Ice Age glacial thinning and retreat in southwestern British Columbia. Geomorphology, 57(3-4): 16.

Kaab, A., Haeberli, W. and Gudmundsson, G.H., 1997. Analysing the creep of mountain permafrost using high precision aerial photogrammetry: 25 years of monitoring Gruben Rock Glacier, Swiss Alps. Permafrost and Periglacial Processes, 8(4): 409-426.

Kaab, A. and Vollmer, M., 2000. Surface geometry, thickness changes and flow fields on creeping mountain permafrost: Automatic extraction by digital image analysis. Permafrost and Periglacial Processes, 11(4): 315-326.

Kenner, R., Chinellato, G., Iasio, C., Mosna, D., Cuozzo, G., Benedetti, E., Visconti, M.G., Manunta, M., Phillips, M., Mair, V., Zischg, A., Thiebes, B. and Strada, C., 2016. Integration of space-borne DInSAR data in a multi-method monitoring concept for alpine mass movements. Cold Regions Science and Technology, 131: 65-75.

Kos, A., Amann, F., Strozzi, T., Delaloye, R., von Ruette, J. and Springman, S., 2016. Contemporary glacier retreat triggers a rapid landslide response, Great Aletsch Glacier, Switzerland. Geophysical Research Letters, 43(24): 12466-12474.

McColl, S., 2012. Paraglacial rock-slope stability. Geomorphology 153–154 16.

Messerli, B., Zurbuchen, M., 1968. Blockgletscher im Weissmies und Aletsch und ihre photogrammetrische Kartierung. Die Alpen, SAC, 3: 14.

Strozzi, T., Delaloye, R., Kääb, A., Ambrosi, C., Perruchoud, E. and Wegmüller, U., 2010. Combined observations of rock mass movements using satellite SAR interferometry, differential GPS, airborne digital photogrammetry, and airborne photography interpretation. Journal of Geophysical Research, 115(F1).

Real-time forecasting of slope kinematics in response to precipitation. Application to Veslemannen (SW Norway)

Antonio Abellan[1], Lene Kristensen[2], Michel Jaboyedoff[3] and Lars Blikra[2]

[1] Scott Polar Research Institute, University of Cambridge, England
[2] Norwegian Water Resources and Energy Directorate (NVE), Norway
[3] Institute of Earth Sciences, Risk Group, University of Lausanne, Switzerland
* Antonio.Abellan@3d-landslide.com

1 Introduction

Modelling the relationships between rainfall, hydrology and deep-seated landslides on a real-time basis and with sufficient response time constitutes a key challenge of early warning and decision support systems. We show here our findings on an autonomous, real-time modelling of slope kinematics at Veslemannen slope (SW Norway), aiming to determine slope-response to precipitation by considering time-dependent aspects of slope behavior. Answering this question will not only increase our understanding of the slope, but also help on the hazard management prior to a potential collapse.

Rock Slope Failures (RSF) around the world generally display creep strain curves characterized by episodic acceleration and deceleration phases in a so-called stick-slip pattern (Prior & Stephens 1972). A sudden increase in pore water pressure and increasing stresses in the landslide body is normally observed after each rainfall episode, revealing a fast infiltration through preferential paths (Corominas et al. 2005; Loew et al. 2012; Blikra et al. 2013; Crosta et al. 2014). This behaviour is normally followed by a progressive decay in velocity reflecting a gradual reduction of water pressure, possibly due to flow diffusion (Iverson 2000). When the movement enters into tertiary creep phase, strain rate is normally characterized by a continuous acceleration until sudden catastrophic failure (Petley et al. 2005; Rose & Hungr 2007; Agliardi et al. 2010). Degrading permafrost also controls the timing and location of RSF (Krautblatter et al. 2013).

Model parametrization in RSF forecasting is normally intricate due to inherently complex geological, hydrological and geomechanical conditions. In addition, epistemic uncertainties also appear due to progressive and/or abrupt changes of slope behaviour in a time-dependent manner (Eberhardt et al. 2004; Petley et al. 2005; Abellan et al. 2015). Calculating slope acceleration and deceleration phases as response to rainfall using inverse modeling and empirically-derived response functions has proven useful before (Belle et al. 2014; Abellan et al. 2015; Bernardie et al. 2015).

2 Available data

We applied the FORESEES model (Abellan et al. under review) to Veslemannen slope, a fast evolving mass movement located in the upper part of Mannen/Børa rock slope, SW Norway (Blikra et al. 2010; Kristensen & Blikra 2013; Skrede et al. 2015; Kristensen et al. in prep). The slope is located on a glacially-shaped valley characterized by exceptionally steep slopes and affected by several highly persistent discontinuity sets (Saintot et al. 2012; Rouyet et al. 2016). The region shows strong climatic seasonality: (a) deep snow cover (more than two meters of snow) with temperatures below freezing point is normally developed during winter; (b) snow melting and thawing occurs during the warm season, when air temperatures range between +1°C and +15°C. Kinematically, the slope accelerates during warmer season following storm events, with peak velocities reaching several cm/day; during the cold season, the slope becomes quiescent/dormant except for small periods of snow melting, as displayed in fig.1. The slope is being continuously monitored by the *Norwegian Water Resources and Energy Directorate* (NVE), and a high level of alert was attained during the last three years (Skrede et al. 2015; Lene et al. in prep). Local environmental data is compiled from

extensometers, a weather station (Fig. 1) and real-time weather forecast provided by the NVE. Remarkably, the slope is not sensitive to external precipitation during cold season, and it only begins to be sensitive to external forcing (both snow melting precipitation) during warm season once the snow cover has been completely melted away. We incorporated a time-varying formulation allowing transient calibration to the system, allowing to account with time-dependent behaviour of the slope (e.g. progressive slope degradation, variation of the hydrological network, freeze-thaw cycles, seasonal variation on the water inflow pattern, snow cover, etc.).

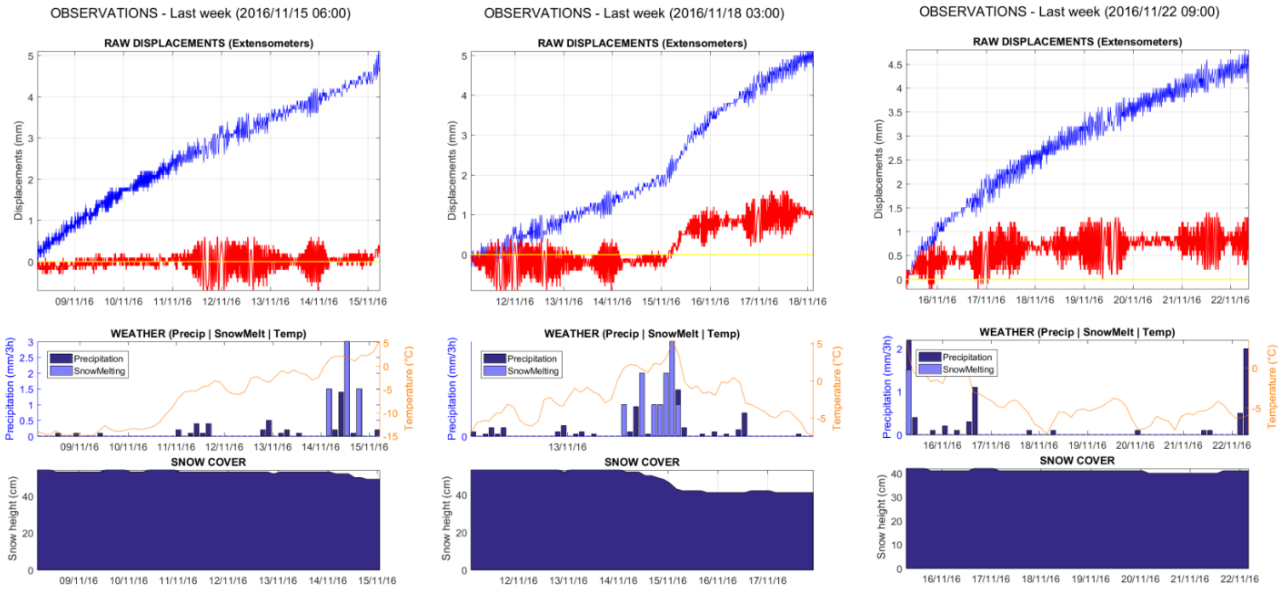

Figure 1. Example of observational data during cold season at three instants of time. Cumulated displacements (upper part), input precipitation and temperature readings (middle part); snow cover (lower part).

3 Model functioning

We utilized a real-time computational model for autonomously predicting the short and long-term slope response to water input. The model uses both effective rainfall and forecast precipitation in addition to surface displacement as input data; the 1D model assumes, visco-plastic rheology, infinite slope conditions, and Mohr-Coulomb failure criteria (FORESEES v.2.0, Abellan et al., under review). The model calculates the main short-term stress variations due to rainfall infiltration using Iverson's (2000) model. A stress-strain equivalence that incorporates both constant and transient terms is formulated and the problem is then inversely solved using non-linear optimization techniques allowing proper calibration of the design variables. Importantly, a transient calibration is utilized in order to account for the time-variant nature of the problem. Upper and lower error bounds were calculated by changing input data variation by +/- 20% in order to account for parametric uncertainties.

A workflow with the main computational steps (implemented in Matlab v.2016a) is shown in Fig. 2. First, a timer schedules the execution of a series of commands, with a delay between executions that is user-defined. The algorithm then attempts to automatically connect to a remote FTP folder, where the observational readings are being recorded in almost real-time. The data is then transferred to a local hard disk and the script begins pre-processing the experimental data (filtering of erroneous values, interpolation, etc.). Next, the algorithm computes slope velocities and minimizes the cost function through optimization of the three design variables (A, B and C, see formulation in fig 2). Once the RMSE drops below a pre-defined limit, or maximum iterations are exceeded, the algorithm generates a series of graphical and numerical outputs and pauses for the user-defined time-delay between executions; finally, the scheduler runs again and starts a new cycle.

Model prognosis was improved by adding weather forecast (one week ahead) imported from the real-time estimations of the Norwegian Meteorological Institute.

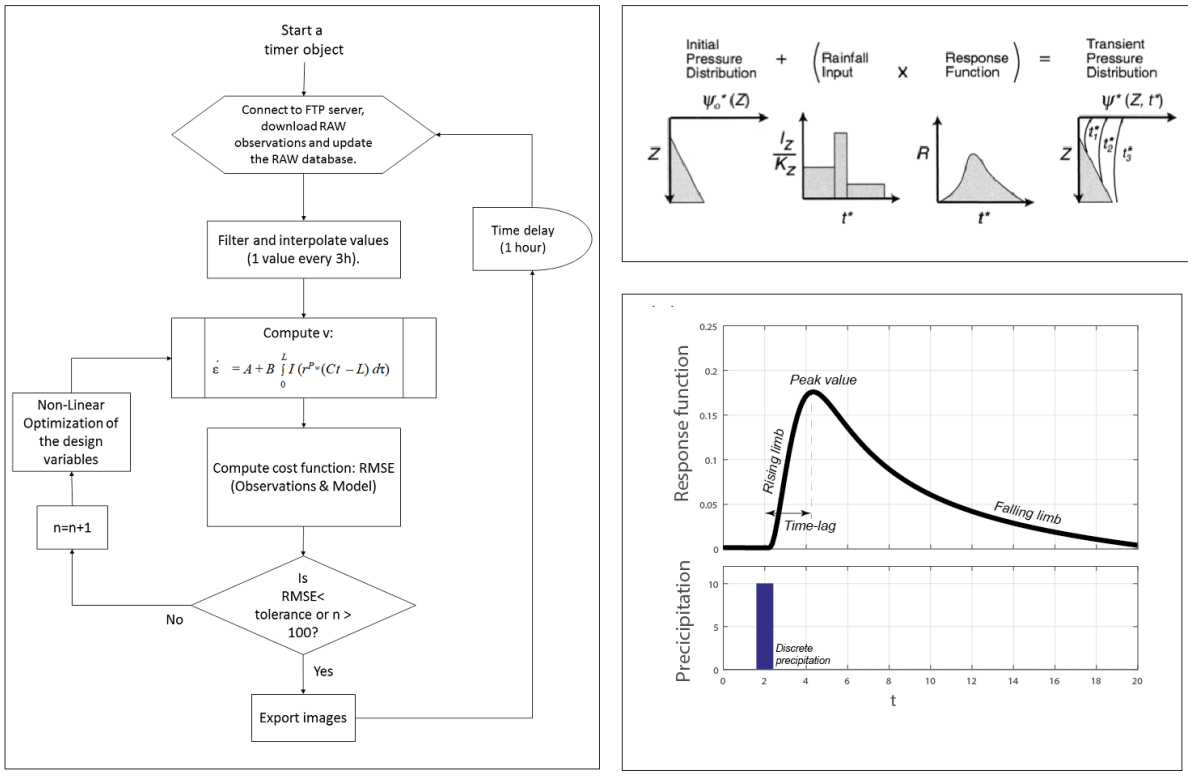

Figure 2. (Left) Model workflow (from Abellan et al. under review); (upper right) Iverson's (2000) infiltration model; (lower right) main components of a response function resulting from input precipitation.

4 Model results

Both effective precipitation and slope deformation were used for inversely calibrating the design variables. Optimization tasks were carried out using different calibration and response function window lengths: an optimal calibration window length of 15 days and an optimal response function length of two days were obtained. A sample of the model results can be seen in Fig.3, showing a close resemblance of the model to the extensometer readings both before a forecast storm (left part), and several days after the storm occurrence (right part). The incorporation of weather forecast into the model allows making realistic evaluations of slope displacements several days ahead on time, with expected accuracy of the prognosis proportional to the confidence on weather forecast.

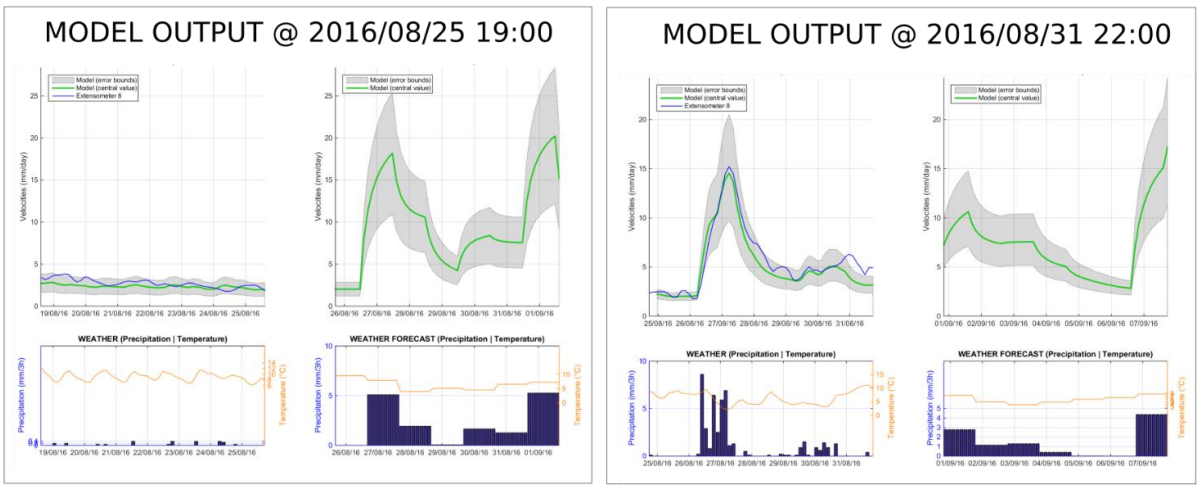

Figure 3. Model output, including error bounds, before and after the arrival of a forecasted storm; (left and right, respectively). A good resemblance is observed between forecast and observed rates of displacement.

5 Conclusions

A real-time processing strategy for autonomously calculating slope kinematics in response to precipitation was shown. The model has been autonomously computing rates of displacements in Veslemannen slope (SW Norway) for more than one year, displaying a clear time-varying behaviour. Our model prognosis was based not only on current precipitation readings but also on local weather forecasts, which has the potential to increase response time for a future implementation of the model outcomes into an Early Warning System. The real-time results can provide a complementary support tool for decision taking during slope accelerations and emergency events.

6 Acknowledgements

We acknowledge the support received by the Norwegian Water Resources and Energy Directorate. AA acknowledges founding from the European Commission, Marie Curie Fellow. [IF-2015-705215].

7 Reference list

Abellán, A., Kristensen, L., Jaboyedoff, M., Blikra, L. Real-time modelling of time-dependent landslide response to precipitation (Under review). Landslides.

Abellán, A, Michoud, C, Jaboyedoff, M, Baillifard, F, Demierre, J, Carrea D, Derron, MH. 2015. Velocity Prediction on Time-Variant Landslides Using Moving Response Functions: Application to La Barmasse Rockslide (Valais, Switzerland) In Engineering Geology for Society and Territory, 2, 323-327. Springer International Publishing.

Agliardi, F, Crosta, GB, Frattini, P. 2010. Forecasting the Failure of Large Landslides for Early Warning: Issues and Directions. In Open Workshop within the frame of the EU FP7" SafeLand" Project (Vol. 82, pp. 50-51) Geol. Survey of Austria.

Belle P, Aunay, B, Bernardie, SN, Grandjean, G, Ladouche, B, Mazué, R, Join JL. 2014. The application of an innovative inverse model for understanding and predicting landslide movements (Salazie cirque landslides, Reunion Island) Landslides, 11(3) 343-355.

Bernardie, S, Desramaut, N, Malet, JP, Gourlay, M, Grandjean, G. 2015. Prediction of changes in landslide rates induced by rainfall. Landslides. 12(3), 481-94.

Blikra, LH, Kristensen, L, Hole, J. 2010. Mannen in Romsdalen: monitoring and data analyses. Technical Report (Aknes/Tafjord Early Warning Centre) Stranda, Norway.

Blikra, LH, Kristensen, L, Lovisolo, M. 2013. Subsurface monitoring of large rockslides in Norway: a key requirement for early warning. Ital. J. Eng. Geol. Environ, 6, 307-314.

Corominas, J, Moya, J, Ledesma, A, Lloret, A, Gili, JA. 2005. Prediction of ground displacements and velocities from groundwater level changes at the Vallcebre landslide (Eastern Pyrenees, Spain) Landslides 2:83–96

Crosta, GB, Di Prisco, C, Frattini, P, Frigerio, G, Castellanza, R, Agliardi, F. 2014. Chasing a complete understanding of the triggering mechanisms of a large rapidly evolving rockslide. Landslides. 11: 747.

Eberhardt, E, Stead, D, Coggan, JS. 2004. "Numerical analysis of initiation and progressive failure in natural rock slopes—the 1991 Randa rockslide." International Journal of Rock Mechanics and Mining Sciences 41.1, 69-87.

Iverson, RM. 2000. Landslide triggering by rain infiltration, Water Resources Research, 36, 1897– 1910.

Kristensen, L, Blikra, L.H. 2013. Monitoring displacement on the Mannen rockslide in Western Norway. In: Marggottini, C., Canuti, P. and Sassa, K. (eds.) Landslide Science and Practice, Springer, Berlin Heidelberg, pp. 251-256.

Krautblatter M., Funk D. & Günzel F. K. (2013): "Why permafrost rocks become unstable: a rock-ice-mechanical model in time and space" Earth Surface Processes and Landforms. Vol 38, Issue 8, 876-887

Kristensen, L, Abellan, A, Jaboyedoff, M, Blikra, L. in prep. Rock Slope instability at Veslemanen slope (Møre & Romsdal county, SW Norway): available data and preliminary analysis. Norwegian Journal of Geology.

Loew, S, Gischig, V, Willenberg, H, Alpiger, A, Moore, JR. 2012. Randa: Kinematics and driving mechanisms of a large complex rockslide. Landslides: Types, Mechanisms and Modeling, p.297.

Petley, DN, Higuchi, T, Petley, DJ, Bulmer, MH, Carey, J. 2005. Development of progressive landslide failure in cohesive materials. Geology, 33(3) 201-204.

Prior, DB, Stephens, N. 1972. Some movement patterns of temperate mudflows: examples from northeastern Ireland. Geological Society of America Bulletin, 83(8) 2533-2544.

Rose, ND, Hungr O. (2007. Forecasting potential rock slope failure in open pit mines. Int J Rock Mech. 44(2) 308-320.

Rouyet, L, Kristensen, L, Derron, MH, Michoud, C, Blikra, LH, Jaboyedoff, M, Lauknes TR. 2016. Evidence of rock slope breathing using ground-based InSAR. Geomorphology.

Saintot, A, Dahle, H, Derron, MH, Henderson, I, Oppikofer, T. 2012. Large gravitational rock slope deformation in Romsdalen valley (Western Norway). Revista de la Asociación Geológica Argentina, 69(3), 354-371.

Skrede, I, Kristensen, L, Hole, J. (2015. J. Geologisk evaluering av Veslemannen – eit mindre fjellskred i utvikling. NVE Report Nr 41–2015. The Norwegian Water Resources and Energy Directorate, Stranda, Norway (In Norwegian)

When does progressive rock-slope failure start and how does it develop in time? An analysis from Norway: a landscape dominated by steep alpine relief excavated by multiple glacial cycles

Reginald L Hermanns[1,2*], Martina Böhme[1], Thierry Oppikofer[1], John Gosse[3], and Ivanna M. Penna[1]

[1] Geohazard and Earth Observation team, Geological Survey of Norway, Norway
[2] Department of Geoscience and Petroleum, Norwegian University of Science and Technology (NTNU), Norway
* reginald.hermanns@ngu.no
[3] Department of Earth Sciences, Dalhousie University, Canada

1 Principles of progressive failure and aim of this contribution

Progressive failure is generally understood as a gravitational slope deformation that lasts over a certain period of time and accelerates prior to catastrophic failure. Several studies suggested hypothetical failure curves (e.g., Crosta and Agliardi 2003; Xue et al. 2014), all of them including an initiation, a steady state creep and an acceleration phase that might be extremely short when external trigger mechanisms such as earthquakes or strong rainfall events apply (Hermanns and Longva 2012). Most focus has been given so far to detecting the acceleration phase as this helps to identify the potentially damaging event; the inverse-velocity method has been suggested in order to predict the failure moment and make early-warning and successful evacuation possible (Fukuzono 1985; Voight 1989; Crosta and Agliardi 2003). However, accelerated movement can only be detected when long-term slip rates and initiation of sliding is known. This contribution summarizes three datasets on rock slope failures in western Norway 1) a dataset on unstable rock slopes, 2) a dataset on ages determined by cosmogenic nuclide dating (CN) of prehistoric catastrophic rock slope failures, and 3) a dataset of published (Hermanns et al. 2012, 2013) and preliminary results of CN surface exposure ages of sliding surfaces. This combination of datasets allows improved discussion of initiation and development (creep phase) of failure over time.

2 Unstable rock slopes within Norway

A systematic analysis for unstable rock slopes using aerial photos, satellite-based InSAR, high-resolution airborne LIDAR data, helicopter reconnaissance and field mapping has been carried out in Møre and Romsdal and Sogn og Fjordane (western Norway). A total of 138 unstable rock slopes with post-glacial, gravitationally induced rock slope deformation have been detected so far (Böhme et al. 2011; Saintot et al. 2011; Oppikofer et al. 2015). This dataset is believed to be a nearly complete dataset for unstable rock slopes in the area. Few new sites might however be detected on densely vegetated slopes when the full cover of these counties with high resolution LIDAR data becomes available.

The unstable rock slopes distribute relatively evenly over the gneissic basement rocks of both counties, but cluster in the weaker phyllitic rocks in Sogn og Fjordane (Böhme et al. 2011). Displacement measurements exist for a total of 45 sites. Four of those are classified as high risk objects with continuous monitoring systems installed (Blikra et al. 2016). The remaining sites are followed-up with periodic monitoring with measurement intervals between once in a year to once in five years. Displacement rates are in general below 1 cm/year with the exception of six slopes where displacement rates vary between 1 and 10 cm/year. From monitoring data alone acceleration cannot be detected on any of those slopes except a small compartment of the Mannen unstable rock slope (Skrede et al. 2015). However, back calculations of displacement velocities compared to the total displacement at those slopes indicate that none of the slopes could have been actively deforming with the present-day deformation rate since deglaciation, suggesting either more recent initiation of slope deformation or acceleration.

3 Age of postglacial rock-avalanche deposits in western Norway

We have compiled cosmogenic nuclide (CN) exposure ages of rock-avalanche deposits in the same region in order to compare them to the retreat of the Scandinavian ice sheet. In total 21 rock-avalanche events were dated by their deposits (18) or failure scars (3) (Hermanns et al., in press). We compared the obtained ages to the decay of the Scandinavian ice sheet that was not spatially synchronous but differed regionally and lasted over several thousand years in places (Hermanns et al., in press). One rock avalanche (at Innerdalen at 14.1 ka) occurred when ice existed in the valley (Schleier et al. 2015), which is in agreement with the latest deglacial models (Hughes et al. 2016). Depositional characteristics of ten (48 %) of the rock avalanches suggest ice-free conditions although they occurred within the first millennia following deglaciation. Six events (29%) occurred between 9 and 7 ka at a time when climate was warmer than today (Lilleøren et al. 2012). Finally four events (20 %) appear to be relatively evenly distributed throughout the rest of the Holocene. This result is similar to detailed analyses of rock-avalanche deposits in the Storfjord that attest that 51 out of 109 rock avalanches occurred within the first 3 millennia after deglaciation and 81% of the rock avalanche material was deposited in the fjord in the first millennia after deglaciation (Böhme et al. 2015).

4 CN surface exposure ages of sliding surfaces of unstable rock slopes

In the same region six sliding surfaces of unstable rock slopes have been sampled for CN surface exposure dating: 1. Oppstadhornet, 2. Skjeringahaugane, 3. Middagstinden, 4. Skorgerurda, 5. Ivasnasen, and 6. Storehornet. Results of sites 1 and 2 were published and dating results suggest that sliding initiated when the slopes melted out of the decaying ice sheet at ca. 14.2 and 10 ka respectively (Hermanns et al. 2012, 2013). This correlates with the retreat of the Scandinavian ice sheet for each location (Hermanns et al. 2016). Paleo sliding rates calculated based on the CN exposure ages were compared to deformation rates determined by dGNSS in over ten years and are identical within error margins with the paleo slip rates suggesting that both slopes deformed with a constant rate since deglaciation.

CN exposure ages of sites 4 and 6 suggest that the sliding surfaces became active when the slopes melted out of the ice sheet. At site 4 the sliding surface has an identical age of ~13.5 ka over a length of 22 m which is identical to the age of a rock-avalanche deposit at the foot of the slope. This suggests that no pre failure deformation (within the error limit of the dating method) occurred on the slope and the slope collapsed shortly after ice retreat. Secondary sliding surfaces on the same slope have Holocene ages and indicate a reactivation of gravitational slope deformation. At site 6 the back-scarp and secondary sliding surfaces also have CN surface exposure ages of ~13.5 ka. CN surface exposure ages of the lower parts of the secondary sliding surfaces are identical within error margins. Thus they suggest that these secondary scarps have been active only for a short time that is smaller than the uncertainty limits of the dating method. The back-scarp in contrast is getting progressively younger in downslope direction. The foot of the back scarp has an age of ~8 ka suggesting no deformation was accommodated on the back sliding surface throughout most of the Holocene. At the foot of that slope exists a rock-avalanche deposit. This was dated to an age of ~3 ka, the corresponding failure surface could not be dated yet.

At site 2 the ages spread from c. 4.5 to 0.5 ka: These are younger in downslope direction. The average paleo slip rate calculated for those ages is about twice as high as today's deformation rates determined by dGNSS (0.8 mm/a) indicating thus a deceleration of the slope.

At site 5 we dated the sliding/failure surface of a rock avalanche, the rock-avalanche deposit itself and the sliding surface of an unstable block that is the extension of the failure surface of the rock avalanche. Both surfaces and the deposit have identical ages of ~3.5 ka (Oppikofer et al. 2017) indicating that failure and sliding of the block occurred simultaneously and no acceleration took place prior to failure that was measureable within the uncertainty margins of cosmogenic nuclide dating.

5 Discussion and conclusions

We have compiled large datasets on unstable rock slopes, ages of rock avalanche deposits and ages of sliding surfaces from western Norway. Our data suggest that rock slope deformation is a wide spread phenomena in the mountains of western Norway. Although post-LGM catastrophic failures occurred predominantly directly following the decay of the Scandinavian ice sheet, rock slope deformation and rock slope failure occurred throughout the Holocene. This is likely not specific to the last glacial cycle. For example, many rockslide scars exist in the Tafjord with no related deposit in the fjord (Oppikofer 2009). Norway was nearly entirely covered by ice sheets not only during the LGM but also during glaciation periods 60 and 90 ka ago and during the previous glacial cycle > 140 ka ago (Svendsen et al. 2004). Glacial cycles cause large changes on rock slopes, that are related to a complete change of the local stress field between glacial cover and deglaciation but also intensive erosion especially on high ridges and at the foot of slopes. Similar to the meltdown of the LGM ice sheet a high concentration of rock slope failures are thus likely to have also occurred following earlier melt down of glacial ice sheets. However, similar to today's situation with 138 unstable slopes a similar amount of unstable slopes likely also existed during previous warm periods that later got covered ("frozen") during following glacial extents.

Two thirds of the dated sliding surfaces became active right after deglaciation and represent unstable slopes with ongoing deformation today. The combination of a large number of early postglacial rock slope failures with a high percentage of sliding surfaces becoming active right after deglaciation shows that climate change in the magnitude of glacial cycles is a first order control on the temporal distribution of rock slope failures in western Norway. However rock slope instabilities may survive slow deformation for thousands of years in the same region.

The observation of longevity of rock slope deformation and a large amount of unstable rock slopes existing today indicates that it is likely that conditions were not very different during other warm periods in the Quaternary, suggesting that unstable rock slopes might survive glacial cycles in a quasi "frozen" state covered under the ice and then become active again. This interpretation is an alternative interpretation to a strong seismic promoter for rock slope failures at the end of the LGM related to isostatic rebound (e.g. Boe et al. 2004; Ballantyne et al. 2014). However, if an unstable slope from an earlier warm period were covered by the LGM glaciation, parts of the unstable rock slopes and especially their foot would be eroded, leaving the upper parts without support, which in turn after deglaciation might promote failure of those "frozen" unstable rock slopes. They will be found as rock avalanche deposits and as slide scar in the morphology, which is documented in our CN data of deposits. If they persist as unstable rock slopes over several thousands of years after deglaciation is questionable but glacial erosion in western Norway does not allow testing for this hypothesis of active unstable rock slopes over several glacial cycles. This is because in western Norway ice sheets were generally erosive and no inherited cosmogenic nuclides from prior to the LGM are left. However in northern Norway large regions exist where glaciers were cold-based and non-erosive. If unstable rock slopes survive glacial cycles our hypothesis could be tested by dating sliding surfaces lying on slopes covered by non-erosive ice.

In the light of progressive failure we have learned from our datasets that only a minor part of unstable slopes initiated in the Holocene. The unstable slopes with fast displacement rates (> 1cm) might belong to this group. The larger part of the dated sliding surfaces date back to the retreat of the ice sheet or the slopes might even have been unstable slopes prior to the LGM. Constant velocity deformation is the most observed behaviour of slowly deforming rock slopes, however deceleration of movement was also observed on one site. Acceleration of movement prior to failure is in general shorter than the resolution of the dating technique and is most effective after glacial retreat; however plenty of those failures might have survived the glacial cycle in a quasi "frozen" state. Preliminary results from northern Norway where cold based ice has been proven support this.

6 Reference list

Ballantyne, CK, Sandeman, GF, Stone, JO, Wilson, P, 2014. Rock-slope failure following Late Pleistocene deglaciation on tectonically stable mountainous terrain. Quaternary Science Reviews 86, 144-157.

Blikra LH, Majala, G, Anda, E, Hallvard, B, Eikenæs, O, Helgås, G, Oppikofer, T, Hermanns, RL, Böhme, M, 2016, Fare- og risikoklassifisering av ustabile fjellparti. NVE-Report 77-2016.

Bøe, R, Longva, O, Lepland, A, Blikra, LH, Sønstegaard, E, Hadlidason, H, Bryn, P, Lien, R, 2004. Postglacial mass movements and their causes in fjords and lakes in western Norway. Norwegian Journal of Geology 84, 35-56.

Böhme, M., Oppikofer, T., Longva, O., Jaboyedoff, M., Hermanns, R., Derron, M.-H., 2015. Analyses of past and present rock slope instabilities in a fjord valley: Implications for hazard estimations. Geomorphology 248, 464-474.

Böhme, M, Saintot, A, Henderson, I, Henriksen, H, Hermanns, RL, 2011. Rock-slope instabilities in Sogn & Fjordane County, Norway: a detailed structural and geomorphological analysis, in: Jaboyedoff, M. (Ed.), Slope Tectonics. Geological Society, London, Special Publications, 351, pp. 97-111.

Crosta, G, and Agliardi, F, 2003, Failure forecast for large rock slides by surface displacement measurements. Canadian Geotechnical Journal 40, 176-191.

Fukuzono, T, 1985. A new method for predicting the failure time of a slope, Proceedings of the 4th International Conference and Field Workshop on Landslides. Tokyo University Press, Tokyo, pp. 145-150.

Hermanns, RL, Longva, O, 2012. Rapid rock-slope failures. Landslides (types, mechanisms and modeling). Cambridge University Press, Cambridge, 59-70.

Hermanns, RL, Gosse, J, Oppikofer, T, Redfield, TF, and Eiken, T, 2016, Expanding Monitoring of rock slope deformation into the geological past by cosmogenic nuclide dating. 3rd Nordic workshop on cosmogenic nuclide techniques, Stockholm, June 8-10, p. 16-17.

Hermanns, RL, Oppikofer, T, Dahle, H, Eiken, T, Ivy-Ochs, S, Blikra, L, 2013. Understanding long-term slope deformation for stability assessment of rock slopes: the case of the Oppstadhornet rockslide, Norway, Proceedings of the International Conference Vajont 1963–2013, Padua, Italy, 8–10 October 2013.

Hermanns, RL, Redfield, T, Bunkholt, H, Fischer, L, Oppikofer, T, Gosse, J, Eiken, T, 2012. Cosmogenic nuclide dating of slow moving rockslides in Norway in order to assess long-term slide velocities, Landslides and Engineered Slopes. Protecting Society through Improved Understanding: Proceedings of the 11th International & 2nd North American Symposium on Landslides, Banff, Canada, pp. 3-8.

Hermanns, RL, Schleier, M, Böhme, M, Blikra, LH, Gosse, J, Ivy-Ochs, S, Hilger, P, in press. Rock-avalanche activity in W and S Norway peaks after the retreat of the Scandinavian ice sheet. Proceedings of the 4th World Landslide Forum, Ljubljana, Slovenia.

Hughes, AL, Gyllencreutz, R, Lohne, ØS, Mangerud, J, Svendsen, JI, 2016. The last Eurasian ice sheets–a chronological database and time- slice reconstruction, DATED- 1. Boreas 45, 1-45.

Lilleøren, KS, Etzelmüller, B, Schuler, TV, Gisnås, K, Humlum, O, 2012. The relative age of mountain permafrost—estimation of Holocene permafrost limits in Norway. Global and Planetary Change 92, 209-223.

Oppikofer, T, 2009. Detection, analysis and monitoring of slope movements by high-resolution digital elevation models. Institute of Geomatics and Analysis of Risk, University of Lausanne, Lausanne, Switzerland.

Oppikofer, T, Nordahl, B, Bunkholt, H, Nicolaisen, M, Jarna, A, Iversen, S, Hermanns, RL, Böhme, M, Molina, FXY, 2015. Database and online map service on unstable rock slopes in Norway—From data perpetuation to public information. Geomorphology 249, 69-81.

Oppikofer, T, Saintot, A, Hermanns, RL, Böhme, M, Scheiber, T, Gosse, JC, Dreiås, GM, 2017. From incipient slope instability through slope deformation to catastrophic failure – different stages of failure development on the Ivasnasen and Vollan rock slopes (western Norway). Geomorphology, accepted with minor changes.

Saintot, A, Henderson, I, Derron, MH, 2011. Inheritance of ductile and brittle structures in the development of large rock slope instabilities: examples from western Norway, in: Jaboyedoff, M. (Ed.), Slope tectonics. Geological Society, London, Special Publications, 351, pp. 27-78.

Skrede, I, Kristensen, L, Hole, J, 2015, geologisk evaluering av Veslemannen-et mindre fjellskred i utvikling. NVE-Report 42-2015.

Svendsen, JI, Alexanderson, H, Astakhov, VI, Demidov, I, Dowdeswell, JA, Funder, S, Gataullin, V, Henriksen, M, Hjort, C, Houmark-Nielsen, M, 2004. Late Quaternary ice sheet history of northern Eurasia. Quaternary Science Reviews 23, 1229-1271.

Voight, B, 1989. A relation to describe rate-dependent material failure. Science 243, 200-203.

Xue, L, Qin, S, Li, P, Li, G, Oyediran, IA, Pan, X, 2014. New quantitative displacement criteria for slope deformation process: from the onset of the accelerating creep to brittle rupture and final failure. Engineering Geology 182, 79-87.

Uma Oya multi-purpose development project: Lessons learned from excavations under high stress conditions

Philippe Nater[1*] and Mousa Hazrati[2]

[1] Pöyry Switzerland Ltd., Zurich, Switzerland
[2] Mahab Ghodss Consulting Engineers, Tehran, Iran
* philippe.nater@poyry.com

1 Introduction

1.1. Main challenge and purpose of the abstract

After finalizing the excavation and the support installation in the main caverns of the Uma Oya MPDP (Multi-Purpose Development Project), cracks in the shotcrete lining of the caverns and in the connecting galleries occurred. This happened during the ongoing work on the inner concrete structure of the caverns. The designers had to give proof to the client that these events will not endanger the integrity of the structures during construction and service life.

As one of the main hazard scenarios potential buckling failure along pre-defined rock slabs in the cavern's side walls was recognized. The potential slabs were formed by the specific discontinuity pattern with sub-vertical joints almost in parallel to the caverns. In case of buckling failure, additional load would have been transferred into the rock pillar between the caverns.

The decisions taken on site during construction were based on long-term monitoring data of which actual examples can be presented. The focus is on readings from load cells on anchors, extensometers and crack meters.

1.2. General outline of the project

The Uma Oya MPDP in the Uva province of Sri Lanka is a classical hydro power plant with the additional benefit of conveying water from the central mountain region to the dry south part of the island. The scheme consists of two catchment areas confined by each a dam. These areas are linked via a low pressure conveyance tunnel of 3.9 km length. A 15.3 km long headrace tunnel starting from the Dyraaba dam guides the design discharge of 19.5 m^3/s past a surge shaft, a valve chamber, a vertical pressure shaft with a length of 630 m, an underground powerhouse with an adjacent transformer cavern both bearing an overburden of almost 700 m and a tailrace tunnel of 3.7 km length.

The main dimensions of the caverns are:

- Powerhouse: Height = 34 m, span = 18 m, length = 72 m
- Transformer cavern: Height = 13 m, span = 14 m, length = 37 m

The powerhouse and the transformer cavern are separated by a rock pillar of 30 m width. The main dimensions and the shape are illustrated in a cross section (Fig. 1).

2 Geology and geotechnical interpretation

The rock mass in the project area consists mostly of massive charnokites of high strength and calc silicate gneisses of which large sections consist of marble. The contact zones often show an anatexis where the rock masses were mixed under high temperature and pressure. The rock is generally massive with only few discontinuities (e.g. at depth of the powerhouse area the RQD is almost 90% - 100%). The main discontinuities are the rock foliation dipping almost perpendicular into the front wall of the caverns and a pronounced sub-vertical joint set parallel to the side walls.

An extensive laboratory testing program was executed revealing a relatively low uniaxial compressive strength of the marbles together with low failure strains. Subsequently the encountered marble was interpreted to be susceptible to brittle behavior. Due to the unpredictable distribution of the lithologies, marble as the material with the lowest strength and the highest brittleness was selected as determinant rock type for design purpose. Characteristic parameters representing the rock mass selected for design were the following:

γ = 28 kN/m^3; E = 16 GPa; ν = 0.25; c = 3.8 MPa; ϕ = 43°

The in-situ stress field and the jacking pressures for pressure tunnel design were investigated with hydraulic fracturing tests in three boreholes all in vicinity of the caverns.

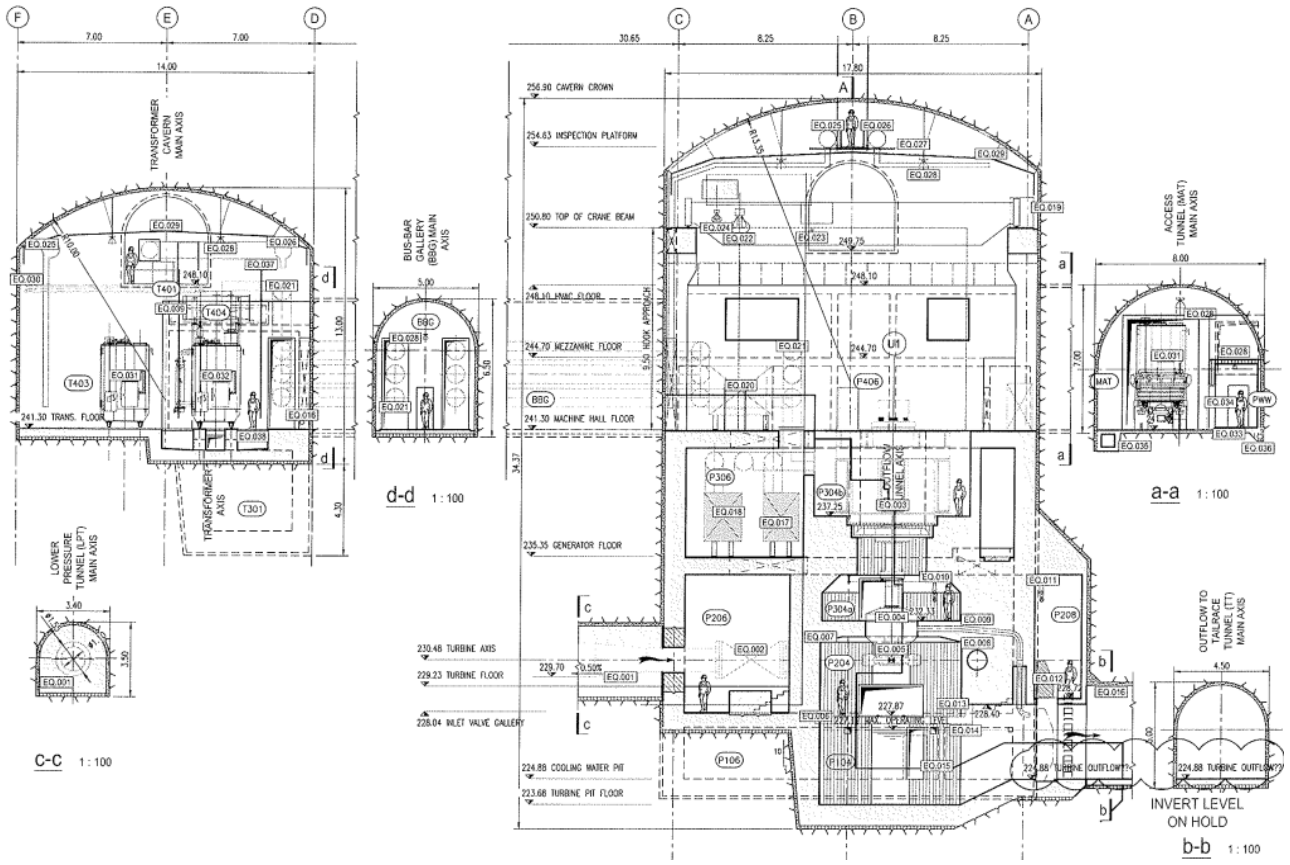

Figure 1. Cross section of the powerhouse and transformer cavern including adjacent tunnels.

3 Design considerations

3.1 Concept

The caverns are designed as self-bearing openings with the inner structure following the “house in house” principle; the inner concrete structure is not intended to carry any significant loads from the surrounding rock mass. Subsequently the rock support needs to be specified for high durability.

The rock support actually consists of mesh-reinforced shotcrete together with fully grouted bar anchors with a length of 8 m and diameters up to 36 mm. The main purpose of the anchors is to stabilize potential wedges in the roof, the side walls and the front walls and constrain the potential slabs in the side walls of the caverns.

3.2 Instrumentation

In the powerhouse cavern instrumentation was foreseen along three cross sections and the front wall. In the transformer cavern two cross sections and the front wall were selected. Both caverns have been equipped with extensometers, load cells on bar anchors and optical convergence pins. In a later stage, 3d crack meters and load cells on pre-stressed cable anchors have been installed.

3.3 Excavation process

All openings in the powerhouse area were excavated by drill & blast method (with exception of the headrace and the tailrace tunnel => both TBM). According to design and specifications, smooth blasting techniques were required to keep the disturbance around the extrados of the openings as small as possible. Additionally, the integrity of the system also relies on the proper application of the support measures especially on complete grouting of the bar anchors and on spraying of shotcrete without shadowing and delamination.

The contractor could not manage to comply with these requirements due to several reasons during the entire construction phase. The powerhouse roof, the connecting galleries and all intersections were left unsupported over a longer period of time – the cavern roofs over several weeks, the connecting galleries over months the intersections partially over years. The initial support installation was not performed according to the specifications and had to be replaced partially.

4 Observations

4.1 Connecting galleries and intersections

In galleries upstream of the caverns, where the in-situ stress increases, local superficial spalling was observed. At almost all intersections the over-stressed rock mass started to form chevron patterns and loosening along the foliation.

4.2 Caverns

Entering the transformer cavern from the access tunnel, a large cuboid block detached from the crown along the foliation plane forming a box shaped excavation instead of an arch roof.

Where the connection galleries between the caverns entered the powerhouse, cracks occurred in the shotcrete both in the caverns' side walls and the galleries support. Opening cracks were even reported up to the middle of the galleries, which was firstly interpreted as a sign of weakening of the rock pillar.

5 Measurements

For illustration, just one example of 3d crack meter readings in one of the connection tunnels is presented here. The graph highlights the need for serious review of any data recognizing, e.g., outliers or reading errors (Fig. 2).

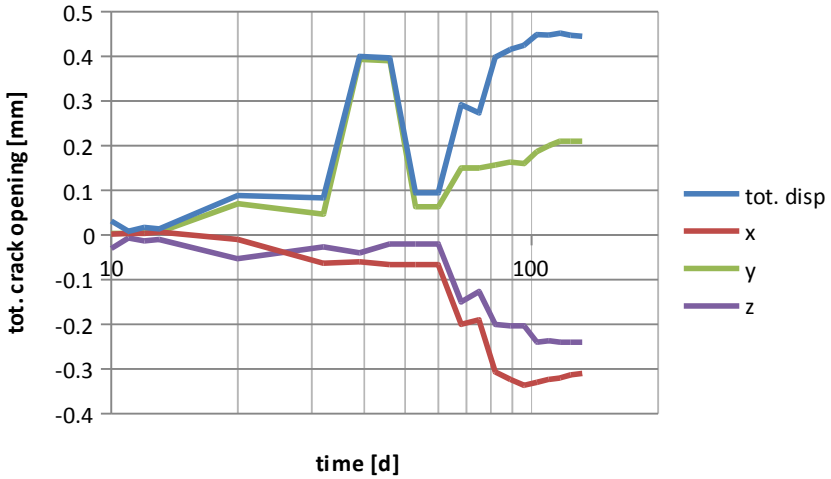

Figure 2. Crack meter reading in the Bus Bar Gallery connecting the powerhouse cavern to the transformer cavern (see Fig. 1).x-direction: along tunnel axis, y-direction: perpendicular to tunnel wall, z-direction: vertical. The graphs contain two uncommented outliers after approx. 40 days.

6 Conclusions

The installation of immediate support is one of the key issues for the limitation of long-term effects in underground structures. As this was not achieved, the rock mass around the openings of the powerhouse perimeter shows signs of overstress together with a continuous increase of measured forces and displacements - which is not terminated by date. Still long-term measurements together with the observations on site do not indicate any tendency towards major instabilities but the situation needs to be observed with care.

The interpretation of measurements and the subsequent decisions should be taken by experts after rational evaluation of the involved phenomena, even though this takes time. On a large construction site with hundreds of people involved and diverging priorities between designer, site supervision, contractor, client and owner, this is not always an easy task.

Progressive failure processes in rock slides: From fractured rocks to the formation of shear zones

Christian Zangerl[1*] and Christoph Prager[2]

[1] University of Natural Resources and Life Sciences, Institute of Applied Geology, Vienna, Austria
[2] alpS GmbH, ILF Consulting Engineers GmbH
* christian.j.zangerl@boku.ac.at

1 Introduction

Compiled field and literature data show that landslides are geologically pre-disposed by the lithological, structural and morphological setting. Concerning the Alps, radiometric age dating data suggest that several active moving landslides represent “old” slope deformations that have been (re-) activated for some 1000 yrs. At several locations, densely foliated and fractured metamorphic rocks (phyllites, schists, gneisses) are widely spread and affected by slowly moving deep-seated rock slides.

According to Cruden and Varnes (1996) rock slides are characterized by a downslope movement of a rock mass on surfaces of rupture i.e. relatively thin zones of intensive shear strain. The landslides presented herein may be classified as “rock compound slides” (according to Varnes’ classification updated by Hungr et al. (2014)). A rock compound slide is characterized by sliding of a mass of rock on a rupture surface consisting of several planes, or an uneven surface, so that motion is kinematically feasible only if accompanied by significant internal distortion of the moving mass. Distinct extensional features i.e. horst- and graben structures at the head as well secondary shear surfaces are characteristic features of this type of landslide.

Furthermore, this type of landslides shows fully persistent basal shear zones, and in some cases also internal shear zones formed through progressive failure processes. It is commonly agreed that shear zones of rock slides originate from to the growth, propagation and coalescence of pre-existing and new fractures as well as rock cataclasis. Based on a variety of field surveys and monitoring data, several slopes show actual gravitational deformation that is determined by sliding processes resulting from shear deformation along discrete shear zones.

Generally, there is little knowledge about the temporal and spatial evolution of shear zones. In addition, there is also a lack in understanding how shear zones form by progressive failure processes. As a consequence, the assessment if a fully persistent basal shear zone has formed is still difficult when direct subsurface investigations such as core drillings or investigation adits are not available.

This contribution aims to highlight open questions for future research rather than to provide final outcomes and conclusions. Beside others, one aim is to initiate a fruitful discussion focusing on the formation and geometry of shear zones of deep-seated rock slides. Field observations focusing on rock mass failure processes of slides and conceptual considerations focusing on the formation of shear zones are presented. Emphasis is given on surface investigations based on mapping and monitoring methods and their ability to develop reliable 3D rock slide models for slope analyses and hazard assessments.

2 Field observations

Based on extensive investigation campaigns numerous case studies are characterized by the existence of fully persistent basal shear zones (e.g. Noverraz et al. 1996). The basal shear zone represents the geological/geomechanical layer between the rock slide mass and the in-situ bedrock below. Structurally, shear zones are heterogeneous and composed of fault breccias (kakirites) and gouges. The material is formed through cataclasis and rock fragmentation and is characterized by

soil-like mechanical and hydraulical properties. The thickness of shear zones can vary considerably whereby zones reaching a few decimeters to several tens of meters are observed. Often, inclinometer measurements show that the shear displacement takes place only in a narrow part of the shear zone, i.e. a result of strain localization. A more detailed description of the structure of shear zones can be found in Strauhal et al. 2017 (and references therein).

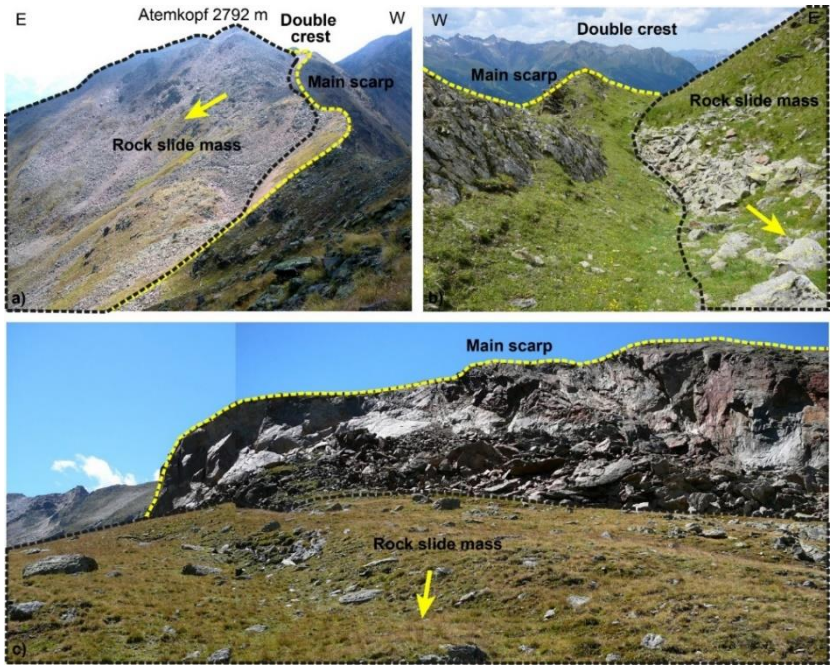

Figure 1. a) Main scarp and double–crested ridge at the Hochmais-Atemkopf rock slide (Kaunertal valley), with a shear offset between 20-50 m. A more detailed description of the case study can be found in Zangerl et al. 2010. b) Double-crested ridge with depression ("Nackental") at the Grastal rock slide (Ötztal valley), with a shear offset of several m. c) Highly active main scarp of the Marzellkamm rock slide (Ötztal valley), with a shear offset of about 10 m.

Often clear features of discrete shearing are exposed in the upper parts of rock slides, where in the scarp region the shear zones daylight due to the offset between the rock slide mass and the in-situ bedrock (Fig 1). In this area scarp planes (Figs. 1a,c) and/or double-/multi-crested mountain ridges ("mountain splitting", Figs. 1a,b) can be observed. Sometimes a discrete lateral boundary between the in-situ bedrock and the rock slide is exposed. In contrast, at topographically lower slope sections and landslide toe areas it is generally more difficult to obtain clear evidences of discrete shear zones. This is due to fragmentation and bulging of the slide mass, intensive rock deformations at the toe of the slope and potential interactions with alluvial valley sediments. In a majority of cases, shear zones are not exposed since they are covered by the rock slide mass itself, but also by slope debris, talus deposits and/or on-lapping debris flow deposits and/or alluvium. Under such circumstances, only subsurface investigations i.e. core drillings and boreholes equipped with inclinometer devices as well as investigation adits can provide reliable data to prove the existence of shear zones.

3 Discussion

Based on literature and on own observations numerous rock slide case studies show fully persistent basal shear zones. These represent "advanced" stages of slope deformation, where progressive rock failure processes resulted in the formation of shear zones. On the other hand, case studies without fully persistent basal shear zones, and thus indicating an early stage of slope failure and deformation, are rare (e.g. Zangerl and Prager 2008). There are only few comprehensively investigated and documented rock slides featuring a basal shear zone in the upper slope section, but without one in the lower slope section. Many of these case studies are characterized by deep-seated

flexural toppling processes where a basal shear zone has not or only partly developed (e.g. Zischinsky 1969).

However, it is assumed that numerous “rock slides” are representing an early stage of slope evolution characterized by only partially formed basal shear zones. This conclusion can be drawn because these slopes move downwards at very low velocities of only a few mm per year and the shear offset in the main scarp area is too small to form a fully persistent rupture surface at the base. According to the classification system by Hungr et al. (2014) these landslides would most likely correspond with the type termed “mountain slope deformation”. This type is characterized by large-scale gravitational deformations of steep and high mountain slopes, featuring scarps, benches, cracks, trenches and bulges, but lacking a fully defined rupture surface. The slope movement rates are typically extremely low and thus can often be detected/quantified only by long-term measurement campaigns. If a fully persistent shear zone has not formed up to now, the shear strain acting on the fractured rock mass was too small and/or strain localization did not occur. This raises some questions, e.g.:

- How much shear strain and slope deformation a fractured rock mass can absorb before the amount of strain localization is sufficient to generate a shear zone?
- How much offset between the rock slide mass and the in-situ rock is required in the scarp region for a fully persistent shear zone to have been formed?
- Can an empirical relationship be established between shear offset in the scarp region, the shear strain in the rock mass and the spatial extent of the basal shear zone?
- Is it possible to draw a conclusion about the existence of a fully or non-fully persistent shear zone without subsurface data but only from surface observations i.e. geological/geomorphological field mapping, analyses of digital elevation models and surface deformation monitoring data?

In mountainous regions worldwide, especially in densely foliated rock masses (e.g. phyllites, schists, paragneisses) thousands of deep-seated rock slides are encountered. For slope stability analyses and hazard/risk assessments there is a need to develop geometrical rock slide models and to characterize the spatial distribution of the (basal) shear zones. The geometry and internal structure of a rock slide has an essential impact on the slope stability, the kinematics, the temporal variable activity behavior and the hydrogeological situation of the landslide system.

However, except for rock slides affecting settlements and infrastructure facilities, usually there is no financial support to perform cost-intensive core drillings by which the existence of fully persistent shear zone can be proven. In other situations difficult rock slide terrain makes subsurface investigations challenging. Answering the listed questions above would facilitate hazard/risk assessment of rock slides, especially when studies for large and remote areas are needed. In addition, feasibility studies where preliminary 3D geometrical rock slide models are required may benefit from these fundamental considerations.

4 Reference list

Cruden, DM, Varnes, DJ. 1996. Landslide Types and Processes. In: Turner AK, Schuster RL (ed) Landslides: investigation and mitigation (Spec. Rep. 247), National Academy Press, Washington D.C., pp 36-75.

Hungr, O, Leroueil, S, Picarelli, L. 2014. The Varnes classification of landslide types, an update. Landslides 11, 167-194.

Noverraz F, (1996) Sagging or deep-seated creep: fiction or reality? In: Senneset (Ed.), 7th International Symposium on Landslides. Balkema, Rotterdam, pp. 821–828.

Strauhal, T, Zangerl, C, Fellin, W, Holzmann, M, Engl, D, Brandner, R, Tropper, P, Tessadri, R. 2016. Structure, Mineralogy and Geomechanical Properties of Shear Zones of Deep-Seated Rockslides in Metamorphic Rocks (Tyrol, Austria). Rock Mechanics and Rock Engineering, 50 (2), 419–438.

Zangerl, C, Prager C. 2008. Influence of geological structures on failure initiation, internal deformation and kinematics of rockslides. Proceeding of the 42nd U.S. Rock Mechanics Symposium / 2nd U.S.–Canada Rock Mechanics Symposium, San Francisco, ARMA 08-063, pp. 1–13.

Zangerl, C, Eberhardt, E, Perzlmaier, S. 2010. Kinematic behaviour and velocity characteristics of a complex deep-seated crystalline rockslide system in relation to its interaction with a dam reservoir. Engineering Geology 112, 53-67.

Zischinsky, U. 1969. Über Sackungen. Rock Mechanics, 1: 30-52.

Different stages of progressive failure in unstable rock slopes in Møre & Romsdal County, western Norway

Thierry Oppikofer[1*], Reginald L. Hermanns[1], Martina Böhme[1] and Aline Saintot[2]

[1] Geological Survey of Norway, Trondheim, Norway
[2] Ruhr University, Bochum, Germany
* thierry.oppikofer@ngu.no

1 Introduction

The valleys and fjords of western Norway are characterized by steep-walled, over-deepened glacial valleys. This Alpine relief, combined with the abundance of brittle and ductile bedrock structures, seasonal heavy precipitation, snow melting, frost cracking periods, and freeze-thaw cycles make many fjords and valleys of western Norway particularly prone to rock slope failures (Blikra et al. 2006). Many rock slope failures occurred shortly (i.e. 1000 to 3000 years) after deglaciation (Blikra et al. 2006; Böhme et al. 2015) and a large number of gravitational deformation structures were formed, possibly caused by the sudden unloading of the steep slopes due to glacial erosion and rapid glacial retreat. These gravitational deformation structures delimit unstable rock slopes, which by continuous deformation might lead to a catastrophic failure and form rock avalanches.

This study presents an inventory of 80 unstable rock slopes located in the Møre & Romsdal County in western Norway (Fig. 1), and investigates their different failure mechanisms and stages of progressive failure evolution. The term "unstable rock slopes" depicts slopes that show signs of significant post-glacial deformation (Hermanns et al. 2012). These investigations are part of the systematic mapping of unstable rock slopes in Norway made by the Geological Survey of Norway and financed by the Norwegian Water Resources and Energy Directorate (Hermanns et al. 2014).

2 Inventory of unstable rock slopes

The national database on unstable rock slopes in Norway (Oppikofer et al. 2015) provides the necessary data for this study. Most field investigations and analyses were made by the Geological Survey of Norway. These comprise geomorphological and engineering geological field mapping (structural measurements), kinematic failure mechanism analysis, periodic displacement measurements (using for example differential GPS, extensometers, but also satellite-based InSAR measurements and terrestrial cosmogenic nuclide (TCN) dating) and estimation of the along-slope elongation (ratio between total displacement and length of slope) (Oppikofer et al. 2017).

The investigated unstable rock slopes are very diverse in terms of failure mechanism, volume, total displacement, and state of activity, whereas the geology is relatively uniform. The study area is located in the Western Gneiss Region and thus mostly composed of various types of gneiss. Of the studied rock slopes, 66 are located in dioritic to granitic gneiss, 9 in augen gneiss, 4 in micaschist, and 1 in metabreccia. However, different structural settings (orientation of metamorphic foliation and other discontinuity sets) lead to very diverse movement types.

The classification of movement type and failure mechanism is based on a combination of international classifications by Hungr & Evans (2004) and Hutchinson (1988), as well as more specific types proposed by Brideau & Roberts (2015) and observations by the authors (for wedge slide along compound, complex surfaces). Tab. 1 shows that one third of the unstable rock slopes are planar slides, which often involve the gneiss foliation as sliding surface (Saintot et al. 2011). Toppling (21%), compound slides (18%) and wedge slides (15%) are also common. Thirteen percent of the unstable rock slopes are DSGSDs, which are generally not considered to be prone to fail in a single, massive rock avalanche event. Yet, many of these DSGSDs include localized instabilities, which in turn might lead

to a catastrophic failure. The volumes range from small instabilities with ~10000 m³ to large deep-seated gravitational slope deformations (DSGSDs) with up to 430 Mm³. Most unstable rock slopes involve volumes ranging between 0.1–1 Mm³ (41%) and 1–10 Mm³ (30%) (Fig. 1).

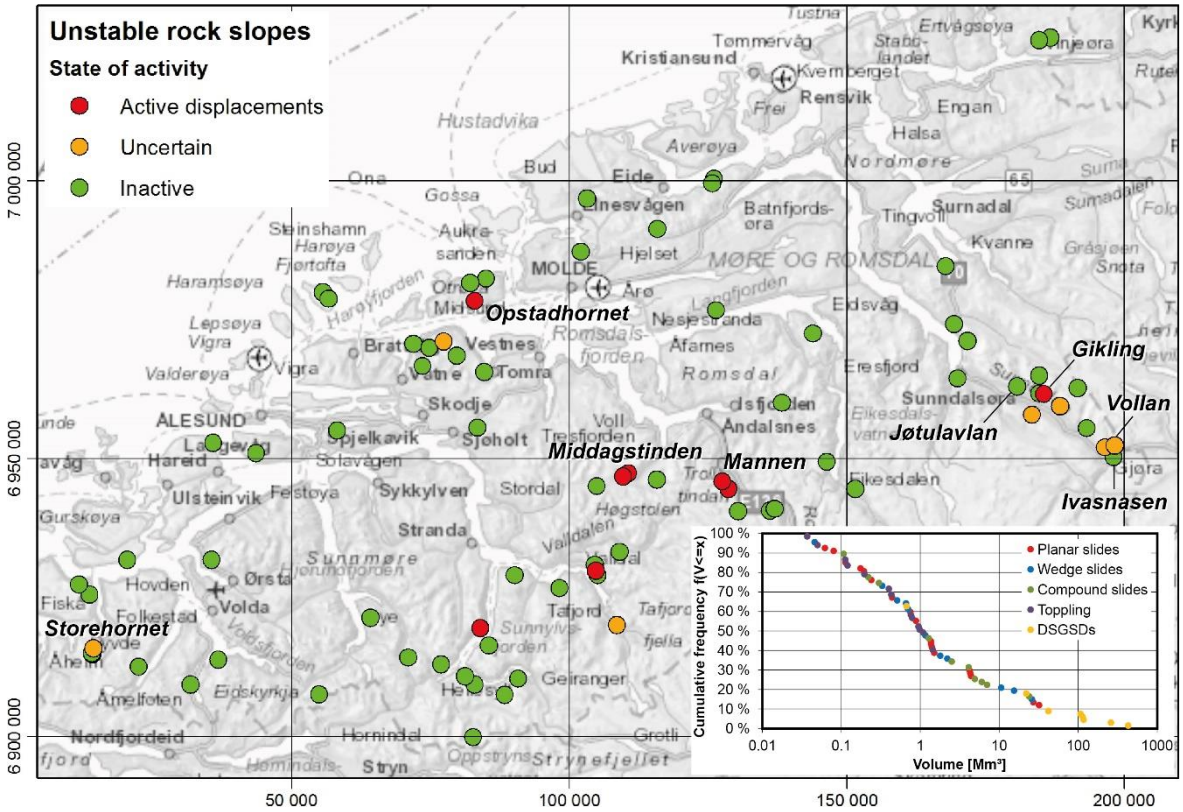

Figure 1. Map of investigated unstable rock slopes in Møre & Romsdal County (western Norway) including their state of activity (coordinates in UTM33N). The inset shows the cumulative frequency distribution of the volume of unstable rock slopes according to their movement type.

Most of the investigated unstable rock slopes in Møre & Romsdal County (65 sites) are at present (most likely with current data and knowledge) inactive (Fig. 1), but were active in the past. The Ivasnasen unstable rock slope, for example, was active ~3500 years ago (based on TCN dating) and is (most likely) inactive since (Oppikofer et al. 2017). Active slope movements are measured at 8 unstable rock slopes (or in smaller compartments of them at least) with velocities ranging from few mm/year to >10cm/year. The state of activity cannot be ascertained for the remaining 7 unstable rock slopes. This state of activity was assessed based on in-situ measurements for 26 unstable rock slopes and InSAR-data for 42 sites, while the remaining 12 sites were assessed solely based on geomorphologic observations and other signs of activity (rockfall, scars of past events, infilling of fractures etc.).

3 Total along-slope displacement and elongation

Regardless of the present state of activity, the total amount of displacements varies greatly between different unstable rock slopes and different movement types and failure mechanisms. While some planar slides for example have moved more than 10 m, other planar slides in similar geological and structural settings have failed catastrophically after less than 1.6 m of pre-failure displacements (Oppikofer et al. 2017). More complex failure mechanisms, such as the active 'wedge slides along compound, complex surfaces' of Opstadhornet and Middagstinden or the 'compound slide' of Storehornet, moved by several tens of meters without leading to a catastrophic failure. The DSGSDs of Gikling and Vollan show total displacements of more than hundred meters leading to division into many smaller compartments, and even to failure of frontal compartments. For Vollan the total along-slope displacement is estimated to ~200 m (Oppikofer et al. 2017). Unstable rock slopes with a

toppling mechanism have usually much smaller displacements (dm to few meters), which is inherent to this failure mechanism that usually affects smaller instabilities (see Fig. 1) and require thus less displacement prior to failure.

Table 1. Movement types of unstable rock slopes in Møre & Romsdal County based on geomorphologic observations and structural field measurements.

Movement main type	Movement subtype	Count		Percentage	
Planar slide	Planar slide (unspecified)	15	26	19	33
	Planar slide along single surface	9		11	
	Planar slide along stepped surface	2		3	
Wedge slide	Wedge slide (unspecified)	3	12	4	15
	Wedge slide along single surfaces	1		1	
	Wedge slide along compound, complex surfaces	8		10	
Compound slide	Compound slide (unspecified)	4	14	5	18
	Bi-planar slide	1		1	
	Topple-slide	7		9	
	Slide with toe outbreak	2		3	
Toppling	Toppling (unspecified)	10	17	13	21
	Toppling along single discontinuity set	2		3	
	Toppling along multiple discontinuity sets	5		6	
Slump without structural control		1	1	1	1
Deep-seated gravitational slope deformation		10	10	13	13

Relating these along-slope displacements to the total length of the slope yields the along-slope elongation, which serves as a proxy for comparing different sites, movement types and failure mechanisms (Jaboyedoff et al. 2012). The along-slope elongation is estimated to 28% for Vollan and at least 13% for Gikling (both DSGSDs), 6% for Opstadhornet, 15% for Middagstinden, and 16% for Storehornet (complex wedge slides and compound slides). For Ivasnasen (rockslide) the measured along-slope elongation is 14% and 2% for Jøtuavlan (toppling). These examples show that similar elongations can lead to very different total along-slope displacements depending on the failure mechanism.

4 Stages of progressive failure

Progressive failure of rock slopes is often described in three stages (e.g. Eberhardt et al. 2004, Stead et al. 2006): from the incipience of slope instability with the initial deformation of the rock mass, a secondary creep phase characterized by steady displacements of the rock mass and, finally, an acceleration phase leading to the failure of the rock slope.

Many unstable rock slopes in Møre & Romsdal County show only very small elongation (<2-3%) with only single open fractures at the back and little to no signs of internal deformation of the rock mass. Those sites are thus thought to be stabilized at an early stage of slope instability, and are stable under present-day conditions. For many cases it is supposed that the open fractures and other signs of deformation occurred shortly after deglaciation, when also most post-glacial rock slopes failures occurred (Böhme et al. 2015; Hermanns et al., in press).

Large elongations are measured for rock slopes that show signs of internal rock mass deformation with several open fractures, scarps, counterscarps and/or rockfall activity. Those slopes are thus likely in the creep stage of progressive failure, yet many slopes are also (most likely) inactive at present.

None of the studied unstable rock slopes (except a small compartment of the Mannen unstable rock slope; Skrede et al. 2015) presents signs of acceleration of displacements, which would indicate the final stage of progressive failure leading to the failure of the rock slope. Yet, it remains to determine

elongation values for different failure mechanisms, failure surface geometries and lithologies above which unstable rock slopes might reach this acceleration phase.

5 Conclusion and perspectives

The 80 unstable rock slopes in Møre & Romsdal County present a large variety of failure mechanisms, volumes and state of activity. Assessing the total along-slope displacement and the total elongation shows significant differences between the different failure mechanisms, but also different stages of progressive failure development.

This ongoing study aims therefore to assess the along-slope elongation for all unstable rock slopes in Møre & Romsdal County, and to relate these elongations to different stages of progressive failure development of unstable rock slopes with different failure mechanisms. Finally, the along-slope elongation might serve as a proxy in understanding an unstable rock slope and its evolution.

6 Reference list

Blikra, L.H., Longva, O., Braathen, A., Anda, E., Dehls, J.F., Stalsberg, K., 2006. Rock Slope Failures in Norwegian Fjord Areas: Examples, Spatial Distribution and Temporal Pattern. In: Evans, S.G., Scarascia Mugnozza, G., Strom, A., Hermanns, R.L. (eds.), Landslides from Massive Rock Slope Failure; NATO Science Series, IV. Earth and Environmental Sciences, vol. 49. Dodrecht, Netherlands: Springer, pp. 475–496.

Böhme, M., Oppikofer, T., Longva, O., Jaboyedoff, M., Hermanns, R.L., Derron, M.-H., 2015. Analyses of past and present rock slope instabilities in a fjord valley: implications for hazard assessment. Geomorphology 248, 464–474.

Brideau, M., Roberts, N.J., 2015. Mass Movement in Bedrock. In: Davies, T. (ed.), Landslide Hazards, Risks, and Disasters, Elsevier, pp. 43–90.

Eberhardt, E., Stead, D., Coggan, J.S., 2004. Numerical analysis of initiation and progressive failure in natural rock slopes - the 1991 Randa rockslide. Int.J.Rock Mech.Min.Sci. 41, 69–87.

Hermanns, R.L., Oppikofer, T., Anda, E., Blikra, L.H., Böhme, M., Bunkholt, H., Crosta, G.B., Dahle, H., Devoli, G., Fischer, L., Jaboyedoff, M., Loew, S., Sætre, S., Yugsi Molina, F.X., 2012. Recommended hazard and risk classification system for large unstable rock slopes in Norway. NGU report 2012.029, Geological Survey of Norway, Trondheim, Norway, 49 p.

Hermanns, R.L., Oppikofer, T., Yugsi Molina, F., Dehls, J., Böhme, M., 2014. Approach for Systematic Rockslide Mapping of Unstable Rock Slopes in Norway. In: Sassa, K., Canuti, P., Yin, Y. (eds.), Landslide Science for a Safer Geoenvironment. Springer International Publishing, pp. 129–134.

Hermanns, R.L., Schleier, M., Böhme, M., Blikra, L.H., Gosse, J., Ivy-Ochs, S., Hilger, P., in press. Rock-avalanche activity in W and S Norway peaks after the retreat of the Scandinavian ice sheet. Proceedings of the 4th World Landslide Forum, Ljubljana, Slovenia.

Hungr, O., Evans, S.G., 2004. The Occurrence and Classification of Massive Rock Slope Failure. Felsbau 22(2), 16–23.

Hutchinson, J.N., 1988. General report: Morphological and geotechnical parameters of landslides in relation to geology and hydrogeology. Proceedings of the 5th International Symposium on Landslides. Rotterdam: Balkema, pp. 3–35.

Jaboyedoff, M., Derron, M.-H., Pedrazzini, A., Blikra, L.H., Crosta, G.B., Froese, C.R., Hermanns, R.L., Oppikofer, T., Böhme, M., Stead, D., 2012. Fast assessment of susceptibility of massive rock instabilities. In: Eberhardt,E.; Froese,C.; Turner,A.K.; Leroueil,S. (eds.) Landslides and Engineered Slopes: Protecting Society through Improved Understanding. London: Taylor & Francis Group, pp. 459-465.

Oppikofer, T., Nordahl, B., Bunkholt, H., Nicolaisen, M., Jarna, A., Iversen, S., Hermanns, R.L., Böhme, M., Yugsi Molina, F.X., 2015. Database and online map service on unstable rock slopes in Norway - from data perpetuation to public information. Geomorphology 249, 69–81.

Oppikofer, T., Saintot, A., Hermanns, R.L., Böhme, M., Scheiber, T., Gosse, J.C., Dreiås, G.M., 2017. From incipient slope instability through slope deformation to catastrophic failure – different stages of failure development on the Ivasnasen and Vollan rock slopes (western Norway). Geomorphology, in press, doi:10.1016/j.geomorph.2017.03.015.

Saintot, A., Henderson, I.H.C., Derron, M.-H., 2011. Inheritance of ductile and brittle structures in the development of large rock slope instabilities: examples from western Norway. In: Jaboyedoff, M. (ed.), Slope Tectonics, Geological Society Special Publications 351. London: Geological Society, pp. 27–78.

Skrede, I., Kristensen, L., Hole, L., 2015. Geologisk evaluering av Veslemannen. NVE rapport 41/2015, Norwegian Water Resources and Energy Directorate, Oslo, Norway, 34 p. (in Norwegian).

Stead, D., Eberhardt, E., Coggan, J.S., 2006. Developments in the characterization of complex rock slope deformation and failure using numerical modelling techniques. Eng.Geol. 83, 217–235.

Estimation of the stress tensor across a stimulated fault zone in the Opalinus Clay, Mont Terri rock laboratory

Christophe Nussbaum[1*], Yves Guglielmi[2], David Jaeggi[1] and Paul Bossart[1]

[1] Swiss Geological Survey, swisstopo, Switzerland
[2] Earth and Environmental Sciences Area, Lawrence Berkeley National Laboratory, USA

* christophe.nussbaum@swisstopo.ch

We present results from a decametre-scale, controlled field stimulation experiment (the FS experiment dedicated to the hydro-mechanical characterisation of in-situ clay fault slip) conducted in a natural fault zone at an overburden depth of 300 m. This experiment was realised in the Mont Terri underground rock laboratory located in the northwestern part of the Jura thrust-and-fold belt of the Alpine foreland (Bossart et al. 2017). The stimulated fault, called the "Main Fault", consists of a 1-5 m-wide N140°-dipping, 50-to-60°SE thrust zone intersecting the Opalinus Clay, an overconsolidated shale formation deposited around 174 Ma (Aalenian/Toarcian). The Main Fault corresponds to a third-order structure interpreted as a blind shear fault bend fold that is detached from the top of the underlying Staffelegg Formation in the hanging wall of the Mont Terri anticline (Nussbaum et al. 2017). We measured fault slip and seismicity induced by fluid-injection in four test intervals distributed in the damage zone and within the core of the Main Fault (Fig. 1A, 1B). Passive seismic monitoring was coupled to a new downhole probe (Guglielmi et al. 2013) that allowed us to conduct high flowrate injections while synchronously recording pressures, flowrate, and the full 3D displacement tensor of induced deformation of the borehole wall and of reactivated slip across the naturally fractured straddle zone (Fig. 1C).

The FS experiment aims at understanding (i) conditions for slip activation and stability of clay faults, and (ii) evolution of the coupling between fault slip, pore pressure, and fluid migration. Results obtained by the experiment are crucial to define mechanisms of natural and induced earthquakes, their precursors and earthquake risk assessment, in addition to providing information on the loss of integrity of natural low-permeability barriers, all important for safety assessment of deep geological repositories of radioactive wastes or CO_2 sequestration.

Four injection tests were conducted: beneath (test 47.2 m), within (test 44.65 m), and above (tests 40.6 m and 37.2 m) the Main Fault core in both boreholes BFS-1 and BFS-2 (see Fig. 1B, interval names refer to their respective depth from the tunnel floor). In addition, a packed-off interval across the upper boundary of the Main Fault at 37.65 m in borehole BFS-1 was designated as a monitoring point using the same deformation probe. Test 37.2 m is the furthest from the fault core and was conducted in mostly intact rock affected by a few polished and striated <10 m-long secondary faults. Test 40.6 m exhibits subparallel faults that may be considered as reactivated bedding surfaces in the damage zone close to the fault core. Test 47.2 m is in a more sparsely fractured zone comparable to the fracture zone at test 37.2 m. We used the following procedure in each test interval: 1) we hydraulically activate the packer inflation from the surface using water conveyed in flexible hoses; 2) then we attach the 3D deformation cage to the borehole wall by oil-pressure actuators, also supplied from the surface (Fig. 1C); and 3) we inject artificial pore-water into the chamber after opening the downhole gage. During the tests, injection pressure is controlled by a surface-mounted pump, while flow-rate, injection chamber pressure, and displacement variations are synchronously monitored at the injection interval and at the 37.65 m monitoring interval. We demonstrated that a 0.4 mm fault slip could be triggered and continuously monitored while the pore pressure was increased by ca. 2.0 MPa above the initial pressure exhibited by the Main Fault (Figs. 1A–C). We also observed that an exponential permeability increase from 10^{-17} to 10^{-13} m^2 occurred in the fault and interpret this to

be associated to creep, episodic slow slip of the fault, and a low magnitude earthquake swarm (Guglielmi et al. 2016).

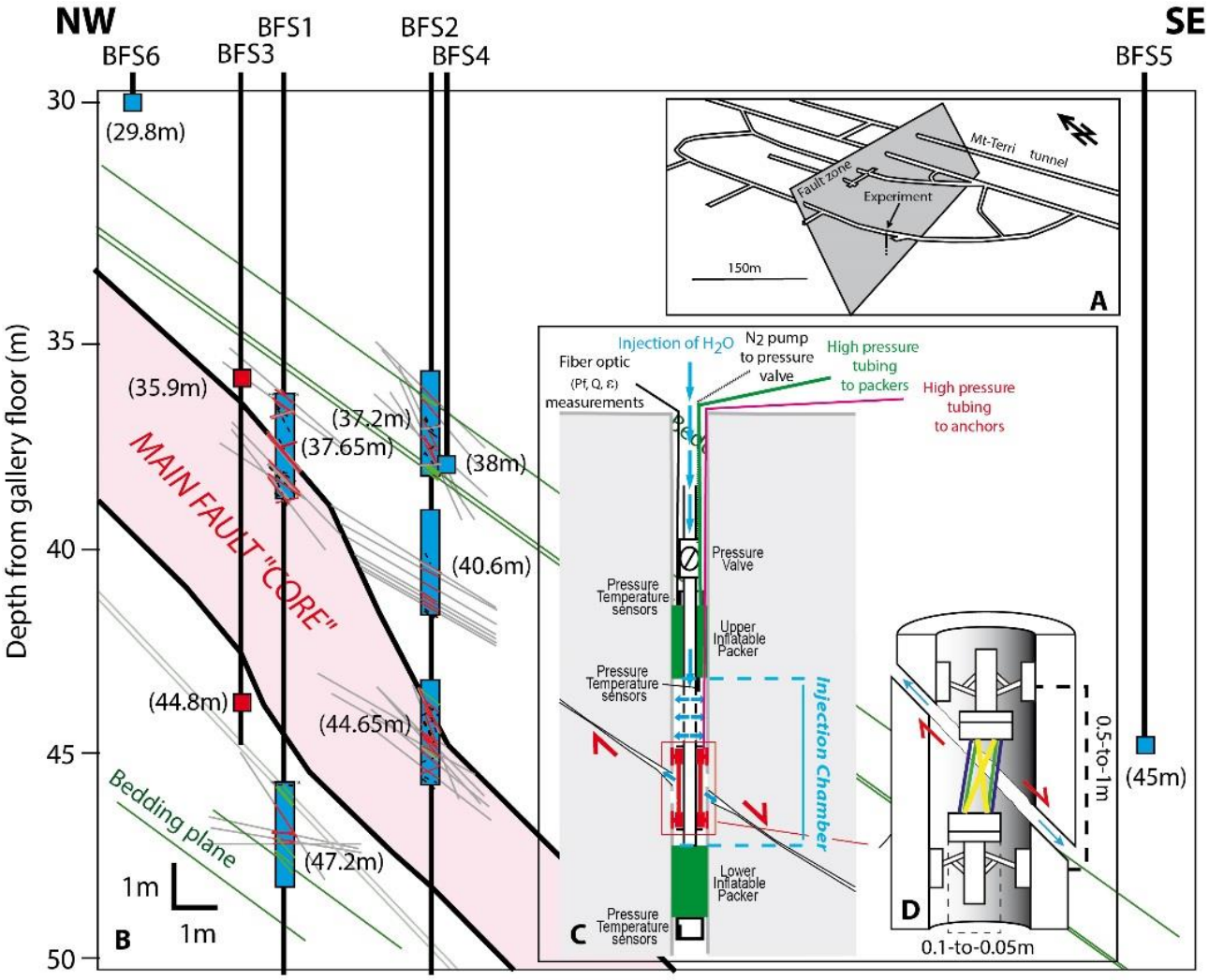

Figure 1. A) 3D view of the Main Fault plane with the location of the FS experiment in the Mont Terri underground rock laboratory. (B) Simplified cross section of the Main Fault with the blue rectangles indicating the location of the five packed-off sections. (C) Test equipment setup; (D) Schematic view of the 3D deformation unit.

Using slip-tendency analysis and “3DEC” numerical software that together enable a fully coupled hydromechanical modelling, we estimate the variability of the stress tensor across the fault zone by fitting the measured 3D displacement vectors with the fault-plane geometry described by optical image logging and drillcore mapping. The three injections made outside the Main Fault core produced mainly opening normal to discrete fault planes with a small shear component. Therefore, these tests provide a precise measurement of the normal stress acting on the activated discontinuities (4.17 MPa). In turn, the orientation of the stress tensor is not well constrained (i.e. the maximum horizontal stress varies between N310 and N340, depending primarily on the orientation of the activated fault planes). The results imply an extensional stress regime for all four tests across the fault zone, in good agreement with the commonly accepted stress tensor for the Mont Terri rock laboratory (Martin & Lanyon 2003). To completely define the stress tensor, we need to adapt the magnitudes to fit the measured displacements and fault hydraulic opening pressures.

Rupture processes within and at the top boundary of the Main Fault are more complex. During injection into the test chamber at 40.6 m in borehole BFS-2, a hydraulic connection with the neighbouring borehole BFS-1 was evidenced by a pressure increase in the monitoring chamber at 37.65 m located ca. 3 m from the injection source. The injection produced a displacement reaching ca. 1 mm

captured by the monitoring probe centred at the top boundary of the Main Fault. We interpret these data as the result of the activation of a minimum of two discrete fracture planes: N43/32E and N50/60E, connecting both test chambers. We explain the measured displacement vectors as propagation of a rupture front along the fault plane oriented N43/32E connecting the test chamber at 40.6 m in the damaged zone to the Main Fault. The rupture is amplified when the fluid pressure wave reached the Main Fault, initially characterised by a reverse displacement and afterwards by a normal reactivation along a N50/60E Main Fault shear plane. This transition over time from reverse to normal movement along the same fault segment might be explained by the propagation of the deformation front with higher shear stress ahead of the area where stresses have been released in association with fluid pressures. Subtle variations of the 3D displacement vectors measured by the deformation-monitoring probe might reveal permeability fluctuations generating small variations of normal stress acting on the reactivated fault planes (on the order of 0.2 to 0.3 MPa). We argue that these variations are sufficient to induce very local changes in the stress regime on the same fault because the deviatoric stress magnitude is low at the shallow depths of this experiment. Thus, the measured pore-pressure oscillations may indicate complex and weak stress variations apparently large enough to trigger slow movement on a fault that is close to a critical state of stress. Our data tend to show clear dynamic stress transfer effects and complex hydromechanical coupling that induce a highly complex fault reactivation. Nevertheless, our approach allows us to consider in greater details the structural complexity of a fault-zone architecture that appears to strongly condition its stability.

Reference list

Bossart, P, Bernier, F, Birkholzer, J, Bruggeman, C, Connolly, P, Dewonck, S, Fukaya, M, Herfort, M, Jensen, M, Matray, JM, Mayor, JC, Moeri, A, Oyama, T, Schuster, K, Shigeta, N, Vietor, T, Wieczorek, K. 2017. Mont Terri rock laboratory, 20 years of research: introduction, site characteristics and overview of experiments. Swiss J. Geosci. DOI 10.10077/s00015-016-0236-1.

Guglielmi, Y, Cappa, F, Lançon, H, Janowczyk, JB, Rutqvist, J, Tsang, CF, Wang, J. 2013. Estimation of permeability, elastic and friction properties of fractured rock masses from in situ hydromechanical testing: the High-frequency Pulse Poroelasticity Protocole (HPPP) testing method. Submitted contribution to the ISRM Commission on Testing Methods, Int J Rock Mech Min Sci and Geomech Abstr special issue.

Guglielmi, Y, Birkholzer, J, Ruqvist, J, Jeanne, P, Nussbaum, C. 2016, Can fault leakage occur before or without reactivation? Results from an in situ fault reactivation experiment at Mont Terri, 13th International Conference on Greenhouse Gas Control Technologies (Lausanne, Switzerland, Nov. 14–18 2016).

Martin, CD, Lanyon, GW. 2003. Measurement of in-situ stress in weak rocks at Mont Terri Rock Laboratory, Switzerland. International Journal of Rock Mechanics & Mining Sciences, 40, 1077–1088.

Nussbaum, C, Kloppenburg, A, Caër, T, Bossart, P. 2017. Tectonic evolution around the Mont Terri rock laboratory, northwestern Swiss Jura: constraints from kinematic forward modelling. Swiss J. Geosci. DOI 10.1007/s00015-016-0248-x.

Evolution and progressive failure of the Preonzo rock slope instability complex (TI, Switzerland)

Sophie Gschwind[1*],Simon Loew[1] and Andrea Wolter[1]

[1] Engineering Geology, Department of Earth Sciences, ETH Zurich, Switzerland
* sophie.gschwind@erdw.ethz.ch

1 Introduction

Fracture and joint patterns in the source areas of rock slope instabilities are often analyzed with structural and kinematic analysis, which has traditionally been considered an important component of pre-disposition and displacement studies prior to failure of such mass movements. These analyses are based on the assumption that fractures are fully persistent and that available surface outcrops represent the statistical conditions of fractures at depth, especially at the elevation of basal rupture planes. However, we have observed several cases where kinematic analyses from surface outcrops are ambiguous, or even misleading regarding kinematic feasibility. An impressive example of such a case is the 2012 Preonzo rock slope failure, where pre-failure kinematic analyses could not explain the observed slope movements and where we have the possibility to compare in detail the pre-failure kinematic analyses with the actual properties of the failed rock mass in the head scarp area and the basal rupture plane. As Terzaghi (1962) and others suggested, for an explanation of the temporal behavior of natural rock slope failures, the interaction between existing natural discontinuities and brittle rock fracture propagation through intact rock bridges must be considered. Failure of a rock mass along complex failure surfaces additionally requires internal deformation of the unstable rock mass body; internal damage accumulates and shear planes develop through progressive failure (Eberhardt et al. 2004). At the Preonzo rock slope instability complex, such rupture planes from different failure events can be analyzed in detail which gives an insight into the structural evolution and progressive failure of brittle rock slope instabilities in time and space.

2 The Preonzo rock slope instability

The Preonzo rock slope instability complex is located on the western slope of the Riviera valley in Ticino, southern Switzerland, above the village Preonzo. The head scarp of the active instability is situated at 1520 m a.s.l., at Alpe di Roscera. The instability complex is made up of crystalline units of the Simano nappe (Penninic domain) and is composed of amphibolitic gneisses and augengneisses that dip about 20-25° to the WSW into the slope, as already described by Willenberg et al. (2009). Over the last 25 years, progressively evolving tension cracks in the head scarp area and displacements of the rock face exposed below these tension cracks were systematically monitored, especially during a phase of increasing rockfall activity and elevated displacement velocities occurring over the last 15 years. The current period of activity comprises three events. In 2002 the first collapse of a significant rock mass of about 150’000 m^3 took place, whereas in 2010 only a small portion of the instability complex failed with about 25’000 m^3. Both events followed periods of heavy rainfall. The most recent event took place in May 2012 (Fig. 1), when about 210’000 m^3 of unstable rock failed in two catastrophic events and exposed the present complex rupture plane. This event was not a total collapse: in the S, a volume of about 120‘000 m^3 of unstable rock remained in place (Figs. 1 and 4). This period of activity was noticed for the first time in 1989, when the opening of a tension crack on the Alpe di Roscera was reported. But in retrospect, already 25 years prior to that, this tension crack can be recognized on aerial images. Crack propagation as visible on these aerial images was analyzed in detail in Gschwind & Loew (2016). Active monitoring of crack opening was started from 1990 on, with an increasing degree of sophistication, with crack meters, reflectors measured by a robotic total station and ground based radar interferometry. Loew et al. (2017) described the operated monitoring system in detail.

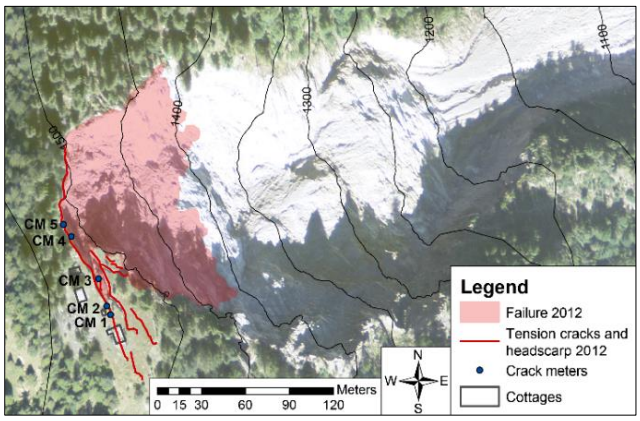

Figure 1. Situation of the headscarp area after the 2012 failure. The extent of the 2012 event is shown in light red and the tension cracks (forming the headscarp in the N) and crack meter locations are indicated in red and blue.

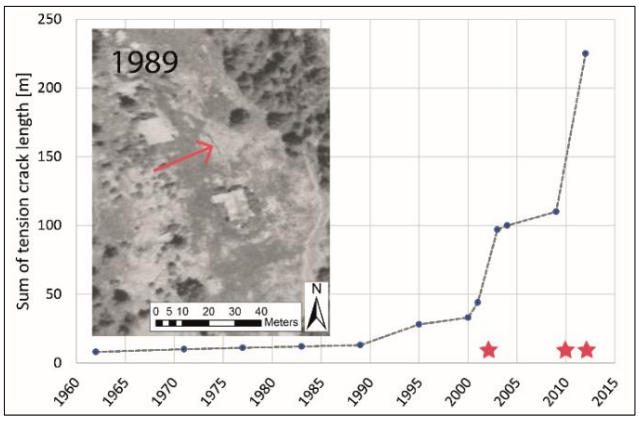

Figure 2. Sum of visible tension crack length from aerial images since 1960 with an example of an aerial image from 1989 (Swisstopo, 2015). The red stars indicate the three events within the actual period of activity.

3 Structures and displacements before the 2012 event

In the area around the instability, four systematic joint sets could be identified. The dominant sets dip steeply with the slope to the E and W and a third set steeply dips to the N. The fourth set is cleavage-parallel and dips about 20-25° to the WSW. Beside these joint sets only a few individual unsystematic joints were measured. The tension cracks at Alpe di Roscera are mainly oriented parallel to the mean slope and share the orientations of the two steeply dipping joint sets to the E and W. Before the 2012 event, only small parts of the tension cracks showed different orientations and the depth was estimated to be more than 10 m.

The analysis of several available aerial images documents a system of tension cracks that continuously grew since the 1960s. The sum of the visible tension crack length, visible on aerial images, is shown in Fig. 2. Whereas the crack length increased steadily until 1989, accelerated crack growth is observed from 1990 on. From 1998 on crack meters were installed that measured the continuous opening of the tension crack. Fig. 3 shows the progressive tension crack opening from 2002 until the most actual event in May 2012. A continuous increase in crack opening velocity can be seen; heavy precipitation provoked short-term acceleration followed by deceleration to antecedent or slightly higher velocities (Loew et al. 2017). After the partial failure in 2012, the movement of the remaining unstable rock mass decreased again to steady displacement rates of less than one cm per year.

4 Structures after the 2012 event

4.1 Discontinuity pattern after the 2012 event

After the 2012 event, the extent and orientation of the tension cracks became clearly visible and the complex rupture surface was exposed. The tension cracks show two main orientations (visible in Fig. 1). They can be related to the steeply E-dipping joint set, and the shorter E-W striking parts, which are shear-dominated, can be related to the steeply N-dipping joint set. Whereas the geometry of the tension cracks can be explained by the mapped systematic joint sets, the geometry of the failure surface below could not be predicted. The complex rupture surface was analyzed by means of photogrammetric elevation models that allowed a detailed mapping of the discontinuities building up the rupture surface. On a macroscale, the failure surface below the tension cracks shows a quite distinct, planar geometry, which dips 45-50° to ENE. On a small scale, the basal failure surface shows a complex stepped structure. There are no persistent discontinuities with consistent orientations for sliding. Whereas the systematic joint sets mapped close to the head scarp on Alpe di Roscera are also visible in the basal rupture plane, many new discontinuities dipping less steeply and favorably oriented for sliding, occur within the basal rupture plane. Almost no discontinuities with

this orientation were encountered in the surrounding areas before the event, whereas about one third of the mapped discontinuities in the 2012 rupture plane dip with 25-60°with the slope (± 40° dip direction).

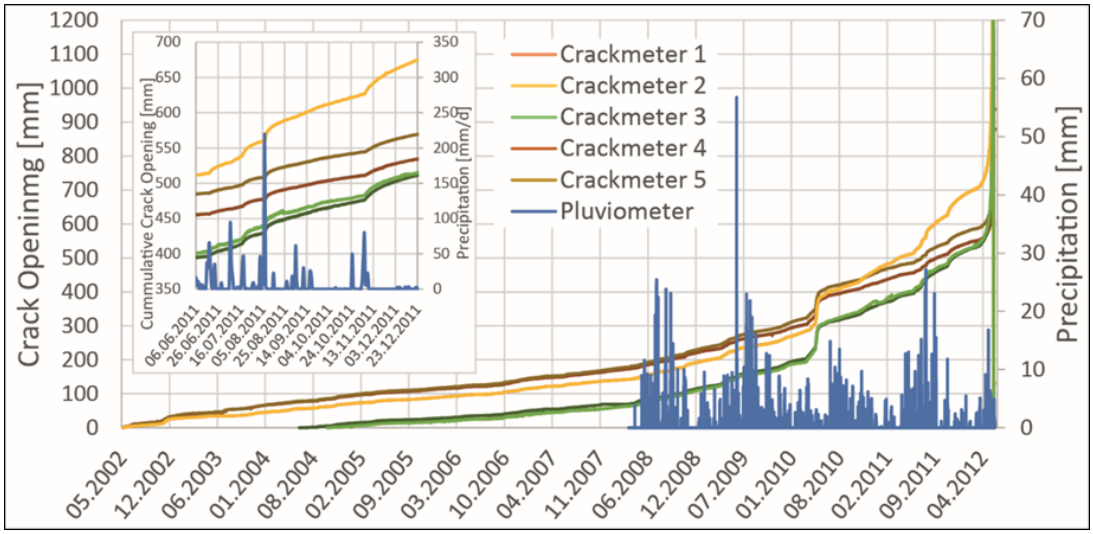

Figure 3. Opening of the tension crack in the headscarp area from 2002 until the 2012 event, continuously measured by crack meters, with zoom into a period of heavy rainfalls and related short-term acceleration.

4.2 Detailed insights into the 2012 rupture plane

In the exposed rupture plane of the 2012 event, several areas are visible that show unweathered, fresh looking areas of stepped, broken rock. In Fig. 4, the remaining unstable block is shown and these areas of unweathered, broken rock are indicated in light blue. We interpret these areas as evidence for the failure of rock bridges that generate newly oriented discontinuities corresponding to the gravitational stresses acting in the unstable rock mass and influencing the kinematics of the rock slope instability. Whereas such failed rock bridges can be identified quite clearly in the steep and tensile portion of the 2012 rupture plane, this is much more difficult along the basal sliding plane, which is partially covered by debris. Some of the discontinuities in the basal rupture plane show a slight roughness because of small steps within the discontinuities (visible in Fig. 5), descending with the slope, which is an indicator for an overall shear-dominated failure through tensile failure of rock bridges, generating these steps, as described by Jennings (1970) and others.

5 Discussion

The evolution of the mapped tension crack length and measured crack opening on the Alpe di Roscera are indications for progressive crack propagation and degradation of the rock mass strength at the Preonzo instability complex. As shown in Loew et al. (2017), until end of March 2012, the displacement evolution can be well reproduced with lab-based creep models, after filtering data from variations in external loading conditions (strong rain fall events, secondary slope failures). Two weeks before failure, a dramatic acceleration occurred that is only partially controlled by variations in external loading conditions. This transition from creep to failure might correspond to a transition from stable to unstable crack propagation. As displacements during the many years before failure mainly occurred in the head scarp area, it is suggested that the fresh tensile rock bridges observed in the head scarp area (Fig. 4) mainly formed through stable crack propagation driven by cyclic variations in water content, pore pressure and/or temperature. As shown by ground-based radar measurements, the rocks at the future base of the unstable landslide did not show significant movements until April 2012. It is therefore hypothesized that progressive deformation in the upper landslide parts gradually increased stress levels at the landslide base until unstable crack propagation through intact blocks lead to catastrophic failure. The analysis of this exposed rupture surface allows

us to explain the mechanisms of such a failure in much more detail than could be done prior to the event.

Figure 4. Photograph of the remaining block (after 2012 event) from below. The right edge of the image shows the main tension crack, which forms the headscarp of the 2012 event, whereas to the left, the remaining hanging block is visible with large areas of freshly broken rock surfaces, indicated in light blue.

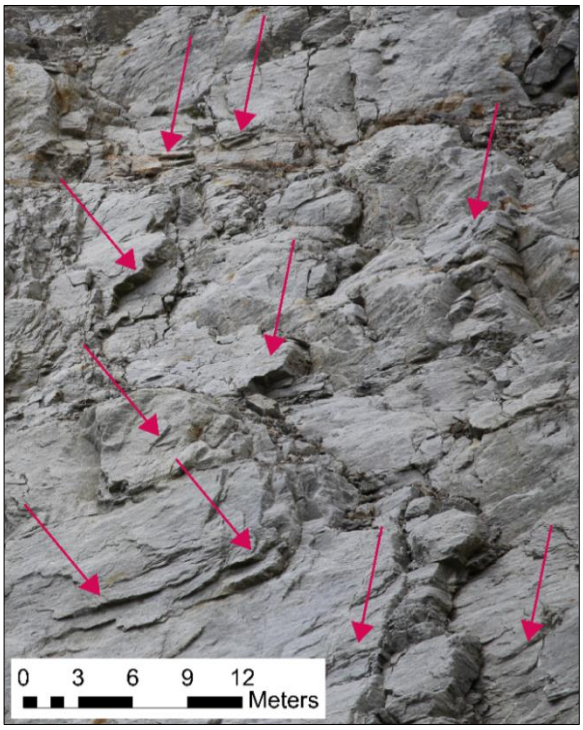

Figure 5. Photograph of the rupture plane near the lower instability boundary of the 2012 failure. The discontinuities show some roughness because of small steps within the discontinuities. Areas containing such steps are highlighted with red arrows.

6 Reference list

Eberhardt, E, Stead, D, Coggan, J. S. 2004. Numerical analysis of initiation and progressive failure in natural rock slopes—the 1991 Randa rockslide. International Journal of Rock Mechanics and Mining Sciences, 41 (1), 69-87.

Gschwind, S, Loew, S. 2016. Reconstruction of the long-term evolution of a catastrophic slope failure at the Preonzo rock slope instability complex (TI, Switzerland). In Stefano Aversa et al. (eds.), Landslides and Engineered Slopes. Experience, Theory and Practice, Proceedings of the 12th International Symposium on Landslides, Napoli, Italy, 12-19 June 2016. CRC Press.

Jennings, J. E. 1970. A mathematical theory for the calculation of the stability of slopes in open cast mines. In Planning Open Pit Mines, Proceedings, Johannesburg, 21 (2), 87-102.

Loew, S, Gschwind, S, Gischig, V, Keller-Signer, A, Valenti, G. 2017. Monitoring and early warning of the 2012 Preonzo catastrophic rockslope failure. Landslides, 14 (1), 141-154.

Swisstopo, Geocatalog, map.geo.admin.ch, 2015.

Terzaghi, K. 1962. Stability of steep slopes on hard unweathered rock. Geotechnique, 12 (4), 251–270.

Willenberg, H, Eberhardt, E, Loew, S, McDougall, S, Hungr, O. 2009. Hazard assessment and runout analysis for an unstable rock slope above an industrial site in the Riviera valley, Switzerland. Landslides, 6 (2), 111-119.

Preliminary results of vibration modes induced by forced dynamic shaking in a quarry rock wall

Danilo D'Angiò[1*], Matteo Fiorucci[1], Luca Lenti[2], Salvatore Martino[3] and Antonella Paciello[4]

[1] Department of Earth Sciences, "Sapienza" University of Rome, Piazzale A. Moro, 5 - I-00185 Rome, Italy
[2] French Institute of Science and Technology for Transport, Development and Networks (IFSTTAR) - Paris East University, 58 Boulevard Lefebvre, F-75732 Paris Cedex 15, France
[3] Department of Earth Sciences, "Sapienza" University of Rome and Research Center for Geological Risks (CERI), Piazzale A. Moro, 5 - I-00185 Rome, Italy
[4] Italian National Agency for New Technologies, Energy and Sustainable Economic Development, (ENEA) - Casaccia Research Center - Via Anguillarese 301, I-00123, Rome, Italy
* danilo.dangio@uniroma1.it

1 Introduction

Rockslides are one of the most hazardous natural events, because of their velocity and rarely detectable precursors. Possible strategies to prevent the risk associated to these events consist in: a) studying the gradual creep-driven deformation of rock mass by setting a proper monitoring system (Loew et al. 2016); b) realizing numerical models also considering progressive failure of rock slopes (Eberhardt et al. 2004); c) coupling microseismic monitoring systems and numerical models, taking in account rock mass damage during time (Xu et al. 2014; Tang et al. 2015); d) analyzing variations of ambient noise as indicators of imminent failure (Got et al. 2010; Lévy et al. 2010).

To investigate long term rock mass deformations due to temperature, wind and rainfalls, the abandoned Acuto quarry rock wall (Frosinone – Central Italy) was selected in Autumn 2015 as test site for the installation of a multi-sensor monitoring system on a rock block prone to failure. The experimental site is included in the carbonatic Monti Ernici ridge. More in particular, Mesozoic wackestone with rudists crops out on the sub-vertical quarry wall with a height ranging from 15 m up to 50 m (Accordi et al. 1986). A geomechanical characterization of the rock mass led to the recognition of four joint sets, here indicated according to dip direction/dip convention: S0 (130/13) corresponding to the limestone strata, S1 (270/74), S2 (355/62) and S3 (190/64) (Fantini et al. 2016). The monitored sector is located in the NW portion of the 500 m long quarry front, which is characterized by the presence of a 64 m^3 densely cracked protruding block, separated from the back quarry wall by a main fracture. The multi-sensor monitoring system consists in two weather stations with air-thermometer, hygrometer, pluviometer and anemometer for wind speed and direction, installed at foot and top of the slope wall, one thermometer for the rock mass temperature, six strain-gauges installed on micro-fractures of the rock mass, four extensimeter installed on open fractures and one optical device. Moreover, a railway track was reproduced near the rock mass, to simulate a real rockfall hazard scenario (Fig. 1).

2 Field experiments

In the Acuto quarry test site, experimental activities took place on July 2016, with the aim of evaluating the vibrations induced in the rock mass by antrophic sources, such as railway traffic. In particular, these experiments consisted in stimulating the rock mass by a vibrodyne, an electro-mechanical excitation device which is able to produce vibrations at fixed frequency and amplitude, to induce stress-strain effects under controlled conditions. During the experiments, the monitoring system was implemented with the installation of a Seismic Navigation System (SNS) array, a ground-based radar able to acquire data both in Real Aperture Radar (RAR) and Synthetic Aperture Radar (SAR) modality and six monoaxial Kinemetrics FBA11 accelerometers cable-connected with a datalogger Kinemetrics K2; the datalogger was provided with an internal tri-axial accelerometer and was set

with a sampling frequency of 250 Hz. Location and ID number of the accelerometers are shown in Fig. 1a-b.

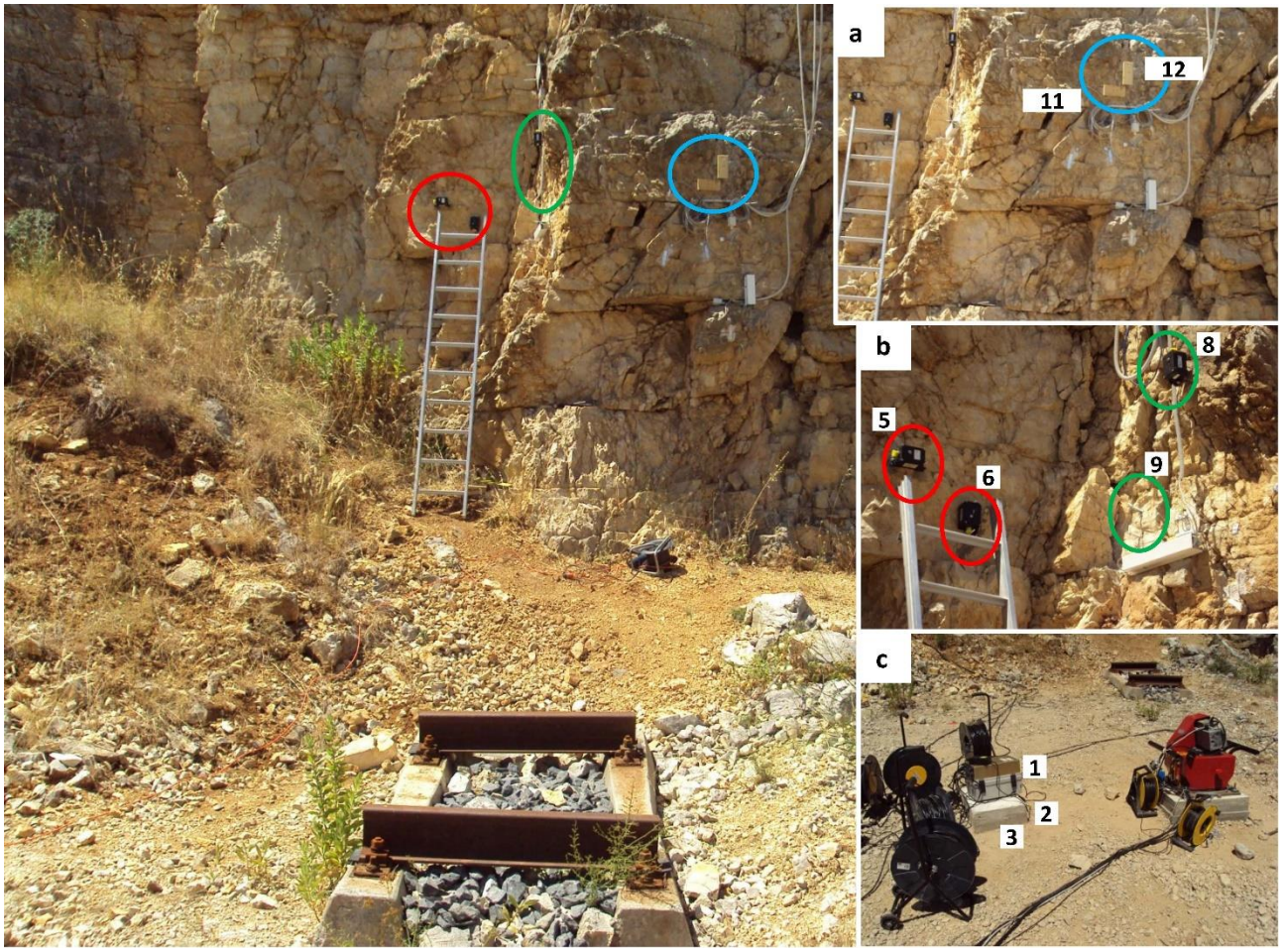

Figure 1. Photographs of the monitored sector of the abandoned Acuto quarry. A railway track was reproduced to simulate rockfall hazard scenario. Positioning and ID number of the accelerometers is shown: in a) on the block front side (blue circle); in b) on the block lateral side (green circles) and on the rock wall (red circles). In c) is shown the vibrodyne (right side) and the datalogger K2 (left side). Photos by Danilo D'Angiò.

2.1 Dynamic tests: preparation and experimental phases

Two concrete bases, spaced 2 m among them, were realized about 8 m far from the rock block and 5 m far from the railway target, to fix the vibrodyne and the accelerometric datalogger. Since the concrete bases were jointed to the underneath bedrock, the vibration produced by the vibrodyne can be considered as completely transmitted to the rock mass wall.

The FBA11 accelerometers were installed partly on the quarry wall and partly on the prominent block; in particular: 2 on the rock wall, 2 on the block lateral side, and 2 on the block front side (Fig. 1).

Such a distribution was chosen to record the effects induced by the controlled vibration at different measurement points and to output different responses among sensors located on the protruded rock block and on the back rock wall. In this way it was also possible to compare the energy content of the input close to the vibrodyne-source (internal K2 accelerometer), with the one recorded on the rock mass.

According to Joswig (2008), a SNS array, devoted to nanoseismic recording of low to very-low intensity vibrations, was installed about 50 m far from the monitored sector, with the aim of locating possible micro-seismic events. This array is constituted by a central three-component station and three vertical-component stations, spaced among them of 120°, at a radial distance of 25 m from the

central station. Each measurement station included one LE-3Dlite MkII seismometer (Lennartz Electronic GmbH) and one REFTEK 130-01 datalogger set at a sampling frequency of 500 Hz.

All the installed devices were set to record data in continuous mode. First of all, undisturbed tracks were recorded (i.e. without anthropic disturbance); in the following, six shaking sequences by the vibrodyne were generated at different frequencies (5 Hz, 10 Hz, 15 Hz, two to 20 Hz and 25 Hz) and time duration (40, 25, 17, 13, 26, 6 minutes respectively). After each shaking sequence the experiment was interrupted for at least one hour, to restore undisturbed vibrational conditions on the rock wall.

2.2 Data analysis

Preliminary spectral and time-frequency analyses have been performed by Geopsy software (www.geopsy.org) to compare the records obtained close to the vibrodyne with the ones obtained on the rock block during the vibrational sequences. The Standard Spectral Ratio - SSR (Fig. 2) obtained on the block (receiver site) respect to the wall (reference site) for the same ground motion component, outputs that in case of both 15 and 20 Hz signals, a seismic amplification exists on the block at 25 Hz. Moreover, only in case of the 20 Hz signal an amplification can be observed at the same frequency on the block. Based on the spectrograms of the recorded signals (Fig. 3), at the lowest generated frequencies (5 and 10 Hz) no energy was received by the rock block and consequently no significant induced vibration was detected. On the contrary, starting from the 15 Hz signal, a very low energy response was detected at the rock block. The 25 Hz and 40-50 Hz frequencies are unfortunately caused by the generator used to energize the vibrodyne, so the data derived from the 25 Hz shaking test are of difficult interpretation.

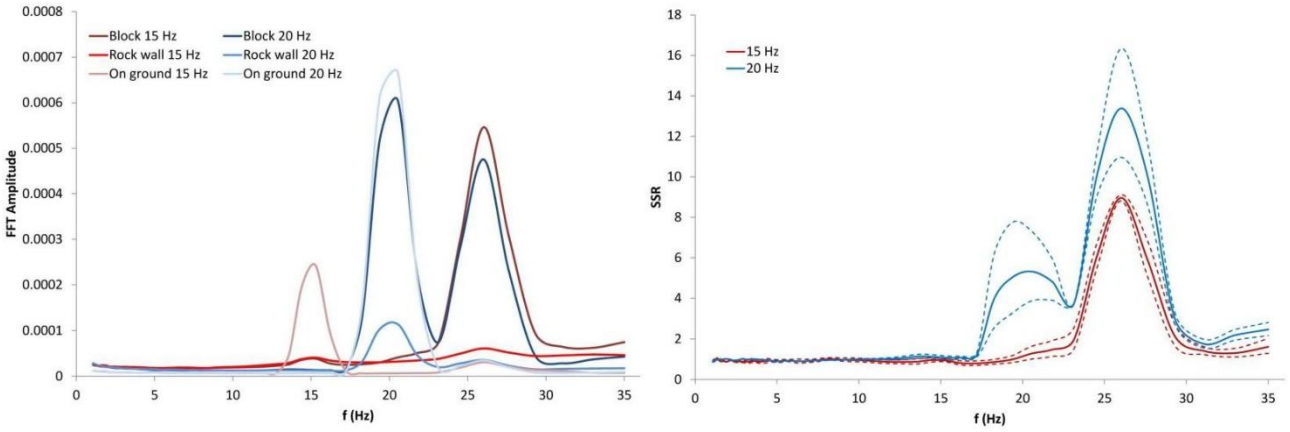

Figure 2. FFT (left side) and block/wall SSR (right side) obtained for the 15 Hz and 20 Hz shaking tests. Dashed lines indicate standard deviation.

Further data analyses will be carried on to evaluate differences among all the accelerometric records and to understand if these dynamic inputs can induce irreversible deformations, that can produce microfracturing and reduce both stiffness and strength of the jointed rock mass. In this regard, the recorded accelerometric signals will be processed to compare their physical features before, during and after the tests performed by the vibrodyne. The so obtained results will be devoted to better focus on further tests, i.e. to carry out tests under more constrained and controlled conditions.

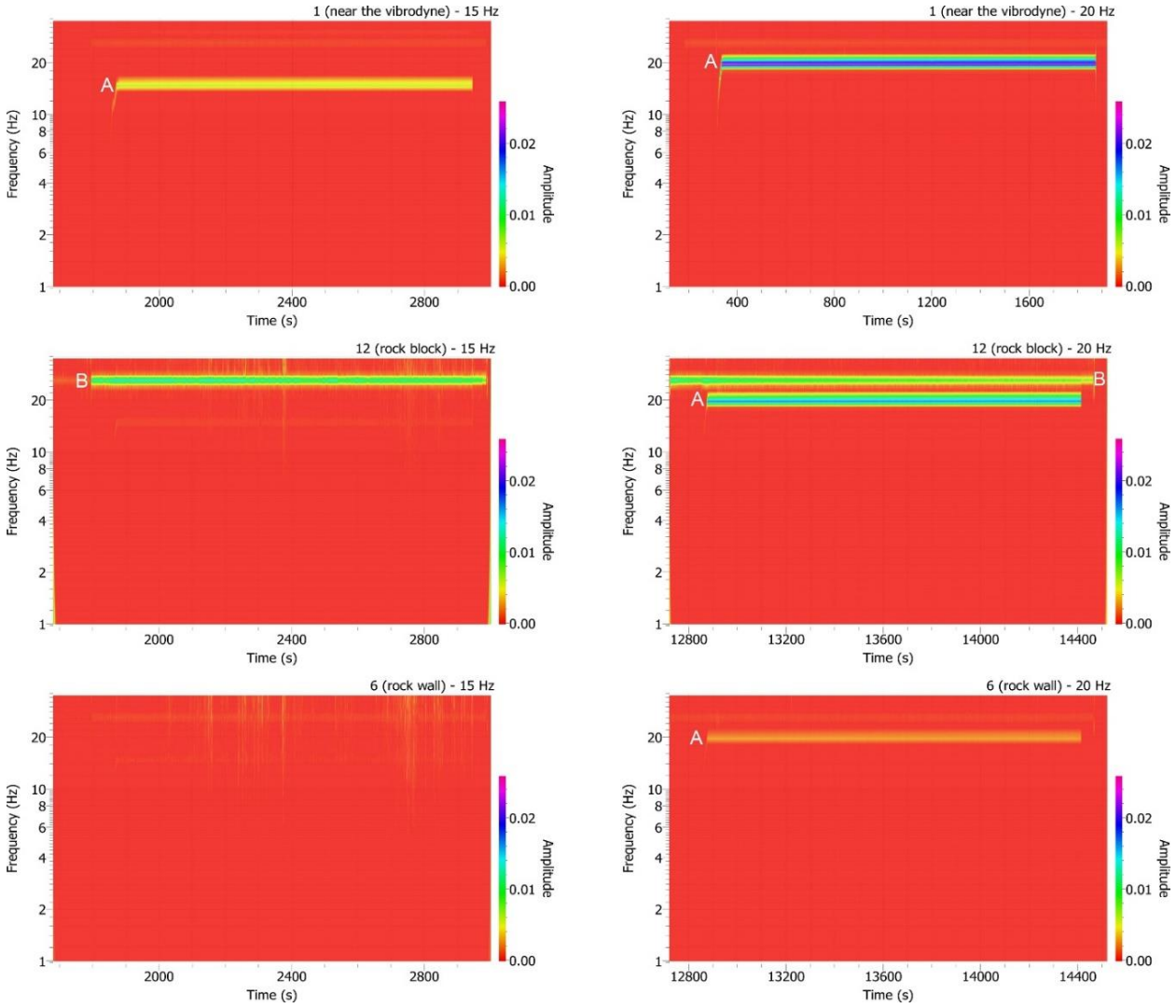

Figure 3. Time-frequency analyses obtained for the 15 Hz (left side) and 20 Hz (right side) shaking tests: near the vibrodyne (up), on the block (in the middle), on the back rock wall (down). Markers on spectrograms indicate frequencies due to vibrodyne shaking (A) and to the generator (B).

3 Reference list

Accordi, G, Carbone, F, Civitelli, G, Corda, L, De Rita, D, Esu, D, Funiciello, R, Kotsakis, T, Mariotti, G, Sposato, A. 1986. Lithofacies map of Latium- Abruzzi and neighbouring areas. Quaderno C.N.R. “La RicercaScientifica”, Roma, 114 (5), 223.

Eberhardt, E, Stead, D, Coggan, JS. 2004. Numerical analysis of initiation and progressive failure in natural rock slopes—the 1991 Randa rock slide. International Journal of Rock Mechanics & Mining Sciences 41, 69–87.

Fantini, A, Fiorucci, M, Martino, S, Marino, L, Napoli, G, Prestininzi, A, Salvetti, O, Sarandrea, P, Stedile, L. 2016. Multi-sensor system designed for monitoring rock falls: the experimental test-site of Acuto (Italy). Rendiconti Online della Società Geologica Italiana, 41, 147-150.

Got, JL, Mourot, P, Grangeon, J. 2010. Pre-failure behaviour of an unstable limestone cliff from displacement and seismic data. Natural Hazards and Earth System Sciences 10, 819-829.

Joswig, M. 2008. Nanoseismic monitoring fills the gap between microseismic networks and passive seismic. First Break, 26, 121-128.

Lévy, C, Baillet, L, Jongmans, D, Mourot, P, Hantz, D. 2010. Dynamic response of the Chamousset rock column (Western Alps, France). Journal of Geophysical Research 115, F4.

Loew, S, Gschwind, S, Gischig, V, Keller-Signer, A, Valenti, G. 2016. Monitoring and early warning of the 2012 Preonzo catastrophic rockslope failure. Landslides, 1-14.

Tang, CA, Li, L, Xu, NW, Ma, K. 2015. Microseismic monitoring and numerical simulation on the stability of high-steep rock slopes in hydropower engineering. Journal of Rock Mechanics and Geotechnical Engineering 7, 493-508.

Xu, NW, Dai, F, Liang, ZZ, Zhou, Z, Sha, C, Tang, CA. 2014. The Dynamic Evaluation of Rock Slope Stability Considering the Effects of Microseismic Damage. Rock Mechanics and Rock Engineering 47, 621-642.

Wongawilli Colliery portal and drift recovery

Roderick Haselden[1*]

[1] Douglas Partners Pty Ltd, Wollongong, Australia
* Roderick.Haselden@douglaspartners.com.au

1 Introduction

During the construction of three new entrances (portals) and inclined roadways (drifts) for an existing coal mine the face and roof of one drift collapsed, resulting in approximately 100 m^3 of material within the roadway and piping extending to the slope in the hillside above resulting in sinkholes. This poster presents the methods used to assess the rock mass, the cause of the collapses and the design and methodology used to recover the portal and drift.

2 Background

Wongawilli Colliery is located approximately 80 km to the south of Sydney, midway up a coastal escarpment that is underlain by a sequence of interbedded sedimentary rocks that includes the Illawarra Coal Measures. Slope instability is well documented within the escarpment, which is generally overlain by colluvium. To construct the mine portal, a bench had been excavated into a steep to very steep hillside exposing the underlying weathered sandstones, siltstone and mudstone.

Support for the drift comprised 200 UC steel sets, supporting a span of approximately 6 m. Sets were installed at 1 m centres, blocked with timber in the roof. Sidewalls were poorly blocked with two 1.8 m long resin rockbolts at mid height to support each leg set. Initial instability was mainly due to roof collapse between the last set and the face, approximately 2 m wide. The face collapsed later on. The mine operator had safety concerns and stopped all work.

3 Inspection and site model

Detailed inspections were carried out to establish a site model and to characterize the rock mass and failures. Inspection of the site found cracking in the shotcrete on both sides of the portal, a number of steel sets had bent and/or settled under roof and lateral loads, significant water seepage from the collapsed rock mass within the drift and two collapses had occurred in the roof and wall of the drift (Fig. 1). These had resulted in piping and unravelling of the soil and rock profile extended to the ground surface in the hillside above the drift resulting in sinkholes, the larger sinkhole being approximately 3 m deep and 10 m wide. Sandstone exposed within the walls of the drift was of very low to low strength and very blocky. A fault with numerous associated joints, running parallel to the face, was exposed in the collapse directly behind the portal shotcrete. The model for the drift is shown in Fig. 2.

The rock mass was assessed using the Rock Tunneling Quality Index (Barton et al. 1974) and the Rock Mass Rating systems (Bieniawski 1989) to have a Q value of approximately 0.1 and an RMR of approximately 25. The values indicated the support installed within the drift to be inadequate for tightly jointed and weak rock mass, which together with the lack of active contact resulted in displacement around the drift. Once confinement was lost, the rock unraveled, resulting in failure to the surface.

Figure 1. Photograph of the collapse within the drift. Note deflection of set in the background and secondary collapses adjacent to the side walls (photograph ©Douglas Partners).

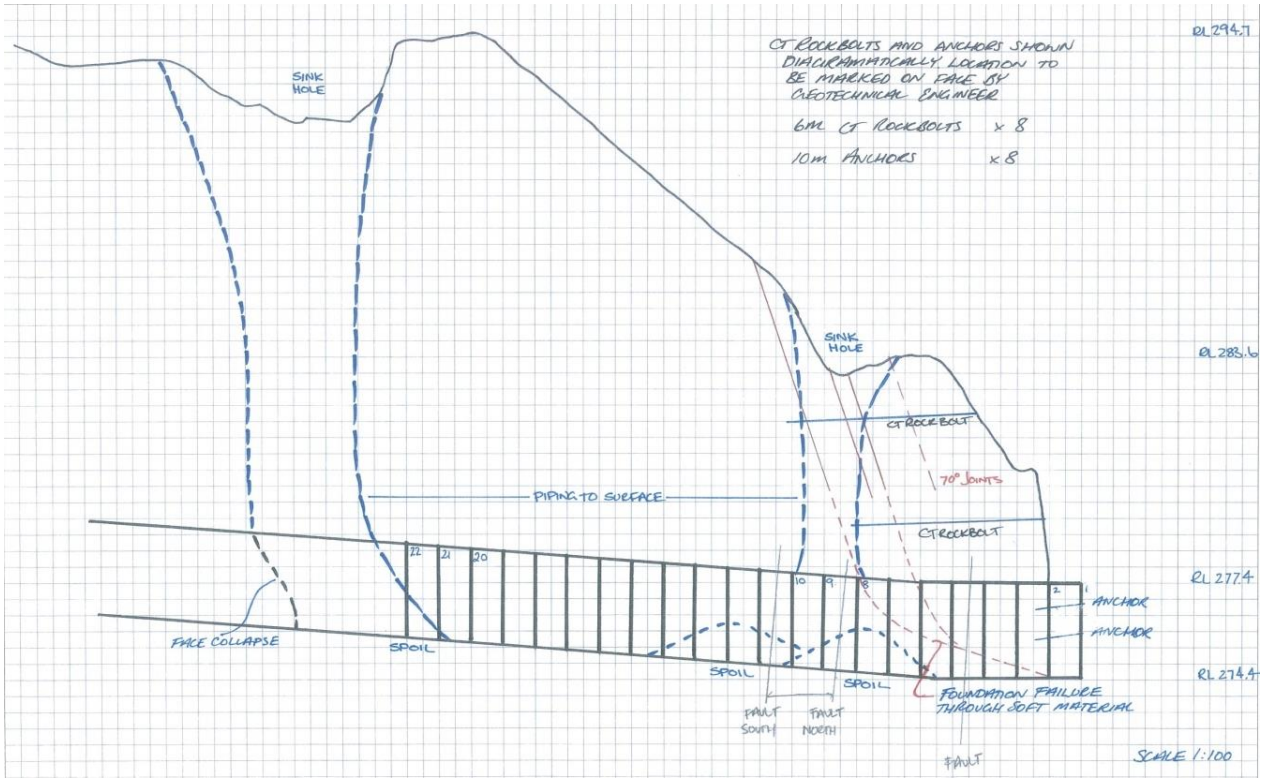

Figure 2. Site model showing the location of steel sets, faulting and piping failures (sketch ©Douglas Partners).

4 Design of support and recovery of the portal face

Due to the instability within the drift extending into the face of the portal and presence of adverse faulting and jointing dipping out of the face, for safety reason it was necessary to stabilize and recover the portal face prior to proceeding to the drift recovery. Support for the face was designed using plane failure analysis described by Hoek and Bray (2001). The support design included 3 and 4 strand tensioned anchors above and adjacent to the portal, rockbolts to stabilize the face around the portal and the construction of two rows of large diameter 'weep' holes to reduce the pore water pressure. Anchors were locked off at 40% of their working load.

5 Recovery methodology and design of support for the drift

Recovery of the drift could commence following lock-off of the portal face anchor support. Support for the sidewalls and roof for the drift was first to be augmented with vertical drains installed followed by systematic fibrecreting, with the fibrecrete tied structurally to the sets to provide active contact between the support and the rock mass. Temporary propping of the set legs (horizontally) and roof (vertically) were to be used where required to make the drift safe. The systematic underpinning of set legs was also recommended due to the excessive settlement observed at a number of sets. On the hillside the sinkholes were excavated to a practical depth of 4–5 m, in 2 m drops, and shotcreted to reduce the load on the face and failed material.

Recovery of the collapsed face and roof comprised a staged methodology for temporary support, which is summarized in Fig. 3 and described below. First the construction of a horizontally arched fibrecrete bulkhead was required in the upper portion of the collapse material at the furthest exposed set, braced off the set legs. Failed material was then removed in a 500 mm layer once the bulkhead had reached a minimum 5 MPa unconfined compressive strength (UCS) and the fibrecrete bulkhead extended before the process was repeated. Once the face was fully supported with a fibrecrete arch, ground improvements comprising the systematic top-down grouting of the collapsed pipe were to commence within the failed material beneath the pipe. Canopy tubes were designed as a beam by a structural engineer to span a length of 5 m, which comprised 10 m long, 100 mm diameter canopy tubes installed at spacings of no more than 100 mm apart, and inclined as flat as possible with bars hooked in the end of each tube to tie into the existing new and additional steel set. Once the ends of the canopy tubes were secured with fibrecrete, partial removal of the fibrecrete bulkhead was to be carried out followed by the removal of collapsed material and immediate fibrecreting of the roof. The removal was to continue top-down with the installation of new sets the excavation continued.

Additional support elements were recommended during inspections carried out during the recovery process including the installation of fiberglass dowels to support the face and a second row of canopy tubes beneath the pipe failure.

At the final inspection the drift had been successfully recovered to a point extending 10 m beyond the piped failure. Ongoing survey monitoring of the recovered section of the drift was to be carried out until it had been confirmed that convergence had stopped. It was also recommended that additional drainage holes were installed through the shotcrete in the sidewalls to prevent the buildup of water pressure behind support.

In summary, the portal and drift were safely and successfully recovered through a staged process of support augmentation, in line with the site conditions, and staged methodology for the recovery of the face and roof through the piped failure. It is paramount that the design of support considers the practicality and safety of carrying out the works, as the risk of failure occurring is typically highest following excavation and prior to construction of permanent support. Where poor ground conditions are encountered, this can require the installation of temporary support in advance of excavation.

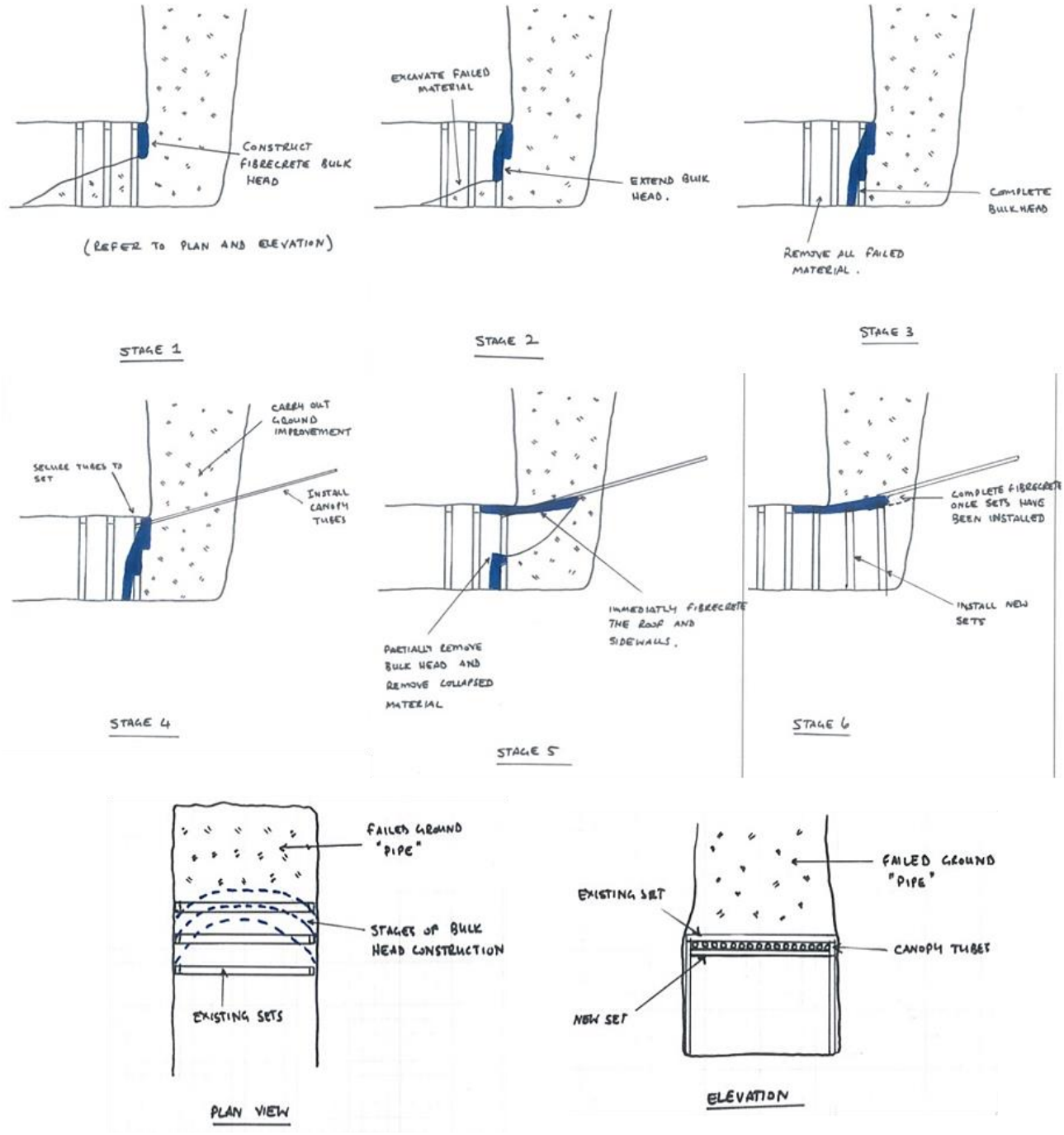

Figure 3. Staged methodology for temporary support for the drift recovery (sketch ©Douglas Partners).

6 Reference list

Barton, N, Lien, R, Lunde, J. 1974. Engineering classification of rock masses for the design of tunnel support. Rock Mechanics 6/4, 189-236

Bieniawski, ZT. 1988. Rock mass classification as a design aid in tunneling. Tunnels & Tunneling, Juli 1988.

Hoek, E, Bray, JW. 2001. Rock Slope Engineering. 3rd Ed, Institute of Mining and Metallurgy, London.

Spatial and temporal evolution of rock fall activity on a failing slope

Andrea Manconi [1*], Franziska Glueer[1] and Simon Loew [1]

[1] Department of Earth Sciences, ETH Zurich, Switzerland
* andrea.manconi@erdw.ethz.ch

1 Abstract

The main goal of this study is to describe the spatial and temporal evolution of rock fall phenomena triggered by rapid slope deformation. To this end, we combine low cost seismic sensors and image processing to study a large instability adjacent to the Great Aletsch glacier in the Swiss Alps, i.e. the Moosfluh slope, which is undergoing an acceleration phase since the late summer 2016. With this analysis, we aim at a better understanding of the relationship between the kinematic behavior of rock slope instabilities and progressive rock mass damage, which may lead to catastrophic failure.

2 Introduction

The Great Aletsch Region is a prominent site located in Switzerland, hosting the largest glacier of European Alps. In this area, glaciers have undergone to several cycles of advancement and retreat, which have deeply affected the geomorphological evolution of the surroundings (Grämiger et al. 2017). The glacier is experiencing a progressive retreat in the order of 50 meters every year, consequently, load is released from the adjacent rocks previously constrained by the ice mass, and slope instabilities might be triggered (e.g., Cossart et al. 2008). In the Aletsch region, a deep-seated slope instability called Moosfluh shows since the 90's a slow but progressive increase of surface displacement (Strozzi et al. 2010). The moving mass associated to Moosfluh affects an area of about 2 km^2 and entails an estimated volume of about 150-200 Mm^3 (Kos et al. 2016). In the late summer 2016, an unusual acceleration of the Moosfluh rockslide was observed.

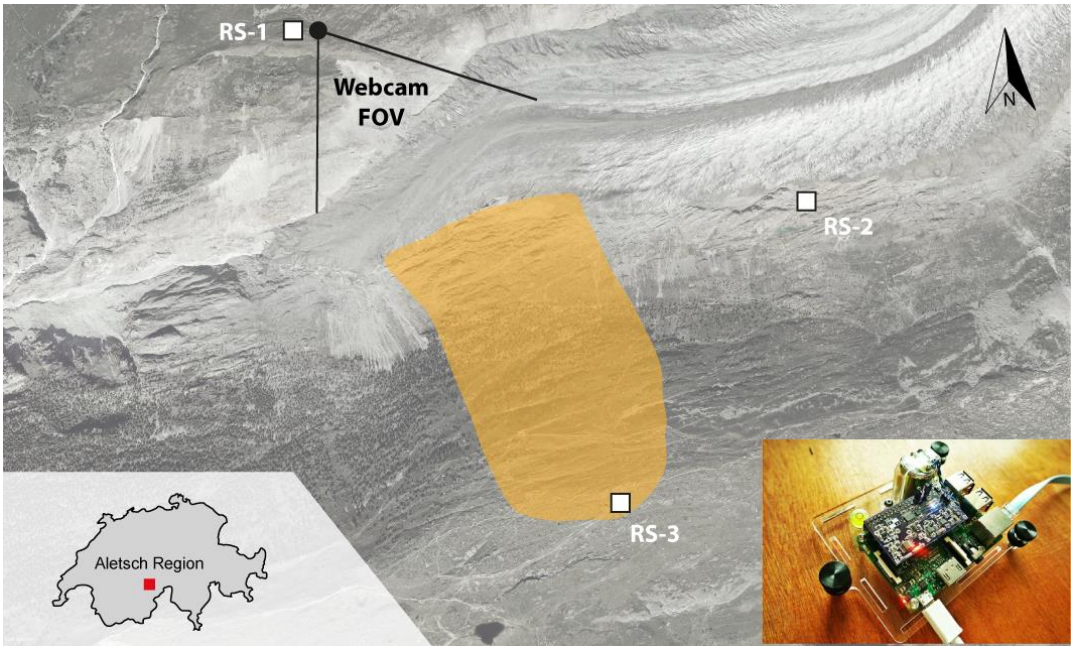

Figure 1. Overview of the area of investigation, the Moosfluh rock slope instability, in the Aletsch region (Swiss Alps). The orange outline shows the area affected by the large surface deformation (up to 0.8 m/day in October 2016) and where most of the rock fall events have been observed. White squares indicate the position of the Raspberry Shake sensors (RS 1-3, see picture in the inset on the bottom right, www.raspberryshake.org).

Compared to previous years, when ground deformations were in the order of few centimeters, in the period September-October 2016 maximum velocities have reached locally up to 0.8 meters per day. Such a critical evolution caused the generation of several deep tensile cracks, and resulted in an increased number of rock failures at different locations of the landside body. These processes have been observed at several other unstable rock slopes prior to catastrophic failure events (Rosser et al. 2007); however, high resolution monitoring data are rare. The main goal of the study is to compare and possibly correlate the spatial and temporal evolution of surface deformation with the occurrence, the location and the size of rock falls events. This may help to better characterize the kinematic evolution of the Moosfluh rock slope, and more in general of large rock slope instabilities showing signs of a potential catastrophic failure.

3 Methods

Due to the limited access to the site, rock falls will be identified and investigated by analyzing the data acquired remotely, including (i) a seismic network composed of 3 Raspberry Shake (RS) seismometers, and (ii) a webcam installed on the opposite side of the Moosfluh slope (see Fig. 1). RS are a low-cost, all-in-one plug-and-go solution developed by OSPO S.A., which integrate vertical velocity sensor (4.5 Hz Racotech RGI-20DX), digitizer, and computer in a single box (100x120x50 mm, 0.35 kg). Installation of the seismometers is planned in middle May 2017, when we expect to record a further increase of deformation and rock fall activity due to the effect of snow melt on the landslide body. Seismic data will be collected and analyzed by using different approaches and algorithms to identify and locate rock fall phenomena (e.g., Manconi et al. 2016). Regarding the webcam data, rock fall processes will be observed and measured by applying Digital Image Correlation (DIC) algorithms. The webcam acquires images every 10 minutes since September 2016, and despite the moderate resolution of the webcam picture (3 MPixel), preliminary results have shown that both surface displacement as well as location of local rock slope failure can be traced (see Fig. 2).

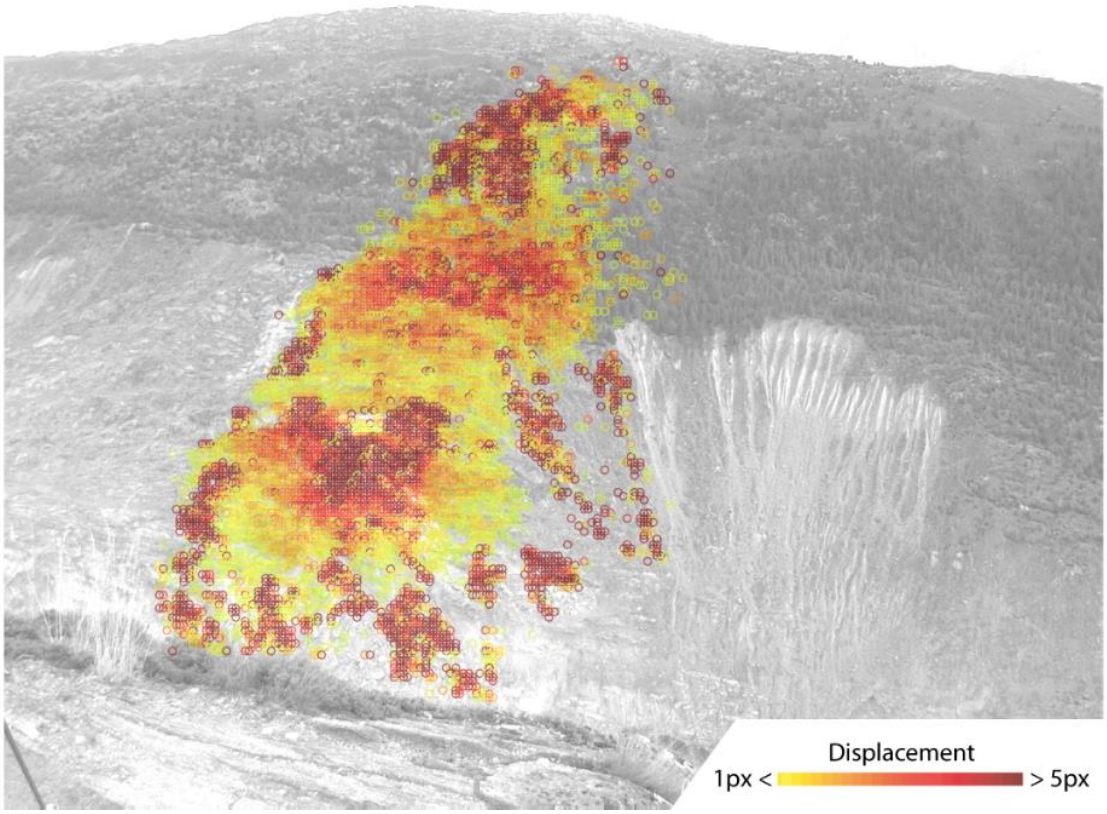

Figure 2. Surface displacements (in pixels) measured via Digital Image Correlation at the Moosfluh rock slope during the acceleration phase experienced in September 2016. Areas characterized by large displacement gradients (dark red) are associated to rock failure events.

4 Summary

In this work, we present preliminary results of a monitoring experiment implemented at the Moosfluh rockslide during the current acceleration phase. We combine DIC analyses on optical imagery and characterization of seismic waveforms acquired from low-cost sensors to gain insights on the physical processes governing the progressive evolution of a large rock slope instabilities towards ultimate failure.

5 Reference list

Cossart, E., Braucher, R., Fort, M., Bourlès, D.L., Carcaillet, J., 2008. Slope instability in relation to glacial debuttressing in alpine areas (Upper Durance catchment, southeastern France): Evidence from field data and 10Be cosmic ray exposure ages. Geomorphology, Paraglacial Geomorphology: Processes and Paraglacial Context 95, 3–26. doi:10.1016/j.geomorph.2006.12.022

Grämiger, L.M., Moore, J.R., Gischig, V.S., Ivy-Ochs, S., Loew, S., 2017. Beyond debuttressing: Mechanics of paraglacial rock slope damage during repeat glacial cycles. J. Geophys. Res. Earth Surf. 2016JF003967. doi:10.1002/2016JF003967

Kos, A., Amann, F., Strozzi, T., Delaloye, R., von Ruette, J., Springman, S., 2016. Contemporary glacier retreat triggers a rapid landslide response, Great Aletsch Glacier, Switzerland. Geophys. Res. Lett. 2016GL071708. doi:10.1002/2016GL071708

Manconi, A., Picozzi, M., Coviello, V., De Santis, F., Elia, L., 2016. Real-time detection, location, and characterization of rockslides using broadband regional seismic networks. Geophys. Res. Lett. 43, 2016GL069572. doi:10.1002/2016GL069572

Rosser, N., Lim, M., Petley, D., Dunning, S., Allison, R., 2007. Patterns of precursory rockfall prior to slope failure. J. Geophys. Res. Earth Surf. 112, F04014. doi:10.1029/2006JF000642

Strozzi, T., Delaloye, R., Kääb, A., Ambrosi, C., Perruchoud, E., Wegmüller, U., 2010. Combined observations of rock mass movements using satellite SAR interferometry, differential GPS, airborne digital photogrammetry, and airborne photography interpretation. J. Geophys. Res. 115. doi:10.1029/2009JF001311.

Interaction of permafrost-affected bedrock and high alpine infrastructure: A distinct element model parameter study

Regina Pläsken[1,2*], Michael Krautblatter[2], Markus Keuschnig[1]

[1] GEORESEARCH Forschungsgesellschaft mbH, Austria
[2] Chair of Landslide Research, Technische Universität München, Germany
* regina.plaesken@tum.de

1 Motivation

Alpine regions show twice the warming rate compared to the global average since the 19th century (European Environment Agency 2009), and high alpine environments are known to be particularly sensitive to temperature changes. Infrastructure which is built in permafrost-affected environments commonly suffers from a reduction in bearing capacities of affected bedrock. The overall aim of this study is to investigate the interaction of changes in bedrock properties induced by a natural decrease of permafrost and the direct effects of high alpine infrastructure.

2 Study site and infrastructure

The study site is situated around the summit station of Kitzsteinhorn cable car (3029 m a.s.l., Austria). It encompasses the north-oriented rock wall of the Kitzsteinhorn, which is made up of calcareous micaschists. The foliation is inclined approximately in the line of the slope with angles between 39° and 52°. Until the mid-20th century parts of the rock wall were covered by a permanent ice face. The current surface of the adjacent glacier is located approximately 100 m below the summit station, which was first built in 1965/66 and refurbished in 1981 and 2010. The rock wall below the summit station is permafrost affected and shows significant seasonality in rock fall activity (Hartmeyer et al. 2016). A cable car station associated with the summit station is anchored to the rock face with pre-stressed rock anchors.

3 Data and methods

3.1 Laboratory testing

Samples of calcareous micaschist were taken and tested extensively in laboratory. Voigtländer et al. (2014) carried out >70 tests on uniaxial compressive strength, tensile (Brazilian) strength and non-destructive tests, all on frozen and unfrozen samples. Elastic moduli, compressive and tensile strength are derived from that raw data.

3.2 Field testing

Geological mapping of the surrounding area and the rock wall below the summit station was carried out (Geoconsult ZT GmbH 2010). Two deep boreholes (30 m) are situated at the study site: one immediately adjacent to the summit station and the other around 45 m below the station. In both boreholes, optical scans were carried out to derive information on discontinuity orientation and condition (Geoconsult ZT GmbH 2014).

In November 2015, two additional rows of 15 pre-stressed rock anchors were installed directly beneath the summit station. The 25 m long anchors are drilled with an inclination of around 3° and a grouted section of 7 m length. Three of these anchors are equipped with load cells, which measure anchor loads every hour.

3.3 Modeling

A preliminary distinct element model was set up in UDEC including the measured parameters described above. Parameters, which could not be derived from laboratory and field testing were determined indirectly from known on-site or transferred off-site values. The estimation of the joint normal and shear stiffness was derived from the elastic modulus and the condition of the rock after Barton (1972) in conjunction with the assumption of similar stiffness characteristics with a physically possible value range of E/G between 2 to 3. For load values, planning documents were used, the missing information on building infrastructure was collected on-site.

For analyzing the influence of the input parameters on the model, a parametric study was carried out. Based on the initial state of frozen rock, both rock and joint parameters were varied and the influence of higher loads was evaluated. As model parameter to be contrasted the Factor of Safety (FoS) was chosen on a comparative basis.

4 Results and discussion

4.1 Laboratory and field testing

Elastic parameters, compressive and tensile strengths are determined in the lab for samples under frozen and unfrozen conditions. The determined values as well as data from geological mapping and borehole scans serve as input parameters for the UDEC model.

Analysis of field data shows that measured anchor load values vary significantly over the course of the year (Fig. 1). After tensioning in December 2015 anchor loads of approximately 485 kN (load cell #9), 470 kN (load cell #12) and 545 kN (load cell #15) were measured. During spring anchor load values decreased, in autumn anchor loads increased again. Load cells show variations between 15% (load cell #15) up to 30% (load cell #9) of the maximum load. Anchor loads represent well-suited proxies for system behavior and provide possibilities for model validation. The observed seasonal pattern seems to be reversible, high anchor load values during winter possibly coincide and agree with the size of the cryosuction-driven increase of freezing pressure in near-surface areas.

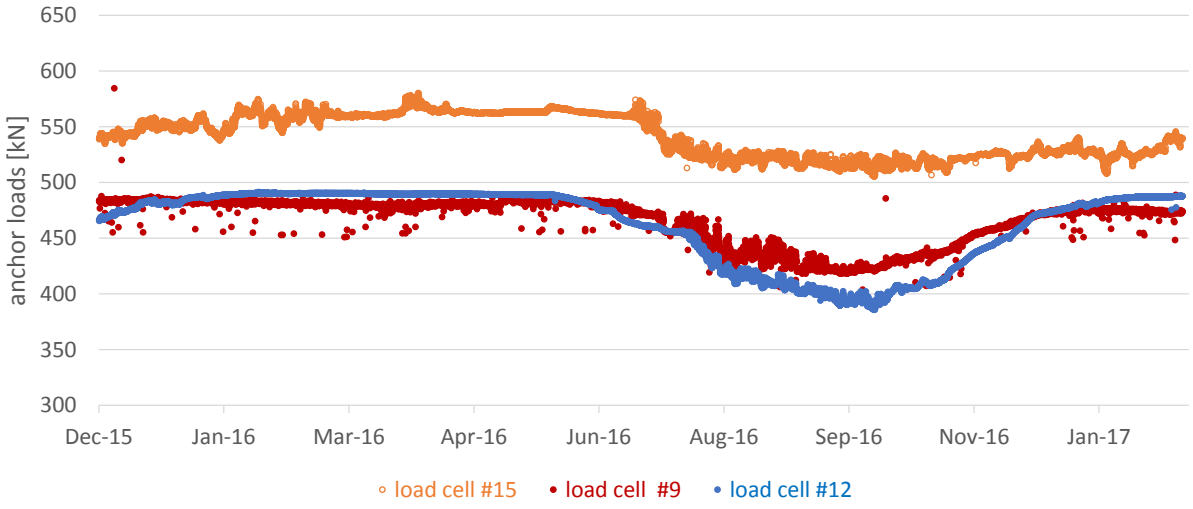

Figure 1. Anchor loads and temperature of anchors beneath the summit station Kitzsteinhorn.

4.2 Modeling

Preliminary model results indicate a mechanical activation of rock immediately above the anchors of the suspension rope due to initial loading. Displacements extend tens of meters up the rock face beneath the summit station (Fig. 2).

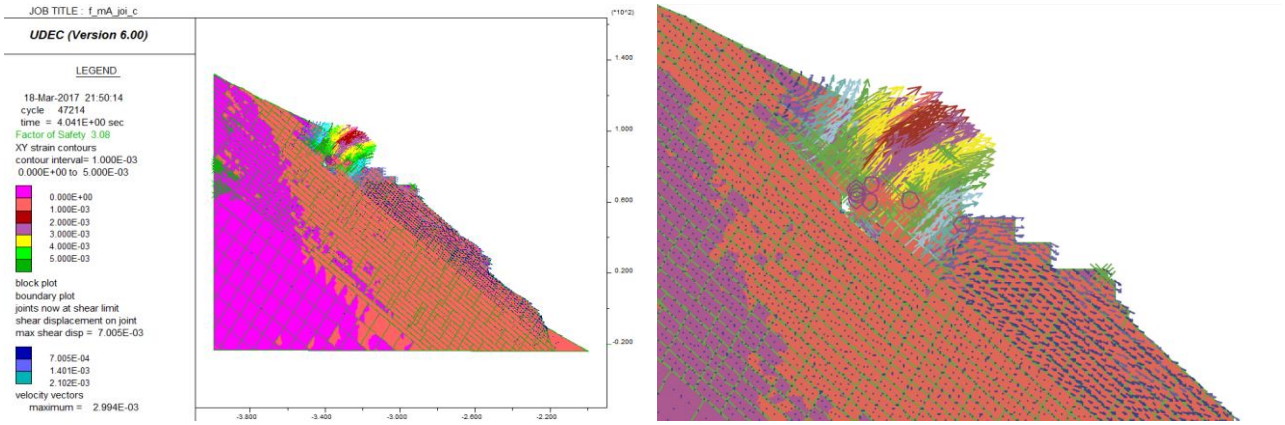

Figure 2. Graphical result representation of initial state, activation of rock mass influenced by summit station.

While the factor of safety does not appear to be strongly influenced by intact rock parameters (frozen, unfrozen conditions), changes in joint parameters (particularly stiffness) and increases in anchor load affect the FoS significantly.

5 Conclusion and outlook

Joints are dominant, so further effort is to be focused on investigating parameters of joint fracture criteria (lab testing, field evaluation). So far elastic joint parameters are derived indirectly, more detailed evaluation of joint stiffness is required. Depending on the physical effects occurring in the upper tens of meters beneath the rock surface, the anchor loads may be used for model validation later.

6 Reference list

Barton, N. 1972. A model study of rock-joint deformation. International Journal of Rock Mechanics and Mining Sciences & Geomechanics Abstracts 9. 579–582.

European Environment Agency. 2009. Regional climate change and adaption. The Alps facing the challenge of changing water resources. Luxembourg.

Geoconsult ZT GmbH. 12.12.2010. Kartierung Gipfelstation. Salzburg. Austria.

Geoconsult ZT GmbH. 20.03.2014. Sicherungsplanung der Felsflanke unterhalb der Gipfelbahn. Salzburg. Austria.

Hartmeyer, I, Keuschnig, M, Delleske, R, Schrott, L. 2016. Rockfall in permafrost-affected Cirque Walls: New Insights on Spatial Variability and Potential Causes derived from a 4-year LiDAR monitoring campaign. Kitzsteinhorn. Austria. speech at 11th International Conference on Permafrost, 20-24. June 2016. Potsdam. Germany.

Voigtländer, A, Scandroglio, R, Krautblatter, M. 2041. Entwicklung geotechnischer Felsparameter des Kitzsteinhorner Kalkglimmerschiefers – Abschlussbericht zum Forschungs- und Entwicklungsvertrag der TU München und AlpS-GmbH. München. Germany.

Rock failure, swelling, sulfate transport and gypsum precipitation in the invert of two road tunnels

Walter Steiner[1*] and Ruedi Krähenbühl[2]

[1] B+S AG, Bern, Switzerland [2] BauGrundRisk, Chur, Switzerland
* w.steiner@bs-ing.ch

1 Scope

Experience from two case histories of tunnels where swelling involving sulfates and gypsum will be presented. Unexpected swelling phenomena were observed of the invert in both tunnels. One tunnel is located at the northern edge of the Triassic Keuper formation in Luxembourg: Tunnel Markusberg of motorway A 13 near Schengen. The other tunnel in the Swiss Alps crosses the formation of Bündner Schist: Gotschna Tunnel of motorway A 28 on the by-pass road of Klosters.

2 Extension of swelling zones and observed heave

In both tunnels the zones with heave are limited in length. In the dual tube motorway tunnel Markusberg the swelling zone extends over about 50 meters, about 200 m from the East portal of the tunnel and severe swelling has been observed, beginning weeks after excavating the horseshoe shaped tunnel. Initially the heave of the tunnel floor was re-excavated and the swollen material removed periodically. In the Gotschna tunnel heave in three different sections, about 100 m long, and spaced about one kilometer each, were observed. Different rates of heave (Tab. 1) are observed in the three sections that depend on type of applied invert or the support pressure.

2.1 Observations in Tunnel Markusberg

The observations at Tunnel Markusberg have been described by Steiner et al. (2015). The swelling zone has a small overburden of 25 m only (Fig. 1), on the ground surface in the vineyard actually gypsum can be observed in the red marl. As substantial heave was observed, a void was left below the roadway and the swollen and heaved ground was periodically removed (Fig. 1).

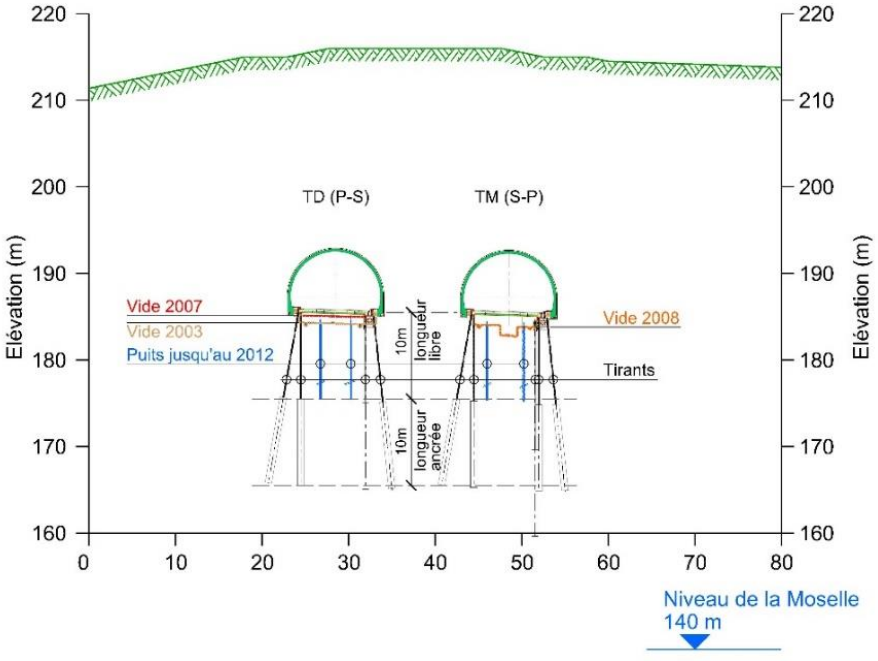

Figure 1. Cross section through swelling zone with void below roadway and tiebacks at edge of tunnel.

In 2003 when the tunnel was opened to traffic a void of about 1.7 m height was left that closed until 2006 to a remaining height of several decimeters only. In 2007 and 2008 a central trench 2 m deep was cut and also the side benches were lowered (Fig. 2).

The layers of bedrock were bent upwards and layers of Gypsum can be seen (Fig. 2) in the excavated a cross-section. The deformation behaviour in the invert and tunnel has been monitored with geodetic surveying since 2003 in the tunnel and with multi-point extensometer below the invert since 2006. Heave rates of the side are 20 mm/a and an estimated support pressure of 300 to 500 kPa applied in this zone. Below the invert the rate of heave is 60 mm/a and the support pressure is estimated as 60 kPa.

Figure 2. The upward bent ground layers in the void below the roadway. The estimated heave is 2 to 3 m.

2.2 Observed behaviour in the Gotschna tunnel

In the Gotschna tunnel three sections, each of about 100 m length with different types of support in the invert and different overburden (Tab. 1) experience swelling (Gall & Krähenbühl 2014).

Table 1. Deformation zones (DZ) and swelling phenomena observed in the Gotschna tunnel

Deformation zone with swelling phenomena: chainage (m)	Overburden (m)	Rate of heave (mm/a)	Support pressure in invert (kPa)	Invert type
DZ 1 (2030–2170)	380	12–15	40–80	Flat invert arch (sheared off)
DZ 2 (2514–2549)	380	20	20	Prior to placing tiebacks
DZ 2 (2514–2549)	380	4	325	Tiebacks in invert
DZ 3 (3300–3380)	230	0.5–1	500	Invert slab

In Fig. 3 support pressure versus rate of heave are plotted for the Gotschna tunnel in the left diagram and for Markusberg and Gotschna together in the right side diagram. With higher support pressures the rates of heave reduce and with a support pressure of 500 to 700 kPa the heave appears to cease. These "swelling" pressure are substantially less than swelling pressures determined in laboratory tests (Steiner et al. 1989; Steiner 1989 2007; Kirschke 2010).

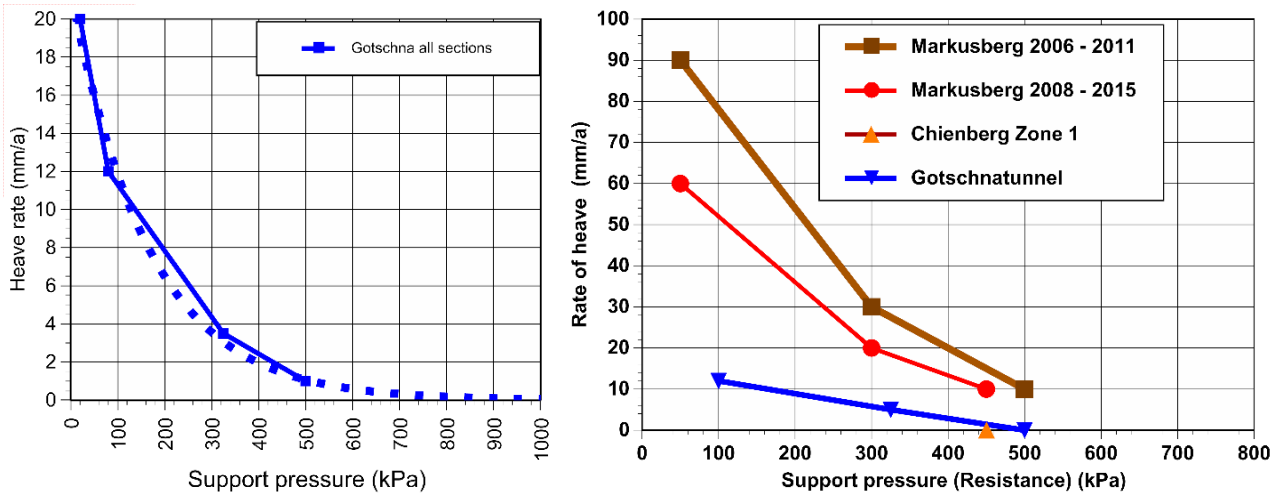

Figure 3. Heave rates versus support pressures in Gotschna tunnel (left) and comparison with the Markusberg tunnel (right).

3 Analyses of brittle failure (or tension cut-off)

Analyses have been carried out to estimate the size of the zone with excavation damage, as proposed by Steiner et al. (2010, 2011), Kaiser et al. (2010), and Amann et al. (2010). For the Markusberg tunnel analyses were carried out with RS2 (Phase2 V9) with estimated parameters. For the Gotschna tunnel triaxial tests had been carried out on samples from two deformation zones: DZ1 and DZ2 (Tab. 2). For the overburden of the tunnels and the associated strength parameters (Fig. 4) stress to strength ratios were calculated indicating an excavation damaged zone around the tunnel of one half to one tunnel radius depth.

Table 2. Strength parameters for rock in swelling zones at the Gotschna and Markusberg tunnels.

Tunnel Name	Rock type	Friction angle Φ' (°)	Cohesion c'	UCS $\sigma_c = 2c\,(N_\Phi)$	N_Φ
Gotschna	Kakirit	27	8 kPa	26.11 kPa	2.6629
	Bündnerschiefer massive	45	4 MPa	19.3 MPa	5.8284
	Bündnerschiefer sheared	28	1 MPa	3.3 MPa	2.76
	Dolomite & Gypsum	45	2 MPa	9.6 MPa	5.8284
Markusberg	Marl with Gypsum	34	1.5 MPa	20 MPa	3.53
	Red Marl (Keuper)	34	0.4 MPa	5 MPa	3.53

4 Synthesis of observations, analyses and monitoring

The synthesis of the field observations, the monitoring of displacements and analyses have given insight in the mechanisms that lead to gypsum swelling. The formation of fissures or flow paths by stress redistribution and tensile failure is followed by percolation of water that dissolves sulfates from anhydrite (James 1992). The sulfate concentration will increase and under sufficient pressure may be kept in solution or with the aid of accessory minerals such as chloride, otherwise sulfates may precipitate and form gypsum (Nüesch et al. 1995). In tunnel Markusberg (Steiner & Maquil 2015) very high concentrations (20 g/l) of sulfate and chloride were observed. The crystallization of gypsum will create stresses in the ground that will charge the tunnel lining and as a reaction will lead to a compression of the rock in the damaged zone. Fissures will close and percolation will be reduced until it ceases. These in-situ pressures are substantially smaller than the swelling pressure determined in laboratory tests as observed by Steiner (1993, 2007) and Alonso et al. (2013).

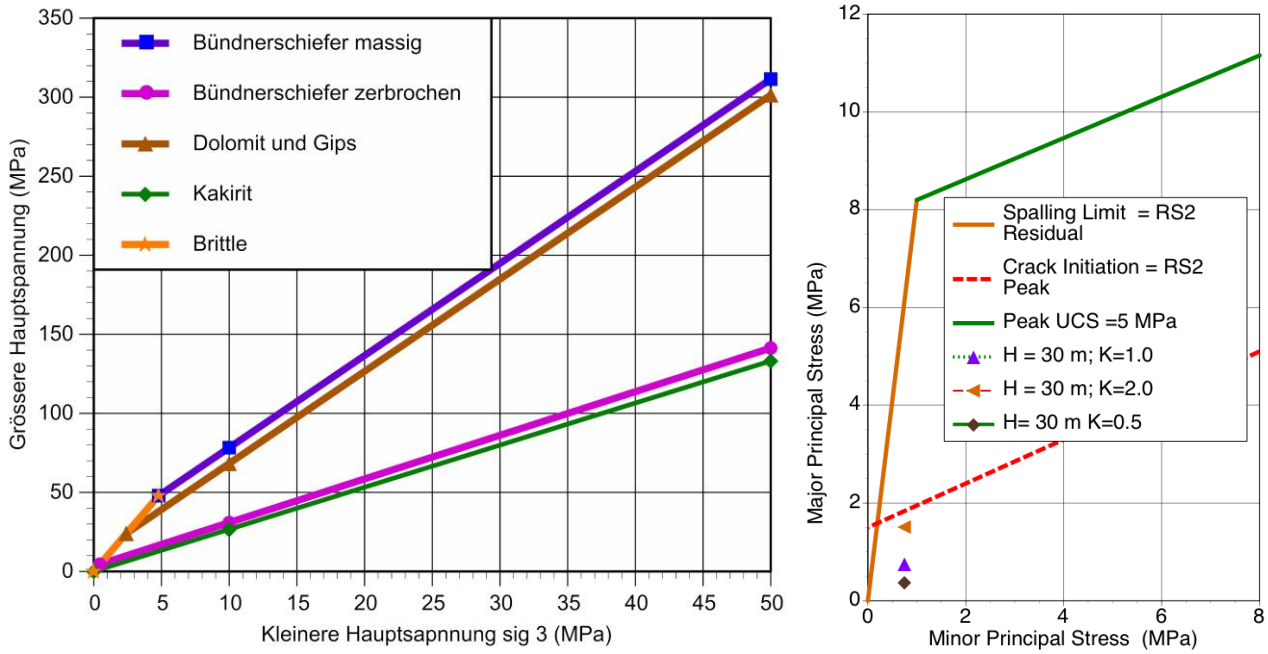

Figure 4. Tri-partite strength envelopes for Gotschna rock (left) and Markusberg Marl (right) according to Kaiser et al. 2010 and Steiner et al. 2010.

5 Reference list

Alonso, E. E, Berdugo, I.R. & Ramon, A.; 2013. Extreme expansive phenomena in anhydritic gypsiferous claystone: the case of Lilla tunnel, *Géotechnique* 63, No. 7, pp.584-612.

Amann, F., P.K. Kaiser and W. Steiner, 2010. Triggering swelling potential of anhydrite clay rocks by brittle failure processes. Eurock 2010, Lausanne, Switzerland, 339 -342.

Amann, F.; Ömer Ü.; S. Löw; P. Kaiser, 2013. Bruchprozesse und in-situ Beobachtungen von Brüchen im Gipskeuper. Research report 2011/006 ASTRA, Engineering geology, ETH Zürich;

Gall, R.; Krähenbühl, R. (2014) Quellerscheinungen im Gotschnatunnel, Kolloquium Tunnel in anhydritführendem Gebirge, IGT_ ETH Zürich, 20 S.

James, A. N. (1992) Soluble Materials in Civil Engineering, Ellis Horwood, New York.

Kaiser, P.K. and Kim B.-H. 2008. Rock Mechanics Challenges in Underground Construction and Mining. In: 1th Southern Hem. Int. Rock Mech. Symposium.: 23-38, Australia.

Kaiser, P.K. with contributions by F. Amann and W. Steiner, 2010. How highly stressed brittle rock failure impacts tunnel design. Eurock 2010, Lausanne, Switzerland, 27-38

Kirschke, D. 2010. Lösungsansätze für den Tunnelbau in quell- und schwellfähigem Gebirge, Geomechanik und Tunnelbau 3 (5), 547 – 556.

Nüesch, R.; Steiner, W.; Madsen, F. (1995) "Long time swelling of anhydritic rock, mineralogical and microstructural evaluation", *Proc. 8th International Conference on Rock Mechanics*, Sept. 25-30, 1995, Tokyo, Japan, pp 133 -138.

Steiner W, P K Kaiser, G Spaun (2010) Role of brittle fracture on swelling behavior of weak rock tunnels: hypothesis and qualitative evidence, Geomechanics and Tunnelling, 3(5), 583-596.

Steiner W, P K Kaiser, G Spaun (2011) Role of brittle fracture on swelling behavior of weak rock tunnels: evidence from tunnelling case histories, Geomechanics and Tunnelling, 4(2), 141-156.

Steiner, W (2007) Einfluss der Horizontalspannungen auf das Quellverhalten von Gipskeuper, *Felsbau* 25/1, S. 15 – 22.

Steiner, W. (1993) "Swelling rock in tunnels: Characterization, effect of horizontal stresses and Construction Procedures", *Int. Journal of Rock Mech. and Mining Sciences.,* Vol. 30, No.4, pp.361- 380.

Steiner, W.; Rossi P.P., and Devin, P. (1989) "Flatjack Measurements in the Lining of the Hauenstein Tunnel as a Design Base for the New Wisenberg Tunnel", *Proceedings International Congress on Tunneling*, Toronto.

Steiner, W. (1989), "Wisenbergtunnel, Bahn 2000", *Veröffentlichungen der Fachgruppe für Untertagbau des SIA der Tagung Juradurchquerungen* , Délemont, SIA-FGU, Tagungsbericht D 037, Zurich, S.69-80.

Steiner, W. & Maquil, R., Didier, G. 2015. Observations of swelling and associated phenomena in Markusberg Tunnel, Schengen, Luxembourg, Shale Symposium, Proc. ISRM 2015, Montreal, Canada.

The effects of stress path and strain rate on the confined compressive strength and failure mode of brittle rocks

Matthew J. Brain[1*], Nick J. Rosser[1], Saskia J. De Vilder[1] and Neil Tunstall[1]

[1] Department of Geography, Durham University, United Kingdom
*matthew.brain@durham.ac.uk

1 Background

Recent studies have demonstrated important links between the strength and failure mode of brittle rock materials, how they respond to varying principal stress conditions and stress paths, and resultant field-scale responses, manifest as differences in the pattern and nature of slope failures and landform and landscape evolution (Diederichs 2003; Leith et al. 2014). However, the influence of strain rate in driving differences in intact rock strength and failure mode is less well constrained (cf. Amann et al. 2011). Furthermore, how differences in stress path and strain rate influence future failures by controlling if, where and when progressive fracture can develop has not previously been considered in sufficient detail.

2 Approach

In contrast to most conventional confined compression tests that employ an increase in axial load to cause failure, we focus on the effects of both slow and rapid (near-instantaneous, quasi-dynamic) reductions in confining pressure on the compressive strength and failure mode of rock samples. We consider the former (slow loss of confining pressure) to be representative of a longer-term, gradual loss of hillslope material, driven by small-scale but continuous rockfall activity. The latter (rapid loss of confining pressure) mimics stress conditions in remnant hillslope materials during and following large slope failures that cause a sudden reduction in lateral confinement of remaining, unfailed materials.

3 Results

We present results of laboratory tests undertaken on a medium- to coarse-grained sandstone (unconfined compressive strength = 51.0 ± 10.6 MPa). We undertook a series of confined compression tests over a confining pressure range of 1 to 10 MPa. Our results indicate that differences in strength and failure mode occur where strain rates differ, despite (un-)loading along the same stress path (constant axial load, reducing confining pressure). A gradual, controlled reduction in confining pressure causes minor, but not insignificant, strengthening relative to standard axial loading tests, though we observed standard shear failure typical of confined compression (Fig. 1a). In contrast, rapid reduction in confining pressure causes an increase in compressive strength relative to baseline axial loading tests, but results in greater rock fragmentation upon failure, indicative of hybrid shear and tensile axial splitting modes (Fig. 1b,c). These effects are most pronounced where the major principal stress at failure exceeds the unconfined compressive strength of the rock. However, we also demonstrate that rapid unloading of rock at relatively low major principal stresses can cause microcracking and damage that is sufficient to weaken the rock, acting as a catalyst for the onset of progressive failure. Using numerical modelling of rock slope failures, we considered the locations within a slope that stress conditions and unloading rates that can cause high rock fragmentation can exist. We found that such locations are most likely to occur in rapid, very deep-seated failures that occur during large seismic events.

4 Implications

Our results have important implications for post-failure development of landslides in terms of the magnitude and frequency of rockfall activity, the propensity for large-scale slope failure and the significance of antecedent conditions and slope failure activity in influencing susceptibility to progressive fracture.

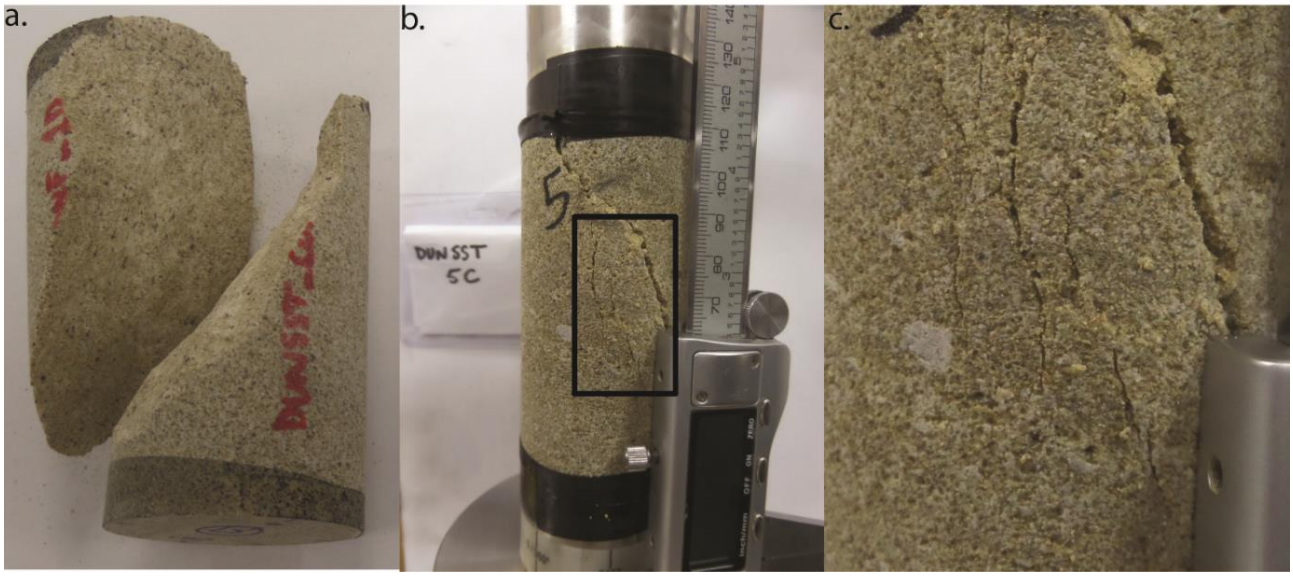

Figure 1. Photographs of post-failure condition of sandstone samples tested along the same stress path (constant axial load, reducing confining stress) but at different rates of confining stress reduction. a. standard shear failure where confining stress is reduced gradually. b. hybrid shear and tensile splitting failure where confining stress is reduced near-instantaneously. The contents of the black box in b. are shown in more detail in c., where sub-vertical cracks are evident adjacent to the main shear surface. Both samples shown are ~96 mm high and ~48 mm in diameter. ©N. Tunstall/M. Brain.

5 Reference list

Amann, F., Button, E.A., Evans, K.F., Gischig., V.S., Bluemel., M. 2011. Experimental study of the brittle behaviour of clay shale in rapid unconfined compression. Rock Mechanics and Rock Engineering, 44, 415 – 430.

Diederichs, M.S. 2003. Manuel Rocha Recipient : Rock fracture and collapse under low confinement conditions. Rock Mechanics and Rock Engineering, 36, 339 - 381

Leith, K., Moore, J.R., Amann, F., Loew, S. 2014. Subglacial extensional fracture development and implications for Alpine Valley evolution. Journal of Geophysical Research : Earth Surface, 119, 62 – 81.

Lifetime of rocks – from subcritical to critical crack growth and dynamic triggered failure

Heinz Konietzky[1*], Wei Chen[2], Wengang Dang[1], Xiang Li[2] and Xin Tan[3]

[1] Geotechnical Institute, TU Bergakademie Freiberg, Germany
[2] Central South University, Changsha, China
[3] Hunan University, Changsha, China
* heinz.konietzky@ifgt.tu-freiberg.de

1 Introduction

Stability and serviceability of brittle rocks or rock masses is mainly governed by load level and strength, whereby three processes can be distinguished: sub-critical crack and critical crack growth under constant or slowly changing load and dynamic triggered failure. Some selected recent research results with respect to (1.) continuum and discontinuum based numerical approaches considering subcritical and critical crack growth under constant load (Chen et al. 2014, 2015, 2016; Konietzky et al. 2009, 2015; Li et al. 2014, 2015, 2016; Tan et al. 2016) and (2.) first results of the stability of discontinuities under complex dynamic loading obtained by dynamic shear box tests (Dang et al. 2016a,b) are presented.

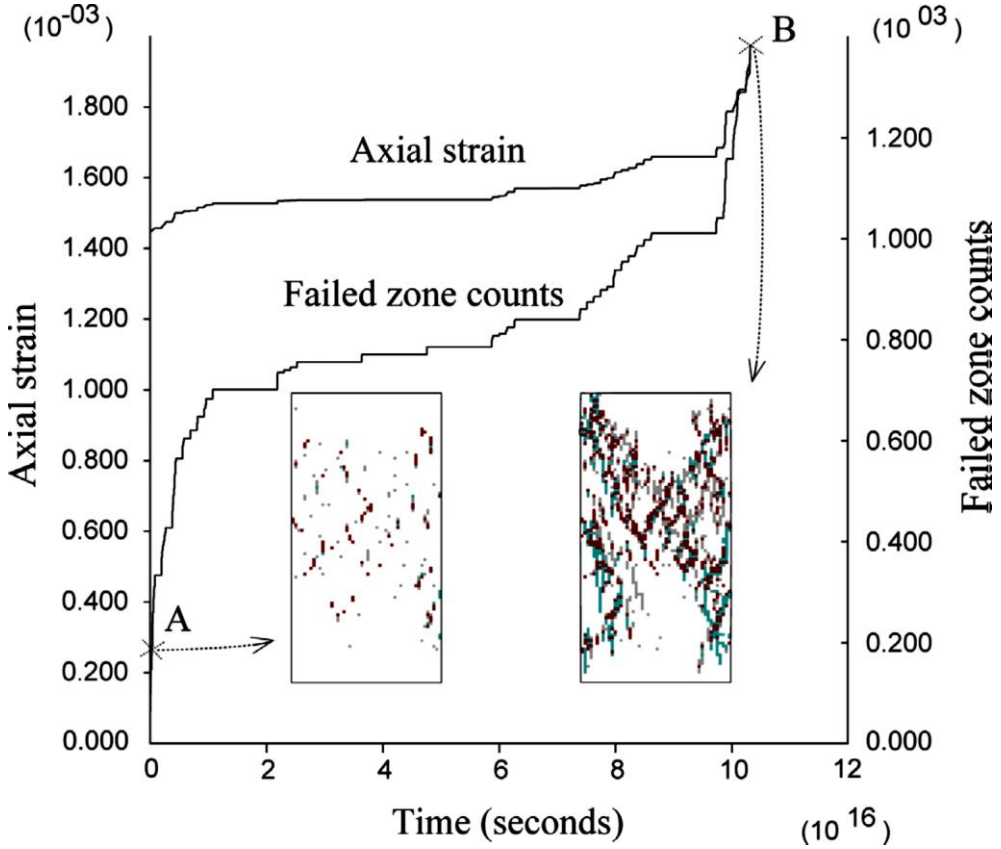

Figure 1. Damage evolution of a rock sample under uniaxial compressive load assuming stochastic initial microcrack distribution.

2 Damage evolution due to subcritical and critical crack growth

Macroscopic fracturing is considered as the result of the growth and coalescence of microcracks. Based on fracture mechanics, subcritical (based on Charles or Charles-Hillig equations) and critical crack growth (linear elastic fracture mechanics) can be distinguished and used to determine the life

time of rocks under loading using stress and crack-size dependent crack propagation velocity. Exemplary, Fig. 1 shows numerical simulation of damage evolution over time in terms of failed zone counts and axial deformation of a rock sample under uniaxial compression, which reveals primary, secondary and tertiary creep phases. This model assumes the existence of a huge number of microcracks with different length and orientation following certain stochastic distributions.

3 Stability of discontinuities under complex dynamic loading

Dynamic shear box tests have revealed several interesting features. One of them is a phase shift between normal and shear force, whereby shear force is lagging. This leads to varying actual (dynamic) friction coefficients *k* defined as actual ratio between shear to normal stress like shown in Fig. 2. Consequently, a simple superposition of static and dynamic forces and assumption of constant friction coefficients will lead to wrong predictions. These findings are important for earthquake research as well as landslide phenomena under dynamic excitation.

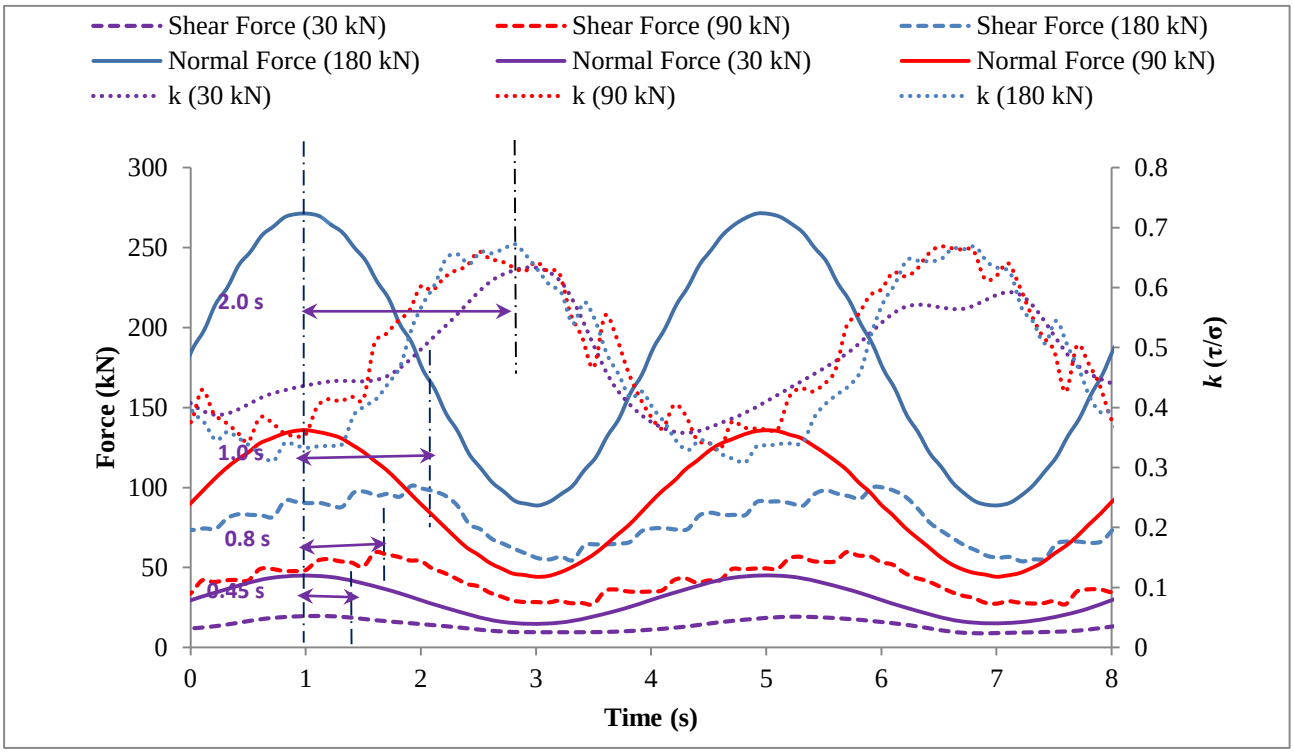

Figure 2. Forces and actual friction coefficient vs. time for dynamic normal load test (shear velocity 3 mm/s, normal impact frequency 0.25 Hz, normal loads 30 ± 15 kN, 90 ± 45 kN and 180 ± 90 kN).

4 Conclusions

Lifetime of rocks depends on both, loading situation and initial damage constellation, which can be described by stochastic distribution of microcracks in terms of orientation and length. If loading is below short-term strength subcritical crack growth will lead to growth and coalescence of microcracks and finally critical crack growth will lead to macroscopic failure. Both, continuum based and discontinuum based approaches are suited to model this kind of damage evolution which can cover primary, secondary and tertiary creep (creep rupture). This kind of approach is valid for brittle rocks under static loading. In case of dynamic loading pre-existing fractures are the dominant feature in respect to potential instability. Direct shear tests have revealed, that dynamic impact in terms of load level, frequency and shear velocity have significant influence on shear resistance. Therefore, in addition to the quasi-static subcritical and critical crack growth processes, the dynamic stability / instability of pre-existing fractures / faults have to be considered.

5 Reference list

Chen, W, Konietzky, H, Tan, X, Frühwirt, T. 2016. Pre-failure damage analysis for brittle rocks under triaxial compression. Computers and Geotechnics 74, 45-55.

Chen, W, Konietzky, H, Abbas, SM. 2015. Numerical simulation of time-independent and -dependent fracturing in sandstone. Engineering Geology 2, 118-131.

Chen, W, Konietzky, H. 2014. Simulation of heterogeneity, creep, damage and lifetime for loaded brittle rocks. Tectonophysics 633, 164-175.

Konietzky, H, Tan, X, Chen, W. 2015. Time-dependent DEM based fracture simulations at the grain-size level for brittle heterogeneous solids., Proc. 4th Int. Conference on Particle Based Methods, Barcelona, Spain, 41-51.

Konietzky, H, Heftenberger, A, Feige, M. 2009. Life time prediction for rocks under static compressive and tensile loads - a new simulation approach. Acta Geotechnica 4, 73-78.

Li, X, Konietzky, H, Li, X. 2016. Numerical study on time dependent and time independent fracturing processes for brittle rocks. Engineering Fracture Mechanics 163, 89-107.

Li, X, Konietzky, H. 2015. Numerical simulation scheme for time-dependent crack growth in hard brittle rock. Acta Geotechnica. 10, 513-531.

Li, X, Konietzky, H. 2014. Simulation of time-dependent crack growth in brittle rocks under constant loading conditions. Engineering Fracture Mechanics 119, 53-65.

Tan, X, Konietzky, H, Chen, W. 2016. Numerical simulation of heterogeneous rock using discrete element model based on digital image processing, Rock Mechanics Rock Engineering. 49, 4957-4964.

Dang, W, Konietzky, H, Frühwirt, T. 2016a. Direct shear behavior of a plane joint under dynamic normal load (DNL) conditions. Engineering Geology. 213, 133-141.

Dang, W, Koniettky, H, Frühwirt, T. 2016b. Rotation and stress changes on a plane joint during direct shear tests. Int. J. Rock Mech. Min. Sci., 89, 129-135.

Investigating the long-term behaviour of brittle rocks: Visco-elastic creep parameters and time-to-failure

Chrysothemis Paraskevopoulou[1*] and Matthew Perras[2]

[1] School of Earth and Environment, University of Leeds, United Kingdom
[2] Department of Earth Sciences, ETH Zurich, Switzerland
* C.Paraskevopoulou@leeds.ac.uk

1 Abstract

Understanding how rocks deform over time can lead to elimination of conservatisms in regards to excavation-design, especially, in the case of nuclear waste repositories where the lifetime of these projects exceeds one million years. Such projects are designed to be constructed in good quality rocks, which can behave in a brittle manner. It is commonly assumed that brittle rocks are unlikely to exhibit time-dependent deformations. In this study it is proven that not only can brittle rocks deform over time with different rates but also the expected failure time is dependent on the visco-elastic parameters of the specific rock specimen.

2 Introduction on time-dependent behaviour of rocks

In the literature (Singh 1975, Aydan et al. 1993, Malan et al. 1997, Hargos et al. 2008, Brantut et al. 2013, Paraskevopoulou et al. 2016, Paraskevopoulou 2016) time-dependency of rock under load has been widely discussed. However, in practice, there is often a miscomprehension and misinterpretation of the different time-dependent phenomena, and the mechanisms involved. The main time-dependent phenomena are defined and summarized in Fig. 1.

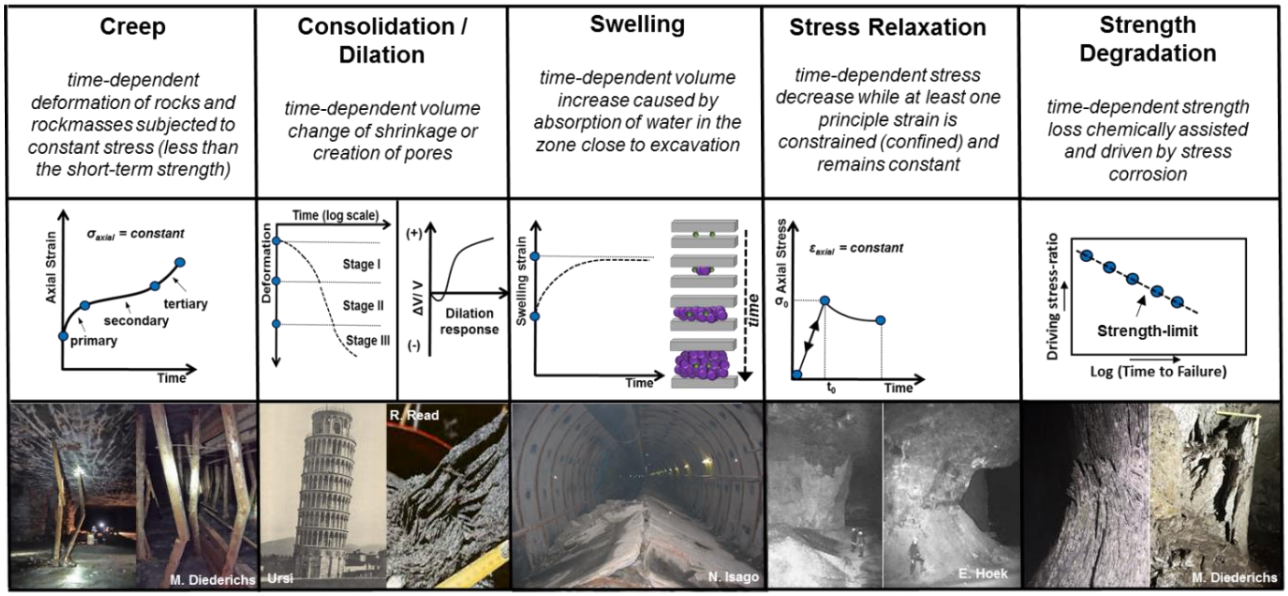

Figure 1: Examples of time-dependent phenomena (with photo acknowledgements given), the behavioural response with time and a description of the phenomena commonly associated with geotechnical engineering (Paraskevopoulou 2016).

Fig. 1 illustrates examples of failures in geotechnical engineering due to these phenomena (column on the left), their main behavioural characteristics with time (middle column), and a description of the process involved (right column) are shown. This paper focuses on investigating the time-dependent behaviour of brittle rocks under a constant (controlled) stress-state by performing a series of uniaxial static load (creep) tests on two types of limestone. The primary focus is on the creep behaviour and

associated degradation and how these related mechanisms influence the time to failure of the laboratory samples. More specifically, this study examines the long-term behaviour of the two types of limestone (Jurassic and Cobourg) and also investigates if a stress threshold exists below which the rock will cease to fail.

3 Damage evolution and failure in brittle rocks

At least four distinct stages of the brittle failure process in compression tests can be identified if the stress-strain response is monitored during loading, as shown in Fig. 2. These stages are: i.) closure of preexisting cracks; ii) linear elastic behaviour; iii) stable crack growth; and iv) unstable crack growth, which leads to failure and the peak strength (the point of maximum stress). These damage or crack growth thresholds have been defined by the International Rock Mechanics Committee on Spall Prediction as CI for Crack Initiation and CD for Crack Damage, respectively (Diederichs and Martin 2010). At increasing stress levels between CI and CD the cracks accumulate and grow in a stable manner. However, if the load or axial stress is held constant between these thresholds, time-dependent crack growth occurs leading to time dependent deformation. Loading above the critical damage threshold (CD) marks the growth of cracks in an unstable manner during Unconfined Compressive Strength (UCS) testing. If the axial stress is maintained at a stress level in excess of CD, accelerated creep rates may occur that can lead to a sudden failure of the specimen (Schmidtke and Lajtai 1985).

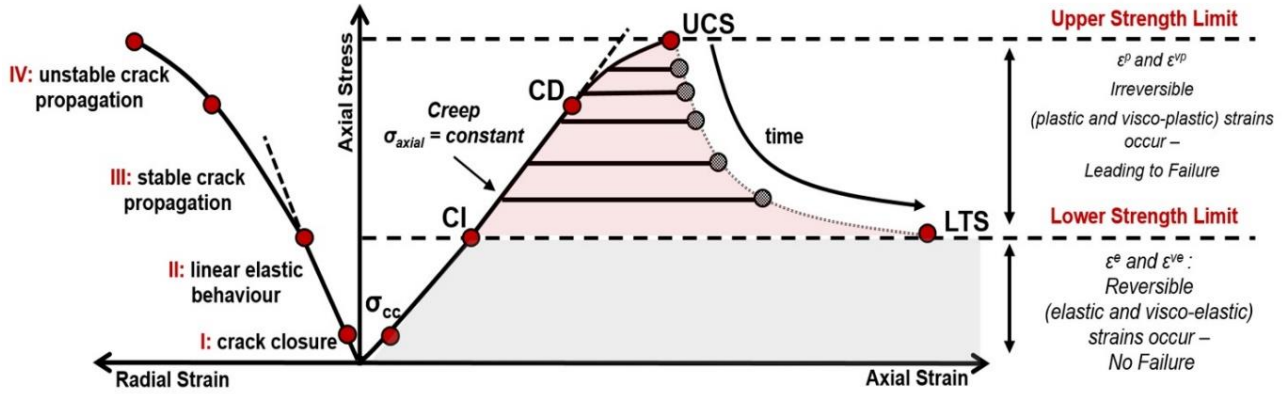

Figure 2: Schematic representation of the stress - strain response and stages of brittle rock fracture process and evolution of the short-term strength of the material to its long-term strength when subjected to a constant stress conditions, (where: σ_{cc} – stress level at crack closure, CI – crack initiation, CD – critical damage, UCS – unconfined compressive strength, σ_c – applied constant stress) (Paraskevopoulou, et al. 2017).

4 Laboratory testing

Two testing series were performed for assessing the long-term creep behaviour, the first was on Jurassic limestone and the second on Cobourg limestone samples. Single-step tests were conducted on 10 Jurassic and 4 Cobourg samples, which were held at stress levels above CI for seconds to several weeks until failure occurred. Most of the single-step tests fail within the first few hours and those that did not reach failure after several days to weeks were terminated and unloaded. Single-step tests are practically convenient but require more specimens to fully cover the spectrum of the expected range of the time to failure.

The static load testing began at load levels close to the peak strength. Subsequent tests were conducted at lower driving stress levels approaching the CD threshold and below. In these tests, the target constant stress is applied and maintained by controlling the axial load while measuring the strains (axial and lateral) as they increase as the sample proceeds to failure. Samples loaded close to the peak strength fail catastrophically into many fragments, while samples loaded below CD fail in a less violent manner.

5 Data analysis

The results from laboratory testing on the two types of limestone (Jurassic and Cobourg) are presented in Fig. 3 using the driving stress-ratio. The closed-filled symbols on Fig. 3 refer to the samples that reached failure. The samples that did not fail are illustrated with open-filled symbols. The samples closer to the CD threshold are expected to fail. They could be outliers or more likely they were stronger than the average UCS value, which is typically used to normalize the time to failure plot. Test with driving stresses close to and below the CI threshold exhibit no failure for the duration of the test. Many of the test results with a driving stress greater than 0.6 would be expected to fail when compared to literature data (Paraskevopoulou et al. 2017).

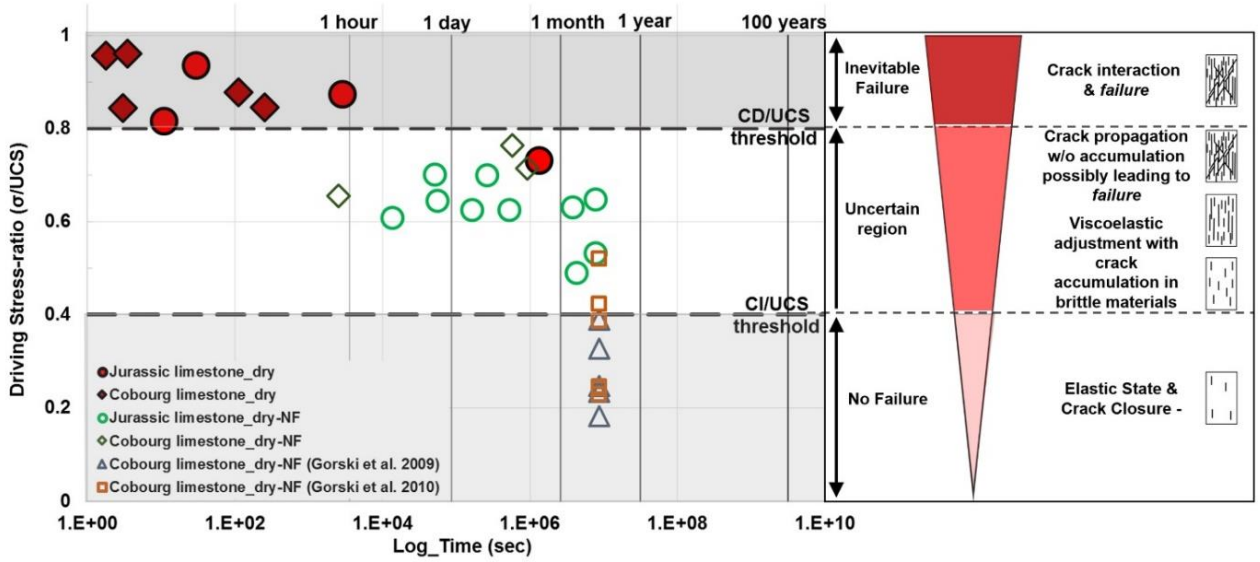

Figure 3. Static load test data of Jurassic and Cobourg limestone performed at room temperature in dry conditions (where the driving stress-ratio is the stress level at failure to unconfined compressive strength of the material). The 'NF' in the legend indicates that these samples or tests did not fail whereas the 'F' denotes that these samples or tests reach failure (Paraskevopoulou, et al. 2017).

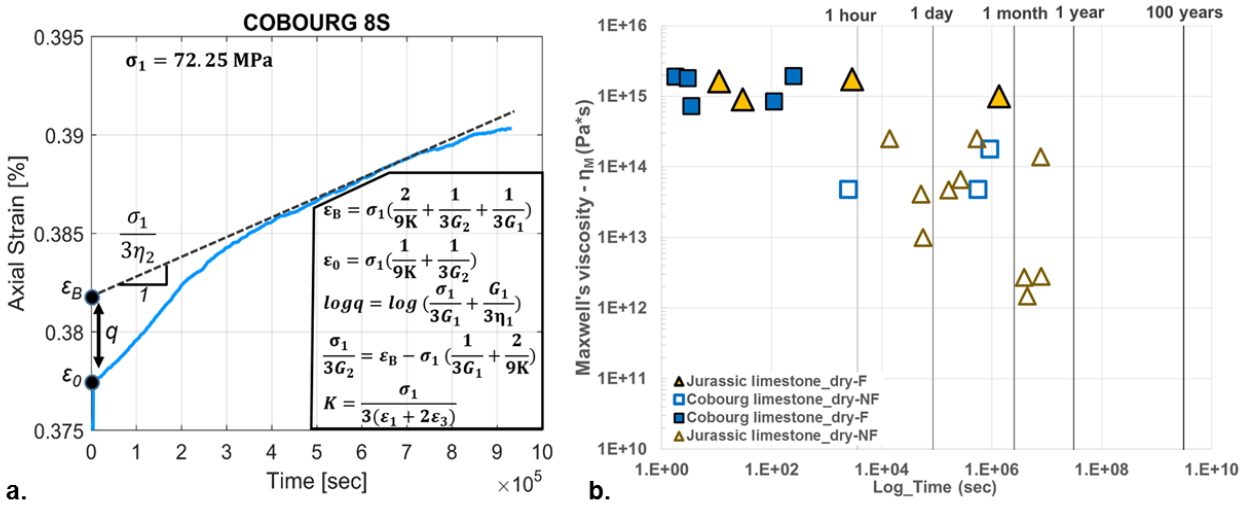

Figure 4. a.) Example to illustrate the estimation of the visco-elastic parameters for the Burgers creep mode. I Where: ε_1 is the axial strain, ε_3 is the radial strain, σ_1 is the constant axial stress, K is the bulk modulus, η_1 and η_2 refer to Kelvin's and Maxwell's model viscosities, G_1 and G_2 is Kelvin's and Maxwell's shear modulii, ε_0 is the axial strain at time zero when the axial stress begins to be held constant and ε_B is the axial strain attained at infinity due to time-dependency. b.) the Relationship between Time and Maxwell's viscosity. The static load tests were performed at room temperature in dry conditions.

When the data set is compared to the visco-elastic creep parameters and more specifically the viscosity of the Maxwell's model (η_2), which determines the rate of viscous flow (Fig. 4a), it shows a clear separation between samples that failed and those that did not, as shown in Fig. 4b. Viscosity is the resistance of matter to flow. The less viscous a material is, the easier it is to flow. This is in agreement with the results of this study. It is shown that the more viscous samples did reach failure (shown Fig. 3 with filled shapes) whereas the less viscous tended to creep more as they are prone to flow. It can be noted that there is a threshold in viscosity below which the samples exhibit creep behaviour without creep leading to accumulated damage. This means that the creep behaviour can take place without damaging the rock and leading to failure.

6 Concluding remarks

This paper illustrates the importance of understanding the behaviour of brittle rocks subjected to driving stress between CI and CD. Driving stresses near or below the CI stress level show no failure whereas above the CD threshold failure can be expected within 1 hour to a few days. In the uncertain region, it is assumed that failure will take place eventually, however more data from similar tests should be taken into consideration. However, the expected failure time is dependent on the visco-elastic parameters of the specific rock specimen. It is suggested that deriving visco-elastic parameters from the strain – time curves of similar tests can be an important indicator of the failure, since the magnitude of the Maxwell viscosity or the rate of flow according to the secondary or steady state on the creep curve could be used as an indicator for failure.

7 Reference list

Aydan, O., Akagi, T. and Kawamoto, T. 1993. The squeezing potential of rocks around tunnels; Theory and prediction. J. Rock Mech Rock Eng. 26(2), pp. 137-163.

Brantut N., M.J. Heap, Meredith P.G. and Baud P., 2013. Time-dependent cracking and brittle creep in crustal rocks: a review. J. Struct. Geol., 52, pp. 17–43.

Diederichs, M., S. and Martin, C.D. 2010. Measurement of spalling parameters from laboratory testing. In Proc. of Eurock, Lausanne, Switzerland.

Hagros, A., Johanson E., Hudson J., A., 2008. Time dependency in the mechanical properties of crystalline rocks: a literature survey. Possiva OY, Finland.

Malan, D. F., Vogler, U., W., and Drescher, K., 1997. Time-dependent behaviour of hard rock in deep level gold mines. J. S. Afr. Inst. Min. Metall., 97, pp.135-147.

Paraskevopoulou, C., Perras, M., Diederichs, M.S., Löw, S., Lam, T. and Jensen, M., 2017. Time-dependent behaviour of brittle rocks based on static load laboratory testing. Journal of Geotechnical and Geological Engineering.

Paraskevopoulou, C., Perras, M., Diederichs, M.S., Amann, F., Löw, S., Lam, T. and Jensen, M. 2016.The three stages of stress relaxation - Observations for the long-term behaviour of rocks based on laboratory testing. Journal of Engineering Geology.

Paraskevopoulou, C. 2016. Time-dependency of rocks and implication in tunnelling, Ph.D. Thesis, Queen's University, Canada.

Singh, D.P. 1975. A study of creep of rocks. Int. J. Rock Mech Sci & Geomech, 12, pp. 271-276.

Schmidtke, H. and Lajtai, Z. 1985. The long-term strength of Lac du Bonnet granite. J. Rock Mech. Min. Sci. Geo., 22, pp. 461–465.

Influence of sample geometry on constant-strain relaxation tests on limestone

Matthew Perras[1*], Patrick Hädener[1], Kerry Leith[1], Simon Loew[1] and Chrysothemis Paraskevopoulou[2]

[1] Department of Earth Sciences, ETH Zurich, Switzerland
[2] School of Earth and Environment, University of Leeds, United Kingdom
* matthew.perras@erdw.ethz.ch

1 Introduction

One of the most common tests to measure time-dependent behaviour and time-to-failure is a creep test, where the load is help constant and the strains are measured with time. A less commonly conducted test on rock specimens is a relaxation test, where one of the sample strain levels is held constant and the stress change is measured with time. A recent study by Paraskevopoulou et al. (2017) identified that the relaxation behaviour appears to be equal and opposite to the creep behaviour, as illustrated in Fig. 1. In this extensive study on two different limestones, the procedure of how to conduct a relaxation test on brittle rocks was examined for cylindrical specimens was examined. A current study, presented here in, has been initiated on prismatic specimens to examine the influence of specimen shape on the relaxation behaviour of brittle rocks.

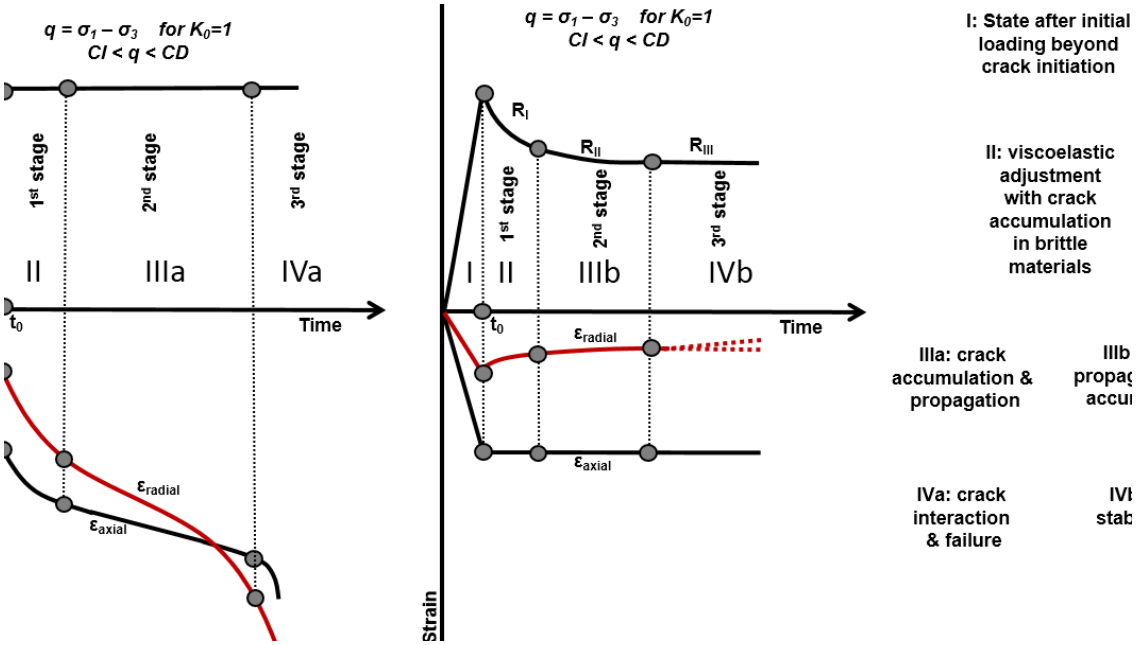

Figure 1. Stress (q) and strain (Ɛ) behaviour of creep (left) and relaxation (right) tests, along with descriptions of the crack behaviour during the different stages (Paraskevopoulou et al. 2017).

The Jurassic limestone, from northern Switzerland, and the Cobourg limestone, from Southern Ontario, Canada have been tested in this study. The Jurassic specimens are dominantly fossil rich, whereas the Cobourg specimens have irregular fossil rich layers mixed with argillaceous layers. The latter is the potential rock mass for Canada's low and intermediate level nuclear waste repository.

The influence of specimen shape on compression tests, as well as other test types, has been examined on a variety of materials and several authors (e.g. Li et al. 2011). However, many of these studies have focused on the height to width (radius) ratio of individual geometries and less on a variety of specimen geometries from the same material. A collection of studies, including this one,

that have tested cylindrical and prismatic specimen geometries under uniaxial compressive conditions are shown in Fig. 2 to illustrate the influence on the mechanical properties.

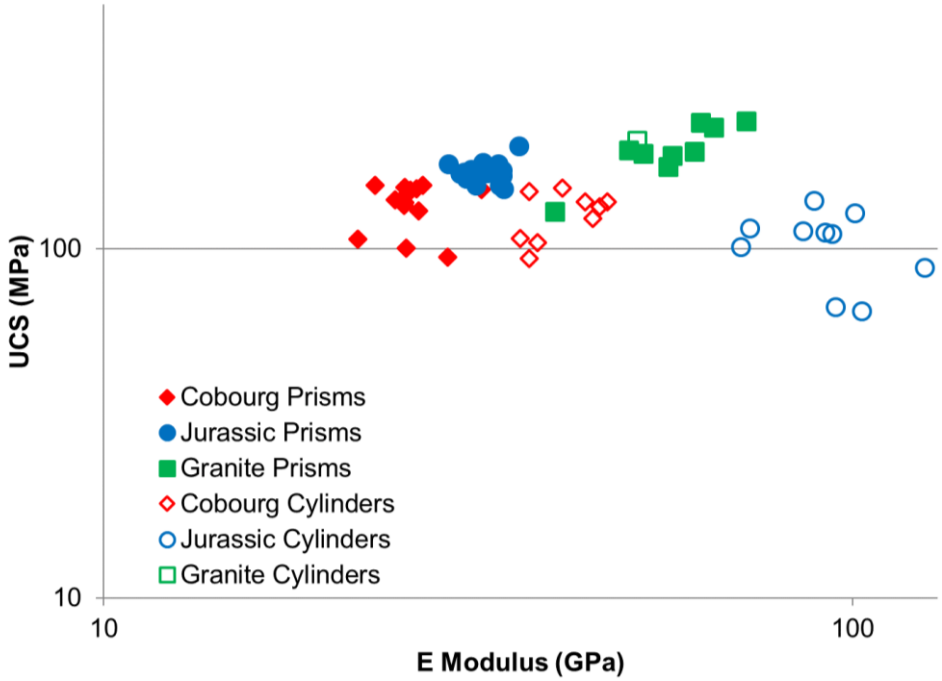

Figure 2. Influence of specimen shape on the mechanical properties of limestone (this study) and granite (Li et al. 2011).

In this study, the prismatic stiffness is much less than the cylidrical stiffness by 2-3 times, although the strength is higher for the prismatic specimens. Another study by Li et al. (2011) on granite specimens indicates that this difference maybe less. The prismatic specimen geometry was selected such that the surface area of the end faces for load would be similar to that of the cylidrical specimens. This should eliminate influences bases on the grain size to specimen size, as has been discussed by others (Bewick et al. 2015). The possible influence of specimen specific stiffness due to variations in the mineralogical content will be investigated at a later stage of the current study.

2 Constant-strain relaxation testing methods

The uniaxial compression tests have been used to set the target strain levels for the relaxation tests. Paraskevopoulou et al. (2017) examined relaxation tests that held either the radial or the axial strain constant and found that the axial strain controlled tests resulted in a more consistent overall behaviour. For the current prismatic tests, the average axial strain at different percentages of the average compressive strength have been used as target strain levels on single stage tests (i.e. one load target per specimen). For a comparison of multi-stage versus single stage relaxation tests, the reader is referred to Paraskevopoulou et al. (2017). To summarize the relaxation test methodology and analysis used in the current study, the steps are listed as follows:

- Specimen is loaded, similar to a standard uniaxial compressive test following the ISRM (1979) method, to the targeted axial strain level using a servo controlled compression machine.
- The axial strain level is held constant and the stress and radial strain is monitored until the 3rd stage of stress relaxation (see Fig. 1) is reached.
- The specimen is unloaded to 5 kN and the axial strain behaviour is monitored for 2-4 hours to understand the amount of plastic strain that has accumulated in the specimen during loading and relaxation.
- The temperature and relative humidity is measured throughout the test.
- A thermal correction is applied to the stress relaxation and radial strain to account for both the thermal strain of the specimen and the sensor frame.
- The stages of stress relaxation for the stress-time and radial strain-time are determined.

- The maximum stress relaxation, from peak load to the start of the 3rd stage of stress relaxation is determined.

3 Prismatic sample geometry influence on constant strain relaxation

The general behaviour, as illustrated in Fig. 1 based on observations from cylindrical specimens by Paraskevopoulou et al. (2017), holds true for the prismatic specimens as well. From the stress-time and radial-strain curves of the prismatic specimens, the same three stages of stress relaxation (RI, RII, RIII) are observed for both limestones and are similar over the full range of the driving stress ratios examined. The time to reach the start of the third stage of stress relaxation is also similar between the cylindrical and prismatic specimens.

Although the three stages are observed for the prismatic specimens, the magnitude of the maximum stress relaxation is greater for the prismatic specimens than the cylindrical, as shown in Fig. 3. The difference increases slightly as the driving stress increases, as indicated by the exponential trend lines. A linear trend line for the cylindrical Jurassic test results has the best R^2 (0.65) value compared to an exponential trend (0.61), however, the cylindrical Cobourg trend line is best represented by the exponential fit with an R^2 (0.68). All trend lines have similar R^2 values between 0.62 to 0.68.

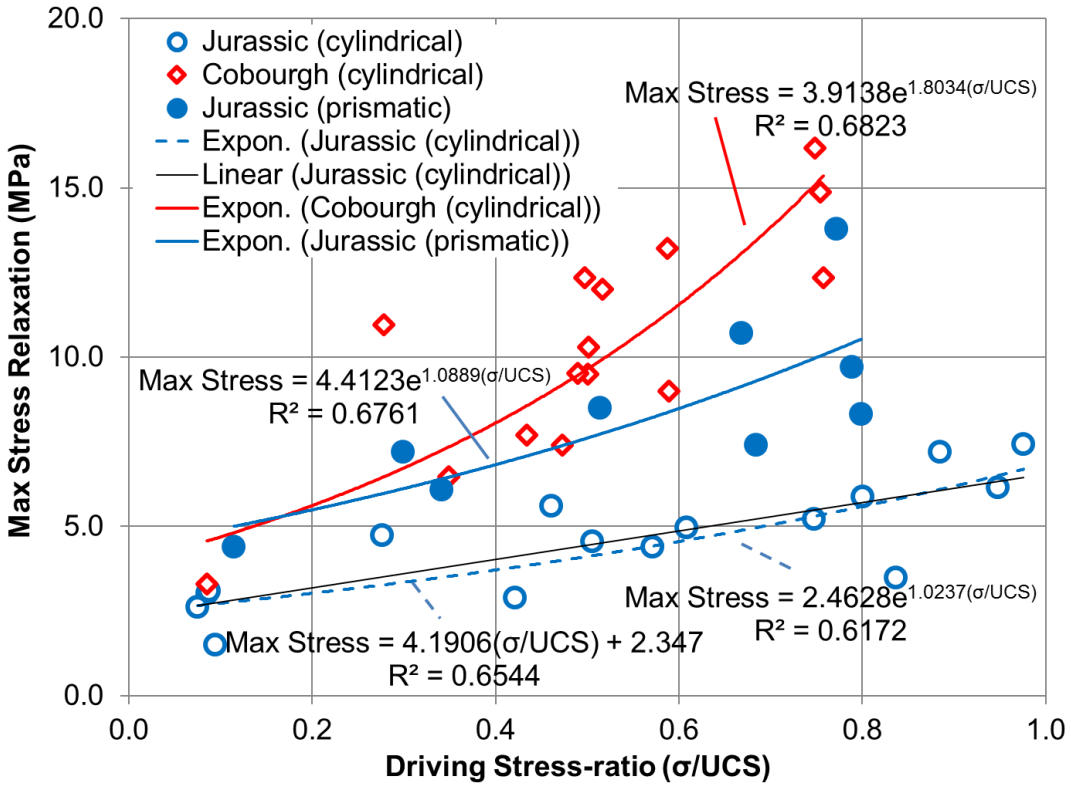

Figure 3. Comparison of the maximum stress relaxation between cylindrical and prismatic specimens of Jurassic and Cobourg limestone showing more stress relaxation for prismatic specimens.

4 Discussion

During UCS testing and on some of the high driving stress prismatic specimens cracking was often observed to occur first on the corners, as shown in Fig. 4. However, although occurring on the corners, these cracks tend to terminate before the end of the specimen. A simplistic 3D elastic numerical model indicated that the corners of the prismatic specimen influences the stress flow within the specimen differently than in a cylindrical one. The corners cause a draw down in the stresses at the corners such that at any one elevation within the sample the stress on the corner is lower than that

inside the specimen and lower than the stress on the center of the face of the specimen. In comparison, the stress is more evenly distributed within the cylindrical specimen with the same stress level across any elevation contour, as indicated in the numerical results of Fig. 4.

The stress distribution with the specimen will influence the fracture initiation and propagation. For the same material, under the same load on the platen, the prismatic specimen will have a larger outer shell of low stress magnitude which will surpress crack growth and limit crack propagation within this region. This would tend to increase the strength as higher loads are required to drive cracks towards the outer edges of the specimen to finally fail the specimen.

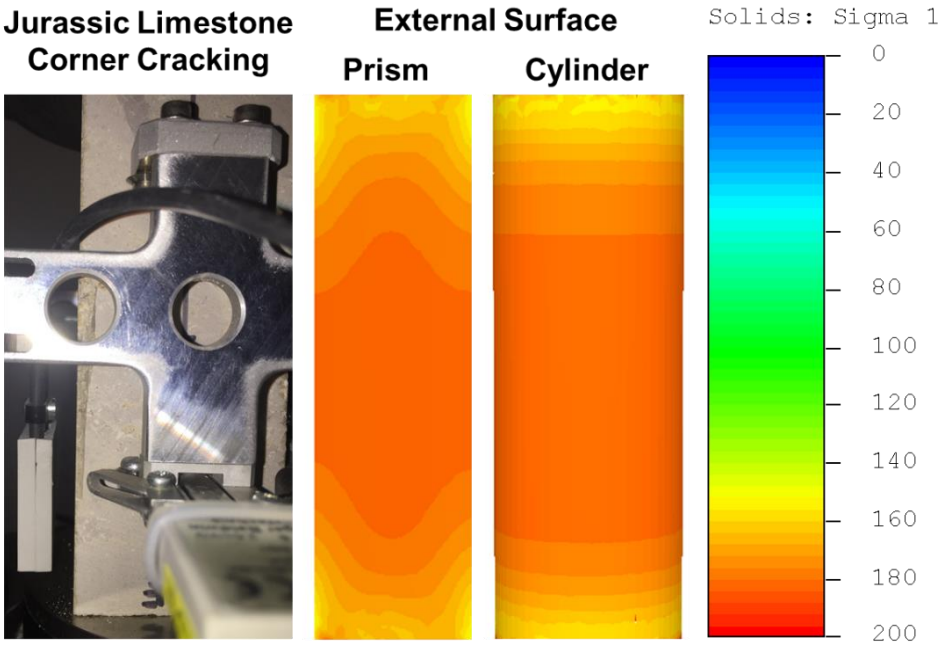

Figure 4. A close up of corner damage on a prismatic specimen of Jurassic limestone during a relaxation test (left) and simplified 3D elastic numerical model of prismatic and cylindrical specimens, showing the external surface stress contours of the maximum stress in MPa.

5 Conclusions

A constant strain relaxation test is a less commonly conducted time-dependent test than a constant stress creep test. Both tests examine potential *in-situ* conditions and behaviours that could occur around underground excavations or other natural situations (faults, slopes, etc.). The advantage of a relaxation test is that the third stage is reached within a short time frame compared to the third stage of a creep test on a similar brittle rock. The findings from this study indicate that this time frame is similar for both cylindrical and prismatic samples and that the general stress-time and radial strain-time behaviour is similar. There is however a difference in the magnitude of the maximum stress that relaxes during the test, with the prismatic specimens resulting in more stress relaxation than the equivalent test on a cylindrical specimen. This is at least partially related to how the stresses are distributed throughout the different specimen geometries, as indicted from the difference in the stiffness and peak strength of the UCS test results and based on a simple 3D elastic numerical model. Other potential influencing factors, such as variations in specimen mineralogy, will be investigated as the study continues. Never the less, this study indicates that there is some influence on uniaxial compression and constant strain relaxation tests from the specimen geometry.

6 References

Bewick, RP, Amann, F, Kaiser, PK, Martin, CD. 2015. Interpretation of UCS test results for engineering design. 2015 ISRM Congress, Montreal, Canada.

Li, D, Li, CC, Li, X. 2011. Influence of sample height-to-width ratios on failure mode for rectangular prism samples of hard rock loaded in uniaxial compression. Rock Mechanics and Rock Engineering 44(3), 253-267.

Paraskevopoulou, C, Perras, M, Diederichs, M, Amann, F, Loew, S, Lam, T, Jensen, M. 2017. The three stages of stress relaxation – Observations for the time-dependent behaviour of brittle rocks based on laboratory testing. Engineering Geology 216, 56-75. DOI: 10.1016/j.enggeo.2016.11.010.

Subcritical crack growth in complex stress field at the nuclear waste disposal site in Olkiluoto, western Finland

Topias Siren[1*]

[1] Department of Civil Engineering, School of Engineering, Aalto University, Helsinki, Finland
* topias.siren@aalto.fi

1 Introduction

In the geological nuclear waste disposal concept, the knowledge of long-term behavior, especially related to rock strength, is of high importance for long-term safety. An *in situ* experiment to investigate rock mass strength was conducted in Olkiluoto at Posiva's ONKALO underground characterization facility, located in Western Finland. The Posiva's Olkiluoto Spalling Experiment (POSE) was executed at the depth of -345 m, in a complex rock stress field and lithology. After executing the experiment a back-calculation phase followed to develop the predictive capability (Valli et al. 2015).

2 Methodology

The eight years of experience and research on the rock strength in ONKALO and executing the POSE *in situ* experiment reveal that the rock mass failure is governed by fracture growth on lithological borders. A two-fold failure criterion was proposed (Siren et al. 2015b) based on the onset of rock mass damage at 40 MPa and a peak rock mass strength of 90 MPa.

The confirming site investigations (Siren et al. 2015b) also indicated that the construction-induced (EDZ_{CI}) and stress-induced excavation damage (EDZ_{SI}) could be distinguished within the EDZ. An indication of this was the discovery of an EDZ_{SI} fracture in the tunnel floor under tensile conditions (Fig. 1) revealed while a section of the floor was wire sawed. The fracture had no characteristics of blasting or natural fracture processes and later Koittola *et al.* (2016) confirmed with a fracture mechanics simulation that a tensile stress field could be the driving factor of the observed fracture.

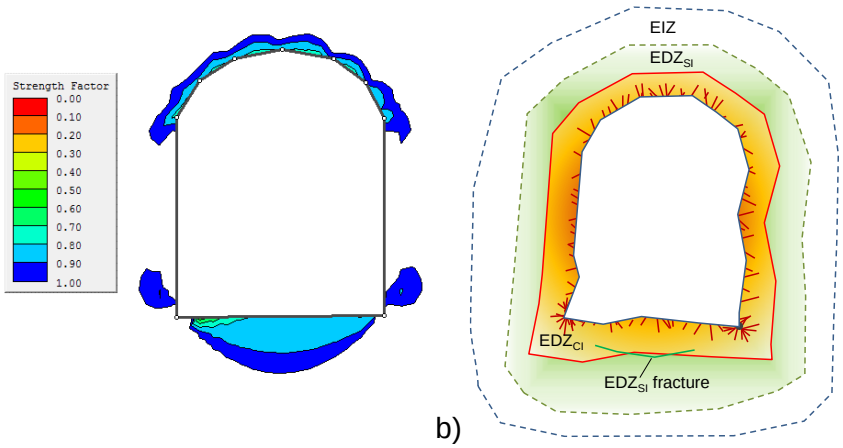

Figure 1. a) Areas to prone to tensile failure at depth of -430 m assuming proposed in situ stress model I and average tensile strength 8.9 MPa for Gneissic rocks (Siren et al. 2015b) modelled using Rocscience software Examine2D based on boundary element method, and b) conceptualization of EDZ_{CI} and EDZ_{SI}.

In the First Phase of the POSE experiment three new fractures initiated subcritically in the first two experiment holes. The first two fractures were localized, after boring of the first hole (Ø1.5 m), in mica-rich layers and rock type contacts, which were known to be relatively weak. The third, subvertical fracture was observed in the wall of the second hole after boring had been completed. Also in the third Phase, a subcritical failure at a mica-rich layer was observed. (Siren *et al.* 2015a)

Despite the similar UCS strengths, the two major rock types in ONKALO behave totally different when confined in true-triaxial tests (Behrestaghi *et al.* 2016). The damage initiates and propagates in veined gneiss (VGN) in lower stresses than in pegmatitic granite (PGR). The PGR shows a significant amount of AE activity while withstanding high stresses (up to 240 MPa). The VGN fails at fairly low stresses while failure progresses along the foliation plane. The VGN shows transverse anisotropic behavior that was needed to be taken in account in the back-calculation of the experiment results.

3 Conclusions

The true-triaxial testing results correspond to the observed behavior *in situ*. Based on the prediction-outcome work, discrete modelling programs are more useful when predicting rock mass behavior and taking into account the subcritical crack growth of the rock material, when applicable. The crack growth velocity (Charles 1958; Atkinson 1984) is very low in regions I and II (10^{-8} to 10^{-18} s^{-1}) and therefore it is reasonable only to consider the meaningful crack growth velocities that can be measured in the laboratory (Region III), see Fig. 2.

For detailed back-calculations the rock material was divided in three components, as shown in Fig. 2, and based on the *in situ* observations, a laboratory testing campaign to study rock creep properties was started, while transversely isotropic material models were included in a fracture mechanics program FRACOD2D (Shen *et al.* 2016). Linking the observation of subcritical crack growth and stress-induced excavation damage, it can be argued that stress is driving subcritical crack growth at the investigation site. Despite the structurally controlled failure and subcritical crack growth, the rock damage is limited in dimensions, and the site well-suited for nuclear waste disposal.

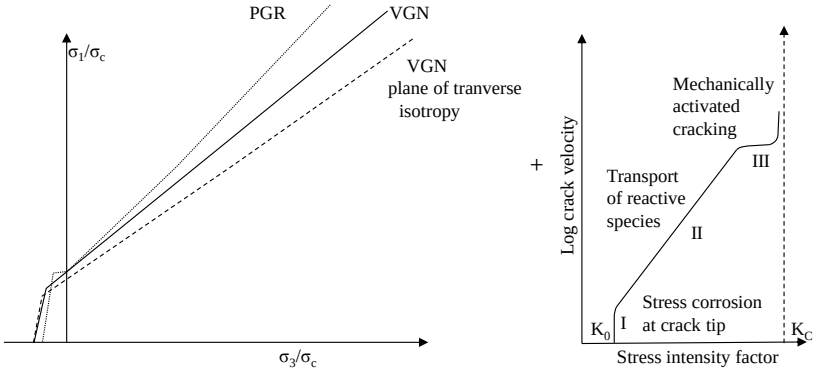

Figure 2. Behavior of ONKALO rocks under different principal stress conditions, and a concept of subcritical crack growth behavior (reproduced after Atkinson 1984), observed with veined gneiss.

4 Reference list

Atkinson, BK. 1984. Subcritical Crack Growth in Geological Materials J. Geophys. Res. 89, pp. 4077-4114.

Charles, RJ. 1958. Static Fatigue of Glass.J. Appl. Phys. 29, pp. 1549-1560.

Behrestaghi, MHN, Young, RP, Suikkanen, J. 2016. ONKALO POSE Experiment - Strength, Deformation and Seismic Response of Olkiluoto Isotropic Pegmatitic Granite and Anisotropic Migmatitic Gneiss under a State of True-Triaxial Stress. Working Report 2016-41. Eurajoki: Posiva Oy.

Koittola, N, Suikkanen, J, Siren, T. 2016. Methods To Study, Model And Confirm The Existence Of Stress-Induced Excavation Damage Zone. 7th Int. Sym In-Situ Rock Stress May 10-12, 2016, Finland.

Siren, T, Hakala, M, Valli, J, Kantia, P, Hudson, JA, Johansson, E. 2015a. In situ strength and failure mechanisms of migmatitic gneiss and pegma-titic granite at the nuclear waste disposal site in Olkiluoto, Western Finland. Int. Jour. Rock Mech. Min. Sci., 79, pp. 135-148.

Siren, T, Kantia, P, Rinne, M. 2015b. Considerations and Observations of Stress-Induced and Construction-Induced Excavation Damage Zone in Crystalline Rock. Int. Jour. Rock Mech. Min. Sci. 73, pp. 165-174.

Shen, B, Shi, J, Rinne, M, Siren, T, Suikkanen, J, Kwon, S, Min, KB. 2016. Two-dimensional displacement discontinuity method for transversely isotropic materials. Int. Jour. Rock Mech. Min. Sci., 2016;83;218–230.

Valli, J, Hakala, M, Wanne, T, Siren, T, Suikkanen, J. 2015. ONKALO POSE Experiment – POSE Back Analyses Plan. Working Report 2015-22. Eurajoki: Posiva Oy.

Time to failure - progression of joints by subcritical crack growth and stress corrosion cracking in quartzite

Anne Voigtländer[1*], Kerry Leith[2] and Michael Krautblatter[1]

[1] Department of Civil, Geo and Environmental Engineering, Technical University of Munich, Germany
[2] Department of Earth Sciences, ETH Zurich, Switzerland
* a.voigtlaender@tum.de

1 Subcritical crack growth and stress corrosion cracking

Progressive deformation of rocks, e.g. by creep (Rutter 1972; Itô & Sasajima 1980; Brantut et al. 2012) and fatigue (Attewell & Farmer 1973; Costin & Holcomb 1981; Ko & Kemeny 2013), at low magnitude near constant stresses is facilitated by different subcritical mechanisms causing gradual irreversible damage, commonly termed subcritical crack growth (Atkinson 1984; Atkinson & Meredith 1987). Subcritical crack growth is an effective means of facilitating time-dependent material degradation (Atkinson 1984; Brantut et al. 2013; Nara et al. 2013). These mechanisms include plastic (Atkinson & Meredith 1987), as well as brittle deformations (Atkinson & Meredith 1987; Nara et al. 2013). These mechanisms are enhanced in the presence of chemically active fluids, such as water (Atkinson & Meredith 1981; Lawn 1993).

An interaction of chemical and mechanical processes, as postulated in stress corrosion cracking (SCC), reduces brittle fracture toughness, and therefore increases subcritical fracture propagation velocities. SCC involves a range of range processes, including stress enhanced dissolution (as described by the Charles' law), hydrolysis and embrittlement, and a reduction of surface energies which in turn reduces cohesive forces and promotes granular disintegration. To better understand the coupling of chemical and mechanical processes in stress corrosion cracking and subcritical crack growth, we set up single edge notch bending (SENB) creep tests, mimicking natural conditions.

2 Experimental methods

Six Alta-Quartzite samples (AQ 1-6, 300x30x70 mm) were brought to failure in stepped SENB creep tests. The load was increased over months in steps of 5-10 % of the intact wet flexural strength determined in preliminary tests, starting at 10% for samples AQ1-3 and at 50 % for samples AQ4-6 (Tab. 1). Samples were pre-cracked to ~ 50 % (F= 4000 N) of the intact strength in a standard SENB testing frame with 10 N/s. Straining of the sample in the long-term tests was measured using electrical resistivity strain gages 2 mm below the notch, and four samples were supplied with distilled water in the notch (AQ 1-2, 4-5). To assess the influence of dissolution in the wet samples, this water was dripped in and captured for analysis of silica content by Atomic Absorption Spectrometry (AAS). Scanning Electron Microscopy images were taken of failed dry and wet samples to allow a surface texture analysis and fractography of fracture planes, to better define and discriminate chemo-mechanical mechanisms of stress corrosion and subcritical crack growth.

3 Results

Measured crack-tip strains during the wet tests were up to an order of magnitude higher, than similarly loaded dry samples, and approached tertiary creep at 70-80 % of the dry maximum loads (Tab. 1, Fig. 1).

Probing of the captured water from the wet samples, with the Atomic Absorption Spectrometry method, detected no silica above the lower detection limit of 50 µg/L, indicating minimal stress enhanced dissolution occurred during the tests or re-precipitation within the fracture.

Table 1. Loading protocol: Load is applied in stages of a percentage, % of KIC (KIC =~1.5 MPa m½, modulus of rupture of 20 MPa). For wet conditions distilled water was dripped in the notch with a medical drip device, after the first load step. Strain of bold samples in Fig. 1.

sample	1.	condition	2.	3.	4.	5.	6.	7.	8.	9.	10.	11.	
AQ 1	10	wet	20	30	40	50	60	70	set up failed				
AQ 2	10	wet	20	30	40	50	60	70	failed				
AQ 3	10	dry	20	30	40	50	60	70	80	85	90	95	failed
AQ 4	50	wet	60	70	80	85	90	failed					
AQ 5	50	wet	60	70	80	85	90	failed – data erroneous					
AQ 6	50	dry	60	70	80	85	90	95	100	failed			

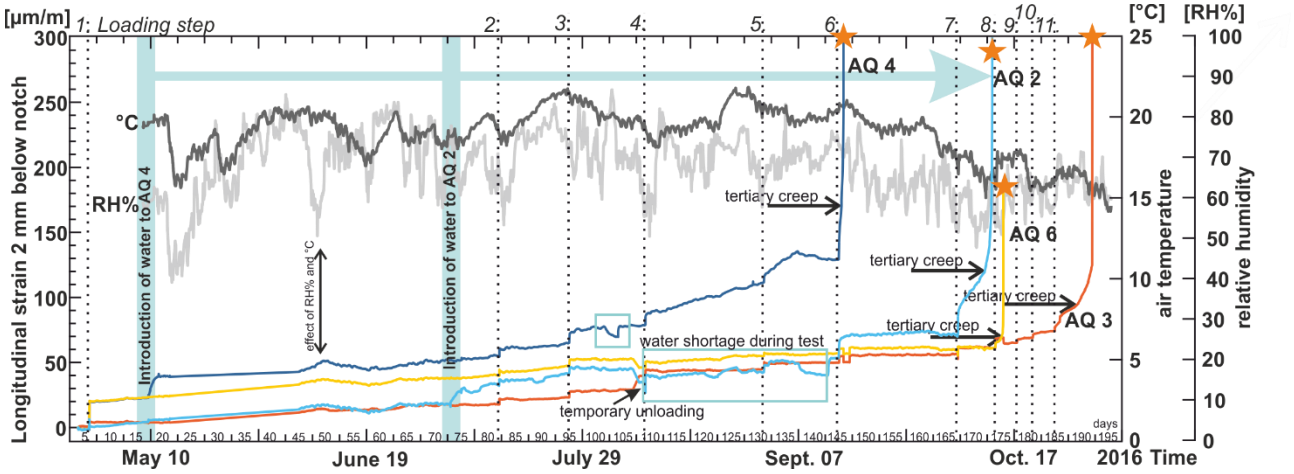

Figure 1. We observed distinct differences in creep strain curve between dry and wet samples, both in rate and elongation. Strain is measured longitudinal with strain gages glued 2mm below the noch tip. Loading followed the protocol in (Table 1). Increments of strain without additional load, in AQ 2 and AQ 4 (blue lines) are associated with the introduction of water (blue vertical line) after a bedding period. Fluctuations of strain in the wet samples are due to blockage in the water supply and refillment. Wet samples failed at lower loads than the dry samples. In addition to strain we monitored relative humidity and air temperature within a 3 m range of the set up throughout the testing period (%RH light grey thick line, C° dark grey thick line). Sudden drops in humidity and temperature rise appear to increase the strain of both dry and wet samples.

Scanning electron microscopy (SEM) of the fracture path of the quartzite samples reveals various morphologies indicating surface alteration, such as etching pit patterns aligned parallel to the principal stress direction (Fig. 2b), terrace dissolution in the plane of the principal tensile stress (Fig. 2c), countering of a highly- to non-corroded surface, and fractures paths following microstructural predispositions, e.g. foliation and cleavage planes (Fig. 2a-f). On the dry fracture surfaces, a variety of breakage patterns are found, highlighting the local stress variability as the fracture progresses (Fig. 3a-b).

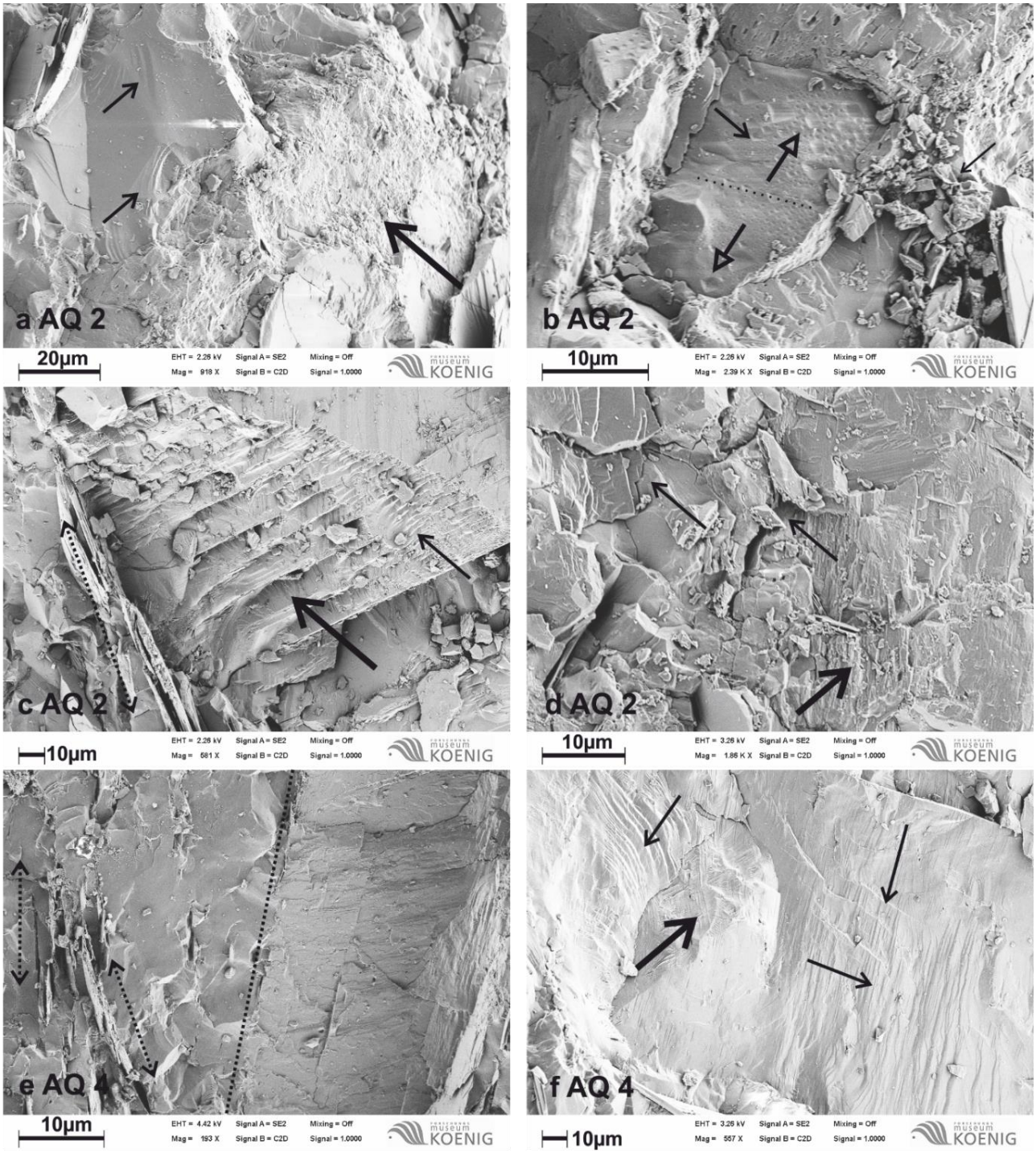

Figure 2. Fracture path surface textures of Alta quarzite wet samples AQ2 (a-d) and AQ4 (e-f), principal stress direction out of plane. Scanning electron microscopy reveals brittle as well as chemically altered surfaces, e.g. in a, conchodial breakage (light arrows) next to irregular dissolution-precipitation surfaces (thick arrow). b shows etch pits aligned parallel to the principal stress direction (extension) along a crack (dotted line). Terrace dissolution and precipitation in c exposes cleavages at different scales of the quartz grains. Note various slightly vertical aligned plates of mica sticking out of plane in c and e. Stress variations and elastic mismatch, ease the formations of microcracks, arcs and steps as well as microblock formations (d). Crystal plane orientations favor different surface textures countering grains of highly- (e right side) to non-corroded chonchodial fracture surface (e, left side). Subcritical crack growth direction variability at different scales (thin arrows), e.g. gradual steps and series of arcs of exposed planes as well as the smoothing out of edges (thick arrow) by dissolution and precipitation is observed in f (images A.V.).

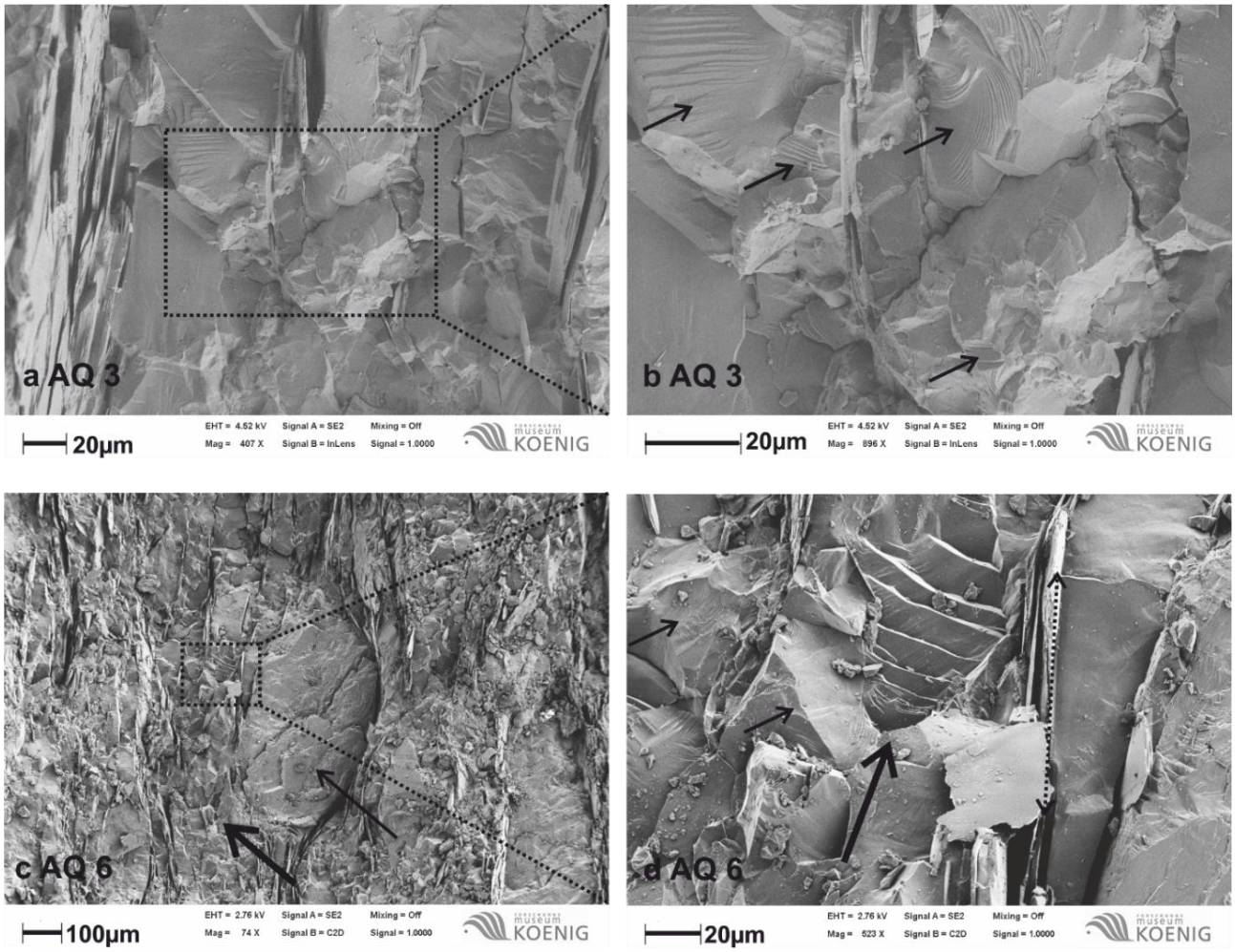

Figure 3. Fractographic images of dry samples AQ 3 (a-b) and AQ 6 (c-d). Scanning electron microscopy reveals brittle and conchodial breakage pattern (a). Fractures do not necessarily follow grain boundaries, but cuts transgranularly through (b, thin arrows). Indicating dynamic brittle rupture. c gives an overview of the rather blocky (thick arrow) and rough surface structure, in line with the principal out of plane stress direction. Mica plates stick out aligned near vertical along the foliation plane (dotted arrow in d). Grain size of quartz varies (large grain with adjectant small grains, thin arrow) as well as the distribution of mica. The enlarged view in d reveals brittle fracture surfaces of various kind and progression directions, such as conchoidial patterns, with an overall smooth surface and sharp edges (thin arrows), as well as graded steps (thick arrow) (images A.V.).

4 Main findings

4.1 Progressive fracturing of quartz

The presence of water in a stressed rock accelerates progressive failure by altering the kinetics at the crack tip. Dry samples AQ3 and AQ6 creep and fracture in a pure brittle fashion at high loads. The macroscopic failure of the dry sample is thus controlled by the stress intensity. The introduction of water to samples AQ1-2 and AQ4-5, caused an increase in strain by altering the mechanical behavior of the materia (Fig. 1).

4.2 Subcritical crack growth surface fractography

Dry surfaces indicate not only dynamic rupture seen as conchoidal breakage, but also progressive local fracture e.g. by subcritical crack growth, forming microblocks and graded steps (Fig. 3) transecting quartz grains. Dry and wet fracture surfaces show varying propagation directions in subcritical as well as dynamic cracking, being lead or routed by stress concentration, microcracks and stress dissipation as well as interactions with inherited structures, resulting in exposed flat cleavage

surfaces and arrests at mica plates, which pose an elastic contrast to the brittle quartz grains (Figs. 2 and 3). Distinct imbricated arcs and gradual steps are present in the fracture surfaces of wet samples, indicating local regions of dynamic propagation and arrest.

4.3 Stress corrosion cracking

Fracture surface features in the wet samples reveal chemo-mechanical coupling (Fig. 2), indicating progressive fracturing was enhanced in the presence of water, though analysis of water samples indicated dissolution was not prevailing in the bulk fluid.. Our observations rather point to a combination of creep, e.g. plastic and brittle deformation and corrosion, e.g. both embrittlement and dissolution-precipitation. In the wet samples more grain and cleavage surfaces are exposed, indicating subcritical crack growth in the presence of water localizes along grain boundaries and interfaces, where stresses concentrate and sensitization of the local resistance is enhanced chemically and physically by the presence of water.

Chemo-mechanical interactions are likely to facilitate progressive fracture of surface bedrock in natural settings. Stress corrosion cracking is thus likely to be an important control on the promotion of rock slope failure, bedrock incision and building material damage.

5 Reference list

Atkinson, B. K. (1984), Subcritical Crack Growth in Geological Materials, *J. Geophys. Res. Solid Earth*, *89*(B6), 4077–4114, doi:10.1029/JB089iB06p04077.

Atkinson, B. K., and P. G. Meredith (1981), Stress corrosion cracking of quartz: a note on the influence of chemical environment, *Tectonophysics*, *77*, T1–T11, doi:10.1016/0040-1951(81)90157-8.

Atkinson, B. K., and P. G. Meredith (1987), The theory of subcritical crack growth with applications to minerals and rocks, in *Fracture Mechanics of Rock*, edited by B. K. Atkinson, pp. 111–166, Academic Press, London, Orlando, San Diego, New York, Austin, Boston, Sydney, Tokyo,Toronto.

Attewell, P. B., and I. W. Farmer (1973), Fatigue behaviour of rock, *Int. J. Rock Mech. Min. Sci.*, *10*, 1–9.

Brantut, N., P. Baud, M. J. Heap, and P. G. Meredith (2012), Micromechanics of brittle creep in rocks, *J. Geophys. Res.*, *117*(8), 1–12, doi:10.1029/2012JB009299.

Brantut, N., M. J. Heap, P. G. Meredith, and P. Baud (2013), Time-dependent cracking and brittle creep in crustal rocks: A review, *J. Struct. Geol.*, *52*(1), 17–43, doi:10.1016/j.jsg.2013.03.007.

Costin, L. S., and D. J. Holcomb (1981), Time-dependent failure of rock under cyclic loading, *Tectonophysics*, *79*(3–4), 279–296, doi:10.1016/0040-1951(81)90117-7.

Itô, H., and S. Sasajima (1980), Long-term creep experiment on some rocks observed over three years, *Tectonophysics*, *62*(3–4), 219–232, doi:10.1016/0040-1951(80)90194-8.

Ko, T. Y., and J. Kemeny (2013), Determination of the subcritical crack growth parameters in rocks using the constant stress-rate test, *Int. J. Rock Mech. Min. Sci.*, *59*, 166–178, doi:10.1016/j.ijrmms.2012.11.006.

Lawn, B. R. (1993), *Fracture of Brittle Solids*, 2nd ed., edited by E. A. Davis and I. M. Ward, Cambridge University Press, Cambridge.

Nara, Y., H. Yamanaka, Y. Oe, and K. Kaneko (2013), Influence of temperature and water on subcritical crack growth parameters and long-term strength for igneous rocks, *Geophys. J. Int.*, *193*(1), 47–60, doi:10.1093/gji/ggs116.

Rutter, E. H. (1972), On the creep testing of rocks at constant stress and constant force, *Int. J. Rock Mech. Min. Sci.*, *9*, 191–195.

Understanding progressive rock failure using ultrasonic tomography and numerical simulation

Qi Zhao[1*], Aly Abdelaziz[1], Tai-Ming He[2], and Kaiwen Xia[1] and Giovanni Grasselli[1]

[1] Department of Civil Engineering, University of Toronto, ON, M5S 1A4, Canada.
[2] Key Laboratory of Seismic Observation and Geophysical Imaging, Institute of Geophysics, China Earthquake Administration, Beijing 100081, China.
* q.zhao@mail.utoronto.ca

1 Introduction

Understanding progressive rock failure and monitoring the stability of underground excavation zones, such as tunnels and underground mines, are critical to their operational safety. Many tunnels and underground structures are constructed under high-stress conditions, and stress redistribution may occur during and after the excavation. Stress redistribution generates energy imbalance in the rock mass, resulting in damage of the rock that impact the stability of underground structures (Chang and Lee 2004). Therefore, evaluating the progressive failure and damage mechanisms of rock at different stress levels are of great importance to geo-hazard assessment and operational safety of underground structures.

In this study, we address this problem using an experiment at the laboratory scale, coupled with ultrasonic tomography (UT) and numerical simulation. A time lapse two-dimensional (2D) UT observation was conducted on a granite slab under uniaxial compression. This test was then reproduced using the combined finite-discrete element method (FDEM). The entire deformation and failure processes were studied using this combination of technologies at the macroscopic and microscopic scales.

2 Material and method

2.1 Sample and compression test

The rock sample investigated in this study was a coarse-grained granite (Fangshan granite) slab 220 mm long, 110 mm wide, and 30 mm thick. This granite consisted of three main mineral phases: Feldspar (67%), Quartz (23%) and Biotite (10%), with an average grain size of 2.6 mm. The sample was tested by applying a uniaxial stress and a UT survey was conducted initially (0 MPa) and at intervals of 20 MPa applied stress.

2.2 Ultrasonic tomography (UT)

The ultrasonic wave velocity is influenced by many factors including: pressure, microcrack density and orientation, and pore fluid properties. Extracting information on these factors from wave velocity using tomography provides a non-destructive approach to image the rock interior and is ideal to study the property changes of the rock during compression tests (Paterson and Wong 2005).

In this study, 26 transducers were placed onto the sides of the sample (Fig. 1). Note that the 6 transducers on the top and bottom of the sample were embedded into the loading frame. Each UT observation was conducted in four stages, and in each stage transducers on one edge served as sources, while transducers on the other three edges acted as receivers. The recorded arrival time was then used for an iterative inversion to obtain the 2D velocity map of the sample.

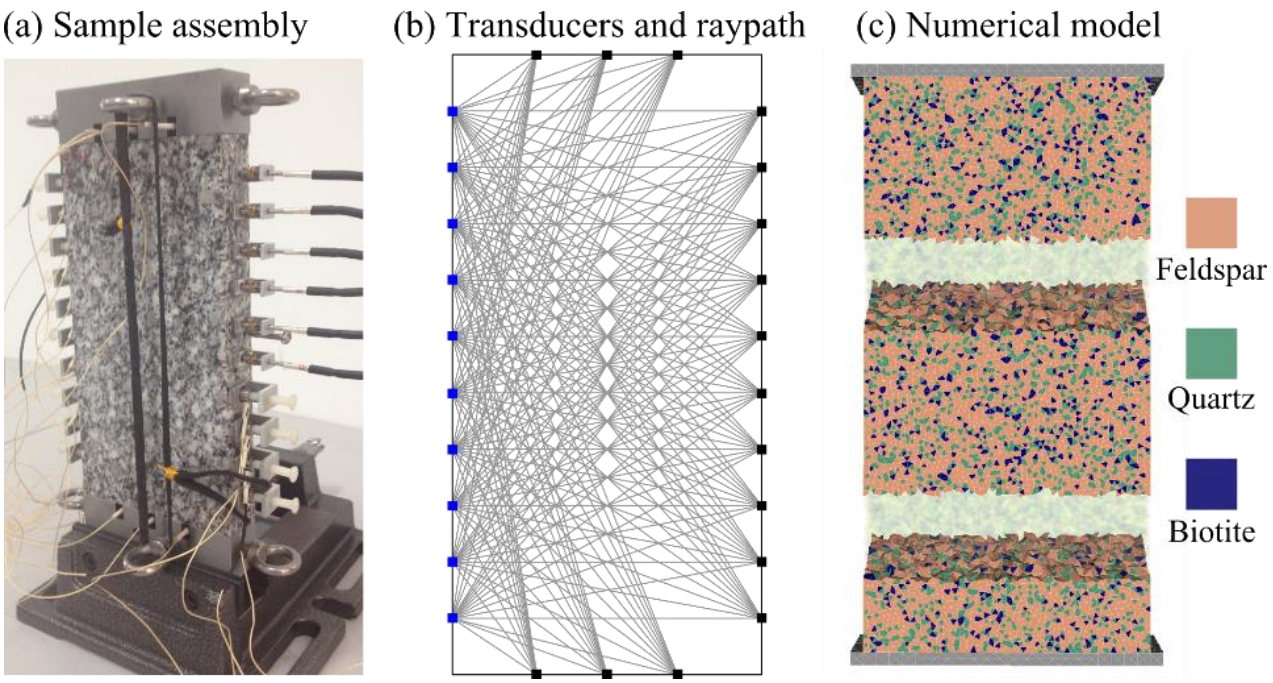

Figure 1. (a) The sample assembly used in the compression test. (b) An example of one stage of the ultrasonic tomography, and transducers on the left edge served as sources. (c) The FDEM numerical model (parts of the model were made transparent to illustrate the model interior mesh topology).

2.3 Combined finite-discrete element method (FDEM)

The FDEM model takes advantage of the finite element method in dealing with elastic deformations and the discrete element method in simulating solid interactions related to fracturing and progressive breakages. FDEM has been proven to provide insights into the failure processes of rocks and associated seismic activities (Lisjak et al. 2013; Zhao et al. 2014, 2015).

The FDEM model consisted of a 220 mm × 110 mm cross-section plane of the block representing the rock sample and two blocks at the top and bottom of the rock sample representing the loading platens. The model was meshed with a finite-element mesh with the element size comparable to the actual grain size. The heterogeneity of the sample was incorporated into the model by assigning different mineral properties and their corresponding relative abundance to the sample domain, using a stochastic spatial distribution.

3 Results and discussions

The emergent simulated mechanical properties were in good agreement with the respective experimental values (Tab. 1).

Table 1. Properties of the sample and corresponding results of the FDEM model

Properties (unit)	Sample	FDEM model
Compressive strength (MPa)	136	138
Poisson's ratio (-)	0.2	0.21
Young's modulus (GPa)	57	61

The initial non-linear portion of the stress-strain curve, approximately from 0 to 50 MPa, measured in the laboratory, was explained due to the closure of microcracks in the sample. Such an effect was not considered in the FDEM modelling, which resulted in a difference in total strain of about 0.02% (Fig. 2). The rock sample failed abruptly at the peak stress during the laboratory test. This abrupt failure was well reproduced in the simulation with a significant stress drop observed immediately after the peak stress. The simulation was terminated shortly after the peak stress point, when a catastrophic fracture formed splitting the sample.

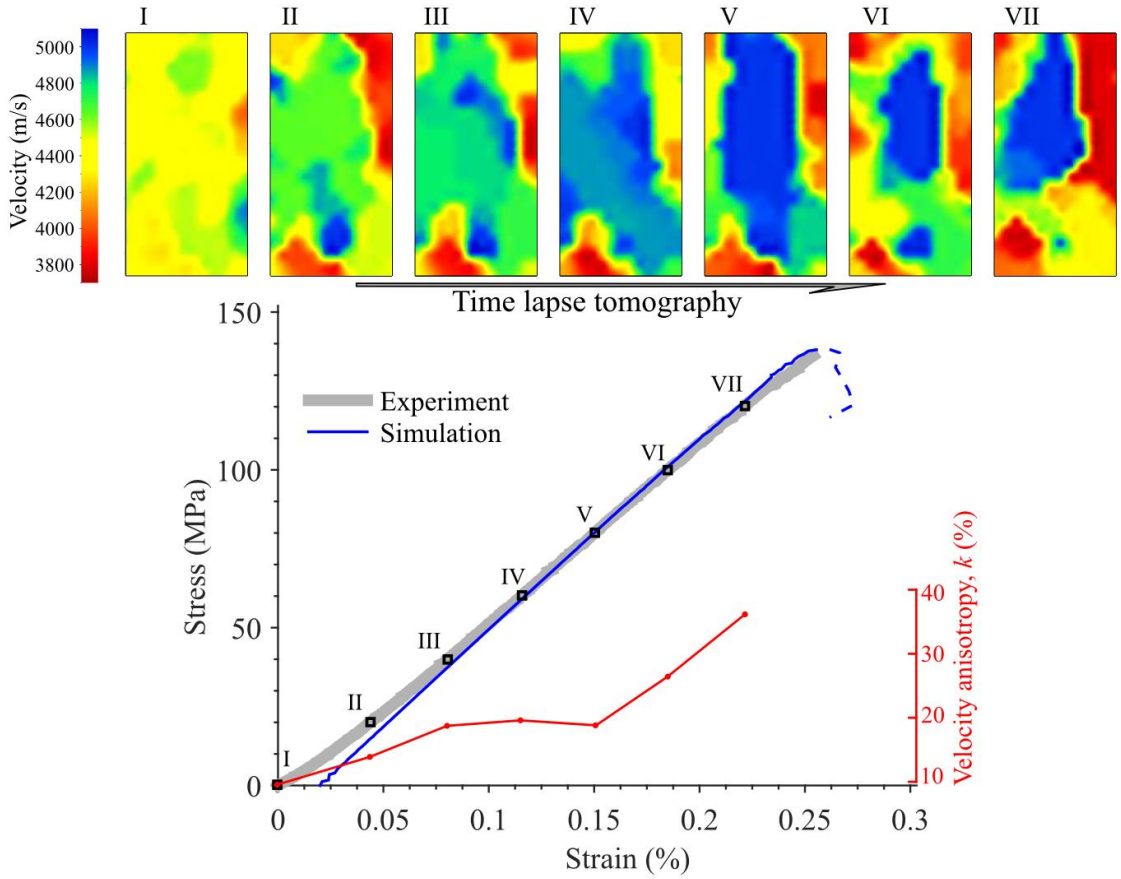

Figure 2. Stress-strain curve of the experiment and the simulation. Note that the strain of the simulated curve is shifted to compensate for the non-linear portion of the experimental curve. I–VII indicate the stress levels under which UT observations were carried out. Velocity anisotropy (k) under these stress levels is also shown.

Tomography results showed that the velocity of the sample at 0 MPa was relatively uniform (Fig. 2I). As the stress increased to 20 MPa, two low velocity areas developed at the north-east and south-west parts of the sample, while the remaining part had slightly increased velocity (Fig. 2II). The velocity in the high velocity zone increased consistently from 20 to 80 MPa, with its size relatively stable (Fig. 2III−V). From 80−100 MPa, the size of the high velocity zone decreased and concentrated towards the center of the sample (Fig. 2V–VI). At 120 MPa, the sizes of low velocity zones increased significantly with further decreased velocity, and the high velocity zone retracted to the north-middle part of the sample (Fig. 2VII).

Next, we calculated the velocity anisotropy (*k*) following Babuška (1984) and examined it as a function of the axial stress (Fig. 2). It has been observed that initially *k* increased gradually from 0 to 40 MPa due to closure of microcracks in the loading direction. Between 40 to 80 MPa, *k* was relatively stable; however, after 80 MPa (~60% of the compressive strength), *k* increased quickly, indicating a rapid damage accumulation in the rock.

Upon reaching 120 MPa, the UT observations depicted the progressive damage accumulation in the rock sample; however, the rock sample failed rapidly as the stress continued to increase without the possibility to run an additional UT measurement. The numerical simulation results were thus used to enhance our understanding of the damage process at this critical stress level (Fig. 3). Numerically we could examine the microcracking (i.e. acoustic emission or AE) and compare it to the observations of the tested sample (Fig. 3). Prior to the peak stress, AE activity scattered throughout the sample volume, with tensile fracturing being the dominant mechanism. After the peak stress, AE events concentrated on the shear band, and a large amount of shear cracks coalesced, forming the macroscopic fracture that split the sample.

The laboratory test and simulation results suggested several precursors of the catastrophic rock failure: (1) decrease of the elastic wave velocity, (2) increase of velocity anisotropy, (3) spatial localization of damage onto the failure plane, and (4) an increase of the dominance of shear failure.

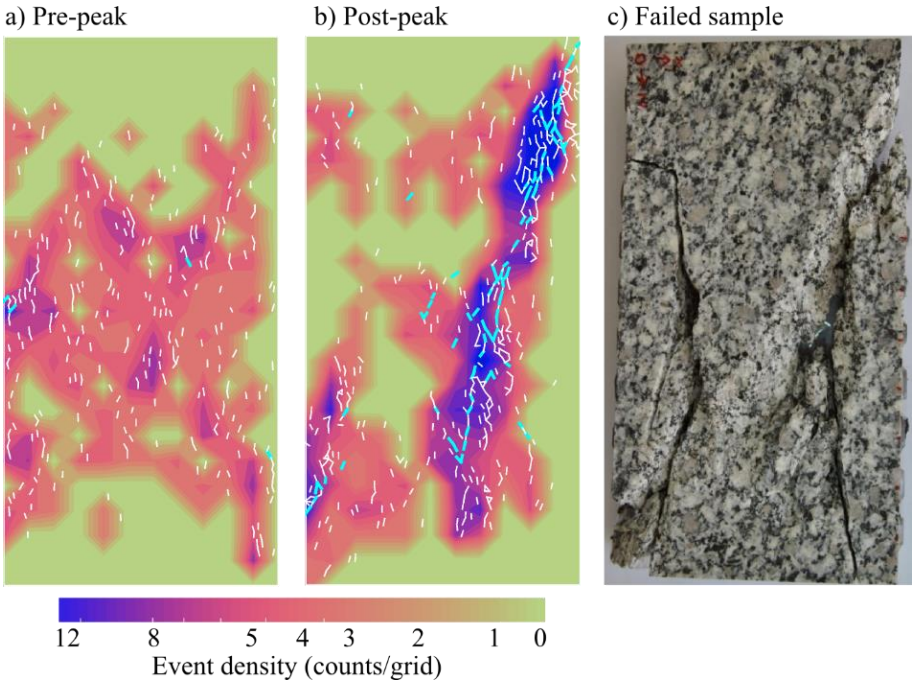

Figure 3. Simulated crack (i.e. AE event) density in space at (a) pre-peak and (b) post-peak stages, and the comparison to the tested rock (c). Thin white dashes represent tensile cracks and thick cyan dashes represent shear cracks.

4 Conclusion

In this study, we employed ultrasonic tomography and numerical simulation to investigate the microscopic and macroscopic behaviors of the progressive failure of a rock sample tested in uniaxial compression. This combination of technologies allowed us to link microcracking (i.e. AE) in the rock to the observed macroscopic behavior. Precursors of catastrophic rock failure were identified based on these results. Such precursors can be obtained from seismological field monitoring, and accompanied by carefully calibrated numerical models, can be used to improve the safety monitoring and control of underground structures. Moreover, these observations may also be useful to forecast natural and induced earthquakes.

5 Acknowledgements

This work has been supported through the NSERC Discovery Grants 341275 & 72031326, CFI-LOF Grants 18285 & 12911, Carbon Management Canada (CMC), Foundation CMG Research Chair Program, and the Special Fund for Basic Scientific Research, IGPCEA No. DQJB13B06 (China).

6 Reference list

Babuška, V., 1984. P-wave velocity anisotropy in crystalline rocks. Geophys. J. Int. 76, 113–119.

Chang, S-H, Lee, C-I. 2004. Estimation of cracking and damage mechanisms in rock under triaxial compression by moment tensor analysis of acoustic emission, Int. J. Rock Mech. Min. Sci., 41(7), 1069–1086.

Lisjak, A, Liu, Q, Zhao, Q, Mahabadi, OK, Grasselli, G. 2013. Numerical simulation of acoustic emission in brittle rocks by two-dimensional finite-discrete element analysis, Geophys. J. Int., 195(1), 423–443.

Paterson, M. S., Wong, T. 2005. Experimental rock deformation: the brittle field, Springer.

Zhao, Q., Lisjak, A, Mahabadi, OK, Liu, Q, Grasselli, G. 2014. Numerical simulation of hydraulic fracturing and associated microseismicity using finite-discrete element method, J. Rock Mech. Geotech. Eng., 6(6), 574–581.

Zhao, Q., Tisato, N, Grasselli, G, Mahabadi, OK, Lisjak, A, Liu, Q. 2015, Influence of in situ stress variations on acoustic emissions: a numerical study, Geophys. J. Int., 203(2), 1246–1252.

Geomechanical characterization of deep geothermal aquifers by field, laboratory and modelling methods

Georg Stockinger[1*], Florian Menschik[1] and Kurosch Thuro[1]

[1] Technical University of Munich, Chair of Engineering Geology, Arcisstraße 21, 80333 Munich
* georg.stockinger@tum.de

The White Jurassic Limestone (Malm) below the basement of the Southern Bavarian Molasse Basin is rich in hydrothermal fluids with temperatures up to 160 °C. These hydrothermal fluids are used to gain profitable, renewable and sustainable energy. Upon now, this resource is gained and used to produce long-distance heating and electricity in several locations in the greater area of Munich (Moeck & Zimmer 2014). However, there is still an increased risk of not discovering fluids the more south the borehole is situated. A concept to reduce this risk is targeted drilling into fracture or fault zones within the Jurassic Limestone Therefore, the rock-mechanical understanding of the surrounding rock of the drilling is of major importance since stress redistribution, fracture initiation and propagation contribute to the borehole stability and the understanding of the connectivity to the aquifer in the near field of the drilling. These influences, in addition to the in-situ stresses in the White Jurassic Limestone in depths of 4000 m have not been investigated satisfyingly.

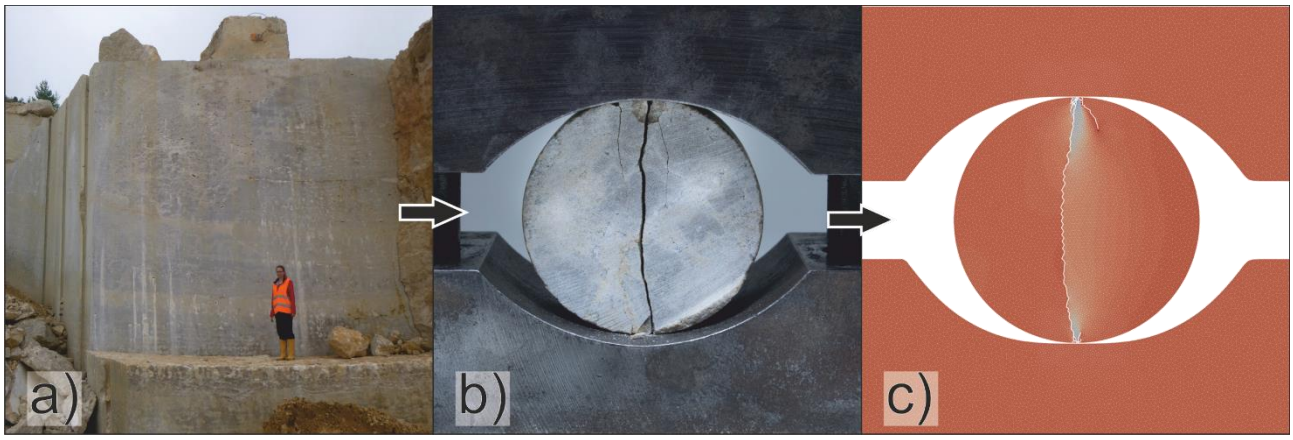

Figure 1. Illustration of the work flow, starting with a) taking samples of dolomite- and limestone in quarries to b) conducting rock mechanical tests on the prepared specimens as we see here the Brazil Test, going over to c) remodeling the determined parameters with numerical modelling to evaluate the parameters as close to reality as possible, © G. Stockinger.

As a first approach to gain rock mechanical parameters for the characterization, so-called “analogue samples” are taken. Later, in the subsequent course of the project “Dolomitkluft”, drill core samples of the deep geothermal borehole will be available. The sampling of the analogue rocks follows lithostratigraphic characteristics of an existing deep borehole and includes dolomite stones as well as limestones from quarries of the Franconian, Swabian and Helvetic White Jura (Fig. 1a). These rock samples are classified petrographically, associated with their original depth and prepared for laboratory testing such as Uniaxial Compressive Strength (UCS), Tensile Strength (BTS), Ultrasonic Velocity (USV) and Acoustic Emission (AE).

Indirect Tensile strength tests after ISRM 1978 (Fig. 1b), conducted on Dolomite stones of different quarries that differ only little in petrography already show variations in σ_t of more than 5 MPa. Thus, we expect that with little change in geology or rather petrography along the borehole, big fluctuations in stress change, crack propagation and borehole stability will occur. In addition, UCS, USV and AE Tests will be performed on the same rock types.

Rocks already sampled at the surface are not influenced by vertical stressed, whereas carbonates, found in a depth of around 4000 m underlay a vertical stress of around 100 MPa and yet not closer known horizontal stresses. Therefore, we try to evaluate the results of the BTS, UCS and AE by remodeling those with the finite – distinct coupled Element code IRAZU (Geomechanica) as shown in Fig. 1c. Subsequently, we are using the above-mentioned parameters to model the rock mechanical behavior in different scenarios with increasing depth and changing horizontal stresses (Geomechanica Inc.). Here, we can already show that – depending on facies – big changes in stress redistribution and fracture propagation occur. These results will then be compared with the conditions found in the borehole in a future project stage to evaluate the reliability of analogue samples for geomechanical predictions in high depth, high stress regimes.

This work is part of the project “Dolomitkluft” and funded by the German Federal Ministry for Economic Affairs and Energy under grant agreement No. FKZ 0324004B.

Reference list

Moeck, I, Zimmer, R. 2014. Tiefe Geothermie in Bayern: Installierte Leistung, Erlaubnis-/Bewilligungsfelder und Erkundung. – Proceedings der Geothermiekongress DGK 2014, 1-11, Essen.

ISRM. 1978. Suggested Methods for determining tensile strength of rock materials. International Journal of Rock Mechanics and Mining Sciences & Geomechanics Abstracts 15, 99-103.

Geomechanica Inc. 2016. Irazu software, Version 1.2 Theory Manual.

The fate of elastic strain energy in brittle fracture

Tim Davies[1*], Mauri McSaveney[2] and Natalya Reznichenko[1]

[1] Department of Geological Sciences, University of Canterbury, New Zealand
[2] GNS Science Ltd, Lower Hutt, New Zealand
* tim.davies@canterbury.ac.nz

1 Introduction

Since linear elastic fracture mechanics (LEFM) was derived from the work of Griffith (1921), it has been assumed that the stored elastic strain energy that is involved in extending a crack in a brittle material becomes potential surface energy associated with the new surface as it is created. Thus the area of new surface that can be created in a fracture episode should be limited by the amount elastic strain energy input before the fragmentation episode. We conducted laboratory and field (rock avalanche) measurements to test this assumption and consistently found more fracture surface area than the assumption would predict. Nevertheless, this result does not affect conventional LEFM because it is unaffected by the fate of the elastic strain energy in brittle failure. We see evidence that the elastic strain energy that causes cracks to propagate in individual grains becomes transient elastic strain, and influences further breakage. This result has broad and growing significance as developing technologies allow ever finer fragments to be detected and measured in brittle fracture.

2 Borosilicate glass fragmentation

Kolzenberg et al. (2013) report dry confined compression tests on borosilicate glass (Pyrex), presenting the elastic strain energy released at failure and total surface area of the fragmented samples. We have carried out unconfined compression tests on dry 10mm diameter and 20 mm long borosilicate glass (Pyrex) cylinders; four tests yielded fragments with estimated total surface area up to 91.8 m^2. Since the specific surface energy of borosilicate glass is established as 4.5 Jm^{-2} (Wiederhorn 1969), this would require about 413 J, but the elastic strain energy available at failure was about 133 J.

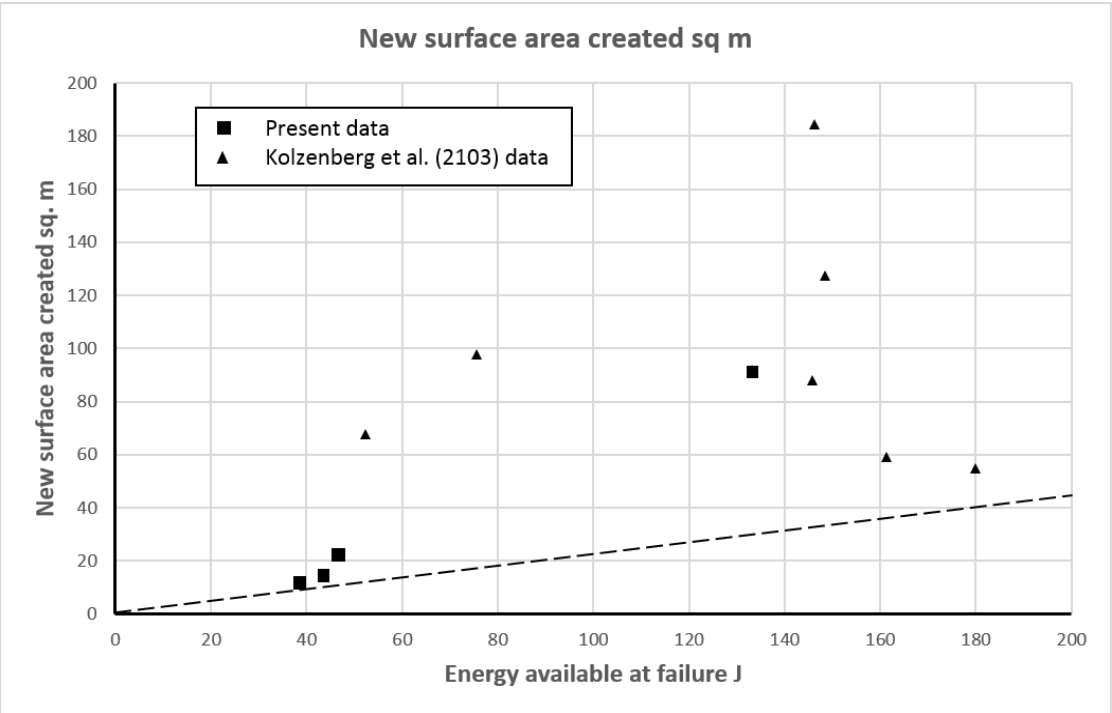

Figure 1. Kolzenberg et al. (2013) data and present data; dashed line shows conventional surface area limit $\gamma = 4.5\ Jm^{-2}$.

Fig. 1 summarises these results; it is evident that in all cases more surface was generated than would be expected if the energy used in creating new surface were lost to surface energy.

3 The Coleridge rock avalanche

At Lake Coleridge, South Island, New Zealand, a 6 x 10^5 m^3 sandstone rock-avalanche deposit was emplaced about 700 years ago (Lee et al. 2009), so its debris is relatively unweathered. The source materials are variably jointed at cm-dm scale. The deposit material is intensely fragmented with angular and very angular clasts of all sizes and a very large proportion of fine material. We sampled the rock-avalanche debris at two distal basal locations in a river-cut exposure. The total fall height of the sampled materials is between 270 m and 320 m, and the horizontal distance from the source to the sample sites is between 840 and 940 m. Laser size analysis of the deposit material showed that to generate the new surface area measured requires a *minimum* of about 2730 J kg^{-1} available from potential energy, if the field value of specific surface energy of sandstone is ≥7 J kg^{-1} (Friedman et al. 1972; Chelidze et al. 1994; Ouchterlony 1982). Since the potential energy available from the fall is about 3000 J $kg^{-1,}$ this leaves only 270 J kg^{-1} to overcome friction in the ~ 900 m horizontl travel distance; this requires that the rock avalanche friction coefficient is < 0.06 – an unrealistically small value. There is thus a strong indication that the potential energy available in the fall is insufficient to generate the new surface area measured, under the assumption that fragmentation consumes energy.

4 Conclusions and implications

As technology allows ever smaller fragments to be measured in rock and other brittle-fracture debris, it has become apparent that an energy-based limit to fragment fineness (“grinding limit”) is unrealistic, especially when it is found that sub-micron fragments are commonly agglomerations of still finer grains (Reznichenko et al. 2012). We have demonstrated that current understanding of linear fracture mechanics is quantitatively unable to account for the amount of new surface created during brittle fracture experiments. An assumption that stored elastic strain is simply released as transient elastic strain at failure allows more realistic analysis and modelling of brittle fracture mechanics, and hence better understanding of, for example, seismic energy release during earthquakes (Davies et al. 2011) and the runout of large rock avalanches (Davies et al. 2010).

5 Reference list

Chelidze, T, Reuschle, T, Gueguen, Y. 1994. A theoretical investigation of the fracture energy of heterogeneous brittle materials. Journal of Physics: Condensed Matter 6, 1957-1868

Davies, TR, McSaveney, MJ, Boulton, CJ. 2011. Elastic strain energy release from fragmenting grains: effects on fault rupture. Journal of Structural Geology 38, 265-277

Davies, TR, McSaveney, MJ, Kelfoun, K. 2010. Runout of the Socompa volcanic debris avalanche, Chile: a mechanical explanation for low basal shear resistance. Bulletin of Volcanology 72, 933–944

Friedman, M, Handin, J, Alani, G. 1972. Fracture-surface energy of rocks. International Journal of Rock Mechanics and Mining Sciences 9, 757-764.

Griffith, AA. 1921. The Phenomena of Rupture and Flow in Solids. Philosophical Transactions of the Royal Society of London A 221, 163-198.

Kolzenburg, S, Russell, JK, Kennedy LA. 2013. Energetics of glass fragmentation: Experiments on synthetic and natural glasses. Geochem. Geophys. Geosyst, 14, 4936–4951

Lee, JA, Davies, TRH, Bell, DH. 2009. Successive Holocene rock avalanches at Lake Coleridge, Canterbury, New Zealand. Landslides 6, 287–297.

Ouchterlony, F. 1982. Review of fracture toughness testing of rock. SM Archives, 7, 131-211

Reznichenko, NV, Davies, TRH, Shulmeister, J, Larsen,' SH. 2012. A new technique for distinguishing rock-avalanche-sourced sediment in glacial moraines with some paleoclimatic implications. Geology 40 (4), 319-322

Wiederhorn, SM. 1969. Fracture surface energy of glass. Journal of the American Ceramic Society 52(2), 99-105.

Ice-related progressive crack growth in rocks

Bernard Hallet[1*]

[1] Department of Earth and Space Sciences, University of Washington, USA
* hallet@uw.edu

1 Introduction

The growth of ice in porous rocks can generate large internal pressures and progressive crack growth. The resulting damage to rock is widely believed to arise from the 9% volumetric expansion of pore water during freezing. This belief is, in fact, at odds with much of the work on freezing of soils and porous solids; under natural conditions, freezing-induced damage in these solids is strongly related to water movement and often largely independent of the specific-volume change of the pore fluid during freezing (Walder & Hallet 1986; Hallet 2006). Herein, we outline the underlying processes, and highlight recent developments to provide an introduction to this rich subject.

2 Underlying processes

The potential of the 9% water-to-ice expansion to cause high pressure in confined spaces is undeniable based on practical experience with, for example, broken bottles in freezers and broken pipes exposed to freezing weather, etc. This expansion may, however, rarely be significant for rocks under natural conditions, because it requires a tight orchestration of unusual conditions. Unless the rocks are essentially saturated with water (unlikely for many situations at the ground surface; Fig. 1 for instance) and frozen from all sides, the expansion can simply be accommodated by the flow of water into empty pores, or out of the rock through its unfrozen sides.

Figure 1. Under ideal conditions -- ample moisture and mild freezing temperature -- intact frost-sensitive cobbles on a beach are reduced to fans of rock slivers within a few decades in Taan Fjord, Icy Bay, Alaska, USA.

The common notion that incipient cracks at the surface of rocks can be wedged open by freezing (as sketched in a number of textbooks) may also be rarely important in nature, because water can leak out of the cracks, and the ice capping the cracks can push out (Davidson & Nye 1985).

Ice growth inside porous rocks has much in common with frost heave of soils, which has received considerable research attention. Less well known is that slow ice growth in soils hydraulically connected to an unpressurized water reservoir over long periods, hundreds of hours, can lead to pressures against a confining piston in a stiff apparatus exceeding 18 MPa (Radd & Oertle 1973). This is far in excess of the internal pressure required for crack propagation in most rocks. Such ice growth (known as segregation ice) is sustained by a supply of water driven thermodynamically along unfrozen films toward growing ice lenses (Taber 1929). Intermolecular forces acting between the mineral surfaces, ice, and water sustain these unfrozen films, and generate significant pressure between mineral and ice surfaces (Dash et al. 2006).

3 Recent developments

This freezing soil-foundation paved the way to an initial model of subcritical crack growth in rock due to freezing (Walder & Hallet 1985). This and a similar model were experimentally validated using acoustic emissions to monitor progressive crack growth in sandstone (Hallet et al. 1991) and measuring sample dilation to monitor ice lensing in chalk (Murton et al. 2006). The theoretical papers on freezing in porous media have recently been updated within the context of a contemporary understanding of pre-melting behavior (e.g. Dash et al. 1995, 2006; Rempel et al. 2001; Rempel 2007). The mathematical aspects of the phenomenon have been developed most recently by Vlahou & Worster (2015) who presented a “mathematical model capable of explaining the physical processes governing fracturing, and establishing the relevance of different parameters. The fracture toughness of the rock, the size of pre-existing cracks and the undercooling of the environment are the main parameters determining the susceptibility of a porous solid to fracturing.” They also consider the dependence of the crack growth rates on the permeability and elasticity of the medium, and conclude: “Thin and fast-fracturing cracks are found for many types of rocks.” The implications of Ice-related progressive crack growth in rocks are broad and rich, as exemplified recently in Rempel et al. (2016).

4 Reference list

Dash, JG, Fu, H., Wettlaufer, JS. 1995. The premelting of ice and its environmental consequences. Reports on Progress in Physics 58(1), 115.

Dash, JG, Rempel, AW, Wettlaufer JS. 2006. The physics of premelted ice and its geophysical consequences, Reviews of Modern Physics 78 (3), 695–741.

Davidson, G, Nye, J. 1985. A photoelastic study of ice pressure in rock cracks, Cold Regions Science and Technology 11 (2), 141–153.

Hallet, B. 2006. Why do freezing rocks break? Science 314 (5802), 1092-1093.

Hallet, B, Walder, J, Stubbs, C. 1991. Weathering by segregation ice growth in microcracks at sustained subzero temperatures: Verification from an experimental study using acoustic emissions, Permafrost and Periglacial Processes 2 (4), 283-300.

Murton, JB, Peterson, R, Ozouf, J-C. 2006. Bedrock fracture by ice segregation in cold regions, Science 314 (5802), 1127-1129.

Radd, FJ, Oertle, DH. 1973. Experimental pressure studies of frost-heave mechanisms and growth-fusion behavior of ice. In: Proc North American Contribution, 2nd Int Conf on Permafrost, Yakutsk, USSR, July, 1973. Washington, D.C. National Academy Press, 377-384.

Rempel, AW. 2007. Formation of ice lenses and frost heave. J. Geophysical Research: Earth Surface 112(F2).

Rempel, AW, Wettlaufer JS, Worster MG. 2004. Premelting dynamics in a continuum model of frost heave. J. Fluid Mech. 498, 227–244.

Rempel, AW, Marshall, JA, Roering, JJ. 2016. Modeling relative frost weathering rates at geomorphic scales. Earth and Planetary Science Letters, 453, 87-95.

Taber, S. 1929. Frost heaving. J. Geol. 37, 428–461.

Vlahou, I, Worster, M. 2015. Freeze fracturing of elastic porous media: a mathematical model, Proc Royal Society A 471

Walder, JS, Hallet, B. 1985. A theoretical model of the fracture of rock during freezing. Bull. Geol. Soc. Am. 96, 336–346.

Walder, JS, Hallet, B. 1986. The physical basis of frost weathering: toward a more fundamental and unified perspective. Arctic and Alpine Research, 27-32.

Subsurface rock damage and healing after earthquakes: What do we learn from geomorphological and geophysical data?

Odin Marc[1,2*], Niels Hovius[1], Christoph Sens Schönfelder[1], Patrick Meunier[3], Luc Illien[1], Manuel Hobiger[4], Ya-Ju Hsu[5], Mako Ohzono[4], Kaoru Sawazaki[7], and Claire Rault[3]

1 Deutsches GeoForschungsZentrum GFZ-Potsdam, Potsdam, Germany
2 Institut de Physique du Globe de Strasbourg - CNRS UMR 7516, University of Strasbourg/EOST, 5 rue Descartes, 67084 Strasbourg
3 Ecole Normale Superieure, Paris, France
4 Swiss Seismological Service (SED), ETH Zurich, Switzerland.
5 Institute of Earth Sciences, Academia Sinica, Taipei, Taiwan.
6 Institute of Seismology and Volcanology, Graduate School of Science, Hokkaido University, Kita 10 Nishi 8, Kita-ku, Sapporo 060-0810, Japan
7 National Research Institute for Earth Science and Disaster Resilience (NIED), Tsukuba, Japan
* odin.marc@unistra.fr

Some studies have suggested that the shaking and deformation associated with earthquakes would result in a temporary increase in hillslope erodibility. However very few data have been able to clarify what causes this transient state and what controls its temporal evolution.

We present integrated geomorphic data constraining an elevated landslide susceptibility to rainfall following 5 continental shallow earthquakes, the Mw 6.9 Finisterre (1993), the Mw 7.6 ChiChi (1999), the Mw 6.6 Niigata (2004), the Mw 6.8 Iwate-Miyagi (2008) and the Mw 7.9 Gorkha (2015) earthquakes. We constrained the magnitude (5 to 20 fold) and the recovery time (1 to 4 years) of this susceptibility change and associated it with subsurface damage caused by the strong shaking (Marc et al. 2015). The landslide data suggest that this ground strength weakening is not limited to the soil cover but also affects the shallow bedrock. Coseismic rock damage is supported by observations of shallow (0 to ~100m) seismic velocity drops constrained with ambient noise waveform correlations within the epicentral area of four of those earthquakes (e.g., Takagi etal. 2012, Hobiger et al. 2015).

For most stations we observe a subsequent exponential velocity recovery (i.e. proportional to $e^{-t/\tau}$) with a τ value in fair agreement with the one estimated based on landslide observation. This recovery dynamic is also consistent with post-seismic processes, namely GPS post-seismic displacement and aftershocks decay (Fig. 1, Marc et al., in review). We analyzed strain time series in Japan and Taiwan and it appears inconsistent with the recovery of landslide susceptibility and shallow seismic velocities. In contrast, surface dynamic strain associated with ground shaking caused by aftershocks display similar relaxation time and may control the subsurface property recovery.

However, two end-member models remain plausible at this stage: one in which repeated shaking causes additional damages that delay internal rock healing similar to the one observed in the laboratory. The other, in which repeated vibration allows progressive compaction and strengthening of the regolith, similar to dynamics observed in granular materials. Further data currently acquired in the Gorkha earthquake epicentral area may allow to clarify the role of aftershocks.

In any case, our data suggest that in tectonically active areas, deep processes may be significant drivers of the subsurface material properties and thus important to understand and forecast a variety of surface processes.

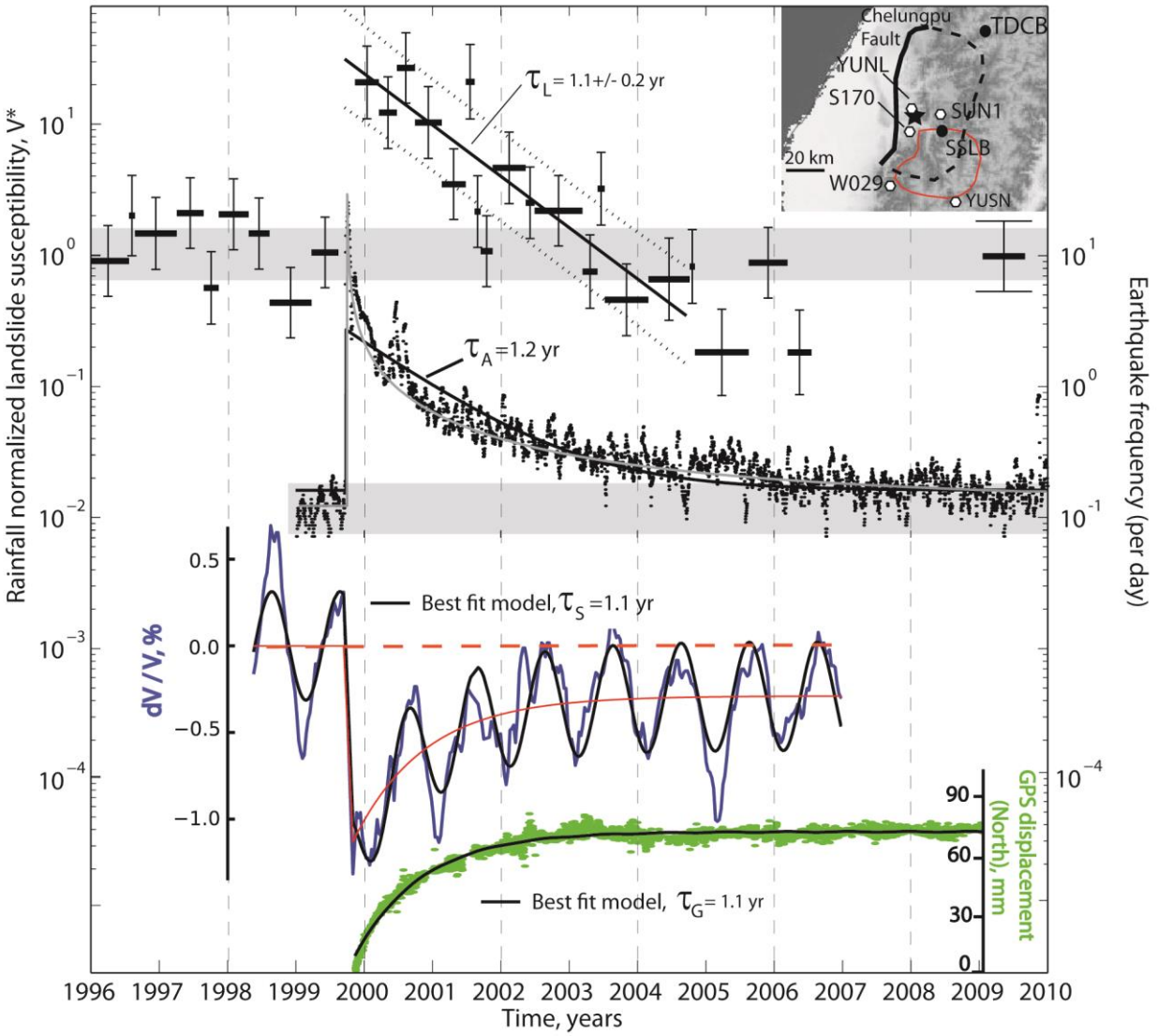

Figure 1. Time series of rainfall normalized landslide susceptibility (black bars), earthquake frequency (black dots), subsurface relative seismic velocity change around seismic station SSLB (blue curve) and northward displacement at GPS station SUN1 (green dots) in the epicentral area of the Chi-Chi earthquake (Taiwan). Best fitting exponential recovery models, with their e-folding time, are shown in black for each time series. Note that a seasonal component is required for the seismic data and that interseismic linear trend has been removed from the GPS curve. Also note the grey line fit of the microseismicity representing a stretched exponential function with a similar relaxation time but better capturing the evolution of microseismicity. Inset: Map of relevant GPS (white octogons) and seismic (black dots) stations in the epicentral area of the Chi-Chi earthquake over a DEM of Taiwan. The fault area is defined by the black dashed polygon, with the rupture trace as a solid line. The area where landslides were mapped is defined by the red polygon.

Reference list

Hobiger, M., U. Wegler, K. Shiomi, and H. Nakahara (2014), Single-station cross-correlation analysis of ambient seismic noise: application to stations in the surroundings of the 2008 Iwate-Miyagi Nairiku earthquake, *Geophys. J. Int.*, *198*(1), 90–109, doi:10.1093/gji/ggu115.

Marc, O., N. Hovius, P. Meunier, T. Uchida, and S. Hayashi (2015), Transient changes of landslide rates after earthquakes, *Geology*, *43*, 883–886, doi:10.1130/G36961.1.

Marc, O., N. Hovius, C. Sens-Schönfelder, P. Meunier, M. Hobiger, Y.-J. Hsu, K. Sawazaki, M. Ohzono, and C. Rault (in Review), Seismic and geodetic constraints on rock damage and landslide hazard after earthquakes. *Science Advances.*

Takagi, R., T. Okada, H. Nakahara, N. Umino, and A. Hasegawa (2012), Coseismic velocity change in and around the focal region of the 2008 Iwate-Miyagi Nairiku earthquake, *J. Geophys. Res.*, *117*(B6), B06315, doi:10.1029/2012JB009252.

The conceptual modeling of the style of rock massif destruction and of its influence on rockslides and rock avalanche formation

Oleg Zerkal[1], Yulia Frolova[1] and Alexander Strom[2*]

[1] Moscow State University, Geological Department, Moscow, Russia
[2] Geodynamics Research Center – branch of JSC "Hydroproject Institute", Moscow, Russia
* strom.alexandr@yandex.ru

1 Introduction

The numerical and physical modeling is the important method of understanding landslide processes. However, when modeling formation and motion of extra-large rockslides and rock avalanches, we face several problems. First, giant size of these features and extreme velocities of their motion intercept their physical modeling with adherence to scaling conditions performed to prove or disprove certain assumptions on mechanism(s) of such rockslides formation and motion. On the other hand lacking of clear and univocal understanding of the nature of such rockslides abnormal mobility complicates selection of motion equation, used for the numerical modeling.

In such situation the "conceptual modeling" when we just qualitatively reproduce any phenomenon or their combination really observed in nature or assumed, based on field observations on the morphology and internal structure of real rockslide deposits, in the lab, seems to be a promising way. It can be exemplified by the successive attempt to model intensive crushing of the rockslide / rock avalanche bodies' internal parts along with retention of the initial mutual position of various lithologies involved in slope failure (Dubovskoi et al. 2008). Such modeling has been performed recently to test some hypotheses proposed to explain formation mechanisms of several large rock avalanches in the Central Asia region.

2 Modeling of the "concealed rock burst"

One of tested hypothesis is that of the "concealed rock burst" that could occur if the slope base composed of the high strength rocks experiences the limit state, i.e. the load exceeds rocks strength. It can lead to formation of the "Prandtl prism" and its instantaneous crush accompanied by effects typical of rock bursts that would supply additional momentum to the collapsing rock mass. It, in turn, increases initial velocity of crushed debris motion and could support its abnormal mobility observed for the numerous case studies. It can be modeled by the uniaxial compression of rock samples in press mould with one side open where forming particles could move after crushing (Fig. 1).

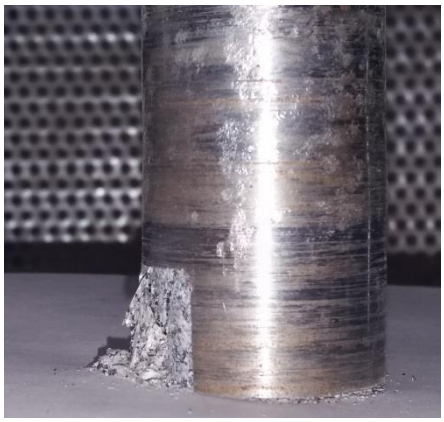

Figure 1. Crushing of the granite sample with strength of ~150 MPa in press mould with "window"

Loading attainable at the base of mountain slopes will be applied. If large number of particles will be formed and will move with high velocity, similar technique could be used for modeling of rock avalanches motion.
Reliable loading attainable at the base of real mountain slopes will be applied. If the experiments will be successful, i.e. large number of particles will be formed and will move with high velocity, similar technique could be used for modeling of rock avalanches motion.

Several highly mobile rockslides demonstrate quite specific spreading of debris over the slope, indicating that after rock massif destruction debris moved not only downslope, according to the gravity

force, but also sidewise, along the slope, outside the headscarp boundaries, forming thin apron blanketing otherwise undisturbed slope (Fig. 2). It is assumed that in such cases rapid or gradual slope deformation starts from the headscarp crown, which result in bulging of the lower part of the slope (the so called "buckling") and its excessive stressing.

When the ultimate strength of this rock mass is exceeded it spalls in all directions, so that some portions of the resultant debris gains momentum directed parallel to the slope.

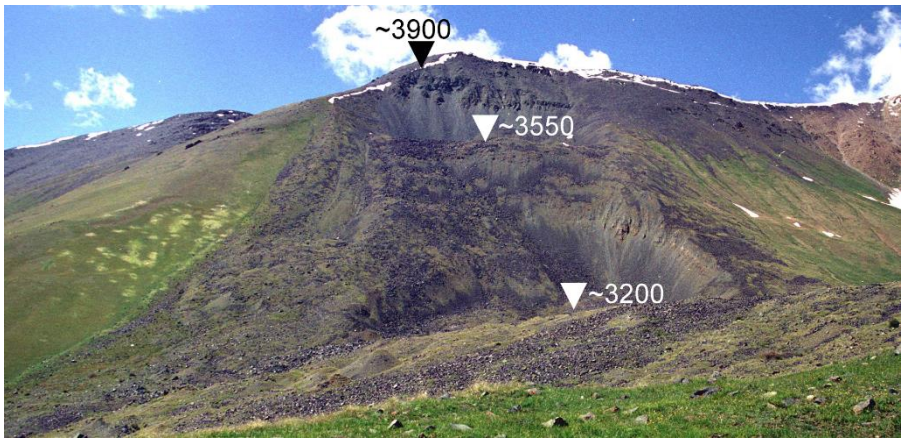

Figure 2. Spur rock avalanche, Central Tien Shan (41.975° N, 75.902° E) with debris apron expanding over the slope outside from the headscarp limits.

3 Modeling of secondary rock avalanches' formation

One more phenomenon reflecting stress state transformation, this time within the moving debris, that can be reproduced in the lab qualitatively – the formation of so called "secondary rock avalanches" (Strom 2006, 2015). In such cases part of the collapsing rock mass that collides with the opposite valley wall or entered sharp valley constriction forms compact body at the slope base or rockslide dam, while part of it is "ejected" being abnormally mobile. Moreover, the runout of such secondary rock avalanches sometimes exceed that of rock avalanches of comparable volume and descend that did not overcome any obstacles on their way (of the "primary" type). It was hypothesized that this affect is associated with momentum transfer from rapidly decelerating part of the rockslide body to its part retaining possibility of further motion (Strom 2010). It could be modeled by comparison of runout of rapid granular flows created by any way that move over unconfined surface with those meeting either one oblique obstacle (i.e. opposite valley slope) or two such obstacles representing valley constriction typical of the " secondary rock avalanches" of the "bottleneck" subtype (Strom 2010, 2015). Some results of such "conceptual modeling" of the abovementioned phenomena and processes will be presented.

4 References

Dubovskoi, AN, Pernik, LM, Strom AL. 2008. Experimental simulation of rockslide fragmentation. Journal of Mining Science, 44, Issue 2, 123–130.

Strom, AL. 2006. Morphology and internal structure of rockslides and rock avalanches: grounds and constraints for their modelling. In: Evans, S.G.; Scarascia Mugnozza, G.; Strom, A.; Hermanns, R.L. (Eds.) Landslides from Massive Rock Slope Failure. NATO Science Series: IV: Earth and Environmental Sciences, Vol. 49, 305-328.

Strom, AL. 2010. Evidence of momentum transfer during large-scale rockslides' motion. In: Williams AL, Pinches GM, Chin CY, McMorran TG, Massei CI (eds.) Geologically Active.Proc. of the 11th IAEG Congress, Auckland, New Zealand, 5-10 September 2010, Tailor & Frensis Group, London, 73-86.

Strom, AL. 2015. Possible Causes of Accelerating Landslide Motion in Confined Environment. In: G. Lollino, D. Giordan, G.B. Crosta, J. Corominas, R. Azzam, J.Wasowski, N. Sciarra (eds.), Engineering Geology for Society and Territory – Volume 2, Springer International Publishing Switzerland, 883-885.

Numerical simulation of rockfall due to fracture propagation in rock bridges

Claudio Scavia[1*] and Marta Castelli[1]

[1] Department of Structural, Geotechnical and Building Engineering, Technical University of Turin, Turin (Italy)
* claudio.scavia@polito.it

1 Introduction

The stability of fractured rock slopes is strongly related to the geometrical and mechanical characteristics of natural discontinuities, which concentrate stresses at their tips giving rise to progressive failure of rock bridges. Fracture mechanics makes it possible to take this phenomenon into account assuming discontinuities as cracks and studying their triggering and propagation inside rock bridges. As an example, a Linear Elastic Fracture Mechanics approach to the back analysis of a rockfall triggering phenomenon is presented in this paper, carried out through the code GEOF (Scavia 1995; Castelli 1998), based on the BEM technique of the Displacement Discontinuity Method (DDM, Crouch and Starfield 1983).

2 Description of the rockfall and definition of the geometrical model

The simulated instability occurred in 2004 from an approximately vertical slope made of Urgonian limestone and located in the Vercors Sub-alpine Chain (South-western France).

After the failure a detailed geological and structural survey has been carried out by Frayssines (2005), leading to a complete description of the detaching niche (scar) and the surrounding slope. The main part of the scar is limited by (Figs. 1a and 1b): a mean surface (A) roughly parallel to the front, a bedding joint at the top (B), a lateral sub-vertical surface on the western side (C). The existence of fresh rock zones was observed and measured during the survey in the lower part of surface (A). This zones (52 m²) correspond to the 5% of the total surface and don't show any sign of alteration, in contrast with the rest of the scar, which is coated with a calcite crust.

A detailed digital model shows that the cliff surface presented a prominent overhang before the failure. The failure mechanism can then be a topple, due to tensile fracturing of intact rock zones. The unstable volume is characterized by a prismatic shape with average height (H) around 20 m, width (w) around 2.5 m and length (L) around 50 m, as shown in Fig. 1c.

As rock bridges are quite uniformly represented in the lower part of the scar (Fig. 1), a planar failure can be assumed and a 2D geometrical model can be considered in the numerical analyses, referred to the cross section in the center of gravity (S1-S1- in Fig. 1b). Different 2D models have been obtained with reference to the length and location of rock bridges. Here, the results related to a rock bridge length (h) around 3.4 m are shown, roughly corresponding to the trace of the surveyed rock bridge along the cross section S_1-S_1 (Fig. 1c).

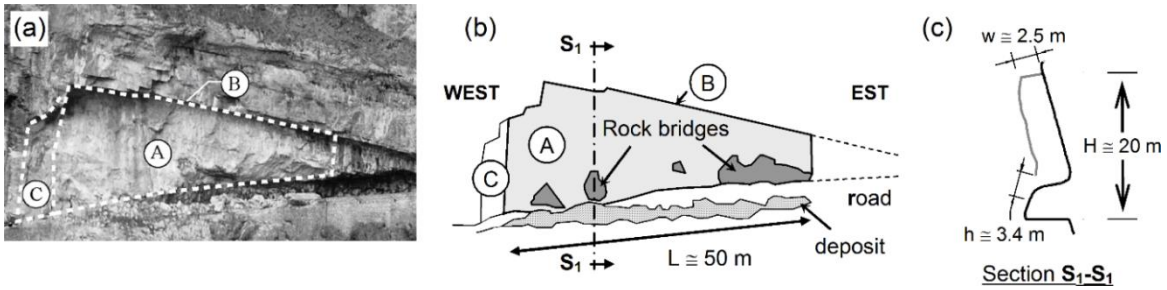

Figure 1. (a) Photography of the scar, (b) instability surface geometry and localization of rock bridges. (c) 2D geometrical model related to cross section S_1-S_1 (h = rock bridge length).

3 Back analysis of the failure mechanism and discussion

In the numerical scheme, the intact material is considered linearly elastic, and each crack is subdivided into a set of N elements, over which the relative normal and tangential displacements (Displacement Discontinuities D_n and D_s) vary according to a given distribution. Knowing the analytical solution for a single element, it is possible to calculate stresses and displacements due to the crack at any point of the elastic body, by adding up the effects of the N elements. The slope formation is simulated through an excavation process applied in steps and the possibility of crack propagation is assessed at each step by evaluating an equivalent stress intensity factor K_{eq} through the computed D_n and D_s and by comparing it with the experimental material toughness K_{IC} (Erdogan & Sih 1963). If such possibility occurs, one element is added at the tip of the crack in the direction perpendicular to the maximum tensile stress. In the analyzed case, fracture toughness was measured through some chevron bend tests that indicated K_{IC}=1,75 MPa·√m (Frayssines 2005).

In the numerical analyses, some DD elements of different length are associated to the external profile of the potential unstable block, the detaching niche and the tips. The excavation was simulated in 10 steps. A tensile propagation of the discontinuity tip was triggered at the end of the excavation and evolved inside the rock bridge until the external profile of the slope, resulting in the formation of a tensile failure surface with length around 4 m. The D_n distribution on the elements making up the global failure surface confirms a toppling mechanism, as shown in Fig. 2a, where both the triggering phase and the coalescence of the rock bridge are indicated. The opening D_n at the moment of triggering is due to the excavation, which induces a tensile state of stress at the tip and the consequent crack propagation. The difference between the two curves in Fig. 2a gives the opening due to crack propagation, which induces a toppling mechanism, highlighted by the deformed geometry obtained at the end of the analysis, as shown in Fig. 2b.

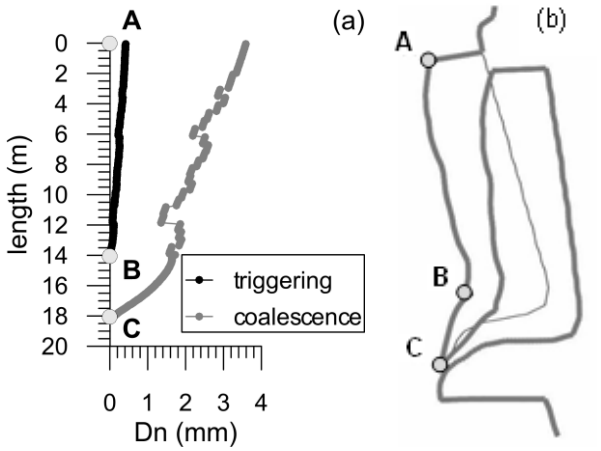

Figure 2. (a) D_n distribution along the detaching niche, at the propagation triggering and coalescence; (b) Deformed geometry at the end of the propagation process (magnification factor = 1000).

This result shows the capability for a fracture mechanics approach to take into account the fundamental role of rock bridges in the stability of a slope. Actually, the uncertainty related to the geometrical and mechanical characteristics of rock bridges is the main obstacle to the application of such approach for prediction purposes. The future development of the research should therefore be related to the development of a probabilistic procedure able to consider the location, extension and mechanical characteristics of rock bridges inside the rock mass as stochastic variables.

4 Reference list

Castelli, M. 1998. Studio della rottura progressiva di strutture in roccia mediante un approccio di Meccanica della Frattura. Doctoral Thesis, Politecnico di Torino, DISTR (in Italian).

Crouch, SL, Starfield, AM. 1983. Boundary Element Methods in Solid Mechanics. London, George Allen and Unwing.

Erdogan, F, Sih, GH. 1963. On the Crack Extension in Plates under Plane Loading and Transverse Shear. Journal of Basic Eng., ASME 85, 519-527.

Frayssines, M. 2005. Contribution à l'évaluation de l'aléa éboulement rocheux (rupture). Doctoral Thesis, Université J. Fourier de Grenoble, LIRIGM (in French).

Scavia, C. 1995. A Method for the Study of Crack Propagation in Rock Structures. Géotechinique 45/3, 447-463.

Transient curve analysis for stress measurements involving progressive rock failure

Robert Corthésy[1] and Maria Helena Leite[1]

[1] Department of Civil, Geological and Mining Engineering, Polytechnique Montréal, Canada
* rcorthesy@polymtl.ca

1 Introduction

In a paper published in 2013, Yaméogo et al. showed how rock failure could affect stress measurements performed using the so-called modified doorstopper technique developed at Polytechnique Montréal. The modified doorstopper stress measurement technique (Corthésy et al. 2016) often categorized as an overcoring technique, consists in recording the recovered strains caused by stress relief at the bottom of a borehole drilled in a rock mass and converting the relieved strains into stresses by using the deformability parameters at the measuring point. The recovered strains are monitored using a specially designed data logger (Fig. 1) which is linked to a modified doorstopper cell. The recovered strains are converted to stresses assuming the rock behaviour is linear elastic and anisotropic. If rock failure occurs during the measurement process, the stress tensor calculated by assuming an elastic behaviour can be wrong. Core discing is probably the most visible manifestation of core failure when performing such measurements, however, even if no visible signs of damage are present, plastic strains can be induced at or near the borehole bottom, affecting the recovered strains and the calculated stresses (Corthésy & Leite 2008). When Yaméogo et al. (2013) published their work, no interpretation model that could account for the progressive failure occurring prior to or during the stress relief drilling process was available. Recently, Corthésy et al. (2016) proposed using the inverse problem approach for interpreting modified doorstopper stress measurements. In this abstract, the potential for using this approach when progressive failure occurs during the stress measurement operations is evaluated.

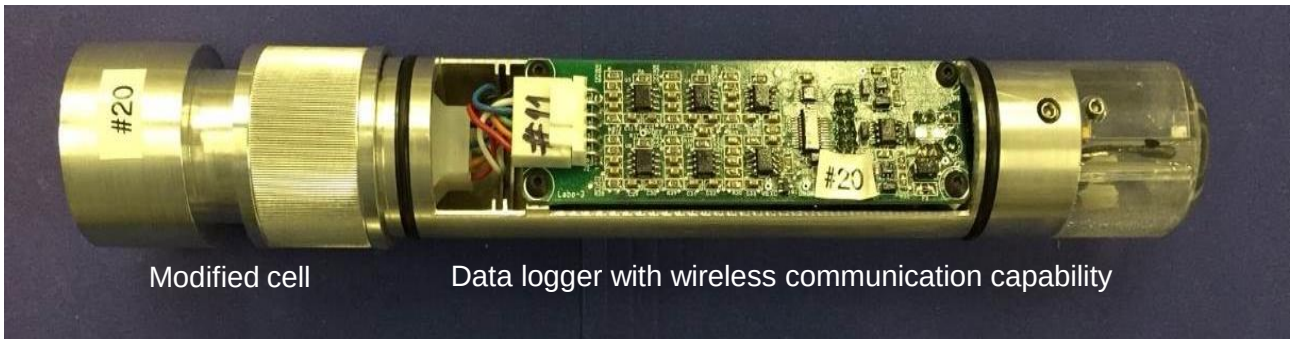

Figure 1. Modified doorstopper cell attached to its data logger with wireless communication capability

2 Methodology

Using Flac^{3D}, the stress relief process for different 3D in-situ stress states in an elasto-plastic cohesion-softening-friction-hardening model simulating the behaviour of brittle rock is used to generate strain recovery curves. Series of analyses are performed, each with a different in-situ principal stress (σ_1, σ_2, σ_3) aligned with the borehole axis. Within the load cases analyzed, the worst stress redistribution at the borehole bottom prior to stress relief drilling is linked to shear failure when σ_3 is aligned with the borehole axis. With σ_2 aligned with the borehole axis, stress redistribution is minimal, while when σ_1 is aligned with the hole axis, stress redistribution mostly affects σ'_3, the minor principal stress at the hole bottom.

The analyses show the stress path found under the rosette during the stress relief drilling process to be highly dependent on which principal in-situ stress component is aligned with the borehole axis and on the ratio between these stress components. Principal stress alignment and relative magnitude also affect the type of progressive failure the core will undergo while drilling, whether tensile, shear, or both.

The strain recovery curves obtained from the elastoplastic numerical analyses performed with Flac^{3D} are then used to calculate the in-situ stresses using two different interpretation methods developed by the authors, initially for isotropic or anisotropic elastic rock behaviour. The first is the RPR method (Corthésy et al., 1994) for Recovered to Peak Ratio, which gives a direct relationship between the far field stress invariant in the plane normal to the borehole axis ($\sigma_x + \sigma_y$) and the far field stress component parallel to it (σ_z), assuming axis z is parallel to the borehole. For isotropic rock, this relationship is only a function of Poisson's ratio and allows adding an equation to an otherwise undetermined system. The RPR method thus allows estimating four far-field stress components from a single measurement, while the conventional approach (Leeman, 1971) leads to an undetermined system of equations with a single measurement. The conventional approach requires three differently oriented boreholes to have the six independent equations needed to calculate six far field stress components. The RPR method requires monitoring the peak strains on the recovery curve plus the recovered strains when complete stress relief is achieved, which is why an in-the-hole data logger was designed. The other method (Corthésy et al. 2016) is based on the inverse problem approach but instead of only taking the peak and recovered strains, it uses a multitude of data points on the strain recovery curves using transient information as the stresses are gradually relieved from the core. One of the advantages of this method is that if progressive rock failure occurs during the stress relief drilling process, the portion of the recovery curve affected by plastic strains may be eliminated, minimizing the stress calculation errors.

3 Results

Fig. 2 is an example of strain recovery curves for both elastic and elastoplastic behaviour, for a simulated load case where the applied major in-situ stresses are $\sigma_x = \sigma_3 = 62$ MPa, $\sigma_y = \sigma_1 = 142$ MPa and $\sigma_z = \sigma_2 = 113$ MPa, z axis being parallel to the borehole. It can be observed that the recovered elastic and elastic-plastic strains are very similar until the stress relief drilling advance *(L/D)* reaches approximately 0.5, *L* being the drilling length and *D* the core diameter. Past this point the ε_{xx} and ε_{yy} values start moving apart, being the farthest when the stress relief process is complete, which is the location where the strains used in the conventional interpretation method are taken. Fig. 3 shows that for this load case, no failure has affected the center of the borehole bottom prior to initiating stress relief drilling. The calculated stresses using the transient curve analysis and the RPR method are shown in Fig. 4 where they are compared to the applied stresses. The advantage of the transient analysis method is evident for this load case. It should be noted again that the conventional interpretation method (Leeman, 1971) cannot be used with a single measurement.

Another example follows, this time with σ_3 parallel to the borehole axis ($\sigma_x = \sigma_2 = 118$ MPa, $\sigma_y = \sigma_1 = 139$ MPa and $\sigma_z = \sigma_3 = 65$ MPa). In this case, discing of the core occurs as shown in Fig. 5 where the dark zones represent tensile plastic strain localisation. This failure mode is also visible through the shape of the strain recovery curves which shows a sharp slope increase as seen in Fig. 6. The problem with the sudden stress drop caused by discing is that the strains are not relieved at a regular pace as shown by the elastic recovery curves (ela). To be able to correctly apply the inverse problem approach, it is necessary to give more degrees of freedom to the solution and allow for an adjustment of the drilling rate (*L/D* ratio). In this case, a bilinear model is used to adjust the *L/D* ratio and Fig. 7 shows the adjustment of the recovery curves from the plastic analysis (simulated field data) with the curves generated by the inverse problem approach identified as *transient* on the graph.

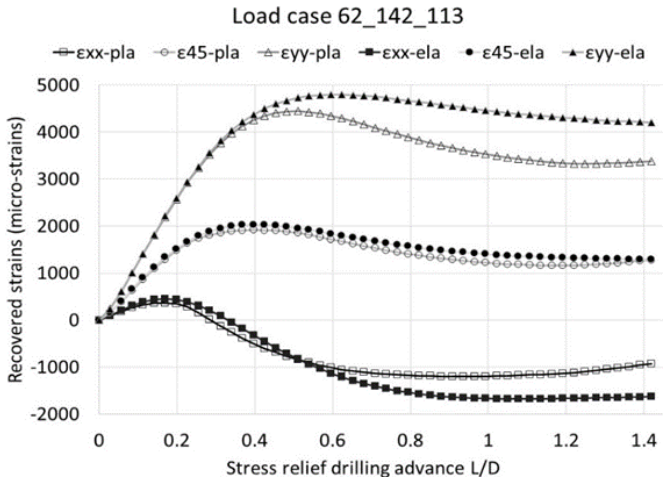

Figure 2. Elastoplastic and elastic strain recovery curves for load case 62-142-113.

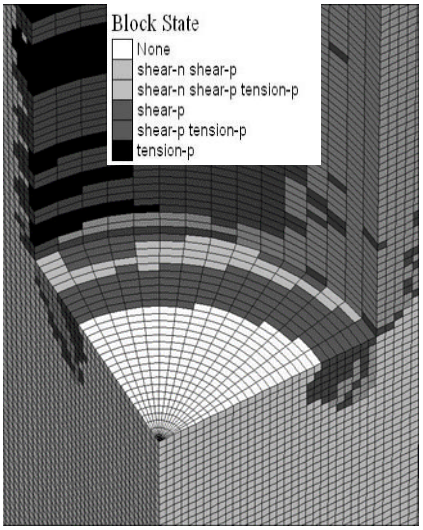

Figure 3. Borehole bottom failure states prior to initiating the stress relief process for load case 62-142-113.

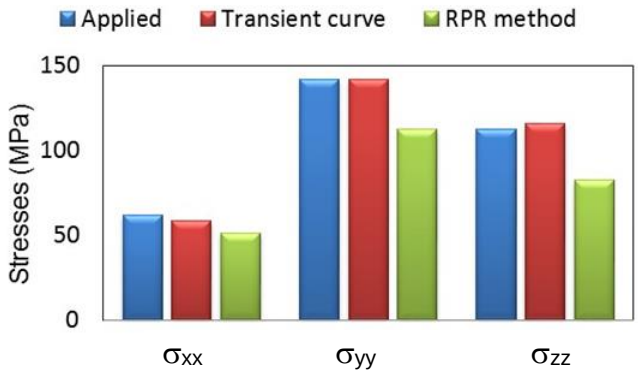

Figure 4. Calculated stress magnitudes using different approaches for load case 62-142-113.

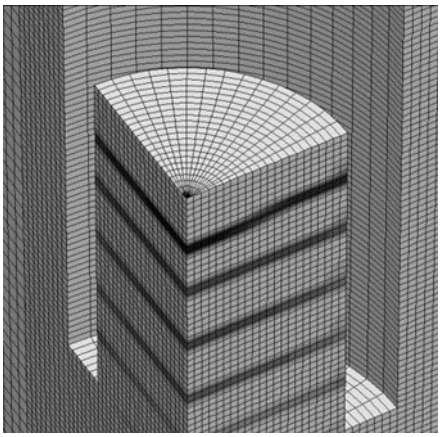

Figure 5. Core discing observed for load case 118-139-65.

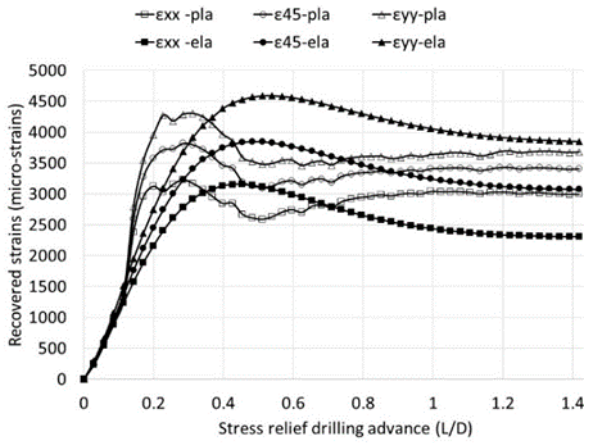

Figure 6. Strain recovery curves obtained from elastoplastic and and elastic analyses for load case 118-139-65.

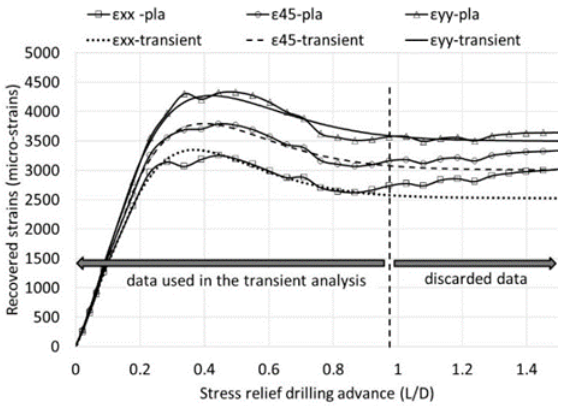

Figure 7. Strain recovery curves obtained from transient analysis using the inverse method superposed to elastoplastic strains for load case 118-139-65.

Fig. 8 shows a comparison of the applied and calculated stress magnitudes obtained from the inverse problem (transient curve) method, giving an excellent match and the RPR method which fails at giving acceptable results, especially for σ_{zz} which is found to be negative and causes an important

underestimation of both σ_{xx} and σ_{yy} due to the influence of σ_{zz} on the equations involved in the RPR method.

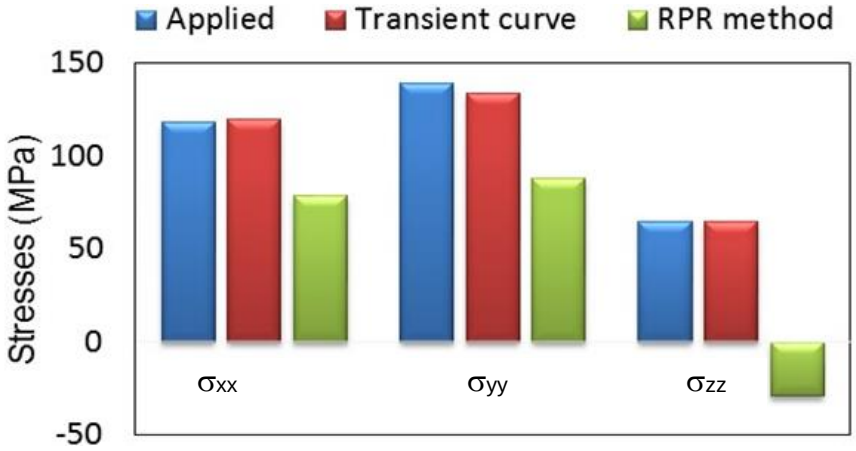

Figure 8. Calculated stress magnitudes using different approaches for load case 118_139_65.

4 Discussion

The results presented in this abstract are considered representative of what could be observed if the rock behaved according to the assumptions made in the numerical models used to generate the data. The use of a cohesion-softening-friction-hardening constitutive law for simulating brittle rock behaviour during coring operations was validated by the authors using experimental data published in the literature (Corthésy & Leite 2008). Note that no elastic parameters softening was programmed in the model which could nonetheless be implemented in further studies of this complex problem. Moreover, the load cases analyzed impose a principal in-situ stress to be parallel to the borehole axis. This situation was found to be the most critical in terms of shear or tensile stress magnitudes causing rock failure at the borehole bottom or during the stress relief drilling operation. Finally, departure from a linear elastic behaviour can easily be detected when using a numerical model which allows to generate an elastic solution which is directly compared to the elasto-plastic one. In practise however, the linear elastic recovery curves are unavailable and the detection of non-elastic behaviour must be based on observations of the shape of the strain recovery curves which may become irregular as shown in Fig. 6, by comparing the two strain invariants which can be calculated with a four gauge rosette and by observing damage on the recovered cores, like the initiation of discing.

5 Reference list

Corthésy R, Leite MH, He G, Gill DE. 1994. RPR method for the Doorstopper technique: Four or six stress components from one or two boreholes. Int J Rock Mech Min Sci 31(5), 507-516.

Corthésy R, Leite MH. 2008. A strain-softening numerical model of core discing and damage. Int J Rock Mech Min Sci, 45, 329–350.

Corthésy R, Leite MH, Vézina C, Ouellet AC. 2016. Application of the inverse problem to stress measurement interpretation in anisotropic rock. 7th Int. Symp. On In-Situ Rock Stress, Tampere, 10-12 May 2016, 309-319.

Leeman ER. 1971. The C.S.I.R. "Doorstopper" and triaxial rock stress measuring instruments. Rock Mechanics 3(1), 25-50.

Yaméogo ST, Corthésy R, Leite MH. 2013. Influence of rock failure and damage on in situ stress measurements in brittle rock. Int J Rock Mech Min Sci 61, 118-129.

Process of the first cracks generating between two neighboring holes under incremental static loading in brittle rocks

Shobeir Arshadnejad[1]

[1] Department of Mining Engineering, Mahallat Branch, Islamic Azad University, Mahallat, Iran.
s_arshadnejad@yahoo.com

1 Introduction

One of the main methods in hard rock quarry mining is the controlled fracture method that is carried out by the introduction of a slowly advancing crack by Non-Explosive Expansion Material (NEEM). The method of rock breakage is without noise and vibrations and its operation, compared to blasting method, is more controllable, very safe and easy and without extra undesirable cracks in the rock block (Hinze and Nelson, 1996; Gambatese 2003; Huynh, et al. 2009; Laefer, et al. 2010).

In this method, some circular holes are drilled closely with equal length, diameter and spacing (center-to-center distance) in a rock block. Subsequently, the holes are filled by the NEEM, which it can be expanded and generates an incremental static loading into the holes after about two to four hours. If the spacing of the holes to be adequate, it will create a crack between two neighboring holes and the rock will fracture along the high-stress concentration path between the holes. In this paper will be try to introduce a new numerical modelling approach for showing location and length of the first cracks around the holes and predicting of the crack growing path with the geometry.

2 Experimental data and a case study

A granite quarry mine was selected as a case study entitled “Ahrar Mine” which it has located near to Natanz in Iran (Fig. 1). Some laboratory tests have been done on the granite specimens for measuring of some rock mechanics’ properties such as uniaxial compressive strength, Brazilian tensile strength, Young’s modulus, Poisson’s ratio, specific gravity and fracture toughness by ISRM standard methods (Fowell, 1995), (Tab. 1). Process of rock fracture in due time by the NEEM has been shown in Figs. 1 and 2. The drill holes were 38 mm with 1 to 3 meters depth and the average of the hole’s spacing was 12 cm (10-14 cm) in the mine.

Table 1. Mechanical properties of the granite (Arshadnejad 2010)

Parameters	σ_c (MPa)	$\sigma_t\sigma_t$ (MPa)	E (GPa)	v	$\gamma\gamma$ (kN/m^3)	K_{IC} (MPa$\sqrt{m}$)
Ave. value	131.6	7.2	70.6	0.25	26.4	1.3
Standard dev.	3.2	0.42	2.3	0.011	0.31	0.08

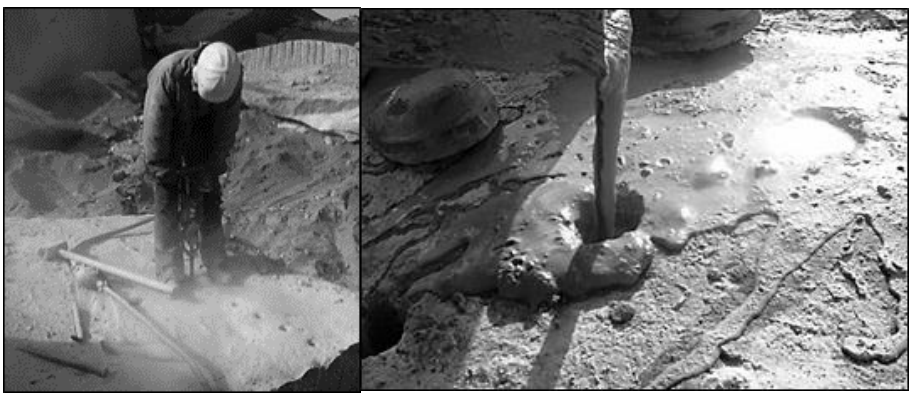

Figure 1. Left: Drilling of a rock block in the granite mine. Right: NEEM into the hole.

Figure 2. Process of rock fracture by the NEEM after 24 hours. Left: Crack generation after 8 hours. Right: Crack opening after 24 hours.

3 Stress distribution around the holes

When there are two neighboring holes in a plate loaded internally, stress concentration will occur between the holes if distance between them is not far. The maximum elastic stresses (stress concentration) were examined by several methods, such as photoelastic analysis (Joussineau, et al. 2003), direct strain measurement (Chong, et al., 1987) and numerical modeling (Yan 2007). Howland (1929) investigated the stress distribution around an infinite row of equal size circular holes spaced equally in an infinite elastic plate. If the type of external loading is tensile in biaxial, two empirical models were developed by Schulz in 1942 and Peterson in 1974. Arshadnejad and his colleagues (Arshadnejad, et al. 2009) suggested two empirical models to determine of stress concentration factors (tangential and radial stresses) between two neighboring holes under internal pressure by numerical modeling. Tangential stress distribution between two holes can be calculated by Eq. 1 and the stress concentration factor in the equation can be evaluated by Eq. 2.

$$\sigma_\theta = C_\theta . P \left[\frac{d}{2r}\right]^2 \tag{1}$$

$$C_\theta = 1.1715 \left[\frac{d}{s}\right]^{0.124} . \nu^{-0.025} \tag{2}$$

Where σ_θ is the tangential stress, C_θ is the stress concentration factor, r is the radial distance of the considered point from the hole center, d is the diameter of holes (m) and S is the edge-to-edge distance between two neighboring holes (hole spacing) (m), υ is Poisson's ratio of rock, P is the internal pressure of the hole (pressure of the NEEM) (MPa). There is an experimental model for evaluation of NEEM's pressure which it has been developed by some experimental measurements (Arshadnejad 2016).

$$P = 0.512\, E^{0.122} T^{0.429} . e^{0.0108\, \boldsymbol{d}} . e^{0.0139\, \boldsymbol{CaO}} \tag{3}$$

Where P is the pressure of the NEEM (MPa), E is Young's modulus of the rock (GPa), T is the temperature in Celsius, d is diameter of the hole (mm), and CaO is the lime content in the chemical combination of the NEEM (%) (Usually it is between 80 and 90 percent).

4 Birth of the first crack holes

If tangential stress around the hole obtains a value equal to tensile strength of the rock, first cracks will be born on the line passing through the center of the holes in both sides of the holes. Because there is stress concentration in the location and the process can be repeated by the time. When there is a crack in a solid, stress intensity factor can controls the process of crack growing based on the LEFM. But evaluation of the first crack length is very important which it needs to calculate the stress intensity factor (in mode I) for this special geometry. There is an experimental relation for determining of the stress intensity factor as follow (Tada, et al. 2000; Fig. 3).

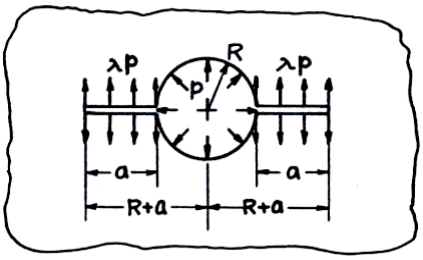

Figure 3. Geometry of the cracks in both sides of a circular hole under internal loading (Tada, et al. 2000).

$$K_I = F_\lambda(S').P\sqrt{\pi a} \quad (4)$$

$$F_\lambda(S') = (1-\lambda)F_0(S') + \lambda F_1(S') \quad (5)$$

$$F_0(S') = (1-S')[0.637 + 0.485(1-S')^2 + 0.4S'^2(1-S')] \quad (6)$$

$$F_1(S') = 1 + (1-S')[0.5 + 0.743(1-S')^2] \quad (7)$$

$$S' = \frac{a}{R+a} \quad (8)$$

$$\lambda = \frac{a}{\sqrt{R.t'}} \quad (9)$$

Where K_I is the stress intensity factor in mode I ($MPa\sqrt{m}$ $\mathrm{MPa}\sqrt{\mathrm{m}}$), P is the internal pressure of the hole (MPa), a is the crack length (m), $F_\lambda(S')$ is a geometric function, λ is a parameter of normalized thickness of the plate, S' is a parameter of normalized crack length, R is the radius of the hole (m) and t' is the thickness of the plate (m) which it is considered one meter, usually.

Eq. 4 can be rewritten in a new form for calculating of the crack length. But it is clear that there is parameter a in both sides of the equation, then it needs to solve by a close loop such as a flowchart which has been shown in Fig. 4 (a' is the calculated value of a in each step).

$$a = \frac{1}{\pi}\left[\frac{K_{IC}}{F_\lambda(S')P_i}\right]^2 \quad (10)$$

Where K_{IC} is the maximum stress intensity factor or fracture toughness of the rock ($MPa\sqrt{m}$ $\mathrm{MPa}\sqrt{\mathrm{m}}$), P_i is the minimum pressure of the hole which it needs to generate the first crack. Therefore the tangential stress on edge of the hole has to equal to the tensile strength of the rock (σ_t). The parameter can be calculated by apply of the stress concentration factor (Eq. 2).

$$P_i \times C_\theta = \sigma_t \quad (11)$$

$$P_i = 0.854\,\sigma_t\left[\frac{d}{s}\right]^{-0.124}.\nu^{0.025} \quad (12)$$

Therefore length of the first crack has been calculated by the relations and the results are in Tab. 2. The minimum pressure of the hole which it needs to generate the first crack in this case was 6.84 MPa based on the data from Tab. 1 and Eq. 12. The crack length is 42 mm and it is close to result of numerical modeling (43.5 mm) and experimental data from the mine (38 mm).

Table 2. Calculation of the first crack length

λ	S'	$F_0(S')$	$F_1(S')$	$F_\lambda(S')$	*a* (m)	*a'* (m)

0.13784	0.5	0.404125	1.342875	0.534	0.019	0.040
0.292231	0.679494	0.239102	1.184715	0.515	0.040	0.043
0.313095	0.694323	0.226586	1.17406	0.523	0.043	0.042
0.303834	0.687914	0.231978	1.178628	0.520	0.042	0.042

5 Crack growth by numerical modelling

If the stress intensity factor is equal to the rock fracture toughness, cracks can be grown. Subsequently, the crack will grow however as the crack length increases, the stresses on the crack tip decreases. Nevertheless, by increasing the stress induced from the hole due to application of NEEM, in due time, the stress intensity on the crack tip will again increase up to the level of rock fracture toughness. Thus, again the crack will grow farther and this cycle of events will repeat until the maximum pressure of the NEEM.

In this study, will be tried to find a communication between the analytical approach and numerical modeling of the first crack. A finite element computer code (Phase^2) has been applied for numerical modeling. View of the modeling is in plan and the type of field stress was constant condition. It is necessary to consider the body force condition have not to be selected and six nodal triangular elements were utilized. The crack has been modeled by a discontinuity element (no-tension). Mohr-Coulomb criterion and Bandis-Barton criterion are semi analytical models to predict of discontinuity behavior in rock. The second criterion needs surface strength and geometry of the crack but there is no imagination about geometry of crack before its generating. Then Mohr-Coulomb criterion was selected without cohesion (C = 0) and 30 degrees friction angle. Mesh density on crack tip and its around is higher than other points. Experience in this research shows that the average length of the elements at the crack tip need to be less than one third of each part of discontinuity element's length. Last version of Hoek-Brown criterion (Hoek, et al. 2002) has been employed for evaluating of behavior of the rock substance.

At each stage the crack was extended according to the size of failure zone at vicinity of the crack tip. After that next model is made by the new extended crack and new orientation of the crack and increased load. This process will be continued to fracture surface to be stopped.

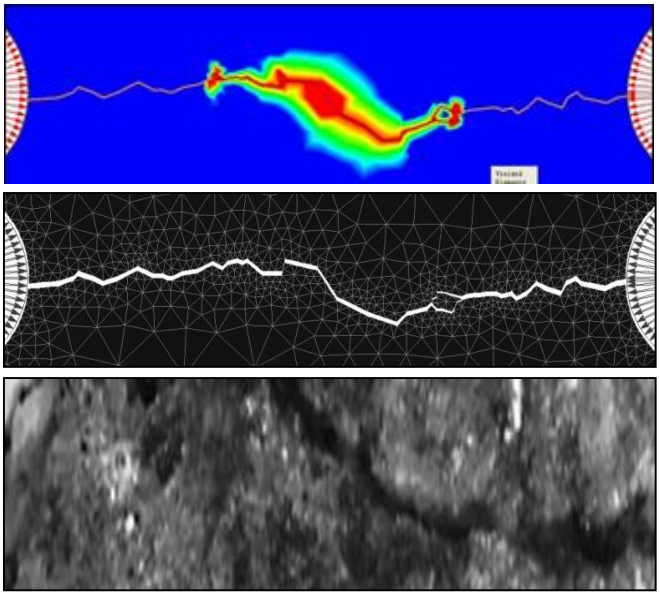

Figure 4. Crack growth by FEM and a picture from the case study (Step 3).

6 Conclusions

If two neighboring holes are enough close together, stress concentration will occur and it will cause to generation of first cracks. Length of the cracks depends to tangential stress due to pressure of the

NEEM and tensile strength and fracture toughness of the rock. The results show that the new suggested equation and the algorithm for calculation of the first crack length had an adequate accuracy. There was a case study in a granite mine in Iran and many measurements were recorded there. Results of numerical models showed that if size of elements near the crack tip to be less than one third of each part of discontinuity element's length, accuracy of the crack path prediction can be acceptable. This research shows that Mohr-Coulomb criterion without cohesion and with basic friction angle (30 degree) is a suitable model for crack's elements and Hoek-Brown failure criterion is adequate model for rock substance.

7 Reference list

Arshadnejad, Sh., 2016. Study on performance of non-explosive expansion materials by experimental approach. Journal of Earth Engineering 1, No.1, 509-514.

Arshadnejad, Sh., 2010. A model for analysis of rock fracture in granite due to non-explosive expansion material. PhD Thesis, Azad University, Science and Research branch, Iran.

Arshadnejad, Sh., Goshtasbi, K., Aghazadeh, J., 2009. Stress concentration analysis between two neighboring circular holes under internal pressure of a non-explosive expansion material. J. Yerbilimleri 30, No.3, 259-270.

Chong, K.P., Harkins, J.S., Kuruppu, D.M., Leskinen, A.I.L., 1987. Strain rate dependent mechanical properties of western oil shale. Proceedings, 28th US Symposium on Rock Mechanics, USA, 157-164.

Fowell, R.J., 1995. Suggested method for determining Mode I fracture toughness using cracked chevron notched Brazilian disc (CCNBD) specimens. ISRM Commission on Testing Methods, Int. J. Rock Mech. & Mining Sciences 32, No.1, 57-64.

Gambatese, J.A., 2003. Controlled concrete demolition using expansive cracking agents. J. Constr. Engrg. & Mgmt. ASCE 129, No.1, 98-104.

Gholinejad, M., Arshadnejad, Sh., 2012. An experimental approach to determine the hole-pressure under expansion load. The Southern African Inst. of Mining & Metallurgy, SAIMM 112, 631-635.

Hinze, J., Nelson, A., 1996. Enhancing performance of soundless chemical demolition agents. J. Constr. Engrg. & Mgmt. ASCE 122, No.1, 193-195.

Hoek, E., Carranza-Torres, C., Corkum, B., 2002. Hoek–Brown failure criterion – 2002 edition. NARMS-TAC, University of Toronto Press, 267–273.

Howland, R.C.J., 1929. On the stress in the neighborhood of a circular hole in a strip under tension. Transaction of Royal Society, London, Series A 229.

Huynh, M.P., Laefer, D.F., 2009. Expansive cements and soundless chemical demolition agents: state of technology review. Magazine of concrete research 61, 100-106.

Joussineau, GH.D., Petit, J.P.B., Gauthier, D.M., 2003. Photoelastic and numerical investigation of stress distributions around fault models under biaxial compressive loading conditions. Tectonophysics 363, 19-43.

Laefer, D.F., Ambrozevitch-Cooper N., Huynh, M.P., Midgette, J., Ceribasi, S., Wortman, J., 2010. Expansive fracture agent behaviour for concrete cracking. Magazine of concrete research 62, 443-452.

Peterson, R.E., 1974. Stress Concentration Design Factors. John Wiley & Sons, New York.

Schulz, K.J., 1942. On the state of stress in perforated strips and plates. Neth. Royal Academic Sciences 1, 45-48.

Tada, H., Paris, P.C., Irwin, G.R., 2000. The stress analysis of cracks Handbook. (Third Edition), The American Society of Mechanical Engineers, Professional Engineering Publishing Limited.

Yan, X., 2007. Rectangular tensile sheet with single edge crack or edge half-circular-hole crack. J. Eng. Failure Analysis 14, 1406-1410.

Damage-based time-dependent simulation of the progressive failure of large alpine rock slopes

Federico Agliardi[1*], Federico Riva[1], Giovanni B. Crosta[1] and David Amitrano[2]

[1] Department of Earth and Environmental Sciences, University of Milano-Bicocca, Italy
[2] ISTerre, Université Grenoble Alpes, France
* federico.agliardi@unimib.it

1 Introduction

Large slopes in alpine environments undergo a complex long-term evolution from glacial to postglacial conditions through a transient period of paraglacial readjustment. During and after this transition the interplay among rock strength, topographic relief and morpho-climatic drivers can promote different types of slope instability, from sudden failures to large, slow (yet potentially catastrophic) rockslides. Deep-seated rockslides are commonly characterised by time-dependent displacements with superposed "long-term creep" components, often considered as evidence of progressive (sub-critical) slope failure (Amitrano & Helmstetter 2006; Lacroix & Amitrano 2013), and "seasonal creep" components resulting from coupling between hydrological triggers and landslides (Cappa et al. 2014; Crosta et al. 2014). Modelling the progressive failure of large rock slopes is key to predict future displacements and potential catastrophic evolution for risk analysis and early warning. Failure forecast for "mature" rockslides with well-developed sliding shear zones and weakened, permeable landslide masses mostly relies on analytical, statistical or numerical models accounting for the hydro-mechanical response of landslides to rainfall or snowmelt (Guglielmi et al. 2005; Crosta & Agliardi 2003; Crosta et al. 2014). Nevertheless, the geometry, internal structure, strength and hydrology of rock slopes are usually poorly known and likely evolve throughout deglaciation and paraglacial adjustment.

Understanding the long-term evolution and progressive failure of large rock slopes requires that we account for time-dependent effects of unloading during deglaciation, permeability and fluid pressure fluctuations, ongoing displacement, and fracture development (Riva 2017; Riva et al, in review). All these aspects are related to a convincing description of rock mass damage processes, from a sub-critical (progressive) to a critical (catastrophic) stage. Nevertheless, time-dependent damage evolution under gravitational load and variable external drivers remains poorly explored. Other open issues include: a) difficult use of time-dependent rheological models, unable to account for localization unless a shear zone is pre-defined; b) largely unknown spatial and temporal patterns of water occurrence in the slope during and after deglaciation (Ballantyne 2002); c) limited understanding of the relationships between brittle failure and permeability on the scale and under stress conditions typical of rock slopes; and d) uncertainty in material property upscaling and model calibration for time-dependent models. In this context, we developed DaDyn-RS, a tool simulating the damage-based, time-dependent long-term simulation of real large rock slopes in alpine environments.

2 Model implementation: DaDyn-RS

We developed a 2D Finite-Element model in Matlab™ (Riva 2017; Riva et al, in review) starting from the approach previously used by Amitrano et al. (1999) and Amitrano & Helmstetter (2006) to simulate brittle creep, crack damage and localization in laboratory rock deformation. By combining a continuum damage mechanics law and a macroscopic time-to-failure law, the model is able to reproduce the entire range of slope creep behaviors, from primary (decelerating) to tertiary (accelerating) stages (Fig. 1). Both instantaneous and progressive failure are simulated depending on the local stress state using an elastic interaction model accounting for damage by the progressive reduction of the effective rock deformation modulus at each element. The finite-element scale implementation

of these formulation allows the model to reproduce problem-scale phenomena as emerging processes, including: damage localization, creep stages, and rupture event statistics. We upgraded the model for application to real (large) rock slopes by implementing major new features. Material property upscaling is introduced to account for the strength, deformability and heterogeneity of rock masses, according to an equivalent continuum approach. We evaluate rock mass properties using the Hoek-Brown approach through Geological Strength Index (GSI; Hoek and Brown 2002; Hoek and Diederichs 2005), estimated at outcrops or from borehole data (Agliardi et al. 2016). We developed a specific model calibration approach integrating evidence/measures of slope displacements and field estimates of rock mass damage through the GSI (Riva et al. 2016). We introduced a time-dependent simulation of valley deglaciation, whose timing is calibrated on absolute or relative chronological constraints and interacts with the model time-to-failure law. As a major implementation, we introduced a damage-dependent fluid distribution and hydro-mechanical coupling scheme, with water occurring in "permeable element clusters" undergoing brittle damage, dilatancy and connectivity to slope surface. Thus, evolving patterns of damage set the slope hydrology and affect hydro-mechanical coupling and progressive slope failure.

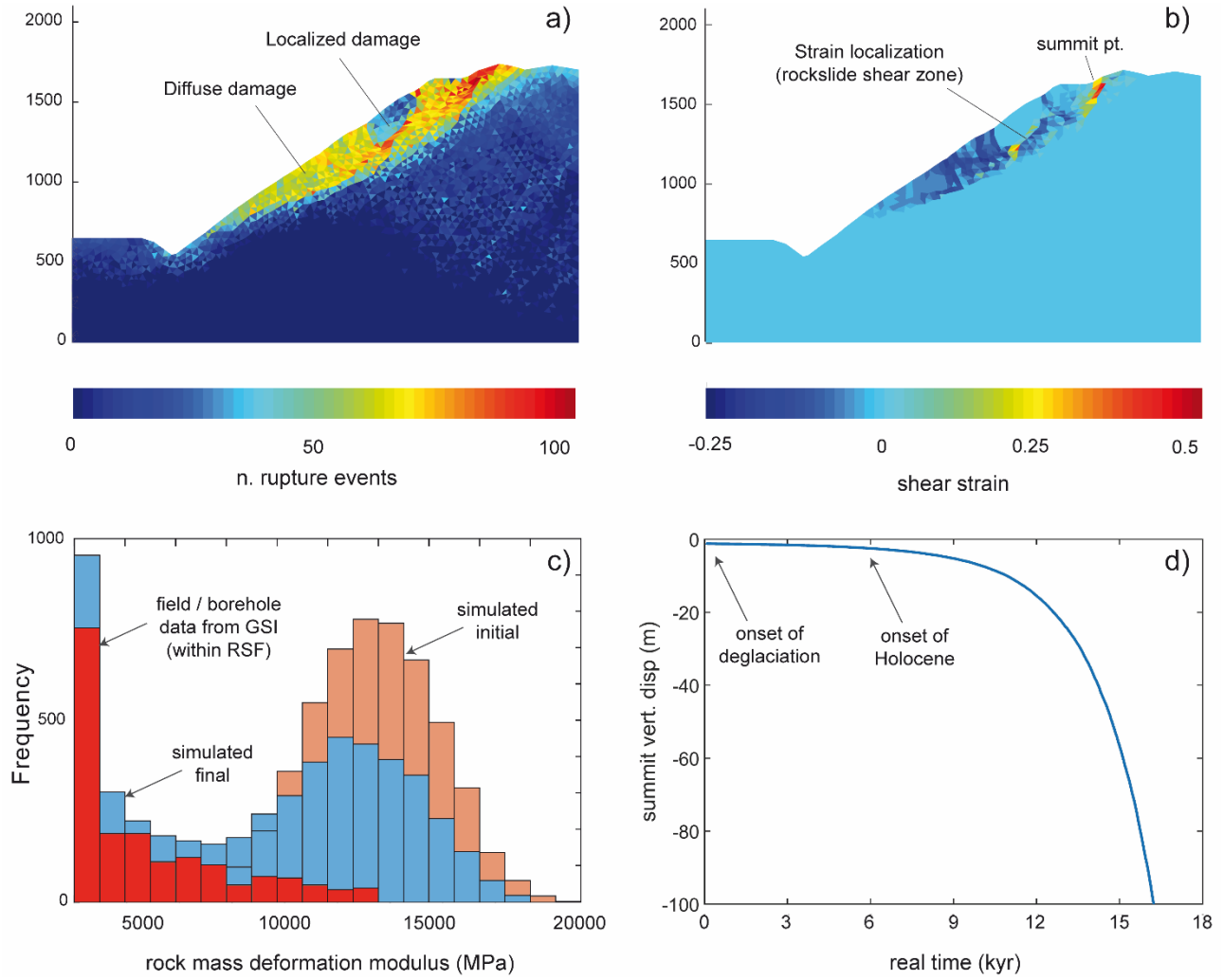

Figure 1. Results of Dadyn-RS simulation on a large deglaciated rock slope with upscaled material properties: a) cumulative number of damage events; b) accumulated shear strain in model elements; c) statistical distributions of rock mass deformation modulus values at the start vs. end of simulation. Simulated values are compared to field data (from GSI); d) displacement-time creep curve for a specified monitoring location.

3 Model application

We first tested DaDyn-RS performance with parametric analyses of synthetic case studies, to investigate the effect of the different model parameters (strength, damage, and creep parameters, as well as mesh size) and the role of groundwater on slope damage and failure mechanics. Then, we applied DaDyn-RS to real slopes located in the Italian Central Alps, namely: a) the Spriana slope, the site of a 50 Mm^3, well-documented active rockslide (Agliardi and Crosta 2014; Riva et al. 2016); and b) the Saline slope, affected by an active Deep Seated Gravitational Slope Deformation (Agliardi et al. 2001; Crosta and Agliardi 2003). Starting from borehole records and field survey data, we used the GSI as a damage proxy to identify field "damage domains". These represent the damage signatures of different long-term slope evolution processes. We constrained deglaciation timings and scaled model results to 'real time' using available field and literature constraints. Model parameters were calibrated by matching field and simulation data of slope instability geometry, kinematics, damage distribution (diffuse vs localized), and displacements (Fig. 1).

From Last Glacial Maximum to present conditions, our model proved to effectively reproduce, in an explicit time-dependent framework, the progressive development of damage-induced permeability, strain localization and shear zone differentiation at different times between the Lateglacial and the Mid-Holocene climatic transition. Different mechanisms and timings characterize different styles of slope deformations (rockslide vs DSGSD), consistently with available dating constraints. DaDyn-RS is able to account for different long-term slope dynamics, from slow creep to the delayed transition to fast-moving rockslides. The model revealed emerging behaviors including transition from dilatant (permeable) to contractive (sealing) shear zones controlling slope hydrology and progressive failure patterns. Simulated timings of slope failure support a very long "paraglacial" period of subcritical rock mass damage.

4 Reference list

Agliardi, F, Crosta, GB. 2014. Long and short-term controls on the Spriana rockslide (Central Alps, Italy). In Landslide Science for a Safer Geoenvironment, 243-249. Springer International Publishing.

Agliardi, F, Sapigni, M, Crosta, GB. 2016. Rock Mass Characterization by High-Resolution Sonic and GSI Borehole Logging. Rock Mechanics and Rock Engineering 49(11), 4303-4318.

Amitrano, D, Grasso, JR, Hantz D. 1999. From diffuse to localised damage through elastic interaction. Geophysical Research Letters, 26(14), 2109-2112.

Amitrano, D, Helmstetter, A. 2006. Brittle creep, damage, and time to failure in rocks. Journal of Geophysical Research: Solid Earth (1978–2012), 111(B11).

Ballantyne, C.K. 2002. Paraglacial geomorphology. Quaternary Science Reviews 21(18), 1935-2017.

Crosta, GB, Agliardi, F. 2003. Failure forecast for large rock slides by surface displacement measurements. Canadian Geotechnical Journal 40(1), 176-191.

Guglielmi, Y, Cappa, F, Binet, S. 2005. Coupling between hydrogeology and deformation of mountainous rock slopes: Insights from La Clapière area (southern Alps, France). Comptes Rendus Geoscience 337(13), 1154-1163.

Hoek, E, Carranza-Torres, C, Corkum, B. 2002. Hoek-Brown failure criterion – 2002 Edition. Proceedings North American Rock Mechanics Society. Toronto, July 2002.

Hoek, E, Diederichs, MS. 2005. Empirical estimation of rock mass modulus. International Journal of Rock Mechanics and Mining Sciences 43(2), 203-215.

Lacroix, P, Amitrano, D. 2013. Long-term dynamics of rockslides and damage propagation inferred from mechanical modeling. Journal of Geophysical Research: Earth Surface 118(4), 2292-2307.

Riva, F, Agliardi, F, Amitrano, D, Crosta, G.B. 2016. Damage-based long term modelling of a large alpine rock slope. In Landslides and Engineered Slopes. Experience, Theory and Practice. Proceedings of the 12th International Symposium on Landslides (Napoli, Italy, 12-19 June 2016).

Riva, F. (2017) Damage-based long-term modelling of paraglacial to postglacial evolution of alpine rock slopes. PhD Thesis. University of Milano–Bicocca, Department of Earth and Environmental Sciences (DISAT), 266 pp.

Riva, F, Agliardi, F, Amitrano, D, Crosta, G.B. Damage-based time-dependent modelling of paraglacial to postglacial evolution of real rock slopes. Journal of Geophysical Research: Earth Surface – in review.

The contribution of time-dependent rib deterioration to pillar bursting seismicity at Westwood mine

Kathy Kalenchuk[1]

[1] Mine Design Engineering, Canada
* kathy.kalenchuk@mdeng.ca

1 Introduction

The Westwood mine is located approximately 80 km west of the town of Val-d'Or in Quebec, Canada. Production in the 104-mining block in Zone 2 of the Westwood mine was halted by three large-magnitude seismic events over two days in May 2015 (Fig. 1). These seismic events are technically interesting because mining activities leading up to these events were reviewed and no specific blast (production or development) could be identified as a trigger. Further, these pillar bursting events occurred in the Central Infrastructure Corridor (CIC) well away from ore zone production, where adverse seismicity in mining operations would more typically be anticipated. This paper provides an overview of the seismic events and uses numerical models to demonstrate how geological conditions and mine geometry both contributed to what was considered, by a review panel of experts, to be an unforeseen series of events.

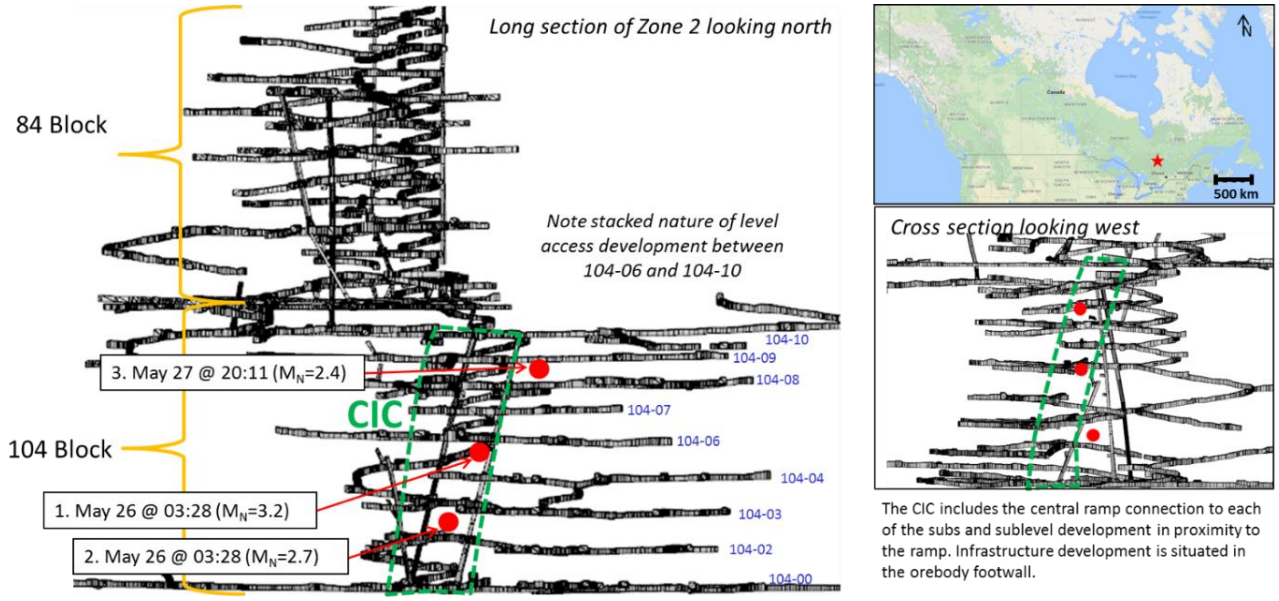

Figure 1. Location of May 2015 large-magnitude events within the 104 mining block. Inset shows Westwood mine location (red star) within the province of Quebec, Canada (modified after Kalenchuk et al. 2017).

2 Numerical back analysis

The main objective of the numerical analyses performed in this study was to improve the understanding of overall rock mass behaviour in Zone 2 at the Westwood mine and to better define the factors that contributed to the May 2015 seismicity. To achieve this, global mine-scale models and local drift-scale models were developed. Model calibration utilized a combination of the available seismic data, underground observations, the condition of boreholes, and inspection of core drill after the events. The global model was developed using FLAC3D (V. 5.0 by Itasca Consulting Group 2012) and included all development and stoping geometries in the relevant mining blocks. Drift-scale modelling utilized Phase2 (V.8.0 by RocScience 2015). Fig. 2 provides a summary of material properties and boundary conditions.

Summary of intact material properties

Unit	Density (10^3kg/m^3)	E_i (GPa)	v	Upper Bound			Parallel to Foliations		
				UCS (MPa)	m_i	Tensile Strength (MPa)	UCS (MPa)	m_i	Tensile Strength (MPa)
U3	2.9	81	0.3	154	10	13.3	120	6	21.9
U4	2.83	49	0.2	104	10	10.0	90	7	12.6
U5	2.87	69	0.24	169	13	11.5	13.5	8	18.5

Summary of rock mass classification (GSI)

Unit	GSI
U3	62 ± 8
U4	54 ± 12
U5	52 ± 12

In situ stress tensors (ranges of magnitude and orientation) utilised during numerical model calibration (bold indicates the base case considered to be the most probable according to the available data)

Principal stress	Magnitude	Orientation (trend/plunge)
σ_1	(1.9, **2.5** or 2.8) × σ_3	000°/00°, **035°/00°** or 055°/00°
σ_2	(1.5, **1.7** or 1.9) × σ_3	090°/00°, **125°/00°** or 145°/00°
σ_3	**σ_v**	**000°/90°**

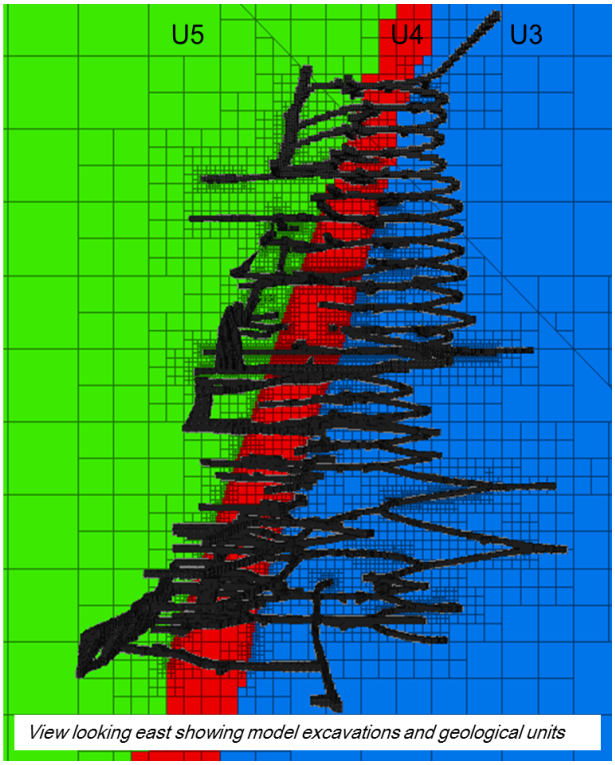

Figure 2. Summary of material propeties and boundary conditions.

The first iteration of numerical simulations focused on the global mine model in order to narrow the range of possible stress tensors and material property combinations. The first iteration of global-scale modelling produced non-unique results. Multiple combinations of boundary conditions and material properties could reproduce the observed ground response. However, these preliminary numerical solutions required either excessively high k-ratios, or un-realistically low material strengths to induce sufficient rock mass yield to drive the pillar failure.

From here, drift-scale numerical simulations were utilized to investigate how progressive, anisotropic rock mass failure around the periphery of excavations may influence inter-level pillar stability. Rib damage is commonly observed at the Westwood mine, and the severity of rib damage varies locally depending on the intensity of rock foliation. Development drives orientated parallel to foliation incur rib damage due to squeezing. This is a progressive mechanism that is well documented in the Val D'Or area (e.g. Mercier-Langevin & Hadjigeorgiou 2011; Potvin & Hadjigeorgiou 2008). Rock mass damage and rib deformations in mine tunnels trending parallel to foliation were contributing to a gradual widening of the effective drift spans (Fig. 3). The wider effective span was influencing pillar performance by decreasing the width to height ratio and, therefore, reducing confinement (σ_3) within the pillars. The influence of progressive rib deterioration at the drift-scale was implemented in the global models by physically adjusting excavation spans. Drifts were widened by 4 m in the north-south direction (each wall offset by 2 m). This geometric reconfiguration results in true widening of EW trending (parallel to foliation strike) drives by 4 m, no widening of NS trending drives, and effective widening of drifts with orientations between EW and NS ranging between 4 to 0 m. This approach to simulation of the effective spans presents an extreme strain softening case as the widened volumes are completely extracted from the models. In reality it would be reasonable to expect that drift ribs would maintain some residual strength and stiffness, these residual parameters are impossible to estimate in the absence of extensive instrumentation data. This calibration of the excavation geometries produced another numerical solution to the back analysis of observed ground reaction; however, in this case, the far field in situ stresses and the assigned constitutive properties were both within more realistic bounds.

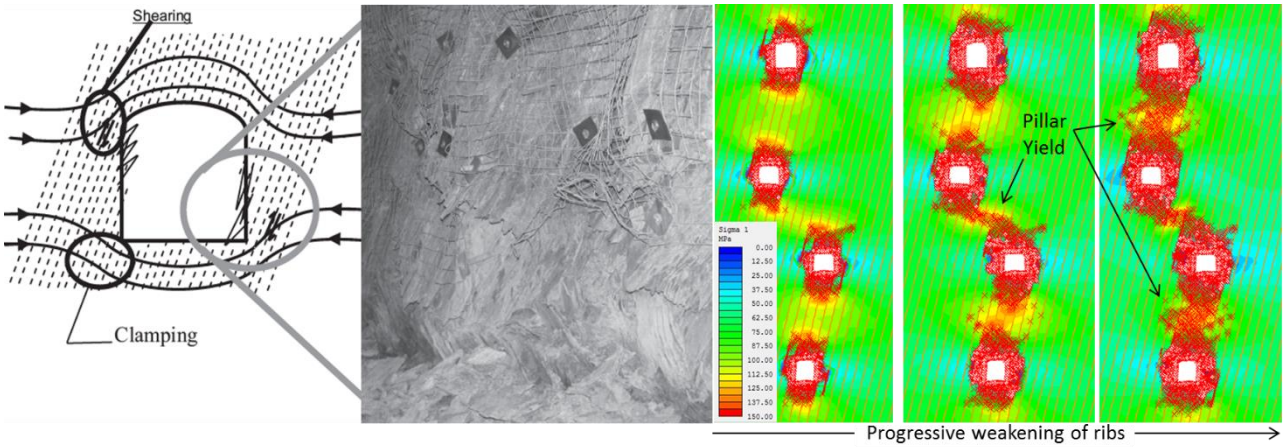

Figure 3. (left) Rib deterioration in strongly foliated ground with high horizontal stress (Potvin & Hadjigeorgiou 2008). (right) Progressive failure of drift ribs contributes to the time depending yield of pillars.

3 Conclusions

The 2015 Westwood mine seismicity is a complex case study where progressive drift-scale rib deterioration was a factor influencing the stability of global-scale mine pillars. Back analysis of observed ground reaction has made it possible to interpret the factors leading up to these pillar bursting events. While multi-scale ground reaction would have been difficult (or impossible) to predict during feasibility and design studies, this back analysis has allowed for the forward simulation of mine plans to formulate risk mitigation through strategic mine planning.

4 Acknowledgement

The author would like to thank Iamgold for permission to present this case study.

5 Reference list

Kalenchuk, K, Mercer, R, Williams, E. 2017. Large-magnitude seismicity at the Westwood mine, Quebec, Canada. *Proc 8th* Int. Conf. on Deep and High Stress Mining. Perth 27–29 March 2017.

Mercier-Langevin, F, Hadjigeorgiou, J. 2011. Towards a better understanding of squeezing potential in hard rock mines, Mining Technology 120, 36–44.

Potvin, Y, Hadjigeorgiou, J. 2008. Ground Support Strategies to Control Large Deformations in Mining Excavations, Journal of the Southern African Institute of Mining and Metallurgy 108, 393–400.

Modeling of hydro-mechanical time-dependent deformation, creep and fracturing of brittle rocks

Tao Xu[1*], Guang-lei Zhou[1], Heinz Konietzky[2] and Chong-feng Chen[1]

[1] Center for Rock Instability and Seismicity Research, Northeastern University, Shenyang 110819, China
[2] Geotechnical Institute, TU Bergakademie Freiberg, Gustav-Zeuner-Str.1, 09596 Freiberg, Germany
[3] State Key Laboratory for Geomechanics and Deep Underground Engineering, China University of Mining and Technology, Xuzhou 221116, China
* xutao@mail.neu.edu.cn

1 Introduction

With the development of deep underground rock engineering, high slope rock engineering, dam base rock engineering and nuclear waste disposition project, the stressed rock mass in most engineering structures in rock is either saturated with water or is subjected to high humidity levels. The problems of the pressure effect including pore water pressure and confining pressure on time-dependent deformation of rock is of great importance in the upper crust. Here we present a constitutive creep model to describe the time-dependent deformation of brittle rocks under different constant pore pressures and confining pressures. First, we formulate the hydro-mechanical coupled time-dependent model and validate the model with experimental data. We then present and discuss the results of the brittle creep simulations. Finally, we discuss the underlying mechanism for the transition to accelerating creep in heterogeneous brittle rocks using the relative roles of the renormalization, the stochastic strength field, the progressive localization, and the transition from tensile to shear events at different stages of damage evolution.

2 Numerical model

When formulating the model in mathematical language, various levels of complexity should be incorporated into each component, with the accuracy and versatility of the model depending on the refinement of the description of each component. For a model used to investigate hydro-mechanical time-dependent deformation of a stressed rock, the coupled effect between the medium deformation and hydraulic components is very important. The model is based on the theory of elastic-damage mechanics and assumes that the damage is elastic and isotropic. The model accounts for material heterogeneity through a stochastic local failure stress field, and local material degradation using an exponential material softening law (Amitrano & Helmstetter 2006). The maximum tensile strain criterion as well as a modified Mohr-Coulomb criterion with a tension cut-off are adopted as two failure thresholds in the model. The tensile strain criterion is preferential since the tensile strength of rock is commonly far below its compressive strength (Jeager et al. 2007). This approach makes it possible to simulate the transition from distributed damage by tensile microcracking to damage where microcracks can interact, coalesce, and ultimately form a shear fracture. The model also describes the temporal and spatial evolution in the medium during the progressive damage process.

3 Modeling results

We apply various axial differential stresses and various constant pore pressures on numerical samples with a geometry of 100 mm × 50 mm to investigate the influence of differential stress and pore pressure on brittle creep. The comparisons between numerical and experimental curves on confined compression and creep tests and the damage and failure processes are respectively shown in Figs. 1–3.

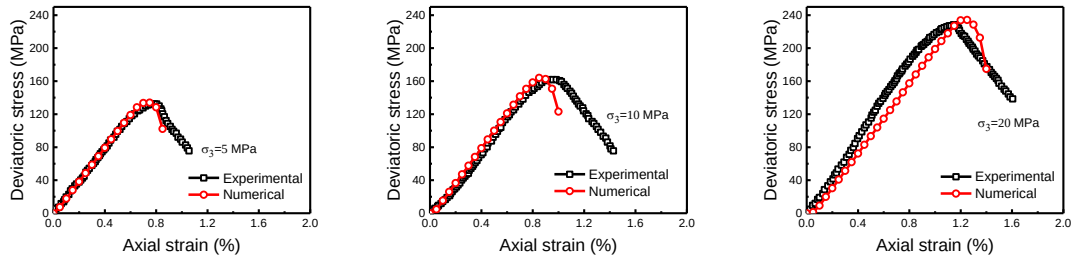

Figure 1. Comparisons between numerical and experimental stress-strain curves of sandstone specimens.

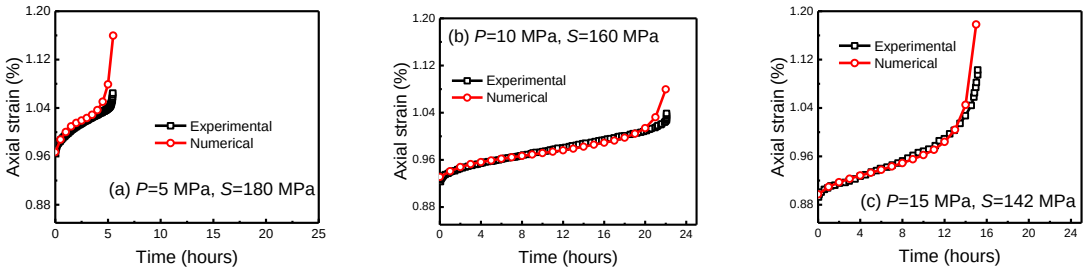

Figure 2. Comparisons between numerical and experimental creep curves at various pore pressures (P) and axial differential stresses (S).

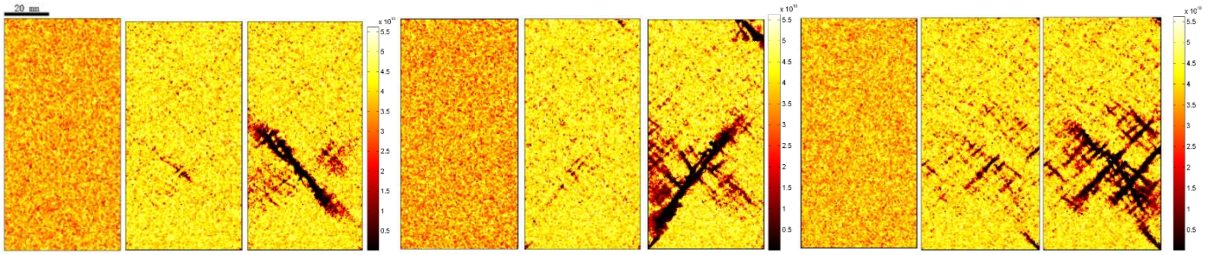

Figure 3. Damage and failure processes of specimens at various differential stress and pore pressures.

4 Conclusions

We presented a numerical model to replicate time-dependent brittle deformation of brittle rock. We simulate conventional brittle creep experiments at various applied axial stresses and various constant pore pressures. The simulation results adequately replicate typical observations of creep tests including tertiary creep. It is observed that the curves of creep strain with time agree well with experimental curves (Yang et al. 2014). More interestingly, we find that the minimum strain rate become smaller and the time-to-failure becomes longer as the applied confining pressure is increased or as the axial stress decreases. We find that the proposed model reproduces the progressive development of fracture processes and the evolution of failure morphology in heterogeneous rocks during creep. Furthermore, the simulations accurately capture the creep damage nature of a classic experimental creep curve. We therefore contend that our time-dependent model is not only able to characterize the time-independent progressive damage up to failure, in particular for samples under uniaxial creep test, but also reveals the time-dependent damage evolution for sandstone under different constant pore pressures and applied axial differential stresses.

5 Reference list

Amitrano, D., Helmstetter, A. 2006. Brittle creep, damage, and time to failure in rocks. J. Geophys. Res. B: Solid Earth, 111(B11): 1–17.

Jeager, J.C., Cook, N.G.W., Zimmerman, R. (Eds.) 2007. Fundamentals of Rock Mechanics. Wiley-Blackwell, Singapore.

Yang, S. Q., Jing, H. W., Cheng, L. 2014. Influences of pore pressure on short-term and creep mechanical behavior of red sandstone. Engineering Geology, 179, 10–23.

Evolution of rock damage zone over different time periods for a horizontal variant of KBS-3 repository design

Johannes Suikkanen[1*], Margareta Lönnqvist[2] and Harald Hökmark[2]

[1] Posiva Oy, Eurajoki, Finland
[2] Clay Tehcnology AB, Lund, Sweden
* Johannes.Suikkanen@Posiva.fi

1 KBS-3 Repository concept

The Swedish and Finnish plan for deep geological disposal of high active spent nuclear fuel is based on the multi-barrier KBS-3 concept. According to the KBS-3 concept, the spent nuclear fuel will be deposited in copper canisters surrounded by compacted bentonite clay at approximately 400–500 m depth in crystalline rock at a selected geological domain. Currently, two design alternatives of the KBS-3 concept exist according to the alignment of the deposited canisters, the vertical KBS-3V variant and the horizontal KBS-3H variant, as illustrated in Fig. 1.

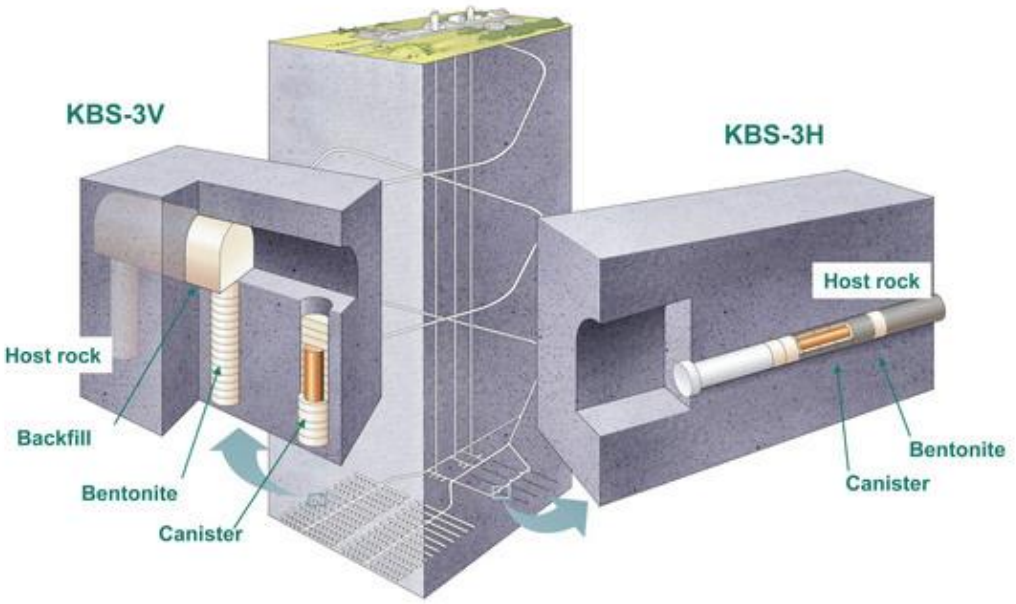

Figure 1. Comparison between vertical and horizontal variants of the KBS-3 deposition concept, figure courtesy of SKB, illustrator: Jan Rojmar.

Posiva Oy is conducting detailed repository site characterization studies at the ONKALO underground research facility, located on the Olkiluoto Island, Western Finland. The site characterization studies are conducted for the purposes of an upcoming safety case, submitted to the reviewing authority as a part of the repository operational license application using the vertical KBS-3V deposition variant as a reference design. However, the horizontal KBS-3H design variant has been kept as an alternative to the vertical KBS-3V case, as the horizontal variant holds the advantage of reducing the need for excavation and subsequent backfilling of deposition tunnels, thus reducing overall costs of the repository closure (Posiva 2014).

2 Drift stability and rock damage zone evolution

The rock mechanics site characterization program of Olkiluoto aims to describe the initial state and properties of the host rock barrier associated with the repository volume. The initial state of the repository acts as a basis for any forward evolution model of the repository system, as it represents

the state of the host rock volume in which the canisters containing the spent nuclear fuel are deposited and sealed into after repository closure. Understanding the initial state and subsequent forward evolution of the repository system is required for demonstrating the operational- and long term safety of the KBS-3 repository design when submitting the operational license application. This paper describes the main outcomes of a rock mechanics evolution study conducted for the horizontal KBS-3H repository design alternative for the Olkiluoto site. For establishing quantitative estimates of the deposition drift stability evolution, the following phases of the repository lifespan were studied and boundary conditions for each phase were derived as the loads, imposed on the repository system and deposition drifts, vary over the whole lifespan.

- The *construction phase* during which the rock transitions from an undisturbed state to the state after excavation of the horizontal deposition drifts. Stress redistribution effects around the openings and drawdown of groundwater pressures. Considered as the *initial state* of the deposition drift.
- The *thermal phase* during which the heat generated by the deposited canisters will increase the temperature of the bedrock and induce thermal stresses. Natural groundwater pressure levels will gradually be restored after the construction, and the bentonite buffer will develop swelling pressure around the deposition drift perimeter.
- The *glacial phase* during which the state of stress will change as a result of the loading and unloading caused by a future ice sheet advancing and retreating over the Olkiluoto site. In addition to the changes in stress, there will also be changes in groundwater pressure.

The issues described in the previous section for each phase of the repository lifespan were addressed using the three-dimensional distinct element code *3DEC*, v. 5.00 (Itasca 2013) and their consequence on drift stability with a two-dimensional boundary element code Fracod^{2D} (Shen et al. 2014). The boundary conditions for the repository models of varying scales during the different phases were derived by linear – elastic modelling with 3DEC, while modelling of detailed deposition drift stability was conducted by coupling the 3DEC boundary conditions with Fracod^{2D}. In particular, the following issues of the drift stability may have influence on the potential migration paths for radionuclides by reducing the transport resistance in the vicinity of the deposited canisters; the extent of the rock damage zone and associated properties of the individual fractures composing the damaged zone, such as fracture aperture.

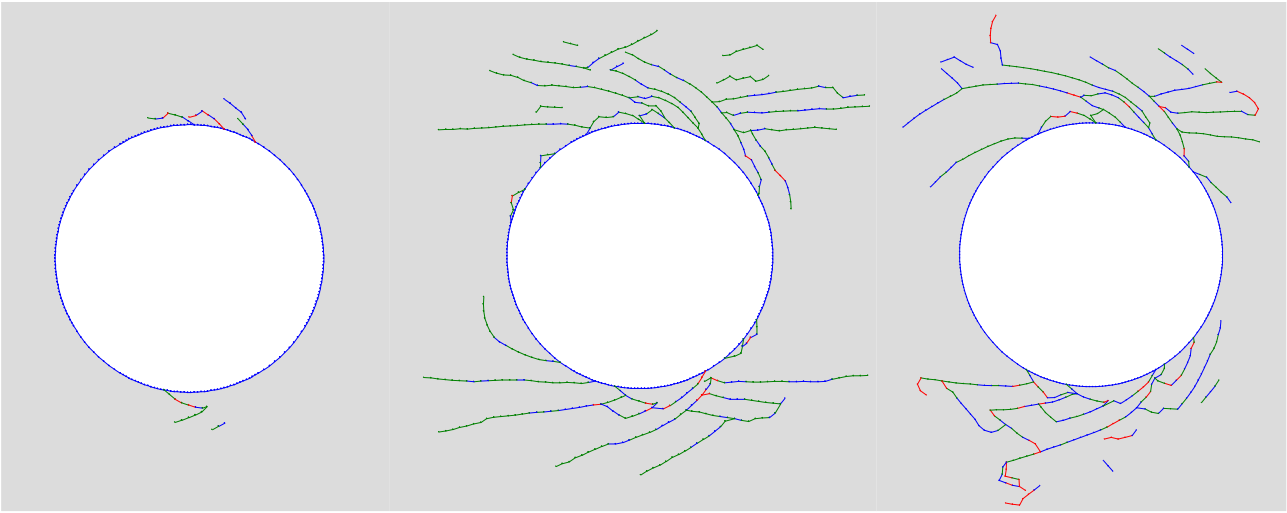

Figure 2. Rock damage zone evolution for a deposition drift around the canister mid-point location during the construction phase (left), thermal phase (centre) and glacial forebulge (right). 5 MPa of bentonite swelling pressure within the drift is implemented starting from the thermal phase (centre). Fractures under tensile conditions are presented in red, fractures that have undergone slipping in green, and fractures that have not exceeded their stability eg. elastic fractures in blue.

The results of the evolution modeling for KBS-3H repository drift stability, with 5 MPa of swelling pressure induced by the bentonite barrier included since the starting of the thermal phase (center),

are presented in Fig. 2. The models of both the thermal phase (center) and glacial forebulge (right) do include the fractures from the previous phases as a starting point eg. glacial model including the fractures from construction and thermal phases. Differences in the fracture patterns of latter phases are present as modelling of progressive rock mass failure through fracture mechanics means is a recursive process, the next result being based on the final result of the previous calculation step. Consequently, the fracture mechanics models do contain inherent randomness and increasing amount of bias when models containing large amounts of calculation steps are being analysed, such as the end glacial scenarios. In order to minimise the inherent bias in the end result, simplifications to the modelling scenarios were being made in a way that the calculation steps could be reduced to a minimum and the models be kept as simple as possible. However, due to the large amount of calculation steps associated with the models of glacial phase, the discretization of boundary stress increments had to be made coarser than in models of previous phases such as the construction- or thermal phases, thus resulting in differing fracture patterns with similar statistics.

From the modeling results, it can be seen that the rock damage zone around the canister location is mainly formed on the floor and roof of the drifts, were the highest tangential stresses prevail. The damage zone around the deposition drift is formed during the thermal phase when horizontal stresses are increased, increasing the stress anisotropy in the vicinity of the drift perimeter, as the canisters emit their excess heat thus causing thermal expansion in the rock mass. The average tangential stress at the drift vicinity reaches its maxima during this phase of the repository lifespan, resulting in reduced aperture on the fractures composing the damage zone around the deposition drift, as illustrated in Fig. 3 showing the aperture data of the damage zone models presented in Fig. 2.

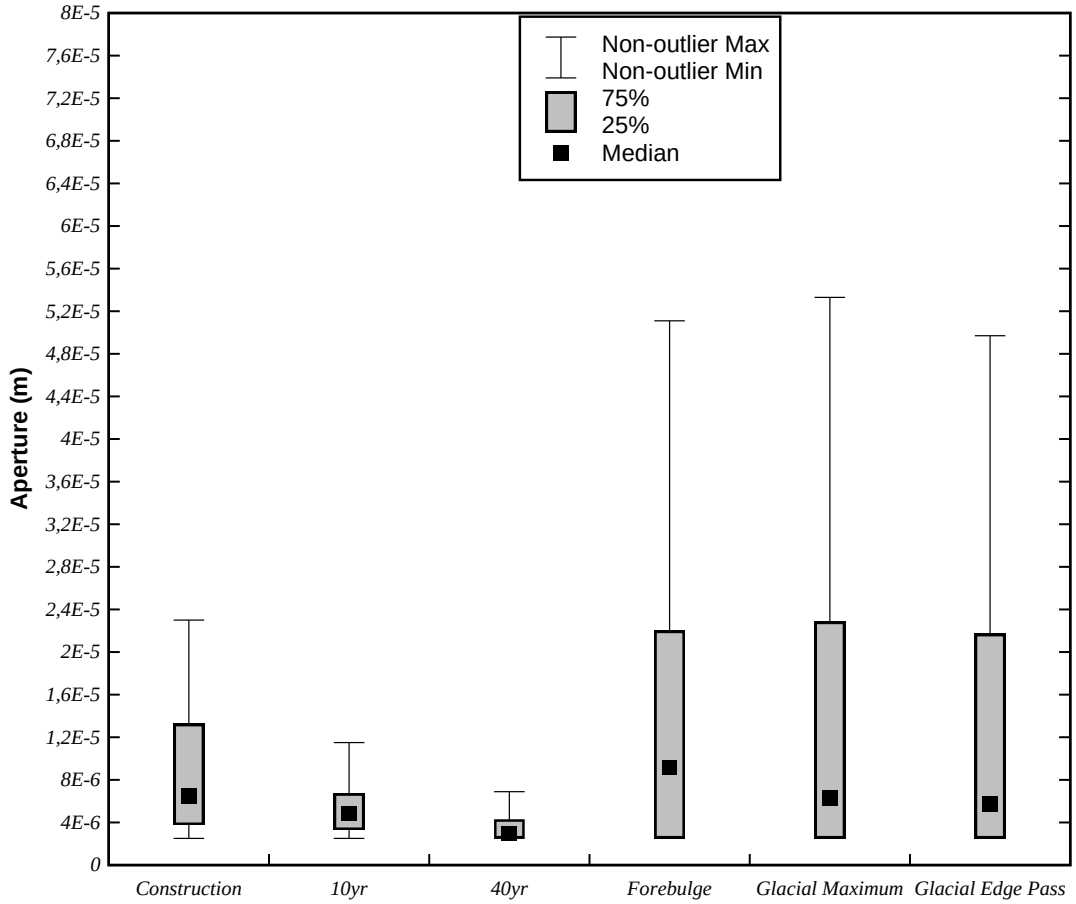

Figure 3. Evolution of rock damage zone aperture for KBS-3H concept deposition drift with 5MPa of swelling pressure having its effect starting from 10 years (10yr) after the start of the thermal period.

During the glacial phase, the state of stress will change as a result of the loading and unloading caused by a future ice sheet advancing and retreating over the Olkiluoto site. The changes in stress are likely to be accompanied by changes in groundwater pressure, with pore pressure level varying in different times of the glacial phase. According to the modelling results presented in this paper, the propagation of the rock damage zone around the deposition drift during the glacial phase around the drift is minor (Suikkanen et al. 2016). However, the deformation of individual fractures associated with the rock damage zone varies with the different phases of the repository lifespan, and the amount of open fractures is increased during the glacial forebulge, and subsequent phases of the glacial cycle, as marked with red elements in Fig. 2 and apertures illustrated in Fig. 3. The increased amount of open fractures during glacial cycle are a result of two distinct processes prevailing at different stages of the glacial cycle. The advancement and retreat of the ice sheet over Olkiluoto site induces stress anisotropy in the vertical plane perpendicular to the deposition drift axis, in comparison to the compressive tangential stress state of the deposition drift during the thermal phase, thus resulting in opening of existing fractures in certain directions while others are closed down. During the time of ice sheet covering the Olkiluoto site all stress components increase in magnitude while excess pore pressure corresponding to 98% of the ice sheet load, considered as an upper limit, is estimated to prevail (Hökmark et al. 2010; Suikkanen et al. 2016). This excess pore pressure decreases the effective normal stress of individual fractures during the glacial maximum resulting in increased aperture while the prevailing rock stress components are increased due to the weight of the overlying ice sheet. The effect of internal drift pressure induced by the swelling of the clay barrier has a pronounced effect with increasing timescale, decreasing the fracture length associated with the deposition drift damage zone and fracture aperture distribution during the glacial phase. However, the effect of swelling pressure is not able to negate the formation of a damage zone around the deposition drift during the thermal phase even with an upper limit of 10 MPa of swelling pressure prevailing within the drift.

3 Reference list

Hökmark H, Lönnqvist M, Fälth B, 2010. THM-issues in repository rock. Thermal, mechanical, thermo-mechanical and hydro-mechanical evolution of the rock at the Forsmark and Laxemar sites. SKB TR-10-23. Stockholm, Sweden: Svensk Kärnbränslehantering AB.

Itasca, 2013. 3DEC – 3-Dimensional Distinct Element Code, User's Guide, v. 5.0. Minneapolis, Minnesota, USA: Itasca Consulting Group Inc.

Posiva Oy. 2014. Description of the KBS-3H Design Variant. Posiva Report 2012-50. Posiva Oy, Eurajoki, Finland.

Shen B, Stephansson O, Rinne M, 2014. Modelling Rock Fracturing Processes: A Fracture Mechanics Approach Using FRACOD. Springer Science & Business Media.

Suikkanen, J, Lönnqvist, M, Hökmark, H. 2016. Analyses of the Stability of a KBS-3H Deposition Drift at the Olkiluoto Site During Excavation, Thermal Loading and Glacial Loading. Posiva Report 2016-16. Posiva Oy, Eurajoki, Finland.

Experimental and numerical simulations via a shear banding model for Mont de La Saxe rockslide

Dattola G.[1*], Alberti S. [1], Crosta G.B. [1] and Wang G. [2]

[1] Department of Earth and Environmental Science – University of Milano-Bicocca
[2] Disaster Prevention Research Institute – Kyoto University
* giuseppe.dattola@unimib.it

1 Introduction

Large rockslides are characterized by complex spatial and temporal evolution, with non-linear displacement trends and significant effects of seasonal or occasional events. Forecasting landslide motion and collapse is a fundamental task for hazard zonation and the design of risk mitigation structures. Consequently, the analysis and modeling of the involved phenomena are very important.

One of the most deeply investigated landslides of the whole Alpine arc is Mont de La Saxe landslide (Fig. 1), located within a deep-seated gravitational slope deformation (DSGSD). This landslide is located at the upper part of the Aosta Valley, NW Italy. The rock slide dimension is of about $8x10^6$ m^3, extends between 1400 and 1870 m a.s.l., over an area of 150'000 m^2 with a horizontal length of about 550, maximum width of 420 m, and average slope gradient of 37°.

The area is subjected to snow fall during the winter (average equivalent rainfall 810 mm ca., data—Mont de La Saxe meteo station at 2,076 m a.s.l.) with a total average precipitation of about 1,470 mm (at the rock slide crown area) and a real evapo-transpiration of about 370 mm.

Aim of this work consists in analyzing this instability by means of an experimental campaign and numerical modelling. The target of this analysis consists in forecasting the landslide displacement and the possible failure.

Figure 1. Photograph of Mont de La Saxe landslide panoramic view

2 Experimental tests

The samples used for experimental tests derived by full core recovery are characterized by a meta-sedimentary sequence. The petrographic characterization have been performed by XRD (X-Ray Diffraction), XRF (X-Ray Refraction) and SEM (Scanning Electron Microscope) with microprobe in addition to laboratory tests on samples from shear zones. Samples from shear zones have different characteristics in terms of thickness of the shear zone, grain size, mineral composition and weathering.

The mechanical characterization of the material has been performed by: standard triaxial tests (Fig. 2) and dynamic-loading ring-shear apparatus (Alberti et al. 2017, submitted). In the drained standard triaxial tests the confining pressure ranges from 600 kPa to over 2,000 kPa. The comparison between the results obtained from the samples in the shear zone and in the near intact zone shows the difference in the mechanical behavior and especially the effects of rock degradation induced by the landslide movement. These experimental data allow the calibration of the material parameters for the successive modelling. Furthermore, the results highlight the mechanism involved in the progressive failure occurring in the shear band. Possible scales effects are not object of the present analysis

The dynamic-loading ring-shear apparatus (DPRI-5, Sassa et al., 1997) has been used to simulate the entire process of failure, from initial static or dynamic loading, by imposing the shear failure, pore-pressure changes, to large-displacement, steady-state shear movement. By means of this apparatus, an experimental simulation of (i) the formation of the shear zone, (ii) the post-failure mobility of high-speed landslides, (iii) the monitoring pore-pressure generation, and (iv) mobilized shear resistance together with shear displacement is carried on.

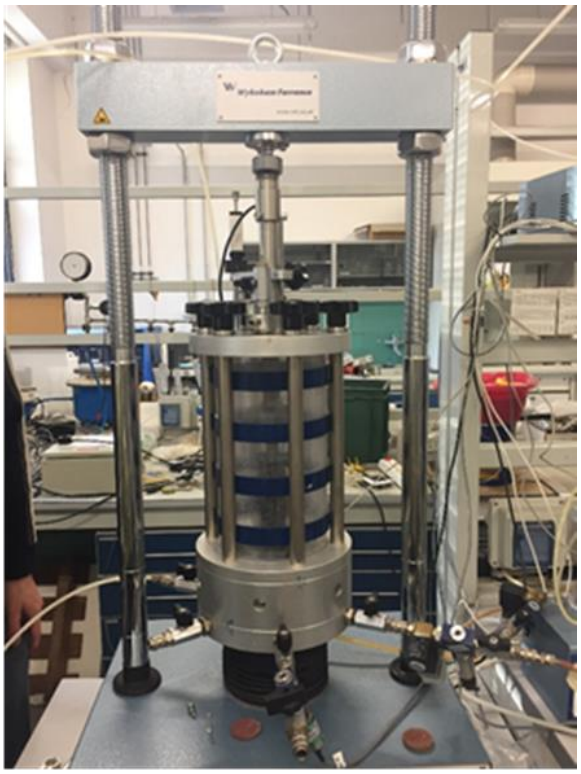

Figure 2. Standard triaxial test apparatus employed for the experimental tests.

3 Modelling and numerical simulations

In order to simulate the mechanical behaviour of the shear band a viscous-plastic model, based on the Perzyna approach, is introduced. By means of this model, the degradation process of the shear

band strength is simulated by introducing a hardening law that takes into account the original and ultimate values of the strength.

The landslide movement is simulated by means of a simplified approach based on a set of interacting blocks sliding on a predefined slip surface (MIB-SA, Crosta et al. 2014; Dattola et al. 2016). This model discretized the landslide mass in a set of independent blocks (Fig. 3a) which are assumed to be rigid bodies. Block motion derives by solving the first momentum equation in which forces considered come from the interaction of blocks and the slip surfaces.

In order to reproduce the sliding motion, the shear band hardening model is introduced in the MIB-SA model. Since the Mont de La Saxe landslide is strongly conditioned by the seasonal trend of the groundwater table (Fig. 3b) , a piezometric surface is reconstructed by the long term in situ measurements using an interpolation tool directly implemented in the numerical code.

A multi-parametric analysis is performed on the most influencing parameters affecting the evolution of the material strength. The simulation shows the evolution of the shear band with time and also its correlation with the water level. Finally, the simulation gives more information about the progressive failure mechanism taking place during the evolution of the rockslide. The numerical simulations gives the evolution of the kinematic variables (displacement, velocity and acceleration) of each block as well as global and local safety factor to provide a basic tool for the prevision of local and/or global instabilities.

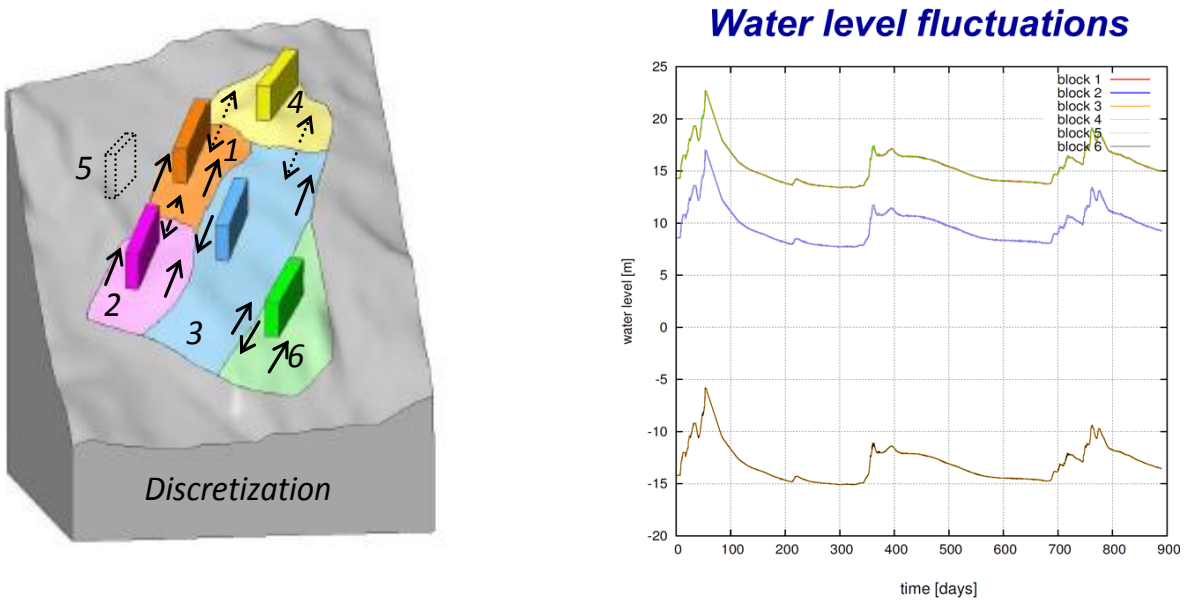

(a) (b)

Figure 3. (a) Landslide Block Discretization in which each colored zone is associated with acorresponding block and the interaction forces between the blocks; (b) evolution of the recorded water level fluctuation.

4 Reference list

Alberti S, Crosta GB, Wang G, Dattola G, Bertolo D 2017. Influence of graphite and serpentine minerals along landslide failure surface. European Geoscience Union conference 2017 (EGU). Submitted.

Crosta, GB, Di Prisco, C, Frattini, P, Frigerio, G, Castellanza, R, Agliardi, F (2014). Chasing a complete understanding of the triggering mechanisms of a large rapidly evolving rockslide. *Landslides*, *11*(5), 747-764.

Dattola G, Crosta GB, Castellanza R, di Prisco C 2016. MIBSA: Multi Interacting Blocks for Slope Analysis. European Geoscience Union conference 2016 (EGU).

Sassa K, Fukuoka H, Wang FW 1997. Mechanism and risk assessment of landslide- triggered-debris flows: lesson from the 1996.12.6 Otari debris flow disaster, Nagano, Japan. In: Cruden DM, Fell R (eds) Landslide risk assessment, proceedings of the international workshop on landslide risk assessment. Honolulu, 19–21 February, pp 347–356.

Beyond debuttressing: Thermo-hydro-mechanical rock slope damage during glacial cycles

Lorenz M. Grämiger[1,2*], Jeffrey R. Moore[1,3], Valentin S. Gischig[1] and Simon Loew[1]

[1] Department of Earth Sciences, ETH Zurich, Switzerland
[2] Dr. von Moos AG, Geological Consulting, Zurich, Switzerland
[3] Department of Geology and Geophysics, University of Utah, USA

* graemiger.lorenz@gmail.com

1 Introduction

Cycles of glaciation drive in-situ stress changes in underlying bedrock as glaciers advance, erode, and retreat, generating damage in adjacent rock slopes and influencing paraglacial slope stability. Glacial debuttressing is frequently implicated as a trigger for paraglacial rock slope failures, despite commonly observed large lag-times between deglaciation and the timing of failure and often without clear mechanical reasoning. Rock slope damage generated during glacial cycles is hypothesized to have a strong role in preparing rock slope failures, however, the mechanics of paraglacial rock slope damage remain poorly characterized.

Glacial cycles mechanically load and unload proximal rock slopes by the changing weight of ice, and in addition produce strongly varying thermal and hydraulic rock-surface boundary conditions tied to the fluctuating glacier (Fig. 1). Bedrock beneath temperate glacier ice maintains near isothermal surface temperatures at ~0 °C. Glacier retreat exposes rock walls to new thermal boundary conditions with strongly varying daily and seasonal cycles, a transition we term *paraglacial thermal shock*. Temperature changes generate thermal strain, inducing thermo-mechanical stresses capable of generating rock mass damage. In addition, high subglacial water pressures near the ice overburden level prevail at the base of temperate glaciers, and affect groundwater conditions in proximal valley flanks. Groundwater recharge by precipitation and snowmelt raises the water table seasonally, which is superposed on changes in hillslope groundwater tied to varying glacial ice elevations. Changing cleft water pressures control effective stresses and the strength of rock mass discontinuities. Together, these thermo-hydro-mechanical stresses act in concert with glacial loading cycles to generate rock slope damage, preparing slopes for future failure.

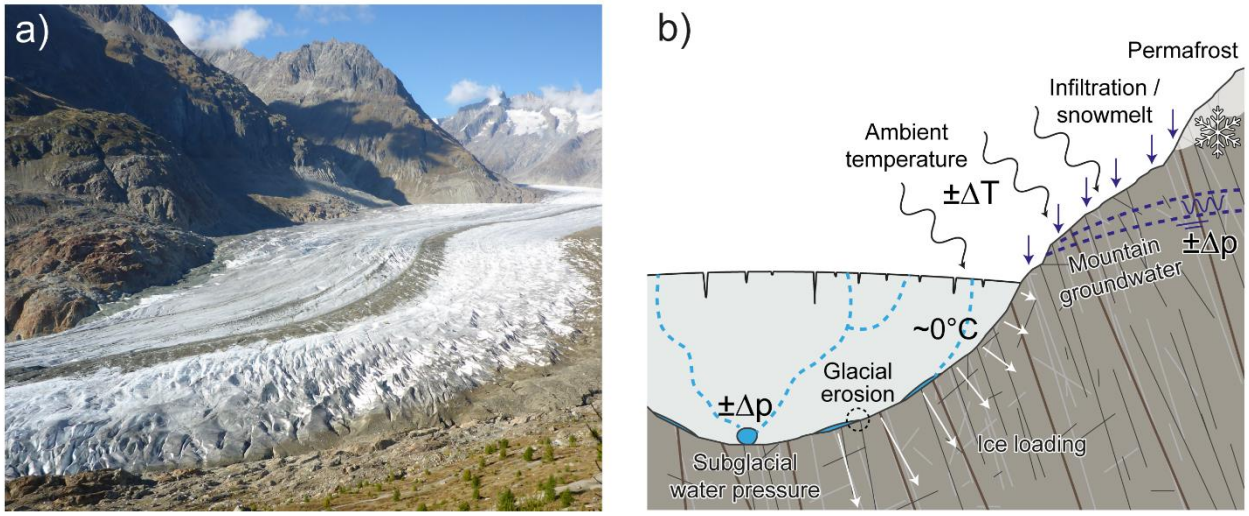

Figure 1. a) The paraglacial environment in the high-alpine region of the Great Aletsch Glacier in Switzerland. b) Conceptual profile of changing paraglacial (i.e., thermal, hydraulic, and mechnical) boundary conditions affecting adjacent rock slopes. (Grämiger 2016).

2 Numerical study of T-H-M rock slope damage and displacement

We study thermo-hydro-mechanical induced stresses and resulting rock slope damage during repeat glacial cycles in the valley of the Great Aletsch Glacier in Switzerland. Following Lateglacial deglaciation, the surrounding valley rock slopes in the Aletsch region experienced several minor glacier cycles during the Holocene. The foliated gneissic rock mass of the Aletsch valley contains several large rock slope instabilities with a concentration around the retreating, present-day glacier tongue. Surface exposure dating of the Driest instability head scarp reveals a Mid-Holocene initialization age (7.4 ± 0.7 ky), matching post-Egesen / pre-Little Ice Age relative ages for the majority of other rock instabilities in the Aletsch Valley. To investigate progressive rock slope damage induced during glacier cycles, we used detailed, conceptual numerical models closely based on our Aletsch Valley study area (Fig. 2). Modeled glacier scenarios represent mapped ice fluctuations at Aletsch, while rock mass strength parameters applied in our models are based on local rock mass characterization. Ground surface temperature measurements, monitoring of subglacial water pressures in ice boreholes, regional spring-line mapping, and monitoring of rock slope deformation at Aletsch each contribute to parameterizing and validating our thermal and hydraulic model boundary conditions.

Our simulations reveal that purely mechanical loading and unloading of rock slopes by ice during glacial cycles generates relatively limited new damage. This result supports our view that glaciers make a poor buttress for adjacent slopes due to the ductile behavior of ice over long time scales. However, ice fluctuations in our models do increase the criticality of fractures in adjacent slopes (bringing them closer to the failure envelope), which may in turn increase the efficacy of additional fatigue processes. On the other hand, bedrock erosion during glaciation (i.e., rock debuttressing) promotes significant new rock slope damage during first deglaciation. The amount of initial damage, inherited from pre-glacial, ice-free topographic and in-situ stress conditions, strongly controls the susceptibility of the slope to new damage from ice loading. The slope response during glacial cycles is path-dependent and varies in damage kinematics: glacier advance in our models enhances toppling failure while glacial retreat promotes sliding. Weaker rock slopes show increased sensitivity to glacial loading cycles, accumulating greater damage and displacements, which in some cases lead to full development of an instability.

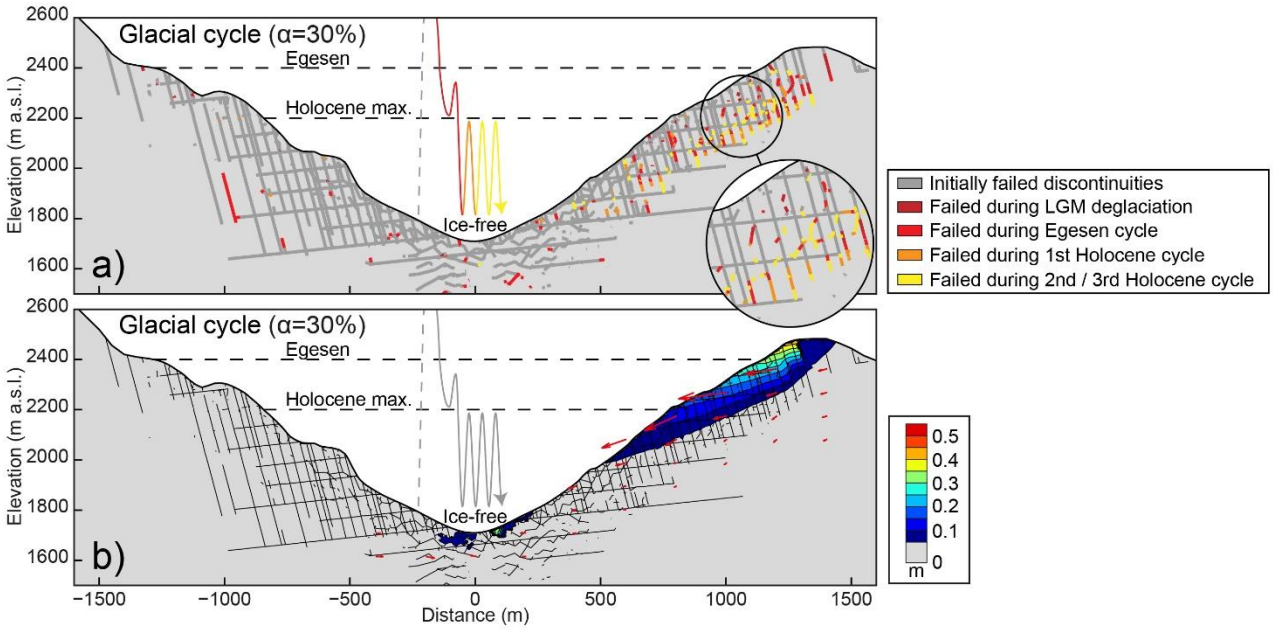

Figure 2. Weakened rock slope affected by repeat purely mechanical glacial loading cycles: a) Spatiotemporal damage distribution as failed discontinuities for a complete glacial cycle (ice-free initialization until end of third Holocene cycle). b) Maximum slope displacement and displacement vectors after a complete glacial cycle with toppling-mode kinematics. (modified from Grämiger et al. 2017).

Changing thermal boundary conditions during glacier retreat and advance in our models affects the temperature regime in the adjacent rock slopes. Thermal strain from long-term temperature changes induces stresses at depths exceeding 100 m, generating significantly more rock slope damage than predicted for purely mechanical loading cycles. Thermal expansion of the rock mass due to warming after glacier retreat causes increased stresses propagating fractures, while cooling during glacier advance results in contraction, reducing joint normal stresses and promoting toppling. First time exposure to seasonal temperature cycles during deglaciation induces a strong but shallow damage front that follows the retreating ice margin. Glacial loading cycles in parallel with thermal stresses (i.e., thermo-mechanical fatigue) are capable of generating significant rock slope damage.

We extend our models by accounting for changing groundwater conditions in proximal valley rock slopes tied to high subglacial water pressures. Glacier loading cycles in parallel with long-term mountain water table variations generate substantial fracture propagation. Major damage occurs during initial ice occupation and first glacier retreat, while subsequent readvances result in minor damage. Superposition of annual groundwater cycles (i.e., hydro-mechanical fatigue) strongly increases rock slope damage during glacial loading cycles, destabilizing the toppling-mode valley flank in our models. The kinematics and dimensions of the predicted instability closely resemble observed characteristics of major landslides in the field at Aletsch. Our results extend simplified assumptions of glacial debuttressing, demonstrating in detail how thermo-hydro-mechanical stresses acting in concert with glacier cycles drive progressive rock mass failure preparing future paraglacial slope instabilities.

3 Reference list

Grämiger, L. M., 2016. Beyond debuttressing: Thermo-hydro-mechanical rock slope damage during glacial cycles. Ph.D. thesis, ETH Zurich.

Grämiger, L. M., J. R. Moore, V. S. Gischig, S. Ivy-Ochs, and S. Loew 2017. Beyond debuttressing: Mechanics of paraglacial rock slope damage during repeat glacial cycles, Journal of Geophysical Research: Earth Surface 122. doi:10.1002/2016JF003967.

Progressive failure, rock mass fatigue and early warning applied to deep-seated rock slope failures

Erik Eberhardt[1*], Doug Stead[2] and Simon Loew[3]

[1] Geological Engineering/EOAS, University of British Columbia, Vancouver, Canada
[2] Department of Earth Sciences, Simon Fraser University, Burnaby, Canada
[3] Department of Earth Sciences, ETH Zurich, Switzerland
* erik@eoas.ubc.ca

1 Progressive failure of rock slopes

The concept of strength degradation and progressive failure represents an important advancement in our understanding of deep-seated brittle rock slope failure. In conventional stability analyses, the strength properties of the rock mass or along a rupture surface on which sliding can occur are assumed to be constant over time. Failure is then explained through the influence of a triggering event, for example a heavy rainfall, which causes disequilibrium between the resisting and driving forces relative to the slope's constant strength. However, this does not properly explain the temporal nature of deep-seated rock slope failures. When a failure does occur, the triggering event rarely stands out as being exceptional, especially when compared to those that had occurred in the past. This suggests that the rock slope must be experiencing some form of strength degradation over time, driving the slope towards an unstable state (Eberhardt et al. 2004).

Strength degradation in these cases has been linked with the progressive failure of intact rock bridges and/or degradation of asperities along a sliding surface. Key studies by Terzaghi (1962), Robertson (1970), Einstein et al. (1983), Eberhardt et al. (2004) and Stead & Wolter (2015) demonstrate that the persistence of natural joints contributing to rock slope failure is generally limited, requiring intact rock bridges to fail to allow mobilization of the rockslide body. This may be associated with the development of a rupture surface and "rock slope collapse", which Hungr et al. (2014) define as sliding occurring on an irregular rupture surface consisting of randomly oriented joints and failed intact rock bridges (e.g., Fig. 1, left). It may also be associated with the development of internal shearing within the slide mass (Martin & Kaiser, 1984), for example in the case of "compound slides". Hungr et al. (2014) define compound slides, as cases involving a well-developed basal sliding surface comprised of multiple planes of uneven curvature such that sliding is kinematically possible only if accompanied by significant internal distortion and shearing of the moving mass (e.g., Fig. 1, right).

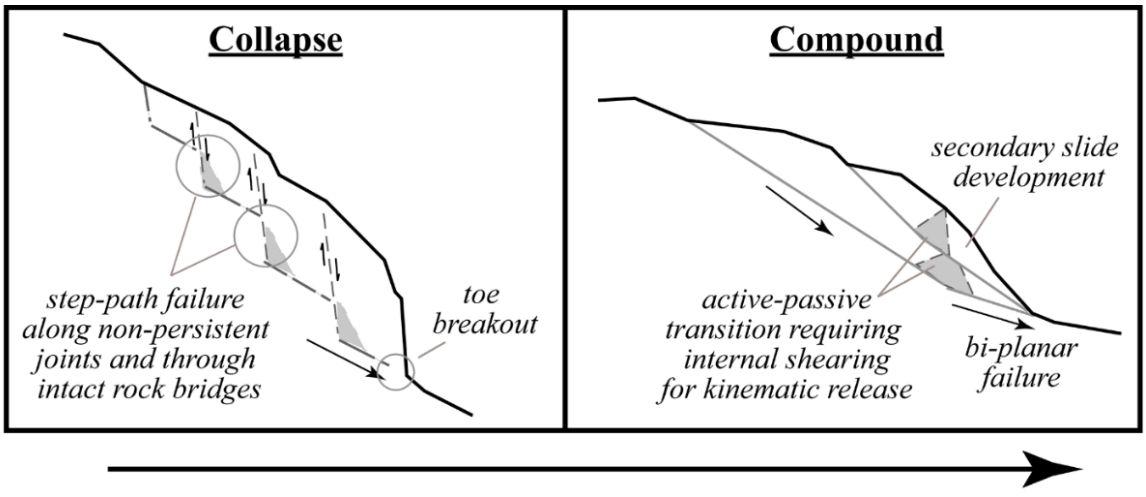

Figure 1. Influence of rock bridge failure and internal shearing on rock slope failure mechanisms.

2 Intermittent slope behaviour and early warning monitoring

Downslope movements arising from deep-seated rock slope instabilities are often episodic, correlating with seasonal precipitation patterns and groundwater recharge. Increased pore pressures reduce the effective stresses along fractures promoting slip, which in turn may cause the slip and dilation of adjacent fractures and/or the rupture of intact rock bridges. Over time, this repeated pattern gradually weakens the rock slope, thus contributing to fatigue and progressive failure (Preisig et al. 2016). In response, rock slopes enter into a pattern of acceleration and deceleration phases. Occasionally these acceleration phases result in episodes of extreme slope movement that are not necessarily triggered by precipitation events of extraordinary amplitude. This introduces significant uncertainty in early warning monitoring; acceleration events may either be an early warning of impending failure, or a false alarm related to localized movements that eventually lock up and subside as the damage state in the slope has not degraded enough to facilitate kinematic release and catastrophic failure.

The suggestion that deformation rates and acceleration events depend on the slope's damage state (governed by its geology) has practical implications for the interpretation of monitoring data. The relationship between deformation rates and driving mechanisms, such as seasonal groundwater fluctuations, can be used to calibrate numerical models and establish the degree of damage and criticality present in the slope. The modeling of seasonal variations further enables reference to be made to time in calculations that are otherwise limited to stress-strain behavior (Fig. 2). This provides a means to assess displacement rate thresholds at which behavior change may occur for a given failure mode, which in turn can be used to establish and constrain early warning alarm thresholds.

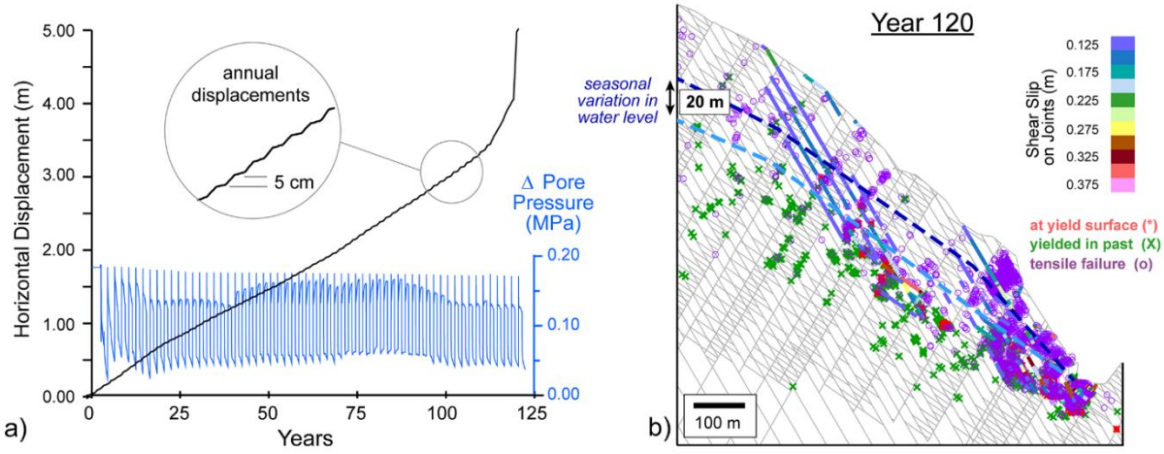

Figure 2. Distinct-element modeling of hydromechanical fatigue, showing: a) cyclic pore pressure input and corresponding slope displacement response with time, and b) slope damage state leading to toe breakout and catastrophic failure.

3 Reference list

Eberhardt, E, Stead, D, Coggan, JS. 2004. Numerical analysis of initiation and progressive failure in natural rock slopes – the 1991 Randa rockslide. International Journal of Rock Mechanics and Mining Sciences 41, 69-87.

Einstein, HH, Veneziano, D, Baecher, GB, O'Reilly, KJ. 1983. The effect of discontinuity persistence on rock slope stability. International Journal of Rock Mechanics and Mining Sciences & Geomechanical Abstracts 20, 227-236.

Hungr, O, Leroueil, S, Picarelli, L. 2014. The Varnes classification of landslide types, an update. Landslides 11, 167-194.

Martin, CD, Kaiser, PK. 1984. Analysis of rock slope with internal dilation. Canadian Geotechnical Journal 21, 605-620.

Preisig, G, Eberhardt, E, Smithyman, M, Preh, A, Bonzanigo, L. (2016). Hydromechanical rock mass fatigue in deep-seated landslides accompanying seasonal variations in pore pressures. Rock Mechanics & Rock Engineering 49, 2333-2351.

Robertson, AM. 1970. The interpretation of geological factors for use in slope theory. In Vanrensburg (ed.), Planning Open Pit Mines, Proceedings, Johannesburg. Cape Town: A.A. Balkema, pp. 55-71.

Stead, D, Wolter, A 2015. A critical review of rock slope failure mechanisms: The importance of structural geology. Journal of Structural Geology 74, 1-23.

Terzaghi, K. 1962. Stability of steep slopes on hard unweathered rock. Géotechnique 12, 251-270.

A Maxwell-Elasto-Brittle rheology for the small and large deformations of geomaterials

Véronique Dansereau[1], Jérôme Weiss[1], Jean-Luc Got[2] and Pierre Saramito[3]

[1] Institut des Sciences de la Terre, CNRS UMR 5275, Université de Grenoble, Grenoble, France*
[2] Institut des Sciences de la Terre, CNRS UMR 5275, Université de Savoie, Le Bourget-du-Lac FRANCE
[3] Laboratoire Jean Kuntzmann, CNRS UMR 5224, Université de Grenoble, Grenoble, France
* veronique.dansereau@univ-grenoble-alpes.fr

1 The small and large deformations of geomaterials

From the continuum mechanics point of view, a number of geomaterials are both (1) damageable elastic solids in which highly localized features emerge as a result of failure and (2) materials experiencing high, permanent strains that dissipate stresses. In this sense, modelling their deformation lies between a solid mechanics (small deformations) and a fluid dynamics (large deformations) problem.

One important example is the Earth's crust, in which brittle fracturing and Coulomb stress redistribution are known to take place and for which scaling properties have been recognized for years (Kagan & Knopoff 1980; Turcotte 1992 and others). Along active faults, co-seismic fracturing activates aseismic creep, leading to deformations that can be larger than those associated with the fracturing itself (Cakir et al. 2012) and to slip rates that decrease progressively over years to decades due to various healing processes (Gratier et al. 2014). Creep relaxes a significant amount of elastic strain, retarding stress accumulation along some portions of faults and concentrating stresses on other locked portions. Hence this dissipative process should be included in earthquakes models (Cakir et al. 2012; Gratier et al. 2014). Another example is sea ice, which deforms rapidly under the action of the wind and ocean drags, in the brittle regime, and for which scaling properties have also been recently recognized (Marsan et al. 2004 and many others). In this case, much larger deformations occur once faults, or ice “leads” (see Fig. 1a, *A*), are formed and divide the ice cover into ice plates called “floes” (Fig. 1a, *B*), as these plates move relative to each other with much reduced mechanical resistance. In sea ice models, these large deformations must be accounted for as they set the overall drift and long-term evolution of the ice pack.

In such contexts, the challenge of the continuum modelling approach lies in the representation of the discontinuities that arise within a material due to fracturing processes using continuous variables and grid-cell averaged quantities. On the numerical point of view, another challenge arises as the methods employed must allow resolving the extreme gradients associated with these discontinuities while limiting the diffusivity associated with advective processes. Here, we present a simple continuum mechanical framework called Maxwell-Elasto-Brittle (Maxwell-EB), built in the view of allowing a transition between the small deformations associated with the fracturing and the larger, permanent, post-fracture deformations, while having the capability of damage mechanics models to reproduce the observed space and time scaling properties of the deformation of brittle geomaterials. The theoretical and numerical development of this new rheological model will be discussed of in two different geophysical contexts: (1) modelling the drift and deformation of Arctic sea ice at regional scales and (2) representing the pre-eruption deformation of a volcanic edifice.

2 The Maxwell-Elasto-Brittle model

The rheological framework combines the concepts of elastic memory, progressive damage mechanics and viscous-like relaxation of stresses (Dansereau et al. 2016). The constitutive law takes the form of the Maxwell viscoelastic model, i.e. :

$$\frac{1}{E}\frac{D\sigma}{Dt} + \frac{1}{\eta}\sigma = K : \dot{\varepsilon} \quad (1)$$

with E, the elastic modulus, η, the viscosity, σ, the stress tensor and $\dot{\varepsilon}$, the rate of strain tensor, and is applied to compressible, elastic solids (hence the dimensionless elastic stiffness tensor, K, defined in terms of the Poisson's ratio, $0 \leq \nu < 0.5$). An important distinction with respect to the original Maxwell model is that the viscosity, η, associated with the stress dissipation term is not the bulk viscosity of the simulated material, but rather an "apparent" viscosity (Lyakovsky et al. 1997; Frederiksen & Braun 2001 and others) that represents its flow resistance averaged over the model grid cell. Like the elastic modulus, E, this viscosity is allowed to evolve both in space and time according to the local level of damage of the material, which represents its degree of fracturation/fragmentation. The ratio of the apparent viscosity and elastic modulus, $\lambda = \eta/E$, has the dimension of a time, and sets the rate of dissipation of the stress through permanent deformations.

Based on previous isotropic progressive damage models (eg., Amitrano et al. 1999 and others), the level of damage is characterized by a scalar variable,d. Damage increases locally when the state of stress becomes overcritical with respect to a Mohr-Coulomb failure criterion and evolves at a rate related to the speed of propagation of elastic waves in the material. To account for various healing processes (refreezing within ice leads, sintering, magma solidification, ...), the level of damage is also allowed to decrease, thereby counterbalancing the effects of damaging over much larger time scales. The coupling between both $E$and $\eta$and $d$is such that over undamaged areas, the mechanical strength of the material (i.e., its elastic modulus) is maximal and its apparent viscosity infinitely large. In this limit, the mechanical response is strictly elastic and the resulting small and highly localized deformations are associated with fracturing processes. Conversely, over highly fragmented areas, all three mechanical parameters (E, $\eta$and λ) decrease, which allows the dissipation of part of the stress into permanent and potentially large deformations. The exact form of the functional dependence of these parameters on the level of damage depends on the nature of the simulated material/process and can be constrained through sensitivity analyses and comparisons to various types of observations. Additionally, the apparent viscosity can be allowed to depend on other properties, such as density (or concentration), as in granular materials (Aranson & Tsimring 2006), or temperature (e.g., Frederiksen & Braun 2001).

The model is developed within the C++ environment RHEOLEF (Saramito 2013a). The numerics is based on finite elements and variational methods. In the case of large deformations, the equations of motion are cast in the Eulerian frame and discontinuous Galerkin methods are used to handle advective processes (Saramito 2013b), as well as rotational and deformational terms that arise the objective derivative of the stress tensor in eqn. (1).

Sensitivity analyses performed in the context of a very simple uniaxial compression experiment with an idealized domain geometry and homogeneous forcing conditions have shown that the Maxwell-EB model, with few independent variables, can represent a large range of mechanical behaviours (Dansereau et al. 2016; Weiss & Dansereau 2016). When varying the one model parameter setting the rate of viscous dissipation of the stress as a function of the increasing level of damage of the material, the model can simulate either a regular, predictable stick-slip with a single damaging frequency corresponding to the prescribed rate of healing or a marginally stable, unpredictable creep-like deformation with temporal correlations in the damaging activity at all time scales below the material's healing time. Over a range of values of this parameter, the model reproduces both the persistence of creeping faults/leads and the activation of new faults/leads with different shapes and orientations. The extreme localization of the deformation in both space and time and the associated scaling properties are represented. Although the rheological framework is isotropic at the element scale, the anisotropy of the elastic interaction kernel is sufficient to generate anisotropy up to very large space scales, through successive elastic interactions between damaged model elements.

3 Geophysical applications

3.1 Sea ice

A first implementation of the Maxwell-EB model on geophysical scales is made in the context of representing the dynamical and mechanical behaviour of sea ice drifting through Nares Strait, a channel of the Canadian Arctic Archipelago (see Fig. 1a). In this case, the ice cover is assimilated as a thin (two-dimensional), compressible plate and plane stresses are assumed. Nares Strait, as other narrow outflow passages of the Arctic, is known for the presence of *ice bridges;* concave arch-like structures across constriction points that remain stable for several months, thereby stopping the flow of ice through the channel, and that are mechanically similar to the concave stress-free surfaces forming in cohesive granular materials (wet sand, soil, grain in a silo, etc). We will discuss the main aspects of these benchmark simulations in terms of the simulated flow and ice coverage conditions as well as the stability and diffusivity of the numerical scheme. In particular, we will demonstrate the capability of the model to represent (1) the strong localization of the ice deformation, (2) the formation of stable ice bridges and self-obstruction to flow and (3) the extreme gradients in ice velocity, thickness and coverage associated with the presence of the ice bridge.

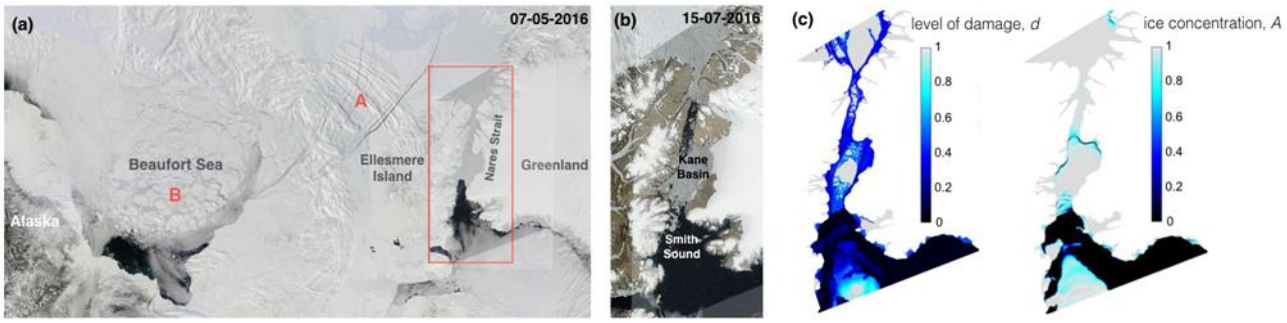

Figure 1. (a) Moderate Resolution Imaging Spectroradiometer (MODIS, NASA/GSFC MODIS Rapid Response at http://rapidfire.sci.gsfc.nasa.gov/imagery/) reflectance image showing part of the western Arctic Ocean on May 7, 2016, with (A) an area where the ice concentration is high and some ice leads are visible (B) an area where the ice cover is highly fractured and divided into ice floes and the ice concentration is low. A stable ice bridge is present in Nares Strait (red rectangle) between Kane Basin and Smith Sound. The grey shading shows the domain coverage of the model simulations. (b) MODIS image of Nares Strait after the break up of this ice bridge. (c) Level of damage (defined here such that $d = 1$ for an undamaged and $d = 0$ for a "completely" damaged ice cover) and ice concentration (ice-covered surface per unit area) in Nares Strait simulated with the Maxwell-EB model.

3.2 Volcanoes

Before a volcanic eruption, the pressurization of the volcanic edifice by a magma reservoir induces earthquakes and damage in the edifice; damage lowers the strength of the edifice and decreases its elastic properties. Inelastic deformations cumulate and lead to rupture and eruption. These deformations translate into measurable surface displacements. We will discuss how the Maxwell-EB model is used to model the pre-eruptive deformation of a volcanic edifice and how available seismicity records and time series of surface displacements measured via satellites (GPS, InSAR) could be used jointly to constrain the model (e.g., Carrier et al. 2015, Got et al. 2017), in particular, the implemented functional dependence of the mechanical parameters (E, η and λ) on the level of damage. Here, preliminary plane-strain Maxwell-EB modelling of the deformation of a magma reservoir and volcanic edifice is presented (see Fig. 2a). The model represents the propagation of damage towards the surface and the progressive localization of the deformation along faults under the pressurization of the magma reservoir (Fig. 2b). This model allows a complete spatio-temporal representation of the rupture process.

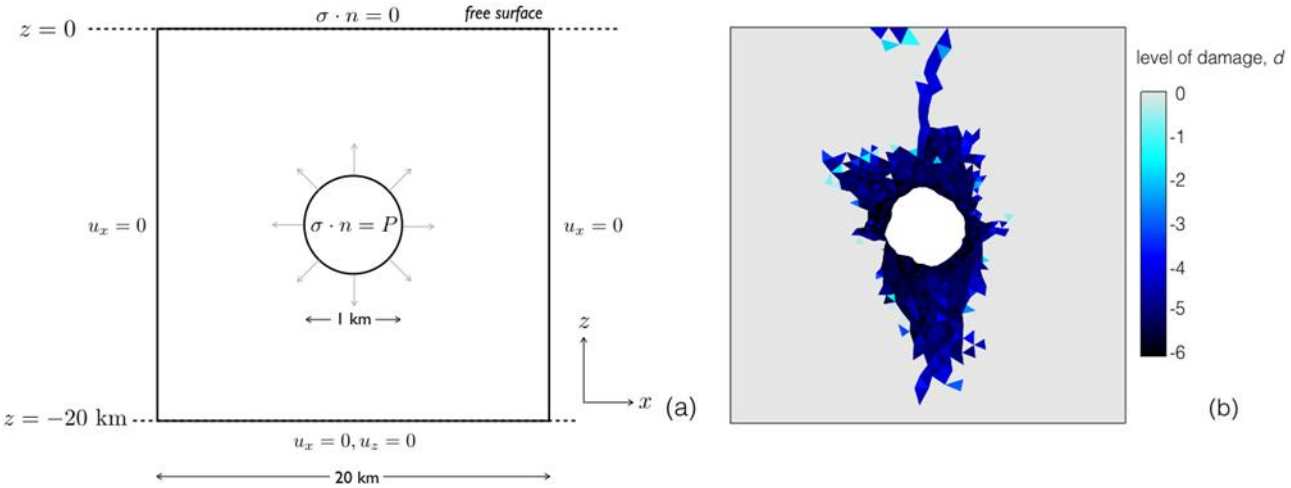

Figure 2. (a) Domain and boundary conditions used in the idealized, plain strain volcano edifice simulations, representing a circular magma reservoir (not to scale) located 10 km below the surface and under homogeneous (outward) pressurization. (b) Simulated deformation and level of damage of the magma reservoir and volcanic edifice (a logarithmic scale is used for the level of damage).

4 Reference list

Amitrano, D., Grasso, J.-R. and Hantz, D. 1999. From diffuse to localised damage through elastic interaction. Geophysical Research Letters, 26, 2109–2112.

Aranson, I. S. and Tsimring, L. S. 2006. Patterns and collective behavior in granular media: Theoretical concepts. Reviews of Modern Physics, 78, 641–692.

Cakir, Z., Ergintav, S., Ozener, H., Dogan, U., Akoglu, A. M., Meghraoui, M. and Reilinger, R. 2012. Onset of aseismic creep on major strike-slip faults. Geology, 40(12), 1115–1118.

Carrier, A., Got, J.-L., Peltier, A., Ferrazzini, V., Staudacher, T., Kowalski, P. and Boissier, P. 2015. A damage model for volcanic edifices: Implications for edifice strength, magma pressure, and eruptive processes, Journal of Geophysical Research. Solid Earth, 120, 567–583.

Dansereau, V., Weiss, J., Saramito, P., and Lattes, P.: A Maxwell elasto-brittle rheology for sea ice modelling, The Cryosphere, 10, 1339– 1359.

Dansereau, V., Weiss, J., Saramito, P., Lattes, P. and Coche, E. Ice bridges and ridges in the Maxwell-EB sea ice rheology, The Cryosphere Discussions, doi:10.5194/tc-2016-276.

Frederiksen, S., and Braun, J. 2001. Numerical modelling of strain localisation during extension of the continental lithosphere. Earth and Planetary Science Letters, 188, 241–251.

Lyakhovsky, V., Ben-Zion, Y. and Agnon, A. 1997. Distributed damage, faulting and friction. Journal of Geophysical Research, 102(B12), 27,635–27,649.

Marsan, D., Stern, H., Lindsay, R. and Weiss, J. 2004. Scale dependance and localization of the deformation of Arctic sea ice. Physical Review Letters, 93(17), 178501.

Kagan, Y. Y., and Knopoff, L. 1980. Spatial distribution of earthquakes: the two-point correlation function. Geophysical Journal International, 62(2), 303–320 .

Got, J.-L., Carrier, A., Marsan, D., Jouanne, F., Vogfjörd, K., Villemin, T. 2017. An analysis of the non-linear magma-edifice coupling at Grimsvötn volcano (Iceland), Journal of Geophysical Research Solid Earth, 122, doi:10.1002/2016JB012905.

Gratier, J. P., Renard, F. and Vial, B. 2014. Postseismic pressure solution creep: Evidence and time-dependent change from dynamic indenting experiments. Journal of Geophysical Research: Solid Earth, 119(4), 2764– 2779.

Saramito, P. 2015. Efficient advanced scientific computing with Rheolef, CNRS-CCSD ed.

Saramito, P. 2013. Efficient C++ finite element computing with Rheolef: vol. 2. discontinuous Galerkin methods, CNRS-CCSD ed.

Turcotte, D. L. 1992. Fractals and Chaos in geology and geophysics. Cambridge University Press, New York, NY, USA.

Weiss J. and Dansereau, V. 2017. Linking scales in sea ice mechanics. Phil. Trans. R. Soc. A, 375, 20150352.

Long-term strength of crystalline rocks

Branko Damjanac[1*]

[1] Itasca Consulting Group, Inc., Minneapolis, USA
* branko@itascacg.com

1 Introduction

Determination of the mechanical response of rock in-situ to applied loads is a central challenge of rock mechanics. This response is controlled predominantly by two scale factors: size and time. The effect of time on rock deformability and strength is a topic of considerable interest in rock mechanics (Einstein & Meyer, 1999). It is of special importance to the geological isolation of highly radioactive nuclear waste, as it is necessary to establish that the rock can isolate the waste from the biosphere for a time period of the order of a million years. This, in turn, implies an understanding of how rock deformability and strength will change over such a period. All materials will creep when subjected to the appropriate long-term loading conditions. At a nuclear waste repository in Precambrian crystalline rock at depths of 400 m to 700 m, loading conditions will be compressive and temperatures less than 100°C. Hence, an important question related to repository design is: “Will the strength decline essentially to zero after such extended periods, or does the rock have a non-zero ultimate strength or ‘threshold’ that can be considered time-independent, for the time-scale of interest?”

2 Time-dependent weakening of crystalline rock

Specimens of crystalline rock subject to creep tests — i.e., sustained constant loading that is below the instantaneous compressive strength — are found to collapse after a period of time. Fig. 1 illustrates a typical series of results obtained, in this case, on cylindrical specimens of Lac du Bonnet (Canada) granite loaded in compression at different constant loads, expressed as a proportion of the “instantaneous” strength. Potyondy (2007) refers to this proportion as the “driving stress ratio.” The majority of the tests were for unconfined loading, but some confined loading results are included.

It is seen in Fig. 1 that the individual tests all were carried out at driving stress ratios greater than 0.6 and for periods of less than two weeks. Clearly, time constraints do not allow laboratory tests to be carried out to obtain data for low stress ratios, so most estimates of the rock strength for extended loading times (of the order of tens to one million years) are obtained by extrapolation from the short-term data. Two such extrapolations are shown:

- a linear extrapolation (black line), which predicts that the rock eventually will reach zero strength, or collapse “under its own weight” in about one million years; and
- a non-linear extrapolation, indicating that the rock has a finite threshold strength that can be sustained for an indefinite period.

The exponential fit (blue curve) suggests that Lac du Bonnet granite has a long-term strength that is of the order of 45% of the UCS for this rock — i.e., the granite is predicted to be able to sustain, indefinitely, a deviatoric stress of ~100 MPa under unconfined loading. The linear extrapolation indicates that the rock essentially will “collapse under its own weight” (i.e., the strength declines to zero) after approximately one million years. Although the data for 10-MPa and 20-MPa confinement in Fig. 1 are quite limited, they appear to exhibit a more rapid rise in “time to failure” than the unconfined data, which supports the possibility of an even higher long-term strength under confinement. This seems logical, as confinement acts to inhibit axial crack propagation, the process by which the rock weakens. Clearly, the difference between the linear and exponential extrapolations leaves an uncertainty in long-term strength prediction that is much too large. Additional evidence of the long-term strength of rocks is required.

Note: LdB1 data are from tests of Schmidtke & Lajtai (1985) on 2:1 aspect-ratio, right-circular cylinders of 31.7-mm dia. LdB2 data are from tests of Lau et al. (2000) on 2.5:1 aspect-ratio, right-circular cylinders of 61-mm dia.

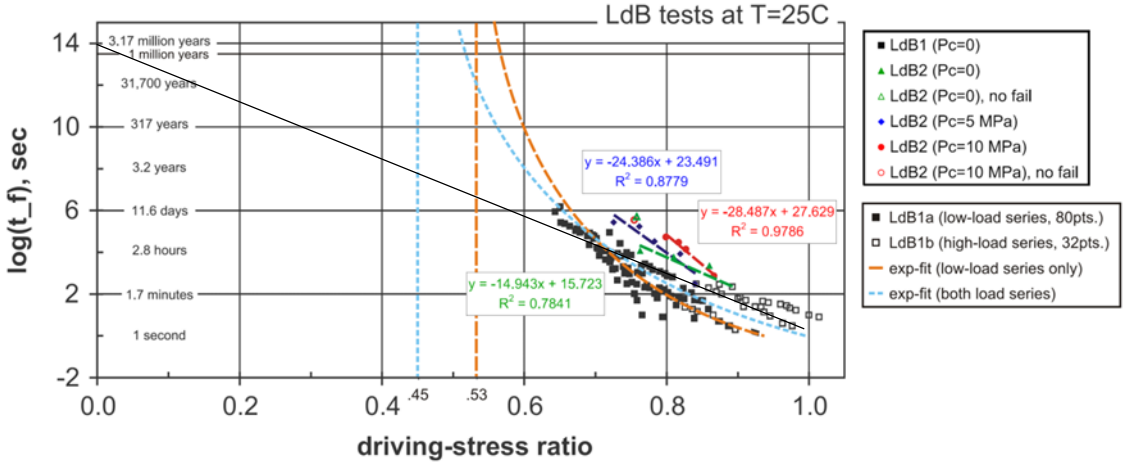

Figure 1. Creep test data for Lac du Bonnet granite showing linear and exponential extrapolation of data (Potyondy 2007).

3 Effect of rock strength reduction on wing-crack propagation

The so-called “wing-crack” model has been used widely in the analysis of tensile crack growth in brittle materials under compressive loads. It is derived from the original analysis by Griffith (1924), which, in turn, was inspired by Inglis’ (1913) analytical solution for the stress distribution around an elliptical crack. Fairhurst & Cook (1966) used the inclined (micro) crack of the wing-crack model as a mechanism to generate local tensile forces normal to the direction of compressive loading in rock and to explain the observed development of cracks parallel to the applied load. Hoek & Bieniawski (1966) demonstrated, experimentally, the propagation of wing cracks from an inclined crack, and the major effect of confining pressure on reducing the development of wing cracks.

The effect of time-dependent strength degradation on the length of a wing crack, and ultimately the strength of rock, can be represented effectively by reduction of the fracture toughness and its effect on propagation of wing cracks. The strength of the rock is reached when the wing cracks become sufficiently long to interact with each other. Thus, it is not only a function of load and rock toughness, but also a function of the spacing of pre-existing cracks or the *level of damage* (at the state) when the time-dependent strength degradation is activated. The analysis presented here considers the effect of toughness reduction on rock strength without direct reference to time. Thus, the time effect is implicit, through its effect on rock toughness (or micro strength).

It is assumed that stress corrosion (Potyondy 2007) is the mechanism of strength degradation. Two necessary conditions for stress corrosion to be active are: 1) the existence of cracks; and 2) tension at the crack tip. In fact, the tensile stress at the crack tip has to be greater than a threshold stress that is proportional to the activation energy (Scholtz, 1972). If the activation energy is neglected, *or assumed to be negligible*, the fracture toughness will decrease to zero with time and the length of the wing crack in the unconfined sample will approach infinity, indicating rock failure. Under those conditions, based on the simple analytical model of Germanovich & Dyskin (2000), the long-term strength of unconfined rock is zero. As will be shown below, a more realistic model, which considers a finite-size sample with discrete rock structure, yields a different result.

The numerical model investigated the effect of toughness (or micro-strength) reduction due to stress corrosion on: 1) the wing-crack length; and 2) the rock strength. A micro-mechanical model was used to represent the brittle rock. In this approach, the domain is discretized into a large number of relatively small blocks — i.e., $d/2a \ll 1$, where d is the block characteristic dimension, and a is the

crack half-length. The blocks, which are polygonal in shape (created by Voronoi tessellation in two dimensions), are assumed to be elastic in these simulations. Inelastic deformation and damage occur along the interfaces or joints between the blocks. Initially, the joints are bonded together, and assigned a specific tensile and shear strength**.** In this model, the bond shear strength is assumed to obey the Coulomb slip law.

The samples with the wing crack were loaded to a number of different levels, represented as increasing fractions of the short-term strength of the cracked samples. The top boundary condition was velocity-controlled (i.e., infinitely stiff) during the short-term strength testing. Once the required load level was reached, the top boundary condition was changed to load-controlled (i.e., infinitely soft) and held constant at this level. The effect of time-dependent toughness reduction caused by stress corrosion was represented in the analysis by a reduction of both tensile strength and cohesion in the joints between the grains ahead of those existing crack tips that were open (i.e., loaded in tension). In other words, the strength was not reduced everywhere throughout the sample, because stress corrosion is considered to take place at the open crack tips only. The micro-strength reduction is implemented in finite increments of 10% of the short-term strength.

Thus, if the sample is loaded at a stress level σ_1, then the driving stress ratio will be σ_1/σ_u, where σ_u is the instantaneous strength of the sample. The critical strength-reduction ratio, r_c, or fraction of strength reduction required to fail the sample — i.e., the number of 10% strength decrements (reduction in crack tensile strength and cohesion or, effectively, reduction in fracture toughness) required before the sample will fail — is defined by

$$r_c = 1 - \frac{\sigma_1}{\sigma_u} \tag{1}$$

The results from the simulations of an unconfined test for a specific axial load σ_1 of $0.16\ \sigma_u$ are shown in Fig. 2. Two states are shown: 1) the initial state, before the strength is reduced; and 2) the final state, after an incremental strength reduction to zero.

There are two interesting observations from this numerical experiment. Based on Equation (1), the sample should have failed for $r = r_c = 0.84$. Because the creep load is reduced in 10% increments in the simulations, this indicates that the sample would not fail at 0.8 reduction, but would fail when the strength was reduced by a further 10% increment, at a stress reduction ratio equal to 0.9 — i.e., $r^3 r_c$. The results of the simulation indicate that the model did not fail; it reached a stable configuration (Fig. 2b) even when the strength was reduced to zero. Also, although analytical considerations indicate that the crack length should be infinite, the wing crack is arrested at a finite length.

The reason for this apparent anomaly is that the numerical model includes a representation of the internal structure of the rock, where the small elastic blocks behave as grains with much greater strength than the bond strength of the contacts between the grains. When the crack becomes sufficiently long, the finite-sized grains effectively blunt the crack tip.

4 Tectonic evidence of a stress threshold in crystalline rock

The difficulty in extrapolating the results of creep tests conducted over days to times of the order of a million years suggests the possibility of examining evidence that may be available from plate tectonics. In this context, it appears that some useful insights can be gained by examining field data with respect to the possibility of a threshold stress in crystalline rock.

Examination of a few situations in stable plate regions provides more convincing evidence. Quarries for dimension stone are selected and developed because the granite is essentially unfractured over a considerable area. The rock is, therefore, of high strength, capable of supporting high stresses. Review of a few examples in the North American Plate, where stresses have been determined or estimated in granite quarries, indicates the existence of a stress threshold. In these cases, the rock is at the surface and essentially unconfined.

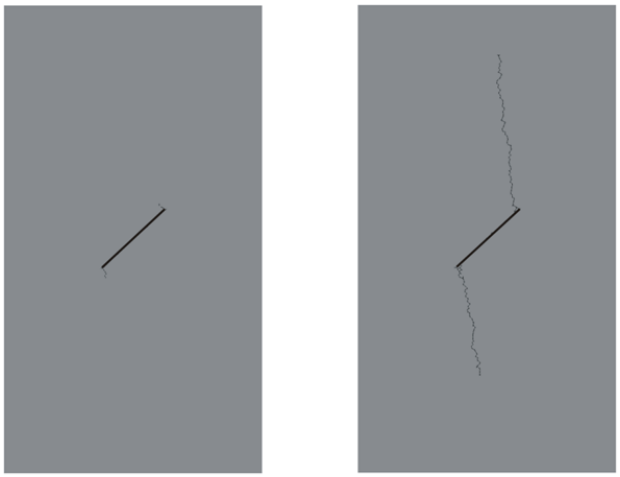

Figure 2. Model configuration and fracturing at two stages during test: Strength reduction at the tip of an unconfined sample with a single crack loaded to 0.16 σ_u.

5 Conclusion

The predominant approach used currently to assess the long-term response of rock is to extrapolate the results of laboratory creep tests, which typically involve loading test specimens over a period of several days, to the much longer times of interest. One of the principal concerns in this extrapolation is to establish whether the rock strength will decline progressively without limit and fail for any non-zero deviatoric stress, or whether it will approach a finite lower limit, or "threshold" stress. This paper has examined evidence for the existence of a threshold stress in crystalline rock, with reference to tectonic data and a numerical model of rock weakening by "stress corrosion" that takes into account the discrete particulate structure of crystalline rocks. The data and the analyses indicate that the long-term strength threshold of intact rock with no pre-existing fractures should be equal to or greater than the crack initiation stress, σ_{ci}, which is in the range of 40% – 60% of the short-term strength.

6 Reference list

Einstein, HH, Meyer. T. 1999. Müller Lecture: Puzzles in rock. In Proceedings, 9th ISRM Congress on Rock Mechanics (Paris, 1999), Vol. 3. G. Vouille and P. Bérest (eds.). Lisse: Balkema.

Fairhurst, C, Cook, N. 1966. The phenomenon of rock splitting parallel to the direction of maximum compression in the neighborhood of a surface. In Proceedings, First Congress of the International Society of Rock Mechanics (Lisbon, September-October 1966), Vol. 1, pp. 687-692. J. G. Zeitlen (ed.) Lisbon: LNEC, 1966.

Germanovich, LN, Dyskin, AV. 2000. Fracture mechanisms and instability of openings in compression. Int. J. Rock. Mech. Min. Sci., 37, 263–284.

Griffith, AA. 1924. The theory of rupture. In Proc., 1st Int. Congr. Applied Mechanics, pp.55-63.

Hoek, E, Bieniawski, ZT. 1966. Fracture propagation mechanism in hard rock. In Proceedings, First Congress of the International Society of Rock Mechanics (Lisbon, September-October 1966), Vol. 1, pp. 243-249. J. G. Zeitlen, (ed.) Lisbon: LNEC.

Lau, JSO, Gorski, B, Conlon, B, Anderson, T. 2000. Long-term loading tests on saturated granite and granodiorite, CANMET Natural Resources Canada, Ottawa, Ontario, Report No. 06819-REP-01300-10016 R00, November.

Potyondy, DO. 2007. Simulating stress corrosion with a bonded-particle model for rock. Int. J. Rock Mech. & Min. Sci.,44, 677–691.

Inglis, CE. 1913. Stresses in a plate due to the presence of cracks and sharp corners. Trans. Inst'n. Naval Architects, London, 1(3), 219-230.

Scholz, CH. 1972. Static Fatigue of quartz. J. Geophys. Res., 77(11), 2104 (April 10).

Schmidtke, RH, Lajtai, EZ. 1985. The long-term strength of Lac du Bonnet granite. Int. J. Rock Mech. Min. Sci., 22, 461–465.

On the progressive failure of gypsum pillars: FEM vs. FEM/DEM approach

Riccardo Castellanza[1*], Stefano Grisi[2], Federico Agliardi[1] and Giovanni Crosta[1]

[1] Department of Earth and Environmental Sciences, University of Milano Bicocca, Milan, Italy
* riccardo.castellanza@unimib.it

[2] Syndial (Eni group), Milan, Italy

1 Introduction

In order to consider the presence of cracks in an abandoned gypsum pillar in numerical simulations, a hybrid method FEM/DEM, which allows the transition from continuum to discontinum, was assumed. By means of a specific numerical code (ELFEN), this approach has been calibrated involving both physical quantities introduced by fracture mechanics and numerical aspects in order to support this hybrid method. Furthermore, the approaches FEM and FEM/DEM have been compared, showing advantages and disadvantages through experimental tests carried out to characterize geomechanical response of the pillar. The interaction domain has been calculated thanks to the implementation of both methods. The meaning of determining this domain is related to the evaluation of failure limit when a coupled system of loads (normal and tangential force and momentum) is acting on pillars. An application to a case study of an abandoned gypsum mine interacting with building in San Lazzaro di Savena (Bologna) is shown.

2 Abandoned Gypsum Mine – specific pillar (P7) chosen

The choice of this pillar is related to its complex and reduntant joints' system, its reduced section and its location. In fact, it was possible to obtain its topography by TLS to furnish a detailed geometrical for the simulation. In the following figure the mine system and the selected pillar is shown.

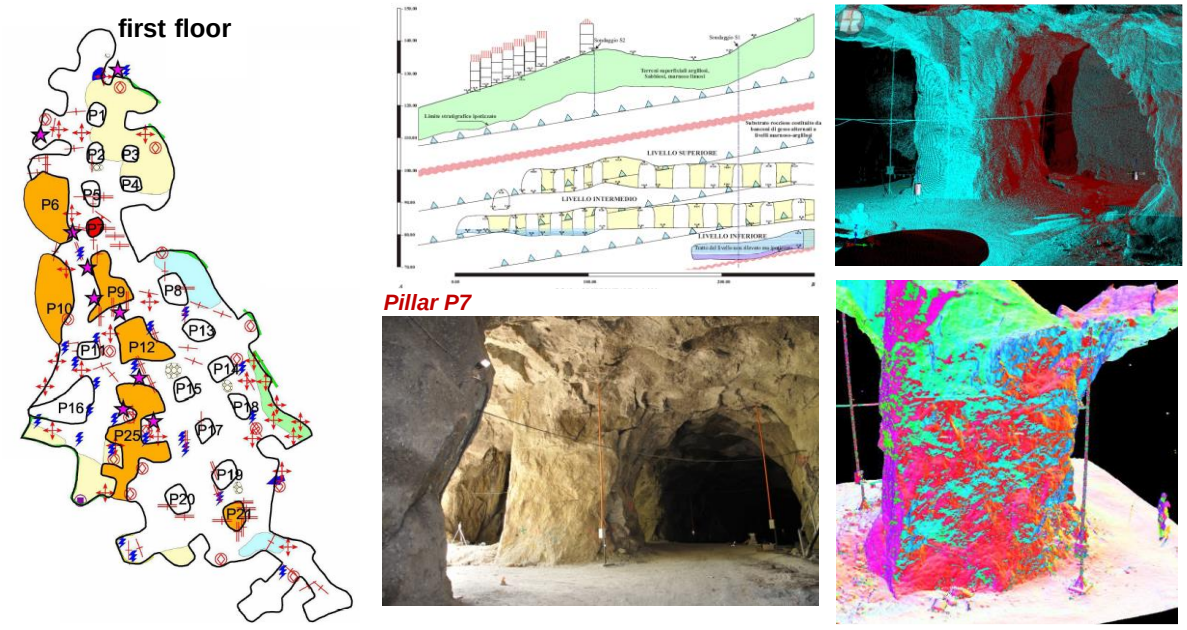

Figure 1. Abandoned mine system and TLS of the selected pillar to be analysed.

3 Laboratory tests (UCS, BT, Triax)

A series of laboratory tests permitted to obtain failure parameters to be inserted both in constitutive model for the continuum approach (FEM) than for the crack propagation model for the discountiuum approach (FEM/DEM).

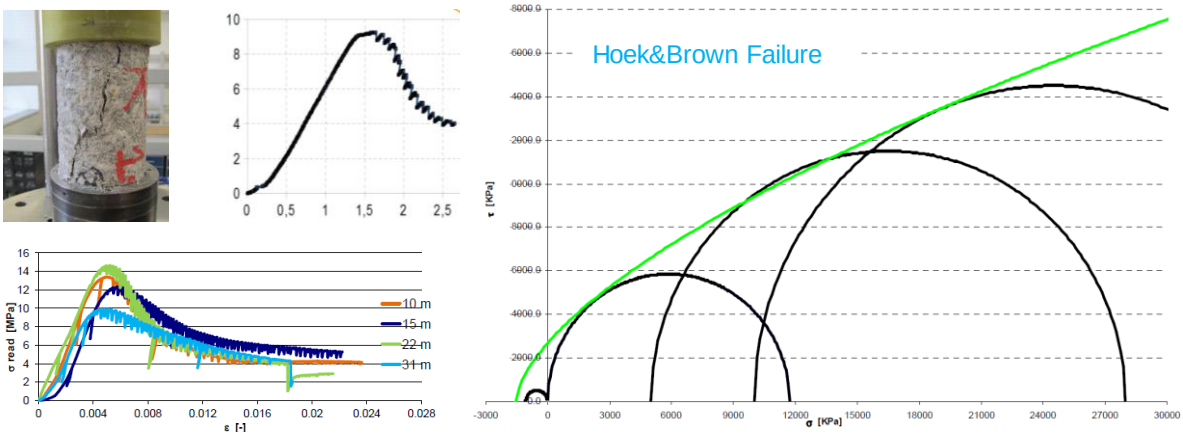

Figure 2. Laboratory tests and failure envelope of the intact rock.

4 A numerical comparison between the two approaches

A coupled system of loads acting on pillar P7 has been simulated. In particular, 3D numerical simulations have been run to calculate an interaction domain represented by normal and tangential force and momentum. Also for the 2D FEM/DEM approach an interaction domain has been built thanks to a simplified solution by choosing two representative sections of pillar P7.. In the following the numerical calibration of the continuum and hybrid approach is shown.

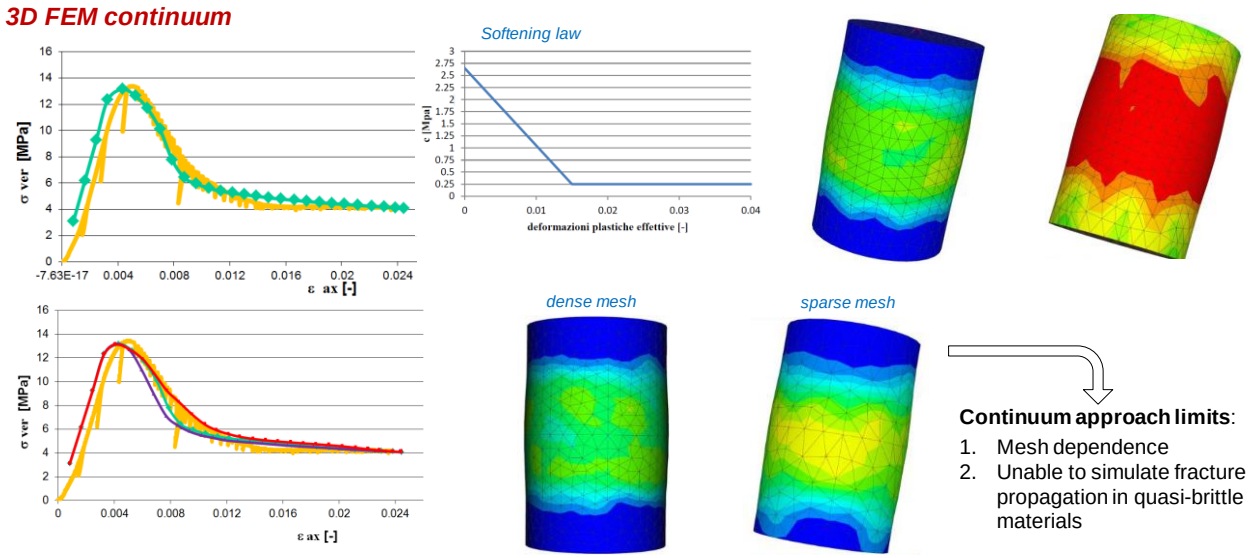

Figure 3. Calibration of the continuum(FEM) approach with a strain softening constitutive model .

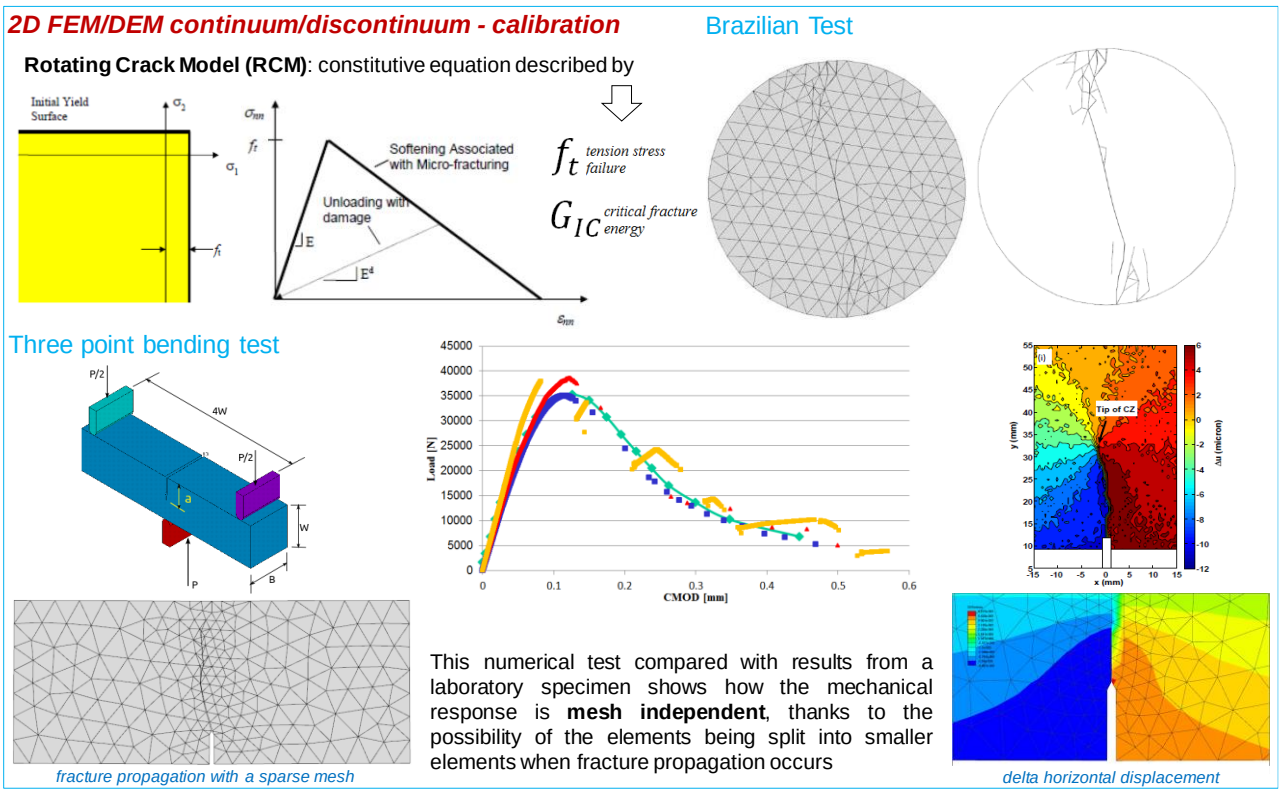

Figure 4. Calibration of the discontinuum (FEM/DEM) approach with a strain softening constitutive model .

5 Simulation of pillar failure

After a numerical calibration process, it was possible to compare the mechanical response of the pillar (real geometry and size) subjected to vertical uniaxial load, using different FEM and FEM/DEM simulation approaches. For the 3D continuum numerical analysis, in this preliminary application we used the same mechanical properties adopted to simulate lab-scale uniaxial tests on intact rock specimens

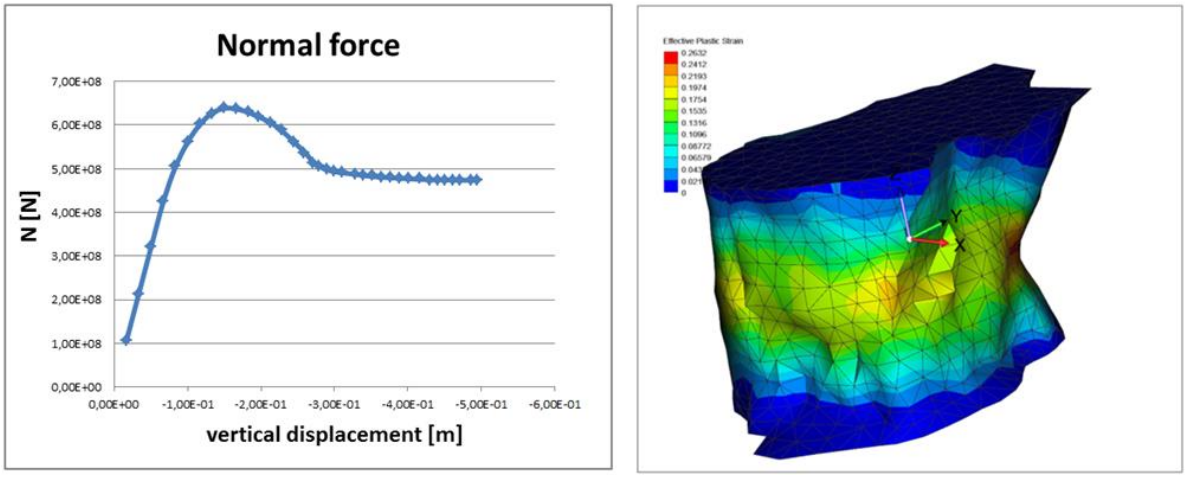

Figure 5. 3D FEM simulation

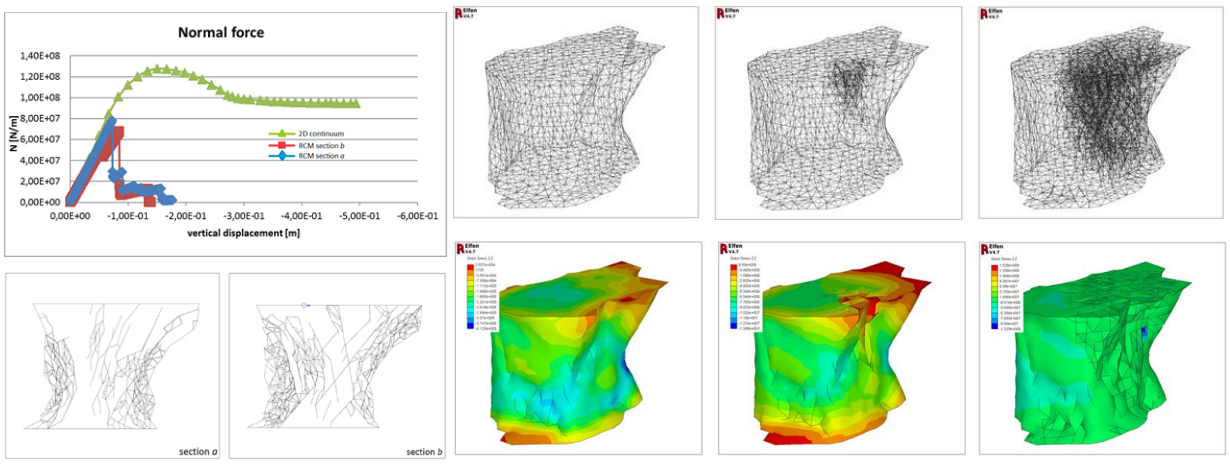

Figure 6. 2D and 3D FEM/DEM simulation

6 Reference list

Castellanza, R. & Orlandi, G. M. & di Prisco, C.& Frigerio, G. & Flessati L. & Fernandez Merodo J.A. & Agliardi F. & Grisi, S. & Crosta G.,2015. 3D numerical analyses for the quanti-tative risk assessment of subsidence and water flood due to the partial collapse of an abandoned gypsum mine. IOP Conference Series: Earth and Environmental Science http://stacks.iop.org/1755-1315/26/i=1/a=012058 ,

Clerk, P.A. & Sellers, E.J. & Owen, D.R.J. 2004. Discrete frac-ture in quasi – brittle materials under compressive and ten-sile stress states. Comput. Methods Appl. Mech. Engrg. 193: 3035–3056.

Duan, K. & Xiaozhi, H. & Wittmann, F.H.. 2003. Boundary ef-fect on concrete fracture and non-constant fracture energy distribution. Engineering Fracture Mechanics 70: 2257–2268.

Eberhardt, E. & Stead, D. & Coggan, J.S. 2004. Numerical analysis of initiation and progressive failure in natural rock slopes—the 1991 Randa rockslide. International Journal of Rock Mechanics & Mining Sciences 41: 69–87.

Elmo, D. & Stead, D. 2010. An Integrated Numerical Modelling Discrete Fracture Network Approach Applied to the Char-acterisation of Rock Mass Strength of Naturally Fractured Pillars. Rock Mech. Rock Eng 43: 3–19.

Lin, Q. & Yuan, H. & Biolzi, L. & Labuz, J. F. 2014. Opening and mixed mode fracture processes in a quasi-brittle mate-rial via digital imaging. Engineering Fracture Mechanics 131: 176–193.

Mortazavi, A. & Hassani, F.P. & Shabani, M. 2009. A numeri-cal investigation of rock pillar failure mechanism in under-ground openings. Computers and Geotechnics 36: 691–697.

Munjiza, A. 2004. The combined finite-discrete element meth-od. London: Wiley.

Pine, R. J. & Coggan, J. S. & Flynn, Z. N. & Elmo, D. 2006. The Development of a new Numerical Modelling Approach for Naturally Fractured Rock Masses. Rock Mech. Rock Engng. 39 (5): 395–419.

Wang, S. Y. & Lam, K. C. & Au, S. K. & Tang, C. A. & Zhu, W. C. & Yang, T. H. 2006. Analytical and Numerical Study on the Pillar Rockbursts Mechanism. Rock Mech. Rock Engng. 39 (5): 445–467

DEEP geothermal energy: a geomechanical view

Martin Potten[1*] and Kurosch Thuro[1]

[1] Department of Engineering Geology, Technical University of Munich, Germany
* martin.potten@tum.de

The use of geothermal energy in Bavaria increased considerably in recent years, and practical experience in geothermal plant operation for heat and power generation has shown a primary need for research. To answer questions related to deep geothermal energy and to concentrate and link operating experience of the operators, the Geothermie-Allianz Bayern (GAB) was founded.

Bavaria has a unique geothermal potential in Germany. In particular, the South-German Molasse Basin south of Munich offers ideal conditions for the development of hydrothermal geothermal energy. The present project aims to reduce the risk of geothermal search in the South German Molasse Basin and to optimize reservoir engineering. For this purpose, the hydraulic effectiveness of disturbances will be investigated by a structure-stress analysis (Reinecker 2010). The disturbance zones near drilled holes will be characterized geologically, seismically and geomechanically. The results provide data for a reference model of the southern Molasse basin. In addition, the local stress situation around the borehole will be evaluated and a geomechanical reservoir model will be constructed using data from the geomechanical near-field analysis (Seithel et al. 2015). In order to complete the database of the mechanical properties of representative types of rock, extensive investigations will be carried out in the laboratory. This will be done with samples from geothermal drillings as well as with so-called analogue samples, which come from geologic or petro-graphic explorations, e.g. quarries.

Furthermore, petrothermal potential in crystalline rocks is focused in the northern part of Bavaria (Riemer 2011). The development and use of this future technology initially requires extensive research, but then it has an outstanding future potential, since the use of geothermal energy is not limited to water in depth (Bauer 2000). Considering local geology, natural stress conditions and geomechanical laboratory parameters, numerical modeling approaches shall show in which part of the investigation area hydraulically division surfaces of defined orientation will appear with priority in case of stimulation measurements. The results will be validated using the above mentioned borehole and exploration analogue data and will serve to predict existing rock anisotropies after stimulation measurements. The slip-tendency analysis is used here to investigate the behavior of already existing interfaces / disturbance zones in a defined stress field. It is used to identify potentially re-activatable faults and to selectively prevent seismic events during fluid injections.

As soon as the results of the laboratory work are available, this will be reached by improving the knowledge about the detection of a local stress field which has a major impact on the hydraulic system of the reservoir of geothermal plant operation. The stress analysis should one the one hand analyses the interaction between the removal of the drilling and the stress relaxation in the borehole. On the other hand it should be researched, how the fractures in the borehole area are spread out and lead to a better connection to the aquifer. One result could be that the hydrothermal water can be obtained mainly in zones, where the critically stresses pass the barrier. In these zones, the pipes have to be installed that the the outcome of this research will be reached to increase profitability and minimize risk of geothermal projects.

This work is being supported by the Bavarian Ministry of Education, Science and the Arts within the framework of the Geothermie-Allianz Bayern.

Reference list

Bauer, W. 2000. Geothermische Verhältnisse des Fränkischen Beckens. Hydrogeologie und Umwelt, 22, Würzburg.

Reinecker, J, Tingay, M, Müller, B, Heidbach, O. 2010. Present-day stress orientation in the Molasse basin. Tectonophysics 482, 129 – 138.

Riemer, A. 2011: Kluft- und Störungssysteme im westlichen Oberfranken und Eigenschaften des Temperaturfeldes mit Fokus auf die Mürsbacher Temperaturanomalie. unpubl. Diploma thesis, Geozentrum Nordbayern.

Seithel, R, Steiner, U, Müller B, Hecht, C, Kohl, T. 2015. Local stress anomaly in the Bavarian Molasse Basin. Geothermal Energy 3:4.

From micro-mechanical to practical engineering approaches to modeling time-dependent rock degradation

Branko Damjanac[1*]

[1] Itasca Consulting Group, Inc., Minneapolis, USA
* branko@itascacg.com

Abstract

The micro-mechanical stress-corrosion model and its implementation in the bonded particle model (BPM) in PFC will be presented. The micro-mechanical models help to understand mechanics of strength degradation but are not practical tools for solution of problems on length- and time-scales relevant for engineering applications. A methodology has been developed and implemented in distinct element codes, which use static-fatigue data (time-to-failure curves), that allow simulation and prediction of damage in the rock mass and stability of excavation as a function of time and evolving stress states. Alternatively, a visco-plastic continuum constitutive model will be presented that can simulate creep (time-dependent deformation) but also associated accumulation of damage and strength degradation. The model uses relatively few input parameters that can be determined from standard creep and strength tests.

Analysis of time-dependent rock masses using the convergence-confinement method

Chrysothemis Paraskevopoulou[1*]

[1] School of Earth and Environment, University of Leeds, United Kingdom
* C.Paraskevopoulou@leeds.ac.uk

Abstract

During the excavation of a tunnel the accumulated wall displacement and the loading of tunnel support is the result of both the tunnel advance and the time-dependent behaviour of the surrounding rockmass. The current approach to analyze the wall displacement increase is based on the convergence-confinement method performed with either analytical (closed form solutions) or the usage of Longitudinal Displacement Profiles. This approach neglects the influence of time-dependency resulting in delayed deformation that may manifest in even minutes or hours after excavation. Failure to consider the added displacements in the preliminary design can result in false selecting the time of installation and the type of support system causing safety issues to the working personnel, leading to cost overruns and project delivery delays. This presentation focuses on investigating and analyzing the total displacements around a circular tunnel in a visco-elastic medium, proposing a new yet simplified approach that practitioners can use which takes into account effect of a time-dependent nature.

Continuum and discontinuum based approaches to simulate time-dependent processes

Heinz Konietzky[1*]

[1] Geotechnical Institute, TU Bergakademie Freiberg, Germany
* heinz.konietzky@ifgt.tu-freiberg.de

Abstract

Modelling procedures based on continuum and discontinuum approaches considering subcrtitical and critical crack growth are presented. For simulations at the grain size level procedures are proposed on how to incorporate grain size, grain shape, mineralogical composition and pore size distributions into the numerical model. The discontinuum based simulations allow to distinguish between intra- and inter-granular fracturing as well as between shear and tensile fracturing. Based on the educational version of FLAC the use of the developed routines is demonstrated. Several examples will show the influence of micro crack size and orientation on the lifetime.

Simulation of fracture initiation and propagation using FRACture mechanics CODe FRACOD

Siren, Topias[1*]

[1] Department of Civil Engineering, School of Engineering, Aalto University, Helsinki, Finland
* topias.siren@aalto.fi

Abstract

The Fracture mechanics code FRACOD2D can model the fracture initiation and propagation using the F-criterion that allows mixed-mode propagation. It can also take into account the rock anisotropy and creep influences under full Thermal Hydoraulic Mechanical coupling. The code has been used in various fields from modelling of borehole breakouts to cavern stability.

ETH zürich

Congressi Stefano Franscini

SFIG SCHWEIZERISCHE FACHGRUPPE FÜR INGENIEURGEOLOGIE

GSGI GROUPEMENT SUISSE DE LA GEOLOGIE DE L'INGENIEUR

FNSNF SWISS NATIONAL SCIENCE FOUNDATION

Schweizerische Eidgenossenschaft
Confédération suisse
Confederazione Svizzera
Confederaziun svizra

Eidgenössisches Nuklear-sicherheitsinspektorat ENSI

ITASCA Consulting Group, Inc.

ISRM International Society for Rock Mechanics